



# **Automatic plant features recognition using stereo vision for crop monitoring**

A Thesis submitted by

**Zainab Mohammed Amean**

MSc Mechatronics Eng

For the award of

**Doctor of Philosophy**

2017

# Abstract

Machine vision and robotic technologies have potential to accurately monitor plant parameters which reflect plant stress and water requirements, for use in farm management decisions. However, autonomous identification of individual plant leaves on a growing plant under natural conditions is a challenging task for vision-guided agricultural robots, due to the complexity of data relating to various stage of growth and ambient environmental conditions. There are numerous machine vision studies that are concerned with describing the shape of leaves that are individually-presented to a camera. The purpose of these studies is to identify plant species, or for the autonomous detection of multiple leaves from small seedlings under greenhouse conditions. Machine vision-based detection of individual leaves and challenges presented by overlapping leaves on a developed plant canopy using depth perception properties under natural outdoor conditions is yet to be reported. Stereo vision has recently emerged for use in a variety of agricultural applications and is expected to provide an accurate method for plant segmentation and identification which can benefit from depth properties and robustness.

This thesis presents a plant leaf extraction algorithm using a stereo vision sensor. This algorithm is used on multiple leaf segmentation and overlapping leaves separation using a combination of image features, specifically colour, shape and depth. The separation between the connected and the overlapping leaves relies on

the measurement of the discontinuity in depth gradient for the disparity maps. Two techniques have been developed to implement this task based on global and local measurement. A geometrical plane from each segmented leaf can be extracted and used to parameterise a 3D model of the plant image and to measure the inclination angle of each individual leaf. The stem and branch segmentation and counting method was developed based on the vesselness measure and Hough transform technique. Furthermore, a method for reconstructing the segmented parts of hibiscus plants is presented and a 2.5D model is generated for the plant. Experimental tests were conducted with two different selected plants: cotton of different sizes, and hibiscus, in an outdoor environment under varying light conditions. The proposed algorithm was evaluated using 272 cotton and hibiscus plant images. The results show an observed enhancement in leaf detection when utilising depth features, where many leaves in various positions and shapes (single, touching and overlapping) were detected successfully.

Depth properties were more effective in separating between occluded and overlapping leaves with a high separation rate of 84% and these can be detected automatically without adding any artificial tags on the leaf boundaries. The results exhibit an acceptable segmentation rate of 78% for individual plant leaves thereby differentiating the leaves from their complex backgrounds and from each other. The results present almost identical performance for both species under various lighting and environmental conditions. For the stem and branch detection algorithm, experimental tests were conducted on 64 colour images of both species under different environmental conditions. The results show higher stem and branch segmentation rates for hibiscus indoor images (82%) compared to hibiscus outdoor images (49.5%) and cotton images (21%). The segmentation and counting of plant features could provide accurate estimation about plant growth parameters which can be beneficial for many agricultural tasks and applications.

# Certification of Thesis

This thesis is entirely the work of ZAINAB MOHAMMED AMEAN except where otherwise acknowledged. The work is original and has not previously been submitted for any other award, except where acknowledged.

Student and supervisors signatures of endorsement are held at USQ.

---

Zainab Mohammed Amean, Student

---

Dr Tobias Low, Principal supervisor

---

Dr Cheryl McCarthy, Associate supervisor

---

A/Prof. Nigel Hancock, Associate supervisor



# Acknowledgments

First and foremost, I would like to thank Allah for helping me complete my educational journey. During the progress of this journey, there have been a number of people whose help I would like to acknowledge. My principal supervisor Dr. Tobias Low for his support, guidance and concern and for pushing this research to places I thought impossible. My associate supervisors Dr. Cheryl McCarthy and Assoc. Prof. Nigel Hancock for their guidance, encouragement and support. I would like to acknowledge the technical and administrative support of the Faculty of Health, Engineering and Science. Also my deep appreciation goes to Miss Sarah Muller for English proof reading of this thesis. I would also like to thank all my friends and colleagues at USQ for their encouragement and support. I would like to thank the Ministry of Higher Education and the University of Technology in Baghdad, Iraq for funding the PhD scholarship.

I am very grateful to my husband and my wonderful sons for their endless love, continuous encouragement and support. Last but not least, I would like to dedicate this work to my parents. I am greatly indebted to them for all their prayers, unconditional support, love and encouragement.

ZAINAB MOHAMMED AMEAN

# Associated Publications

The following publications were produced during the period of candidature:

Mohammed Amean, Z., Low, T., McCarthy, C., and Hancock, N. “Automatic plant branch segmentation and classification using vesselness measure,” *Proceeding of the 2013 Australasian Conference on Robotics and Automation (ACRA2013)*, Sydney, Australia, December 2-4, 2013.

(The work in this paper is presented in Chapter 6).

Mohammed Amean, Z., Low, T., McCarthy, C., and Hancock, N. “Evaluation of stereovision for extracting plant features”, *2013 Society for Engineering in Agriculture Conference: Innovative Agricultural Technologies for a Sustainable Future*, Barton, ACT, Australia, September 22-25, 2013.

(A part of this paper work is presented in Chapter 3).

# Contents

<b>Abstract</b>	<b>i</b>
<b>Acknowledgments</b>	<b>iv</b>
<b>Associated Publications</b>	<b>v</b>
<b>List of Figures</b>	<b>xiii</b>
<b>List of Tables</b>	<b>xxi</b>
<b>Notation</b>	<b>xxiii</b>
<b>Acronyms &amp; Abbreviations</b>	<b>xxvi</b>
<b>Chapter 1 Introduction</b>	<b>1</b>
1.1 Motivation . . . . .	1
1.2 Mobile robot platform in agriculture . . . . .	4

---

<b>CONTENTS</b>	<b>vii</b>
-----------------	------------

1.3	Machine vision in agriculture . . . . .	5
1.4	Plant monitoring systems . . . . .	7
1.5	Research scope . . . . .	10
1.6	Research questions . . . . .	12
1.7	Research aim and objectives . . . . .	13
1.8	Original research contribution . . . . .	14
1.9	Thesis outline . . . . .	16
 <b>Chapter 2 Literature review</b>		<b>18</b>
2.1	Image analysis using 2D image features . . . . .	20
2.1.1	Fruit detection . . . . .	20
2.1.2	Plant detection . . . . .	22
2.2	Image analysis using depth sensing . . . . .	26
2.2.1	Depth sensing in the outdoor field condition . . . . .	27
2.2.2	Depth sensing in a controlled environment . . . . .	30
2.3	Image analysis techniques for leaf and stem detection . . . . .	33
2.3.1	Leaf detection . . . . .	34
2.3.2	Detection of multiple leaves . . . . .	35

<b>CONTENTS</b>	<b>viii</b>
2.3.3 Stem and branch detection . . . . .	41
2.4 Conclusion . . . . .	44
2.5 Research problem . . . . .	49
<b>Chapter 3 Evaluation of the stereo vision system</b>	<b>52</b>
3.1 Introduction . . . . .	52
3.2 Stereo vision technique . . . . .	53
3.2.1 Triangulation . . . . .	54
3.2.2 Camera calibration . . . . .	56
3.2.3 Stereo rectification . . . . .	58
3.2.4 Stereo correspondence . . . . .	59
3.3 Stereo vision specification . . . . .	63
3.4 Cotton plants experiment setup . . . . .	67
3.5 Evaluation of disparity maps for a wide range of parameters . . . .	68
3.6 Chapter summary . . . . .	80
<b>Chapter 4 Leaf segmentation and counting algorithm</b>	<b>82</b>
4.1 Introduction . . . . .	83
4.2 Initial image inspection and evaluation . . . . .	84

<b>CONTENTS</b>	<b>ix</b>
4.3 Algorithm design process . . . . .	86
4.4 Image pre-processing stage . . . . .	88
4.4.1 Background removal process using depth and colour attributes	88
4.4.2 Image segmentation based on hue distribution . . . . .	93
4.4.3 Image enhancement and shape geometrical analysis . . . . .	99
4.5 Depth Discontinuity Segmentation (DDS) . . . . .	109
4.5.1 Disparity Map Denoising technique (DMD) . . . . .	110
4.5.2 Global Discontinuity Segmentation technique (GDS) . . . . .	114
4.5.3 Local discontinuity segmentation–Eight Neighbours Difference technique (ENBD) . . . . .	119
4.5.4 Final leaf segmentation . . . . .	130
4.6 Leaf plane extraction . . . . .	134
4.6.1 Definition of a plane . . . . .	134
4.6.2 Leaf plane extraction method . . . . .	136
4.6.3 Error measurement . . . . .	137
4.7 Chapter summary . . . . .	141
<b>Chapter 5 Evaluation of automatic leaf segmentation and counting algorithm</b>	<b>143</b>

## CONTENTS

x

5.1	Introduction . . . . .	144
5.2	Data collection . . . . .	144
5.3	Leaf counting accuracy - results and discussion . . . . .	147
5.3.1	Effect of lighting . . . . .	150
5.3.2	Effect of leaf orientation . . . . .	160
5.3.3	Effect of leaf size . . . . .	163
5.3.4	Effect of overlapped leaves . . . . .	166
5.4	Chapter summary . . . . .	169

## Chapter 6 Automatic plant branch segmentation using vesselness

	measure	171
6.1	Introduction . . . . .	172
6.2	Stem and branches segmentation algorithm overview . . . . .	172
6.3	Edge detection for stem and branch segmentation . . . . .	173
6.4	Branch extraction using vesselness measure . . . . .	175
6.4.1	Line fitting using Hough transform technique . . . . .	180
6.5	Results evaluation and discussion . . . . .	183
6.5.1	Indoor results . . . . .	183

<b>CONTENTS</b>	<b>xi</b>
6.5.2 Outdoor result . . . . .	186
6.6 Reconstruction of plant segmented parts and 3D localisation . . . .	191
6.7 Chapter Summary . . . . .	194
<b>Chapter 7 Conclusions and Future work</b>	<b>196</b>
7.1 Conclusions . . . . .	197
7.2 Potential application of the research work . . . . .	202
7.2.1 Plant inspection and growth monitoring . . . . .	202
7.2.2 Leaf inclination angle measurement . . . . .	203
7.3 Future work and recommendations . . . . .	204
7.3.1 Development of leaf detection algorithm . . . . .	204
7.3.2 Detection of large and bent leaves . . . . .	205
7.3.3 Development of stem detection algorithm . . . . .	205
7.3.4 Development of 3D model reconstruction . . . . .	206
<b>References</b>	<b>207</b>
<b>Appendix A Stereo vision camera and specifications</b>	<b>233</b>
A.1 Stereo vision camera . . . . .	234



<b>CONTENTS</b>	<b>xii</b>
A.2 Camera specifications . . . . .	234

# List of Figures

1.1	Cotton and Hibiscus plants. . . . .	11
2.1	Main research areas related to this study . . . . .	19
2.2	Depth image segmentation, (a) original image, (b) disparity map, and (c) disparity map after noise filtering and segmentation (Xia et al., 2009) . . . . .	32
2.3	Multiple leaf detection of (a) and (b) using MLP-ASM method (Xia et al., 2013). (a) Top view image of pepper leaves, (b) side view image of paprika leaves. (c) Segmentation of individual leaves using depth sensor (Xia et al., 2015) . . . . .	39
3.1	(a) The geometry of a binocular stereo model, and (b) an undistorted, aligned and measured stereo camera system. . . . .	55
3.2	World point mapped into the image plane using Intrinsic and Extrinsic matrix parameters in pinhole camera model. . . . .	57

3.3	(a) Stereo vision camera during image capture. (b) Cotton plants at an early growth stage . . . . .	67
3.4	Presents different settings for the stereo mask parameter. (b) The disparity map has noise “spikes” in the background and an accurate depth discontinuity for leaves’ boundaries. (c) and (d) have smooth depth and less spike areas in the background, but blur depth discontinuity for leaves’ boundaries. All disparities have a “speckles” area behind the plants. . . . .	70
3.5	Shows different settings for surface size parameters for the disparity images while the images have the same setting for surface difference =1.0 and texture validation =1.0. Stereo mask = 7 for (b). Stereo mask = 9 for (c) and (d). . . . .	73
3.6	(a) and (b), present different settings for surface difference parameter. Both images have the same setting for surface size =200, texture validation =1.0 and Stereo mask = 11. (c) and (d), show different settings for texture validation parameter for the disparity images and have the same settings for surface size =200, surface validation=1 and Stereo mask = 13. . . . .	74
3.7	Present the effects of different settings of the stereo and edge mask parameters on the accuracy of the disparity maps. . . . .	76
3.8	The effects of different settings of the stereo and edge mask parameters on the accuracy of the disparity maps. As the value of stereo mask increased the gaps’ areas decreased. . . . .	79

4.1	Sample of cotton and hibiscus plants. (a), (b), (c) and (d) cotton plants in sunny positions. (e) and (f) cotton plants in shadow conditions. (g) and (h) Hibiscus plants in indoor (g) and outdoor (sunny) positions (h). . . . .	85
4.2	Leaf segmentation and counting algorithm. . . . .	87
4.3	Disparity map for the six selected cotton and hibiscus plants. (a), (b), (c) and (d) cotton plants in sunny condition. (e) and (f) Hibiscus plant in indoor and outdoor (sunny) conditions. . . . .	90
4.4	Filtered disparity map for the six selected cotton and hibiscus plants of Figure 4.1. . . . .	91
4.5	Colour image after depth mask for each of the R, G, and B colour channels for the six selected cotton and hibiscus plants of Figure 4.1. . . . .	92
4.6	HSV colour Transformation for Plant1 side 1 of Figure 4.5 . . . . .	94
4.7	Histogram distribution of the hue channel for the colour images of the six selected cotton and hibiscus plants in Figure 4.1. . . . .	96
4.8	Result from HSV colour space & applying the developed equations for the six selected cotton and hibiscus plants in Figure 4.1. . . . .	97
4.9	Binary image transformation for the six selected cotton and hibiscus plants in Figure 4.1 . . . . .	98
4.10	Median and size filter binary images for the six selected cotton and hibiscus plants in Figure 4.1 . . . . .	100

4.11	Labeled leaves with different colours for the six selected cotton and hibiscus plants in Figure 4.1 . . . . .	101
4.12	Ellipse fitted to each leaf (red outline) for the six selected cotton and hibiscus plants in Figure 4.1 . . . . .	104
4.13	Binary images after the application of ellipse criteria for the six selected cotton and hibiscus plants in Figure 4.1. The number of objects for the hibiscus plant was decreased due to ellipse-fitted criteria.	105
4.14	The equivalent disparity images after application of ellipse criteria for the six selected cotton and hibiscus plants in Figure 4.1 . . . . .	106
4.15	Plant leaves segmented in different colours after using ellipse criteria for the six selected cotton and hibiscus plants in Figure 4.1 . . . . .	107
4.16	Plant leaves overlaying colour images for the six selected cotton and hibiscus plants in Figure 4.1 . . . . .	108
4.17	Plant 3 side 2 colour segmentation showing connected areas 1 and 3 and overlapped area 2. . . . .	111
4.18	Connected leaves of area 1 for Plant 3. Colour image and disparity map (a) before separation; (b) after separation . . . . .	113
4.19	Plant 4 side 1 showing two connected areas 2 separated using the DMD technique . . . . .	114

4.20	Two overlapping leaves (area 2 of Plant 3) and their separation process using GDS technique. The top image shows the overlapping leaves. The disparity map declares the distinct difference between pixels. The lower images present the results after separation. . . . .	115
4.21	Cotton and hibiscus plants with connected areas which have been separated using the GDS technique. . . . .	118
4.22	A disparity map showing a big difference in neighbouring pixels while Equation 4.7 indicates a smooth increment in unique vector $U$ . . . .	120
4.23	Leaves segmented using (ENBD) technique, the red pixel presents the centre of the window, yellow pixels present the eight neighbouring pixels, the blue pixel presents the changed pixel after the application of this technique. . . . .	122
4.24	Leaves segmented using (ENBD) technique, the red pixel presents the centre of the window, yellow pixels present the eight neighbouring pixels, the blue pixel presents the changed pixel after applying this technique . . . . .	123
4.25	Two areas of plant 3 connected by small pixels and the disparity map of the same connected area. . . . .	124
4.26	Disparity map of area 3 connected leaves, (a) sequence of the ZNC technique, (b) disparity map after the separation of the two connected areas using the ZNC technique. . . . .	126

4.27 (a) Colour image of area 3, plant 3 after separation using ENBD and ZNC techniques, (b) Plant 2 final segmentation image after using DDS techniques. . . . .	128
4.28 Cotton and hibiscus plants with connected areas separated using ENBD and ZNC techniques. . . . .	129
4.29 Final leaf segmentations. Column 1 presents results after using the image pre-processing algorithm, column 2 shows result after using DDS. . . . .	132
4.30 Final leaf segmentations. Column 1 presents results after using image pre-processing algorithm, column 2 shows result after using DDS. . .	133
4.31 Two types of plane (a) A 3 points plane with a normal vector (b) Two parallel lines plane . . . . .	135
4.32 Plane extraction process for plant leaf . . . . .	137
4.33 The error in depth between the leaf plane and interpolated plane . .	139
4.34 Plant 1 side 1 in Figure 4.1 with 5 extracted plane and error analysis	140
5.1 Three selected plants from dataset 1 with different sun directions. .	153
5.2 Two selected plants from dataset 3 (small cotton) and dataset 5 (big cotton) with overexposed conditions. . . . .	154
5.3 Steps of segmentation for Plant 3 side 2 from dataset 5 (big cotton) with overexposed and partial shadow conditions. . . . .	155

5.4	Two selected plants from different data sets with low lighting conditions and high segmentation rates, (a) Plant 11 side 2 dataset 6 presents Case 1, (b) Plant 3 side 1 dataset 2 presents Case 2. . . . .	158
5.5	Two selected plants from different data sets with low lighting condition and low segmentation rates, (a) Plant 1 side 2 dataset 6 presents Case 1 (sunset), (b) Plant 1 side 1 dataset 2 presents Case 2 (images under shade). . . . .	159
5.6	Four selected plants with different dominant leaf orientations. Column one, colour image. Column two, result image. . . . .	162
5.7	Plants with different leaf sizes (a) Small leaves; (c) Big cotton with 3 large and bent leaves showing two parts disparity for each leaf; and (e) Big cotton with 3 large and bent leaves showing one part disparity for each leaf. . . . .	165
5.8	Two selected plants with overlapping leaves in flat pose and their segmentation results: (a) unseparated leaves; (b) separated leaves. .	168
6.1	Hibiscus nursery plant (a) Sobel edge detection filter; and (b) Canny edge detection filter. . . . .	175
6.2	Hibiscus nursery plant (a) RGB image, (b), (c) and (d) illustrate output of Frangi vesselness filter with standard deviation $\sigma_s = 0.55$ , 2.55 and 4.55 respectively. . . . .	178
6.3	Different values of area opening operation $x_c$ for the image of Figure 6.2b, (a) $x_c=10$ , (b) $x_c=30$ , (c) $x_c=50$ , and (d) $x_c=70$ respectively.	180



6.4	Typical steps of the branch segmented algorithm: (a) RGB image; (b) vesselness measure output; (c) area opening operation $x_c=50$ ; (d) Hough transform multiple lines output; (e) single line for each branch; (f) assigning different colour for each line; and (g) overlapping those lines with the RGB image. . . . .	181
6.5	Hough transform Accumulator output for the images in Figure 6.6a and 6.6b. The groups are numbered as branch numbers for the image in Figure 6.6a. . . . .	182
6.6	Image of hibiscus nursery plant from different aspects (Column one); the results after stem and branch segmentation algorithm is applied (Column two). The images were taken under indoor conditions, (a), (b), (e) and (f) with artificial light, (c), and (b) with diffuse sunlight	185
6.7	Hibiscus nursery plant, (a), (c) and (e) RGB image; (b), (d) and (e) stem and branch detection results. . . . .	188
6.8	The result of stem detection for 4 big pot cotton plants (350 mm diameter) in sunny conditions . . . . .	190
6.9	Plant part reconstruction of two images of a hibiscus plant to generate a 2.5D model . . . . .	192

# List of Tables

3.1	Stereo and Validation parameter ranges for the Bumblebee2 camera.	69
3.2	The effect of changing the stereo and validation parameters on the disparity maps with their representative figures. . . . .	78
4.1	Final leaf segmentation results for the 8 selected cotton and hibiscus plants in Figures 4.29 and 4.30. . . . .	131
5.1	Cotton plants data set collection. The images were collected during Winter and early Spring of 2014. . . . .	145
5.2	Total segmentation rates of developed algorithm for cotton and hibiscus plants under all conditions. . . . .	148
5.3	Average segmentation rates for cotton plants under different illumination conditions where, A = Accuracy, S = Sensitivity and P = Precision. . . . .	149
5.4	All data sets segmentation results according to leaf orientation. . .	161

---

5.5	Separation rate of DDS algorithm for occluded and overlapping leaves for cotton and hibiscus plants in all conditions. . . . .	166
6.1	Stem and branch segmentation results for 12 hibiscus plant images under indoor conditions. . . . .	186
6.2	Final average of accuracy, sensitivity and precision for the hibiscus plant in indoor and outdoor conditions. . . . .	187

# Notation

$A$	Intrinsic parameters for pinhole camera model
$a, b, c, d$	Plane equation parameters
$b$	Base line of stereo vision camera
$C_l, C_r$	Lenses' centers of the left and right cameras
$D$	Matrix determinant
$Dif_{Img}$	Difference image
$d_l$	Left deviation
$d_r$	Right deviation
$d_s$	Disparity between the left and right camera
$f$	Camera focal length
$f_x, f_y$	Focal length parameters of the intrinsic matrix
$H$	Hessian matrix
$I$	Pixel's intensity value
$I_L, I_R$	Pixel intensity functions of the right and left images
$i$	Image dimension in $x$ axis
$j$	Image dimension in $y$ axis
$Leaf_{Img}$	Leaf image
$LH$	Lower threshold value of hue space
$m$	Column size of the image
$n$	Row size of the image

---

$n_v$	Normal vector
$p_1, p_2, p_3, r_0$	Any points in the plane
$P$	A point in the 3D world coordinate of a binocular stereo model
$P_l, P_r$	Projection points of $P$ in the left and right image planes
$Plane_{Img}$	Plane image
$p_o$	A point in the 3D world coordinate of the pinhole camera model
$p_i$	Projection of $p_o$ in the image plane
$R$	Rotation matrix
$R_l, R_r$	Rotation matrices of the left and right cameras
$R_s$	Rotation matrix of the stereo camera
$t$	Translation vector
$T_l, T_r$	Translation vector of the left and right images
$T_s$	Translation vector of the stereo camera
$s$	Second order structure
$s_c$	Skew coefficient
$W$	Matching block (window) between the left and right images
$x_c$	Threshold value of connected component algorithm
$x_0, y_0$	The optical center in the image plane
$x, y, z$	Camera coordinates axes
$X, Y, Z$	Global coordinates axes
$Th_1, Th_2$	Threshold weighting parameters for ellipse criteria
$U$	Unique vector
$UH$	Upper threshold value of hue space
$Z_{leaf}$	Depth value for the leaf
$Z_{plane}$	Depth value for the interpolated plane
$\beta$ and $c$	Threshold values of smoothing filter
$\kappa_1, \kappa_2$ and $\tau$	Threshold weighting parameters' of hue space

---

$\lambda_1$ and $\lambda_2$	Eigenvalues of the Hessian matrix
$\mu$	Mean value of pixels in hue space
$\rho, \theta$	Hough transform parameters
$\sigma_h$	Standard deviation of hue space
$\sigma_s$	Standard deviation of the smoothing filter
$\mathfrak{R}_\beta$	Blobness measure
$\nu_o$	Vesselness measure

# Acronyms & Abbreviations

2D	Two Dimensional
3D	Three Dimensional
ACM	Active Contour Model
API	Application Programming Interface
ASM	Active Shape Model
CCD	Charge Coupled Device
CSS	Curvature Scale Space
CLAHE	Contrast Limited Adaptive Histogram Equalization
DDS	Depth Discontinuity Segmentation algorithm
DMD	Disparity Map Denoising
ENBD	Eight Neighbours difference
EM	Edge Mask
ExG	Excess Green criterion
ExR	Excess Red criterion
EXGR	Excess Green minus Excess Red criterion
FN	False Negative
FP	False Positive
FPS	Frames Per Second
GDS	Global Discontinuity Segmentation technique
GPS	Global Positioning System

---

HSV	Hue, Saturation, Value
HSI	Hue, Saturation, Intensity
IR	Infrared Radiation
LAI	Leaf Area Index
LAD	Leaf Area Density
LH	Lower Hue threshold
LRF	Laser Range Finder
MLP	Multilayer Perception Classifier
NN	Neural Network
NCC	Normalized Cross Correlation
QFF	Queensland Farm Federation
RGB	Red, Green, Blue
RMS	Root Mean Square Error
RMS2	Second Root Mean Square Error (Step 3, Listing 4.7, Section 4.6.3)
ROI	Region of Interest
SAD	Sum of Absolute Difference algorithm
SDK	Software Development Kit
SM	Stereo Mask
SSD	Sum of Squared Difference algorithm
SVM	Support Vector Machine
TP	True Positive
TOF	Time of Flight Camera
UH	Upper Hue threshold
ZNC	Zero Neighbours Counting



# Chapter 1

## Introduction

### 1.1 Motivation

Agriculture is one of the main resources that supplies humans with fundamental life requirements, whilst at the same time supporting the economic growth of most countries. Typically, conventional agricultural work is carried out manually by farmers and skilled workers. Advancements in technology seek to convert manual and intensive agricultural tasks into automated tasks, relying on mobile robots and machine vision. These autonomous vehicles provide continuous monitoring of the agricultural environment, autonomously acquiring the information and performing the associated tasks (Cheein and Carelli, 2013; Zecha et al., 2013). To accomplish these tasks, these autonomous vehicles require a sufficient number of intelligence sensors to accurately monitor plants and provide relevant data accordingly. This information is then analysed and used in crop management strategies which aim to reduce input resources (water, fertiliser), reduce the chemical stress on humans, and improve farm management efficiencies (Zhang et al., 2002).

Plants usually display a variety of visual parameters which reflect their condition, stress, and survival requirements. Monitoring plant parameters such as vegetative growth, plant height and volume using human vision alone is labour intensive for farmers and agronomists and prone to human weaknesses due to variable eyesight and the results are skewed by lighting, weather conditions and other external factors. Machine vision systems attempt to replicate human vision systems by using visual sensors and image analysis techniques. These intelligence systems can potentially automate the visual assessment of plant conditions in order to provide the required sensing information for many field practices (McCarthy, 2009).

A variety of plant image segmentation issues were solved using 2D image features such as colour, shape, and texture. These features are widely used; however they may vary depending on growth stage, season and image acquisition (Yanikoglu et al., 2014), or they are difficult to detect or identify under different ambient conditions, or for complex plant canopies (Xia et al., 2013). The geometrical analysis of 2D image features is a commonly applied approach for plant parameter estimation. The accuracy of plants' parameter estimation can be affected by image position, overlapping canopy, and the similarities between canopy architectures (Lati et al., 2013).

To overcome these problems that affected the estimation of plant parameters, 3D imaging sensors were introduced for their ability to add another feature specifically depth, to the other already known features such as colour, shape and texture. Recently stereo vision techniques have been widely and successfully used for fruit harvesting in robot applications, and therefore, they are also expected to be equally beneficial for plant segmentation and identification. With the rapid advance in computational power, 3D modelling using stereo vision becomes an attractive alternative to providing adequate details about plant canopies. The reconstruction of

plant canopies in 3D models offers great prospects, where the information on plant canopies with accurate parameters estimation can be acquired (Lati et al., 2013).

Plant identification is a major concern for the vision-based guiding system in precision agriculture applications. Most of the research concentrates on plant identification using a leaf as the main feature with a controlled background. The detection of multiple plant leaves under natural conditions (which may contain interference and overlapping leaves for non-simple plant structure), is a crucial and challenging task for vision-guided agriculture robots (Xia et al., 2013).

Depth information has been widely and successfully used for plant feature identification in indoor (laboratory conditions), (Andersen et al., 2005), or greenhouse applications (Xia et al., 2015). The promising results of plant identification obtained from these indoor and greenhouse applications using depth information, indicate that the field of outdoor study has potential for more challenges and further investigation. The greenhouse environment could present the same effects of outdoor lighting conditions but still there is an advantage over outdoor experimentation as outdoor images can be affected by wind. The wind can cause the plant to oscillate which can result in blurred and poor quality of images. This will affect plant segmentation and identification processes.

The above challenges provide the motivation to develop an image analysis system using a stereo vision sensor which can be used on a robot platform, to identify important plant features and perform automatic monitoring of plant parameters. The proposed system will be capable of segmenting and counting plants' important features (leaves, stem and branches), which can assist plant growth and crop management, therefore it is relevant to review some aspects of that technology. One of these aspects is a mobile robot platform. The recent developments in that field

include some of the commercially available robots used in certain agricultural applications. The following sections illustrate the importance and benefits of using autonomous technology in agricultural applications, and some potential applications for mobile robot platforms and machine vision which could be compatible for this research study.

## 1.2 Mobile robot platform in agriculture

Automatic crop monitoring could be enhanced with a mobile robot platform that can continuously inspect the crop. It is hard to adapt a robot for different agricultural tasks in an outdoor environment and this is mainly due to the agricultural environment being less structured than an indoor manufacturing environment (Armada et al., 2005). The earliest attempts to develop driverless vehicles in agriculture began seriously in the 1960s (Fountas et al., 2007). Machine vision based guidance system technology was introduced in the 1980s, by the potential to combine computers with image sensors (Yaghoubi et al., 2013). Since then, the autonomous agricultural robot has experienced promising developments which open the field for potential autonomous agricultural operations. These robots have been involved in both indoor (greenhouse) and outdoor agricultural applications. Agricultural robots have the ability to implement potentially high-risk and repetitive agricultural functions previously undertaken by one or more people. Examples include crop monitoring and picking in physically awkward circumstances, high speed harvesting and pesticide spraying.

Fruit and vegetable harvesting is both time consuming and tiring work and most researchers have devoted their work to this research area (Billingsley et al., 2006). The results of this research show the use of autonomous vehicles in harvesting

applications can reduce labor costs, enhance operational safety and application accuracy, and increase productivity (Plebe and Grasso, 2001; Yang et al., 2007; Yuan et al., 2010; Si et al., 2015). Furthermore, the autonomous vehicles can provide continuous monitoring of the agricultural environments and supply the farmer with up-to-date and precise information to assist with infield management decisions (Zecha et al., 2013). For example, two types of robotics have been recently developed and launched for the first trial; SwagBot and Ladybird. A SwagBot2 robot was introduced and used for herding and monitoring cattle on a farm (Jukan et al., 2017). This research can be adopted and applied in autonomous farm activities including plant monitoring. The intended adopters of the autonomous farm activities are farmers, where the autonomous sensing is expected to be integrated with existing on-farm operations. The Ladybird robot is a lightweight multi-directional electric vehicle which has been developed to monitor and harvest vegetables (low height crop) in a broad field. This type of robot is equipped with intelligent software which enables it to conduct autonomous farm sensing and manipulation tasks such as mapping, detection, classification, weeding, and harvesting for various vegetable crops (Funnell, 2015). The proposed outcomes intended to be develop in this study could become a potential application for the new agricultural robots which have been recently developed.

### **1.3 Machine vision in agriculture**

A machine vision system becomes an essential tool in precision agriculture applications. Machine vision utilises image analysis to extract useful information for different applications, such as fruit detection and recognition for automatic picking and harvesting machines, which saves labour costs and increases productivity (Plebe

and Grasso, 2001; Van Henten et al., 2002; Zhao et al., 2005; Yang et al., 2007; Wachs et al., 2010; Bulanon et al., 2010; Hayashi et al., 2010; Ji et al., 2012; Bakhshipour et al., 2012; Si et al., 2015; Wang et al., 2016). Precision agriculture intends to monitor plants' characteristics using non-destructive inspection methods for determining product properties. The rapid advancement in sensor technology, data acquisition systems and computer analysis theories have provided important developments in the field of autonomous operations in agriculture. Machine vision uses perception sensors to detect potential plant features and provides continuous monitoring of agricultural environments. Machine vision accords the opportunity to analyse information both within or outside the visible electromagnetic spectrum such as ultraviolet or infrared regions, which the human eye cannot recognise (Cubero et al., 2011).

A machine vision system can be useful also for yield estimation operation. Yield estimation at an early plant growth stage has multiple potential benefits for growers such as, adjusting specific management to increase yield, planning for the harvest method, predicting future market price and crop-load estimation (Okamoto and Lee, 2009; Kurtulmus et al., 2011; Linker et al., 2012; Zhou et al., 2012; Wang et al., 2012; Payne et al., 2013; Gongal et al., 2016). With this in mind, autonomous vehicles have become an important research tool in modern agriculture. For example, an automated image-based detection system for precision weed spot spraying is also a potential technology for preserving crops, minimising weed effects and reducing herbicide usage (Rees et al., 2009). In addition, an autonomous vision guidance of farm vehicles for crop row detection has multiple benefits for farmers such as saving labour costs and time, and enhancing operational safety and efficiency using video camera images (Billingsley and Schoenfisch, 1997), monocular vision (English et al., 2014), or using stereo vision techniques (Rovira-Más et al., 2004; Kise et al., 2005).

Furthermore, machine vision can perform an important role in plant part recognition and identification. Plant identification is a major challenge in the field for a vision based guidance system due to the multiple number of features which need to be identified and due to the complexity of the background (Nesaratnam and BalaMugan, 2015). Analysing leaf and flower images has provided benefits for agronomy and biology for plant species identification (Valliammal and Geethalakshmi, 2011) and also for leaf classification and recognition (Kadir et al., 2013; Wu et al., 2007; Hu et al., 2012). The autonomous inspection and 3D measurement of plant canopies using stereo vision can provide detailed information about plant health, disease propagation path way and autonomous spray treatments (Xia et al., 2009; Li et al., 2009) and drought stress by measuring the leaf inclination angle (Biskup et al., 2007).

In this study, an image segmentation algorithm using a stereo vision sensor has been developed to segment important plant features (leaf, stem) for the purpose of monitoring plant growth, disease inspection and early indication of plant stress. Monitoring plant growth using stereo vision technology has the potential to increase plant productivity in farms and to support the continuous growth of the global population.

## 1.4 Plant monitoring systems

Plant monitoring is an essential task to investigate the growth of the crop and react accordingly if some factor such as water shortage and nutrient stress, plant illness or insect attack is detected. The automated monitoring of plants is a promising process and should be capable of providing accurate and sufficient information about growth development to reflect the true physiological state of plants (Kacira and Ling, 2001). This task can be performed by monitoring and analysing a va-

riety of plant features. The existing technology in this field offers some typical types of measurement sensors which include destructive (contact with the plant) and non-destructive techniques. Some of destructive approaches can be very time consuming and poorly representative of plant canopies. For the sake of convenience and time efficiency, non-destructive methods have been developed and become more prominent in recent times (Meyer and Davison, 1987; Zhao et al., 2012).

The literature reports many approaches to recording plant status measurements using different indicators. For example, plant water status can be measured and estimated by leaf water potential (Huck and Klepper, 1977). This index can be indirectly measured via some plant properties such as leaf thickness change, leaf temperature and growth rate (Lu and Neumann, 1999). The manual observation for leaf angle is another indirect measurement for visible leaf wilting which can reflect plant water stress (Meyer and Walker, 1981; Ehleringer and Hammond, 1987). The development of an image analysis system that can replace some of those measurement tools may be a promising advancement for this field. For example, leaf angle is a good indicator of visible leaf drought stress and wilting which could be measured by the change in the zenith leaflet angle distribution (Biskup et al., 2007).

The estimation of crop canopy properties and measurement such as plant height, width, volume, and growth stage, can provide an applicable tool for crop management decisions (precise fertilizer, pesticide application), according to the crop yield prediction. The structure of the canopy can be characterised by size, shape position and orientation of vegetative elements (Ross, 2012; Weiss et al., 2004). It is not easy to define a canopy structure due to the large amount of information required. Therefore, a canopy structure can be described with only a few variables such as leaf inclination distribution function and leaf area density (Weiss et al., 2004). The Leaf Area Density (LAD) is the portion of one-sided leaf area within a reference



volume, which is defined as a key index for characterising the vertical and horizontal plant canopy structure (Oshio et al., 2015).

Another approach used to estimate foliage density is Leaf Area Index (LAI). The concept of LAI was introduced for the first time by Watson (1947) to describe the relationship of plant growth capabilities and light interception. LAI corresponds to the one-side leaf area per unit ground surface area. LAI can be calculated by integrating the leaf area density over the canopy height (Weiss et al., 2004). The literature reports numerous approaches developed for quantifying LAI including destructive and non-destructive methods (Bréda, 2003; Jonckheere et al., 2004). Due to the considerations of cost, efficiency and convenience, the estimation of LAI using a digital camera has been widely adopted in recent years (Sakamoto et al., 2012). The importance of measuring LAD and LAI is to estimate plant vegetative growth and to measure the relation to interception of light for maximum growth respectively (Weiss et al., 2004; Wolf et al., 1972).

It has been demonstrated that stereo vision technology can offer great prospects to implement an image-based 3D reconstruction model of a plant canopy and an estimation of its growth parameters (Andersen et al., 2005; Lati et al., 2013). The 3D reconstruction model may offer the required information regarding measurement of plant canopies thereby indicating more accurate height, width, leaf area and mass volume measurement (He et al., 2003). In this context, the development of image processing algorithms that can segment and count the leaves of a plant canopy using stereo vision techniques could be useful for estimating LAD or calculating LAI.

---

## 1.5 Research scope

This study will focus on segmentation of important plant features such as leaves, stem and branches, using colour and depth properties. The specific focus of the study is the detection of multiple leaves for non-simple plant canopy in a semi-structured outdoor environment under a variety of sunlight conditions (sunny, shady and cloudy). To implement this task, the depth data from stereo vision sensors, combined with colour information, will be used to develop an image processing algorithm to segment plant images and to solve problems presented by overlapping leaves.

The term semi-structured was employed for the experiment conditions because, images of single plants in pots at outdoor conditions were captured without the complexities of other plants from the same type in the foreground and background. In addition, the images were taken from different directions and angles which might be unobtainable in real field conditions. In contrast, the indoor plants have a more structured environment and there is a greater ability to modify this environment to suit imaging requirements to be more controllable compared with the outdoor environment and real field conditions.

The experiments carried out for this study involve two types of plant (with different structures), namely cotton (*Gossypium hirsutum* L.) and hibiscus (*Hibiscus rosa-sinensis* L.) (Figure 1.1). Hibiscus plants have clearly separated stems, branches, and leaves with adequate space between them. There is no heavy overlapping between stem, branches, and leaves. As such, hibiscus plants have been chosen at the commencement of this study to develop leaf, stem and branches segmentation algorithms. The cotton plant was chosen because it is a major crop in Australia, grown mainly for its fibre and seed oil and planted extensively in Queensland and



(a) Cotton plant



(b) Hibiscus plant

Figure 1.1: Cotton and Hibiscus plants.

New South Wales. According to Queensland Farmers' Federation (QFF, 2012), the cotton industry adds more than \$2.5 billion in value to the Australian economy annually. The growing of cotton consumes large amounts of water, so monitoring cotton plant features in order to indicate plant growth stages can improve water use and efficiency. Therefore, this research focus is more on cotton than hibiscus to develop the leaf segmentation algorithm regarding to the importance of cotton crop. Compared with other major field crops, cotton has perhaps the most complex growth habit, due to its indeterminate growth (Oosterhuis, 2001). This is because the fruiting-to-vegetative growth balance is critical in cotton due to the continuing vegetative growth even after fruiting is initiated. This balance can be affected by crop management (water, fertiliser) and environment (Oosterhuis, 2001). As such,

more than one parameter is used to monitor cotton growth such as; vegetative growth, stem internode length and fruit abscission. The continuous monitoring of plant features, stress and requirements can detect any imbalance between fruiting and vegetative growth which can, in turn, improve management decisions. In that sense, monitoring these parameters using image analysis could be more complicated compared to other plants which have fewer parameters that indicate their growth. Presently, there are no similar reported studies for cotton and it is expected that this study may be applicable to other plants displaying a similar structure.

## 1.6 Research questions

1. *Which important plant features (leaves, stem and branches) can be segmented accurately using vision sensors, to help inform plant characteristics of various growth stages to enhance crop management practices?*
2. *How does the combination of image features such as colour and depth, assist plant image segmentation under varying outdoor lighting conditions, and how do depth gradient properties enhance plant segmentation and which plant part can benefit more from depth segmentation?*
3. *How do the outdoor varied illumination conditions such as sunny, shady and cloudy affect the performance of plant segmentation techniques and can stereo vision aid segmentation in these conditions?*

---

## 1.7 Research aim and objectives

The aim of this research is to develop an image analysis system using colour and depth information captured by a stereo vision camera to recognise the important features of cotton plants (leaves, stems). This system must be capable of segmenting and counting multiple plants' leaves and performing the separation between overlapped leaves using colour and depth properties. The system must also be able to reconstruct the segmented plant parts for the purpose of generating a structural plant model appropriate to various growth stages at different outdoor conditions, to enhance precision of agricultural operations. The structural plant model can be used to monitor plant characteristics for various growth stages at different outdoor conditions, to enhance precision of agricultural operation.

The specific objectives of this study are:

1. Develop an image analysis algorithm which can detect and count multiple plant leaves from the collected images, using image preprocessing techniques with the aid of depth and colour information.
2. Develop an image analysis method capable of separating between overlapping leaves of plant canopies using depth gradient properties.
3. Evaluate the performance of the developed algorithms for leaf segmentation and overlapping separation, mainly using cotton plants images (at different growth stages) and some images of hibiscus plants at a semi-structured outdoor environments under varying light conditions.
4. Develop an image analysis algorithm which can segment and count plant stems and branches.

5. Demonstrate how the developed algorithms can be used to reconstruct segmented plant parts for the purpose of generating a structural plant model and localising leaves and stem in the  $x, y, z$ , coordinates.

In this study, a stereo vision camera is used as the primary sensor to produce colour and depth information. Stereo vision cameras use reliable sensors which work in an outdoor environment under a variety of illumination conditions to produce high resolution depth and colour information (Gai et al., 2016).

## 1.8 Original research contribution

The principal contributions of this research are as follows:

1. Collection of a detailed data set of cotton plant images at different growth stages under semi-structured outdoor environment and varying light conditions. These data sets have been used for the development of the image analysis algorithm for this research study. These data sets can be added to the plant images data sets and could be beneficial for other research studies.
2. Development of an image analysis algorithm that can segment a plant canopy from non-simple background, under semi-structured outdoor environments and varying sunlight conditions (sunny, cloudy and shady).
3. Development of a new technique which can differentiate between overlapping leaves' boundaries, depending on the depth gradient of the disparity map data. This technique can calculate the discontinuity in depth values in a global manner and separate the overlapping items accordingly. This technique can work faster than edge detection techniques which need to calculate the gradient for each pixel in the image and follows another step for leaves' separation.

4. The proposed algorithm depends on the stereo vision sensor images without adding any artificial tags on the leaves. A calibration process is required only once for initial parameter settings. Afterwards, the developed algorithm works adaptively for all data sets under different outdoor conditions.
5. A comprehensive evaluation of the algorithm's performance on cotton plant datasets under a variety of outdoor lighting conditions reveals both the advantages and limitations of the algorithm.
6. Development of an additional algorithm which segments, classifies and counts stems and branches of plants automatically using a vesselness measure technique under direct sunlight.
7. The separation of overlapped (occluded) leaves using depth discontinuity properties under direct sunlight conditions has not yet been reported in the literature.

---

## 1.9 Thesis outline

This dissertation is organised as follows:

**Chapter 2** contains the literature review of the related research published in the same area of this study and discusses the critical art studies. Plant feature extraction using 2D and 3D image sensors, leaf and stem detection and multiple leaves segmentation and occlusion separation are the key elements of the related work for this study.

**Chapter 3** describes the fundamental idea and the essential processes of stereo vision techniques including camera calibration and rectification, triangulation and stereo corresponding process. The chapter also explains the characteristics, properties and limitations of the depth sensor used in this study. A focus on the evaluation of the disparity map in producing an adequate depth information for the plant parts is also presented in this chapter, and a wide range of disparity map parameters was tested and evaluated for optimal combination.

**Chapter 4** illustrates the development process of the proposed leaf segmentation and counting algorithm. The chapter describes in detail the main steps of the developed pre-processing segmentation using colour, depth and shape properties. In addition the chapter presents the development of other segmentation techniques to solve problems presented by overlapping leaves based on gradient discontinuity. A method that extracts a plane from leaf vertices using x, y, z coordinates of depth image is also presented in this chapter.

**Chapter 5** presents the evaluation of the performance of the leaf segmentation and counting algorithm under different outdoor illumination conditions. The images' main issues are presented which significantly affected the performance of the



developed algorithm. The chapter also presents the overall results of the algorithm in segmenting two types of plant leaves which revealed the algorithm's capability and limitations.

**Chapter 6** deals with the automatic branch segmentation algorithm. The chapter presents the experimental tests used to verify the performance of the developed algorithm. The algorithm performance was evaluated for hibiscus in indoor and outdoor conditions and for cotton plants at different outdoor illumination conditions.

**Chapter 7** demonstrates the overall conclusions of this study with respect to the accomplishment of the research objectives. Suggestions for the potential applications of this research and future work recommendations are also presented in this chapter.

# Chapter 2

## Literature review

There are several factors that could inform the design of machine vision systems to detect important plant features, including leaves, stems and fruit. This task can be achieved using a range of sensors to acquire information from the environment and to detect potential features such as colour, shape, texture and depth. Monocular (2D) vision sensors are normally used to segment non-green fruit from other plant parts and an unwanted background. Green fruit and plant leaves need spatial sensors that will work with properties other than colour and shape.

There is a multitude of literature studies concerning green fruit detection in a green leaf environment (Lee, 2006; Kane and Lee, 2007; Okamoto and Lee, 2009) which use spectral and 2D shape properties. Spectral analysis is usually used to segment green fruit from trees which have different spectral characteristics from leaves or to segment small weed seedlings from a soil background (Franz, 1989; Franz et al., 1991*b*). The spectral analysis can be affected by many variables such as plant health, leaf age and illumination conditions therefore, spectral analysis cannot be the basis for individual leaf segmentation.

The intended application of this study is the segmentation of individual leaves from each other, where leaves have quite similar spectral characteristics and 3D shape properties. Recently, depth sensors have been used in autonomous agricultural applications to segment plant parts and give precise positioning data. Many literature studies exist which report important plant feature extraction in a glasshouse environment. The focus of this thesis is on colour and depth sensing to segment important plant features such as leaves and stems at semi-structured outdoor environments under varying sunlight conditions. This chapter reports an overview of the literature studies relevant to the field of this PhD research study. The main research topics are: image analysis for fruit and plant detection using 2D image features, depth sensing in indoor and outdoor conditions, image analysis for plant part detection (leaf, stem), and the detection of multiple leaves. Figure 2.1 shows the main research area related to this study. A brief conclusion and the research problem are also presented at the end of this chapter.

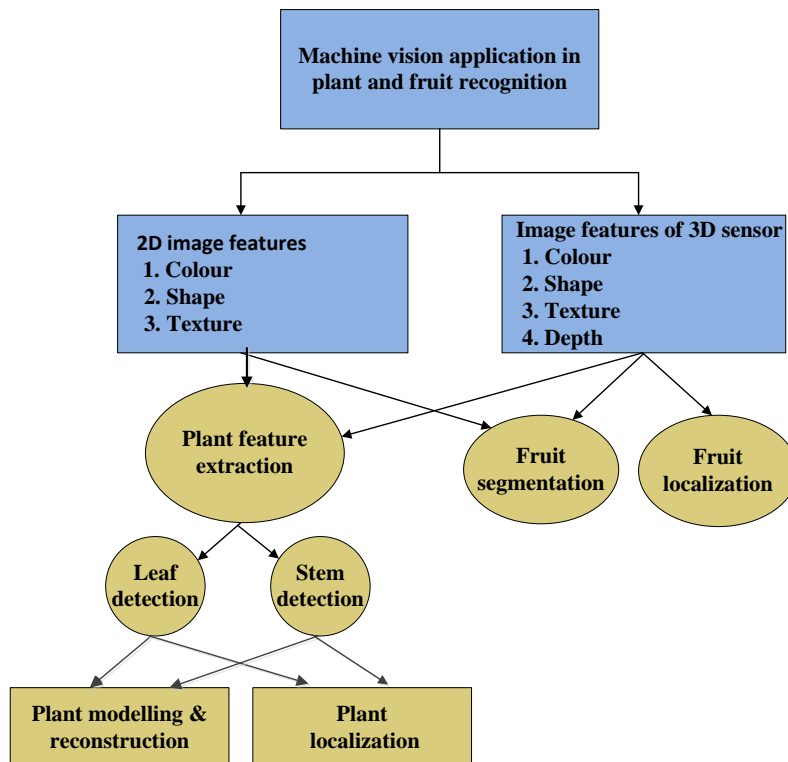


Figure 2.1: Main research areas related to this study

## 2.1 Image analysis using 2D image features

The use of image segmentation techniques depends on image sensors and on application requirements. Various methods of image segmentation techniques have been investigated to extract the important features of plant and fruit. Researchers have often combined two or more image segmentation methods to segment fruit and plant parts accurately. In general, segmentation techniques can be classified according to the 2D colour image sensors (monocular image) which depend on colour, texture, and shape attributes or 3D image sensors which can benefit from depth features.

### 2.1.1 Fruit detection

Colour image segmentation is a popular approach used to identify the region of interest according to its colour. It is widely used in fruit and plant detection for indoor (greenhouse) and outdoor applications. For example, the method based on colour subtraction (G-R) and (G-B) was used by Wang, Zhu and Ji (2008) to recognise cotton for an automatic cotton harvesting robot. Zhou et al. (2012) used other colour indices to detect and count red and green apples for early yield prediction. The red minus blue channel (R-B) was used for green apple detection, while the difference between red and green channel (R-G) was more effective to detect red apples. This method showed a potential yield prediction method; however, the method cannot discriminate between a single apple and a cluster of apples. The apple count depended on the number of pixels in the cluster.

The disadvantages of using the colour feature as a solo feature are: colour feature is influenced by the ambient light conditions, and it has limited capability to detect an individual fruit and to deal with complex surrounding plant structures. The

researchers tried to support colour by the use of other features such as shape (Wang et al., 2012; Si et al., 2015) and texture (Zhao et al., 2005; Linker et al., 2012) to overcome this problem.

Wang et al. (2012) presented an automated crop yield estimation method based on the integration between colour and shape features to segment red and green apples in an orchard. The red and green apples were segmented using hue, saturation and values in the Hue Saturation Value (HSV) colour space. Hue channel information is adaptive for discriminating objects of different colour (Lin et al., 2005). The hue values of the red apple pixels were distributed in two ranges from  $0^\circ$  to  $9^\circ$ , and from  $349^\circ$  to  $360^\circ$  while the hue values of green apples ranged from  $49^\circ$  to  $75^\circ$ . Apple pixels have stronger green than leaf pixels, therefore, a suitable threshold value for the saturation channel was used to differentiate the green apple pixels from the green leaves. The centres of green apples were removed and they could not be detected using saturation segmentation. This is because they have high brightness and low saturation due to the camera flash effect. For that reason, shape features combined with geometrical analysis were used to complete the shape of segmented apple and to detect individual apples in the image. This method performed well for both types of apple; however one limitation remained. The method was only performed at night using artificial light, therefore no results are reported under daylight illumination conditions.

Combining colour, shape and texture features can enhance apple segmentation and improve detection reliability. For example, Linker et al. (2012) proposed another method to discriminate between apples and other objects and to estimate the number of green apples in the plant images depending on colour, shape (contour and arc analysis) and texture (smoothness criteria) properties. Although the method showed high segmentation results when compared to other methods proposed for

instance by Wang et al. (2012) and Zhou et al. (2012), direct sunlight and colour saturation were the main problems with this detection method. The detection accuracy can be enhanced when plant images are captured under controlled lighting conditions (diffuse light).

Studies have been reported on fruit segmentation methods that use colour, edge, image threshold and morphological operational techniques to segment fruit from the tree and background (Plebe and Grasso, 2001; Chen and Yang, 2013; Xiang et al., 2014; Luo et al., 2016). The coverage of the fruits by the leaves is one of the most important problems in fruit detection, therefore these methods introduce another feature of depth, to localise the fruit position in the tree for fruit harvesting robot applications. More details about depth sensing and related segmentation techniques are explained in Section 2.2.

### **2.1.2 Plant detection**

The image processing techniques used to segment plant attributes depend on different factors such as: the scale of plant measurement which ranged from small seedling, plant parts (e.g. leaf, stem) to the dense canopy, the measurement environment (e.g. laboratory, greenhouse or field condition), and the applied application (e.g. yield prediction, plant monitoring and species identification). The segmentation process of plant images becomes more complicated due to the complexity of plant structure and the similarity in colour between the plant and the foliage background. With this in mind, the complexities of the outdoor agriculture environment, including a variety of ambient light conditions and the occlusion between plant parts and their neighbours, make plant image segmentation a challenging task. Machine vision technology offers the potential to identify plant features using

colour, shape and texture (Meyer et al., 1998-b; Tillett et al., 2001).

### 2.1.2.1 Colour feature

Colour can be an effective feature used to segment foliage from background soil for top view image of small seedling crop (Tian and Slaughter, 1998). It is also used to reduce the illumination effect on the scene of the plant image (Perez et al., 2000). Since RGB colour images contain information in red (R), green (G) and blue (B) channels, the image can be segmented according to these channels. Most of the plant image information is found in the green channel. Among several approaches developed for separating green from the image, Woebbecke et al. (1995) found that the modified hue ( $2G - R - B$ ) or *Excess Green* index ( $ExG$ ), was the most effective approach for separating plant from background soil. This is because ( $ExG$ ) produced near binary images and provided a clear contrast between plant parts and background soil (Hamuda et al., 2016).  $ExG$  index was widely used later to enhance plant parts segmentation (leaves, stem) and perform effective discrimination between green and unwanted background (Meyer et al., 1998-a; Lamm et al., 2002; McCarthy, 2009; Guijarro et al., 2011).

Another colour index called *Excess Red* ( $ExR$ ) or ( $1.3R - G$ ) was proposed by Meyer et al. (1998-a) to segment the leaf region from the background but it was not as accurate as ( $ExG$ ). Afterwards, Meyer et al. (2004) combined the two colour indices ( $ExG$ ) and ( $ExR$ ) to produce another effective colour index called ( $EXGR$ ) or ( $ExG - ExR$ ). This method applied the two colour indices simultaneously where ( $ExG$ ) index was used to separate plants region while the background residue was eliminated using ( $ExR$ ) criterion (Neto, Meyer and Jones, 2006; Tang et al., 2009). Meyer and Neto (2008) reported that ( $EXGR$ ) colour index demonstrated

superior segmentation results over the (*ExG*) for plant images taken under different environments (greenhouse or actual field) and various backgrounds (soil or plant residue).

### 2.1.2.2 Shape feature

The use of colour as a solo feature to segment plant image is seldom used when plant images are complicated and more than one image feature needs to be extracted to identify plants. The researcher combined other features such as edge, shape and geometrical analysis information to segment plant image. Shape is the most obvious feature used to discriminate between crop leaf and weed (Guyer et al., 1986; Perez et al., 2000). It is also the most heritable feature which is least affected by environmental conditions such as mean annual temperature and mean annual precipitation (Li et al., 2015). Furthermore, it possesses considerable information that describes the morphological characteristics of plant leaves. Franz et al. (1991a) identified plant species based on individual leaf shape using the Fourier-Mellin correlation method. Chi et al. (2003) fitted Bezier curves to different leaf boundaries to drive the geometric description of the leaf shape. Contour segmentation methods including the length histogram of contour segment and centroid-contour distance were used by Yahiaoui et al. (2006) and Wang et al. (2000) respectively to extract the shape feature of plant leaf for an image retrieval system. Other segmentation methods used Elliptic Fourier analysis which provides complete and accurate descriptions of leaf complex boundary (McLellan and Endler, 1998; Neto, Meyer, Jones and Samal, 2006; Lexer et al., 2009). The geometrical analysis including various simple leaf geometric features such as length, width, area, diameter, aspect ratio and convex area ratio were also used for leaf segmentation (Wu et al., 2007; Pauwels et al., 2009; Kadir et al., 2011a; Söderkvist, 2001; Kaur and Kaur, 2012; Lee and



Hong, 2013).

### 2.1.2.3 Texture feature

Leaf identification using both colour and shape features is still a challenging task due to the fact that leaves of the same plant may vary in terms of shape and colour, depending on plant condition, season and image acquisition (Yanikoglu et al., 2014). As such, adding a texture attribute may provide botanical information about leaf such as leaf pubescence, leaf venation, and also leaf disease or insect damage (Meyer, 2011). Texture feature is normally used to identify various species of grass or broadleaf which need to consider leaf venation, colours and additional canopy structure (Meyer et al., 1998-a). Textural analysis based on Gabor wavelets analysis has been widely suggested for segmenting weeds embedded in canopies and for classifying plant species (Strickland and Hahn, 1997; Tang et al., 2003; Lin et al., 2008). The combination between colour, shape and texture approach was tested by Zhang and Chaisattapagon (1995) for detecting weeds in wheat fields. The results show that the leaf surface coarseness indices determined by Fourier spectra may be effective in discriminating wheat from broadleaf weed species.

The plant leaf texture can be identified also by extracting leaf venation indices. Park et al. (2008) used Curvature Scale Space (CSS) corner detection algorithm for extracting leaf venation characteristics for the purpose of plant classification. Leaf venation features can also be extracted from grey images using morphological operations. Kadir et al. (2011b) used an opening morphological operation to identify vein feature beside colour index and Polar Fourier Transform analysis for foliage plant retrieval. The major problems for leaf texture analysis are leaf orientation or

rotation, image resolution, image illumination (e.g. shadow or background lighting), and the bidirectional reflectance of leaf surfaces (Meyer, 2011) which can result in incorrect classification of plant species. Texture and shape analysis are more effective for horizontal orientation of leaf images taken with balance defusing light conditions.

The 2D image features such as colour, shape, and texture in combination perform a variety of image segmentations. The combination of 2D image features are the most relevant attributes for simple plant identification applications. Adding another image feature or depth has become a promising attribute for identifying complex plant structures.

## **2.2 Image analysis using depth sensing**

Depth is another feature which can be used to enhance the recognition and localisation of plant and fruit parts. The selection of a depth sensor depends on the application task (e.g. fruit picking or plant sensing) and application environment (e.g. in the field, a greenhouse or indoor laboratory applications). Studies in the literature report that a binocular stereo vision system is considered an effective method of depth sensing for outdoor agricultural applications, since it is robust enough to deal with the various ambient illumination conditions (Kazmi et al., 2014). The system involves using two cameras from different views in parallel or alternatively positioned at specified angles, thus the distance between the object and the camera can be calculated.

Other depth sensors such as Microsoft Kinect (Corporation, Redmond, WA USA) and time-of-flight (TOF) cameras can produce accurate depth information pertaining to plant parts. Microsoft Kinect and TOF cameras are active (emitter) sensors

which rely on infrared radiation (IR). These sensors could work in outdoor conditions with some constraints. For example, the Microsoft Kinect sensors can work at night or under a hood shaded from direct sunlight (Nakarmi and Tang, 2012). They are unreliable to produce high quality results under sunlight due to the interference of the infrared spectrum of the sun (Popovic et al., 2017). Some types of TOF cameras can work outdoors in sunlight but they have lower resolution. The estimation of depth is dependent on the traveling time of light that is reflected by the detected leaves however, some light is partially absorbed or transmitted by the leaf surface. Ideally, higher reflectance results in better estimation of depth, yet the sensor could be saturated due to strong reflections which can affect sensor efficiency (Kazmi et al., 2014)

The working limitation of these sensors results in a real challenge when using depth sensing for plant feature extractions under a variety of sunlight conditions. This section reports on the literature which uses depth sensing in fruit and plant detection under outdoor or controlled environmental conditions.

### **2.2.1 Depth sensing in the outdoor field condition**

Depth sensing using a stereo vision technique has been applied in a variety of agricultural applications and tasks. Automated guidance has become an important ingredient of modern agriculture. A stereo vision system has been used to develop navigation algorithms for an automated guidance tractor following crop rows in the field (Rovira-Más et al., 2004; Kise et al., 2005; Hanawa et al., 2012). These studies have used stereo disparity information to determine the position of the crop rows, and to find the central path for the tractor with a target point. Using a stereo vision sensor in an automated guidance system has limitations because the maxi-

imum depth and precision measured by the stereo vision system is limited by the baseline between the cameras. As depth increases, the quality of the distance values decreases rapidly (Weiss and Biber, 2011). To overcome this problem, Rovira-Más et al. (2008) combined the information captured by a stereo camera, a localisation sensor (GPS) and an inertial measurement unit to create 3D terrain maps of agricultural fields. Adding another localisation sensor and an inertial measurement unit was important to enhance the performance of the stereo vision system to create a 3D terrain map.

The literature reports some studies deals with the structural measurement of plants that have been done at outdoor conditions using stereo vision. For example, (Ivanov et al., 1995) find the structural parameters of maize plants such as leaf position, leaf area distribution and leaf orientation for reconstructing a 3D model of plant canopy. The method used top down stereo images and performing destructive analysis of the plant to view the inner leaves, however the properties of the 3D model were not promising. Biskup et al. (2007) introduce a method for measuring leaf angle for soyabean plant under field conditions. The method can track leaf diurnal and nocturnal movements and measuring leaf inclination angle by fitting a plane to the reconstructed 3D leaf surface.

In recent decades, some studies have been performed with fruit harvesting robots using stereo vision techniques, for example: Orange (Plebe and Grasso, 2001); tomato (Yang et al., 2007; Xiang et al., 2014); apple (Si et al., 2015) and grape (Luo et al., 2016). These studies integrated depth with other features such as colour, edge and shape to identify and segment fruit from other parts of the tree. The fruit location in 3D coordinates was measured by using stereo matching techniques. The image segmentation was performed using a variety of colour transformations such as: Hue-Saturation-Value (HSV) color space projection and classification to

segment orange (Plebe and Grasso, 2001); colour difference ( $R - G$ ) and colour difference ratio  $(R - G)/(G - B)$  to recognise Fuji apple (Si et al., 2015); and YCbCr, HSV, HSI,  $L^*a^*b$  components as an effective indicator of grape colour (Luo et al., 2016). Image post-processing techniques were used to eliminate noise and to prepare images for the feature extraction stage including: image thresholding; morphological operation (image dilation, opening and closing operations); labelling image regions according to the area to remove small noise; and filled image holes.

A tree normally includes objects such as leaves and branches which obscure fruits in most situations. In addition, overlapping between fruit is a difficult problem in the research field of machine vision. Therefore, more than one image analysis method is required to segment the important feature of individual fruit for harvesting applications. For spherical fruits, shape detection algorithms and geometrical analysis have normally been used to extract the circular feature. For example, the circular shape feature of an apple was extracted from the fruit contour image using the random ring method (Si et al., 2015). Edge curvature analysis and geometrical analysis of radius measurements were used by Plebe and Grasso (2001) and Xiang et al. (2014) to extract the circular features from orange and tomato images. In addition, Plebe and Grasso (2001) used a circular fitting method to recognise the overlapping citruses. Similarly, the geometric information of the grape clusters and other image features such as edge detection (Canny, 1986) and a Hough line detection (Matas et al., 2000) was applied by Luo et al. (2016) to determine the contour boundary, the centre, and the cutting points of grape berries respectively.

Then, stereo matching process was applied to recognise the 3D positions of the individual fruit (Si et al., 2015; Plebe and Grasso, 2001) and to extract the 3D coordinates of the cutting point on the peduncle and the centre of grape berries (Luo et al., 2016). The results of these proposed methods show that a stereo matching

technique provides accurate results of 3D localisation of fruit. These techniques use depth to determine the distance between the fruit centre and robot gripper for harvesting applications. They rely more on colour, edge, and geometrical analysis to detect an individual fruit. The depth feature can potentially solve occlusion problems as it can differentiate between the objects according to depth values.

Xiang et al. (2014) benefited from the depth feature by using depth information to enhance fruit cluster segmentation as well as measuring fruit location in 3D coordinates. Each cluster of tomatoes was classified as adhered or overlapped type based on the difference in depth between the individual fruit included. Then, edge curvature analysis was used for colour image to segment the adhering region, while edge curvature analysis was used for colour image and depth map to detect different parts of overlapping regions. This method shows a good segmentation rate of 87.9%, to detect individual tomatoes from the cluster under different illumination conditions.

### **2.2.2 Depth sensing in a controlled environment**

Depth sensing has been widely introduced in many applications for plant part detection under controlled environments. A controlled environment can include indoor laboratories, greenhouses and outdoor areas with diffused sunlight or even at night (using artificial light). These sensing techniques can be implemented using Microsoft Kinect sensors, TOF cameras and binocular vision sensors. Most of these applications are devoted to 3D plant modelling and phenotyping. A part of these applications is ranged to deal with simple plant structure recognition, inter-plant distance measurements and to sensing of complex plant canopies.

As an example of using depth for simple plant recognition in a laboratory environment, two methods of applying pesticide were used with the automated guidance of a pesticide spraying robot. Li et al. (2009) used stereo vision technique to detect and to calculate the 3D pest position on the plant leaf. This method used colour transformation to segment pest from the leaf. Then, depth information was utilised to calculate pest position for automatic pesticide robot application.

In the work presented by Xia et al. (2009), depth sensing was used for leaf segmentation as well as for calculating the centre position of each leaf. The disparity map was calculated using Birchfield stereo matching algorithm (Birchfield and Tomasi, 1999). Then, different processes were applied, such as smoothing, depth histogram and thresholding to filter and to segment the disparity map into several areas depending on depth values. Afterwards, shape and size attributes were used to confirm the segmentation for each leaf. The depth value of each leaf was measured by calculating the mean value of depth for the leaf area. The geometry centre of each segmented leaf area presented the 3D position of that leaf where the automatic spray system could project and perform the task. Figure 2.2 <sup>1</sup> presents the plant segmentation steps.

In these two methods, depth information was used to segment simple structured plants in a laboratory environment. Various techniques need to be investigated and applied to deal with complex plant structure, where leaves are overlapping each other. Depth sensing could enhance the segmentation process by adding depth information. The literature reports two methods for multiple leaf detection using depth sensing (Wallenberg et al., 2011; Xia et al., 2015). These methods are discussed in more detail in Section 2.3.2.

---

<sup>1</sup>©[2009] IEEE. Reprinted, with permission, from [(Xia et al., 2009), "A stereo vision based method for autonomous spray of pesticides to plant leaves", Industrial Electronics, July 2009

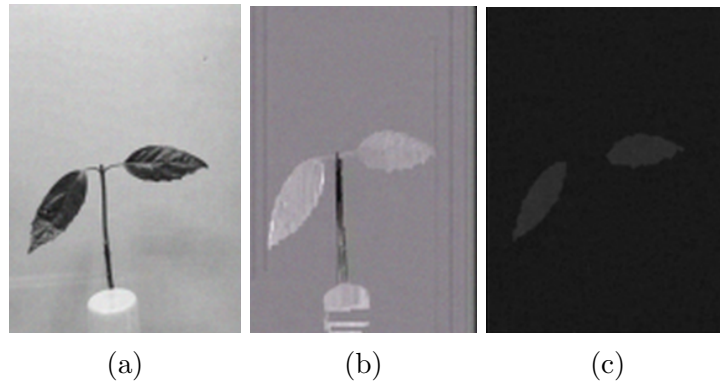


Figure 2.2: Depth image segmentation, (a) original image, (b) disparity map, and (c) disparity map after noise filtering and segmentation (Xia et al., 2009)

Depth sensing is also used for other agricultural applications. The literature reports two studies that use depth sensors to measure row spacing and inter plant distance under a controlled field environment for the purpose of final yield management. In the first study, Nakarmi and Tang (2012) utilised a TOF of light camera (3D sensor) to measure inter-plant spacing sensing for corn plants in controlled conditions. This system can detect the corn stem accurately when the imaging area is covered properly and the camera is protected from direct sunlight. Nakarmi and Tang (2013) used the same sensor to develop a non-invasive machine vision system to detect cotton plant stems. This method produced good results for stem profile detection from images captured at night time in low weed infestation field conditions.

The 3D models of plants can provide detailed structural information about plant growth. The literature reports various studies that have been developed using different depth sensors, for example Chapron et al. (1993) and Takizawa et al. (2005) used stereo vision technique for constructing 3D models of plants canopies at indoor conditions. The plant model was useful to extract some information such as leaf area, leaf shape and plant height. Other indoor applications, such as wilt detection, have been successfully implemented by (Mizuno et al., 2007) using stereo vision and phenotyping analysis techniques using low cost depth cameras (Microsoft Kinect)



(Ch  n   et al., 2012) or Laser Range Finder (LRF) (Kaminuma et al., 2004). The corn plant space sensing in indoor and outdoor conditions has been demonstrated by (Jin and Tang, 2009) using stereo vision from top view images. The method was effectively capable for updating the plant skeleton structures, recognising individual corn plants and detecting their centre positions. The 3D models of plants can provide promising results to interpret plant growth and the plants' structural analysis, however most of these methods are limited to the controlled environment (indoor, greenhouse). Therefore, this research area needs more study and development in order to make it more applicable for outdoor applications.

## **2.3 Image analysis techniques for leaf and stem detection**

The identification of plant parts such as leaves, stems and branches is important for assessing plant growth. The literature reports a variety of studies dealing with plant parts, segmentation using different techniques. Many of these studies are devoted to single leaf segmentation, while some of these studies have analysed the skeleton structure of the plant (i.e. stem, branch). Detection of multiple leaves from one image is a critical issue in real field environments, however there are some studies reported with this focus. The following articles describe plants with a single feature (i.e. one leaf or stem), whilst others analyse multiple leaf detection techniques.

### 2.3.1 Leaf detection

A proper investigation of leaf status is essential for in-field crop management. It is a fundamental process to support crop cultivation, and to monitor plant growth, stress and disease attack (Chaudhary et al., 2012; Arivazhagan et al., 2013; Wspanialy and Moussa, 2016). The literature reports numerous studies dealing with single leaf segmentation for different applications. They were largely motivated on identifying leaves for the purpose of species identification. Typically this type of segmentation relies on having one leaf in the image. (Wu et al., 2007; Kadir et al., 2013; Hu et al., 2012; Cerutti et al., 2013; Yanikoglu et al., 2014; Kalyoncu and Toygar, 2015; Rojas-Hern et al., 2016; Rojanamontien et al., 2016; Husin et al., 2012). Their segmentation task was based on the assumption that there were no overlapping leaves. These studies need to implement two tasks: leaf segmentation and leaf classification. The segmentation tasks were performed using the image processing techniques previously presented in Section 2.1.2 including colour, shape, edge, geometrical and morphological operations. The classification task dealt with identifying shape and texture features. Those features were fed as training data for the classifier part to implement matching and identification processes. The classification process is one of the machine learning applications that can be implemented using several of the machine learning techniques such as Neural Networks (NN), Artificial Neural Networks (ANN), Support Vector Machine (SVM), and Genetic algorithms. The classification process is another wide research area; and, as such, it will not be included in this research study. The detection of multiple leaves is the specific focus of this study, therefore this review will focus on multiple leaf extraction techniques including small seedling and dense plant canopies.

### 2.3.2 Detection of multiple leaves

The automatic detection of individual leaves is a crucial task for different practices in precision agriculture such as plant inspection, micro-spraying and de-leafing (Xia et al., 2013). Leaves on the same plant share the same features, such as colour, shape and texture. With this in mind, multiple leaf segmentation is a challenging task for many reasons including: colour similarities between leaf and background foliage, similar characteristics between leaves on the same plant, plant structure complexity, and leaf occlusion. Therefore, the multiple leaf detection technique needs to address the colour similarity between neighbouring leaves and the different perceived shapes of leaves, and to present different leaf sizes within one image. The presence of different leaf sizes within one image becomes a problem when applying pre-processing techniques, for example the use of morphological operations such as erosion and dilation operators. The erosion and dilation operators require a different structural element to be defined for each different shape and size object in the image. In addition, applying these techniques could remove some of the small leaf sizes from the image, by using an erosion process and other large leaves could be connected to each other by using a dilation process. Therefore, further image analysis techniques are required to implement this task.

The literature reports different techniques for identifying an individual leaf, using a variety of vision sensors. These techniques are based on two main steps: background removal and individual leaf identification. The image analysis techniques used to implement each task depend on some factors such as: image acquisition method (e.g. from top or side view), which can offer a variety of leaf orientation (horizontal or vertical), and also depend on the assumption that leaves are occluded or not. Top view images can offer a horizontal orientation for plant leaves which are completely visible or partially occluded. Different leaf orientations can be seen

from side view images. Although some studies have been reported that deal with multiple leaf detection techniques, most of them are concerned with small seedling or non-complex plant canopies. In general these studies can form two categories: 2D segmentation approach, and 3D segmentation approach.

### **2.3.2.1 2D segmentation approach**

This type of image segmentation relies on the 2D image features such as colour, shape and edge. The first step of segmentation is background removal. Typically this step of segmentation relies on removing a distinct soil background for top view images using traditional pre-processing and segmentation techniques including: colour indices and transformation, image enhancement, thresholding, edge detection and thinning operations. In some studies, the infrared wave band was used to remove the background area since it can provide the best contrast between plant vegetative parts and soil background (Franz et al., 1991a; Franz et al., 1995).

After removing the background part, each individual leaf needs to be identified using internal leaf features. One of the most obvious features is leaf shape. As the images are taken from the top, which provides a complete view for leaf boundaries, the curvature characteristic of leaves can provide an adequate description about each leaf. The literature reports varied techniques for extracting curvature function and recognising leaf boundaries. For example, Franz et al. (1991a) proposed a shape based method for detecting different types of small seedling leaves which are completely visible or partially occluded. The method used Fourier-Mellin correlation procedure (Mitchell and Grogan, 1984) for identifying curvature function. The performance of the Fourier-Mellin correlation algorithm was successful with completely visible leaves but inadequate for describing leaf shape that has relatively

small curvatures or have featureless leaf margin.

Another shape based algorithm was presented by Franz et al. (1995) for identifying completely visible and partially occluded leaf boundaries. The method was based on Sobel edge detection technique (Sobel and Feldman, 1968) for computing the intensity gradient of each pixel. Then, the segmented edge was linked together based on gradient criteria to form a closed and complete leaf boundary for segmenting plant vegetation parts from soil background. The areas of overlapping leaves could be partitioned to multiple regions so each leaf could be identified. User intervention was required at various steps in the process.

Some leaf shapes are quite similar to an ellipse shape, therefore ellipse criteria can be a suitable description of the leaves' curvature function. This criteria inspired Chien and Lin (2002) to propose a method for measuring leaf area, position and orientation of four types of small seedling plant from top view image using elliptical Hough transform technique (Duda and Hart, 1972). The method showed good results for identifying complete and partially occluded leaves for horizontal orientation; however, the method was not adequate for identifying oblique leaves. This method was developed later by adding two side view images and applying the convex hull image processing algorithm (Chien and Lin, 2005). The side view images offered the information missing from top view images. The leaf skeleton information was used to correct leaf area measured by top view image for better estimation.

A variety of machine learning approaches were used for identifying multiple leaves in the plant image. For example, genetic algorithm (Neto, Meyer and Jones, 2006) and NN technique (Pan and He, 2008) demonstrated high performance for extracting individual leaves from canopy images and detecting vegetation pixels from the ground respectively. The use of watershed-based leaf segmentation algorithm is re-

ported in (Lee and Slaughter, 2004; Wang, Huang, Du, Xu and Heutte, 2008; Tang et al., 2009; Nesaratnam and BalaMurugan, 2015), which efficiently extracts plant leaves from a complicated background. However, their segmentation was not based on identifying leaves from occlusion or solving the problem of overlapping leaves.

In order to deal with detecting partially occluded plant leaves, models including a priori knowledge on leaf shapes are required to segment the individual leaves. Franz et al. (1991a) used an ideal leaf model, which is oriented randomly, as a priori knowledge to identify a complete or partially occluded leaf using cross correlation matching method. The method was able to identify leaves with horizontal and non-horizontal orientations. Parametric deformable models including a priori knowledge on leaf shapes was presented to segment the individual weed leaves from the complicated background (Manh et al., 2001). Afterwards, the Active Shape Model (ASM) was used to segment occluded leaves in field conditions (Manh et al., 2001).

A deformable model containing a priori knowledge about leaf shapes was also developed by Xia et al. (2013) to detect damaged and occluded pepper leaves in greenhouses. The quadratic Bezier curve fitting was applied to segment image edges into partial leaf boundaries. Then, the Multilayer Perceptron Classifier (MLP) was used to classify partial boundaries as leaf boundaries or veins. Afterwards, multiple leaf shape models were built using a priori knowledge. A modified ASM was used to implement the matching and identification process. This method was able to identify single, occluded and overlapping leaves and benefit from the advantages of using machine learning techniques such as MLP and ASM. The images were taken from the top side of the plant which offers semi-complete horizontal orientation for leaves facing the camera with a simplified background.

Although good segmentation rates were presented from the methods based on build

leaf models containing a priori knowledge, there were some limitations for applying these methods to other plants which exhibit different leaf shapes rather than computation time cost. Furthermore, Xia et al. (2013) reported that the method was designed to work with complete leaf shape, or at least one edge boundary needed to be in the top view of the leaf image (Figure 2.3a and 2.3b)<sup>2</sup>. As such, some side views and very small leaves (with non-clear curvature boundary) were not detected using this method (Figure 2.3b ).

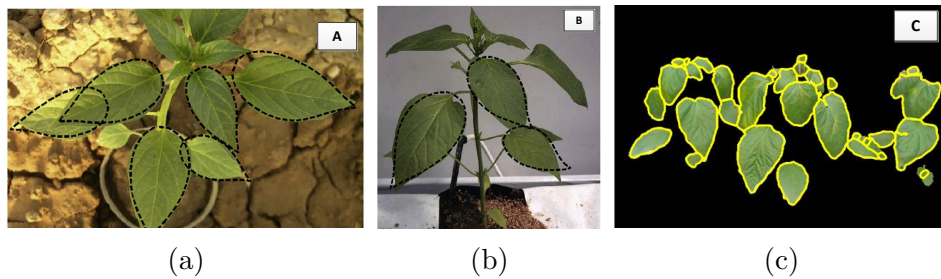


Figure 2.3: Multiple leaf detection of (a) and (b) using MLP-ASM method (Xia et al., 2013). (a) Top view image of pepper leaves, (b) side view image of paprika leaves. (c) Segmentation of individual leaves using depth sensor (Xia et al., 2015)

It is obvious from the above review that extracting shape features was the common motivation to identify plant leaves. This is because shape can provide a distinct feature for plant leaves and can identify complete and partially occluded leaves. Good results can be obtained for images captured from a suitable view which could offer a complete leaf shape of simple plant canopy. Shape feature might not be beneficial for irregular leaf shape, very complicated leaf shape (cannot be identified by curvature functions) or for dense plant canopies.

<sup>2</sup>Figure 2.3a and 2.3b are reprinted from Biosystems Engineering, Vol 116, (Xia et al., 2013), Plant leaf detection using modified active shape models, Page No. 32, ©[2013], with permission from Elsevier.

### 2.3.2.2 3D segmentation approach

The limitation of the shape based method could be addressed by using another feature, or depth for more flexible leaf segmentation method. Xia et al. (2015) proposed another method for segmenting the occluded leaves in a greenhouse environment. Firstly, the plant was extracted from the background using the mean shift clustering algorithm for depth image (Comaneci and Shift, 2002). The gradient vector field was calculated on the depth image. Based on gradient vector field value, the center of divergence was calculated which was used for automatic initialisation of the Active Contour Model (ACM). The occluded boundaries of the overlapping leaves in the depth image were identified using ACM (Xu and Prince, 1998).

The method shows a high segmentation rate for single and occluded leaves (Figure 2.3c <sup>3</sup>). The figure also shows that the images were taken from the side view of plant with front dominant leaves' direction. This view offers a quite complete leaf shape with vertical leaf orientation which is necessary for the segmentation process. By contrast, side view leaves (have image plane larger than 60° angle) which have a small visible area were not detected properly. They might have over segmentation using ACM method. In addition, due to the hardware limitation of Microsoft Kinect sensor, the small size leaves were also ignored. Furthermore, the method cannot segment the occluded leaves showing tiny differences in depth. This is because the method depends on calculating the gradient vector field which depends on the significant difference in depth between boundaries of leaves. The

---

<sup>3</sup>This article is an open access article by Xia, C.; Wang, L.; Chung, B.-K.; Lee, J.-M. "In Situ 3D Segmentation of Individual Plant Leaves Using a RGB-D Camera for Agricultural Automation". *Sensors* 2015, 15, (<http://www.mdpi.com/1424-8220/15/8/20463/htm>), used under the terms and conditions of the Creative Commons Attribution license (<http://creativecommons.org/licenses/by/4.0/>)



boundary of occluded leaves with smooth difference in depth cannot be detected by this technique. In addition, these methods were applied under controlled environmental (greenhouse) conditions. More challenges are expected for detecting leaves in outdoor (uncontrolled) environments and for mature plant canopies.

For dense plant canopies, an active contour model would not be beneficial where plant images present different leaf orientations with irregular shapes. Another method was presented by Wallenberg et al. (2011) to segment leaves from a dense plant canopy. The superparamagnetic clustering algorithm (Blatt et al., 1996) was used to segment plant leaves from the colour and depth images, captured by a Microsoft Kinect sensor. The method was based on the fusion of colour and depth gradient values using a channel representation technique (Zemel et al., 1998; Granlund, 1999). The proposed method used three types of segmentation based on one feature each time: colour, depth, and colour fused within depth gradient values. The results show that the simultaneous use of both colour and depth fusion is more effective and useful than using only one or the other. The method shows good segmentation performance but low detection rate within serious occlusion areas. However, results were limited to a greenhouse environment and indoor using Microsoft Kinect sensor with a limited working depth range (Mozos et al., 2012). Moreover, this method required a supervisor to adjust the depth channel against the colour channel weighting parameters.

### **2.3.3 Stem and branch detection**

Plant stem detection is a potential method for plant growth sensing and plant row spacing measurement. Measuring row spacing and inter plant distance is useful for final yield management, while stem and branch segmentations are used for plant

modelling and plant parts reconstruction. For row spacing and inter-plant distance, two methods were reported from the literature using different techniques:

The first technique was presented by Nakarmi and Tang (2012) to measure inter-plant spacing of corn using a TOF sensor. A skeleton centroid and orientation is determined using a parallel thinning algorithm based on 8-connectivity (Rosenfeld, 1975). This system can detect corn stems accurately when plants are inclined  $\pm 15^\circ$  from the vertical axis under a controlled field environment. In that case, the imaging area needs to be covered properly to protect the camera from direct sunlight.

The second technique for row spacing and inter plant distance was also proposed by Nakarmi and Tang (2012). This technique was developed to overcome the limitation of the first technique (Nakarmi and Tang, 2012), where stems cannot be identified precisely for double or triple plants. This is because plant branches normally have a curvilinear structure with more than  $\pm 15^\circ$  inclination angle from the vertical axis. For that reason, Nakarmi and Tang (2012) enhanced their work using the vesselness measure technique (Frangi et al., 1998). The vesselness measure is based on detecting a typical line profile of reflected light on the colour image (Steger, 1996). This technique was first developed by Frangi et al. (1998) to extract vessels from medical images. A vesselness measure of the Hessian matrix (Frangi et al., 1998) and Hough transform (Duda and Hart, 1972) techniques were used to detect the plant stem profile for different applications. Nakarmi and Tang (2013) used these techniques to measure row spacing and inter plant distance for cotton. The method shows high results for stem profile detection from images captured at night in low weed infestation field conditions.

Stem detection is also useful for measuring nodes and internode length as an indication for vigor, growth and plant stress. The internode length is largely affected by

environment stresses such as water and temperature (Oosterhuis and Kerby, 2008). The distance between main stem nodes indicates several types of plant stresses which are mainly used for water stress that potentially indicates stunted growth. The internode length in cotton can also indicate the amount of vegetative growth (McCarthy, 2009). A short cotton internode length (shorter than 50 mm) could indicate moisture stress while an internode greater than 70 mm can indicate excessive vegetative growth (McKenzie, 1998).

Previous work in cotton was implemented by McCarthy (2009) for cotton plant stem detection for the purpose of water stress sensing. The method used vesselness measures and Hough transform techniques for monocular plant image analysis. The distance between nodes on the cotton main stem was used as a significant indicator of plant water stress and irrigation crop management. The vesselness measure has important advantages comparing with the technique proposed by Nakarmi and Tang (2012). For example, there is no limitation for stem inclination angle from vertical axes as previously mentioned. Therefore, this method is more suitable to extract plant skeleton features that have stems and branches. This work was done under field conditions, however some level of lighting control was achieved by the camera apparatus used.

In addition to indicating water stress, there is an additional benefit from stem internode measurement. Internode length was used as an indication for tomato plant vigor and growth, and presents the salient effects of environmental stresses on the plant (Yamamoto et al., 2016). Recently, a new method for internode detection was presented by Yamamoto et al. (2016). In this method, a tree-based segmentation model (Guo et al., 2013) was used to segment tomato seedlings based on pixel colour classification and a regression tree classifier (Breiman et al., 1984). The classifier pre-training includes manual labeling of the training images into three classes: stem;

leaves; and background. Afterwards, thinning (Zhang and Suen, 1984), and branch cross-point detection (Sarfraz, 2005) techniques were applied to the generated image of the stem. Also, the pixels of candidate nodes were extracted. The method was developed under a glasshouse environment with a clear background behind three types of seedling plants.

In a new study presented by Ji et al. (2016) for branch detection, apple tree branches were identified as obstacles in the navigation of a picking mobile robot. This method showed another approach of threshold segmentation which was based on Contrast Limited Adaptive Histogram Equalization (CLAHE). This method was applied to distinguish between the small grey intensity difference levels. Subsequently, the iterative threshold segmentation was used to extract branches from the image. The result shows high rate of apple branch segmentation (94%) compared to other approaches (Otsu and histogram). Nevertheless, the method has a slower segmentation rate when compared to the histogram method. This technique is effective for branch segmentation because it depends on the image subtraction of apples from the total plant image; whereas apples have different grey levels to branches and leaves.

## 2.4 Conclusion

Several autonomous segmentation algorithms for plant parts have been developed in recent years and have been introduced in different applications. The main goals of these studies has been to increase productivity and to reduce crop input resources. The selection of the desired sensor and segmentation approach depends on the specific agricultural applications and plant features that need to be extracted for that application. From the reviewed literature, the selection of the suitable sensor and

the segmentation approach for different application can be summarised as follows:

1. Vision sensors have been considered the most promising and common sensors used for plant and fruit feature extraction. The published studies use different types of vision sensors to acquire plant and fruit images which need different types of image segmentation. The colour based segmentation method using RGB colour transformation and colour subtraction techniques is very popular for image analysis algorithms and it is more beneficial for non-green fruit detection (Wang, Zhu and Ji, 2008; Zhou et al., 2012).
2. HSV, HSI,  $L^*a^*b$ , YCbCr colour transformations were also used as a common and effective colour segmentation approach which can adaptively discriminate fruits with different colour (Lin et al., 2005). Among several approaches developed for separating interested green area from plant images, *ExG* and *EXGR* indices were found to be more effective in segmenting foliage from background soil for top view images (Woebbecke et al., 1995; Meyer et al., 2004). Colour features have low reliability under different lighting conditions such as changes in atmosphere, season and sunlight. Therefore, supporting colour by other image segmentation features such as shape and texture is important for an accurate plants identification process.
3. Plant and tree images are typically complicated. Therefore, more than one image feature is required to implement segmentation tasks such as: colour, shape, edge or texture. Shape is the most relevant attribute of leaves, as colour is not sufficient to be used alone in plant identification applications. The literature reports some effective techniques used for segmenting leaf boundaries such as Bezier curves (Chi et al., 2003), Elliptic Fourier analysis (Neto, Meyer, Jones and Samal, 2006) and leaf geometrical analysis including length, width,

- area, diameter, aspect ratio and convex area ratio (Wu et al., 2007; Kadir et al., 2011a).
4. Combining texture attributes with colour and shape is also required for some instances when the shape varies due to the plant condition and image acquisition. Texture analysis considering leaf pubescence and leaf venation is useful to inform plant condition and notify leaf disease and insect damage. Texture analysis based on known techniques such as Gabor wavelets and Polar Fourier Transform were used as effective approaches for plant species classification. The species classification based on texture analysis can be affected by leaf orientation or rotation, image resolution, illumination and the bidirectional reflectance of leaf surfaces (Meyer, 2011).
  5. Although the 2D image attributes have an important role in the plants' image segmentation and species classification, nevertheless, most of these application deal with small plant seedlings or one leaf segmentation. The 2D image features might not be sufficient for recognising features of dense plant canopies. In that sense, another image feature or depth needs to be introduced.
  6. Depth sensing using a stereo vision technique has been applied in a variety of indoor and outdoor agricultural applications. A stereo vision system has been used to develop navigation algorithms to determine the position of the crop rows, and to find the central path for the an automated guidance tractor. However, the maximum depth and precision measured by the stereo vision system is limited by the baseline between the cameras. As depth increases, the quality of the distance values decreases rapidly (Weiss and Biber, 2011). Therefore, resorting to alternative sensors (such as GPS and an inertial measurement unit ), is more reliable especially in localisation, navigation and 3D map row detection (Rovira-Más et al., 2008).

7. Stereo vision is more applicable for narrow distance applications such as fruit harvesting robots. These studies successfully identified different types of fruit and measured 3D location in trees such as orange (Plebe and Grasso, 2001), tomato (Yang et al., 2007), apple (Si et al., 2015) and grape (Luo et al., 2016). Shape attributes, edge detection and geometrical analysis were used in these studies for identifying individual fruit, finding fruit locations and solving the fruit occlusion problem. Depth difference information was used to enhance the detection of occluded fruits (Xiang et al., 2014). Therefore, further studies are required that focus on the recognition of overlapping and occluded clusters of fruits using depth.
8. Depth sensing, using different depth sensors, is also used for other plant applications in a controlled environment such as plant part detection (Li et al., 2009; Xia et al., 2009), row spacing and inter plant distance (Nakarmi and Tang, 2012; Nakarmi and Tang, 2013), 3D modelling and plant phenotyping (Takizawa et al., 2005; Ch  n   et al., 2012; Kaminuma et al., 2004). The research using depth sensing for extracting plant structures is mostly limited to controlled environmental conditions. However, there are some studies paying considerable attention to the use of stereo vision for plant parameter identification and 3D modelling at outdoor conditions (Ivanov et al., 1995; Biskup et al., 2007). These studies show an acceptable result which opens the field for further studies focusing on using depth for outdoor plant applications. Therefore, more studies need to be devoted to this research area.
9. For detection of other plant parts, such as stem and leaf, the literature reports some methods for stem profile detection. These methods are implemented using different sensors under controlled environments. The techniques report different accuracy rates with some limitations such as stem detection with

specified inclination angles (Nakarmi and Tang, 2012). The vesselness measure technique was used to extract stem profiles without this limitation, as it was used for curvilinear structure detection (McCarthy, 2009; Nakarmi and Tang, 2012). This method looks promising for stem and branches detection for the purpose of plant 3D modelling and plant parts reconstruction.

10. The literature reports some studies paid considerable attention to multiple leaf segmentation under controlled outdoor and indoor conditions. The focus of these studies is to detect multiple leaves for small seedling plants using 2D segmentation approaches such as Fourier-Mellin correlation (Franz et al., 1991a), Sobel edge detection (Franz et al., 1995) and a modified active shape model (ASM) (Xia et al., 2013). These approaches rely on detecting the curvature characteristic of leaves from top view images which offer a horizontal leaf orientation with complete leaf shape.
11. For mature plant canopies from side view images, the 2D segmentation approaches relying on shape attributes become non beneficial where shape feature is inconsistent for all leaves. In that case, depth feature is becoming a promising attribute. There are some studies focusing on the detection of multiple leaves using different approaches such as colour and depth fusion method (Wallenberg et al., 2011), and active contour model for front dominant leaves' images (Xia et al., 2015). These studies show good segmentation results however they were implemented under controlled illumination conditions. The segmentation of multiple leaves for the plant canopy, under a variety of outdoor illumination conditions using depth, is not reported in the literature.

The related studies in the literature have been reviewed and summarised to assign and highlight the research problem in the following section.



---

## 2.5 Research problem

In agriculture automation, the analysis of 2D image features has addressed a variety of machine vision applications in outdoor conditions, ranging from large scale analysis (weeds) or to dealing with simpler plant structures (small seedlings) (Åstrand and Baerveldt, 2004). The 3D imaging has been commonly applied to indoor applications, for example, plant phenotyping (Chéné et al., 2012; Golbach et al., 2016) and image based plant modelling (Quan et al., 2006). The 3D imaging using stereo vision techniques is also used for outdoor applications such as: fruit picking with harvesting robot applications, crop row detection systems and in field navigation (Kise et al., 2005; Kise and Zhang, 2008; Hanawa et al., 2012). Therefore, additional research and studies need to be undertaken to investigate plant parts detection in outdoor conditions.

The limitation of using 3D imaging sensors in outdoor applications, is due to a large variation in outdoor lighting conditions and most of the 3D imaging technology sensors being designed for indoor applications which limits the use of these sensors for outdoor applications. Therefore using these sensors at outdoor applications may limit the scope or make the system very complex for practical implementation (Kazmi et al., 2014).

Although 2D imaging has addressed some of the assortment of problems in precision agriculture ranging from disease detection (Chaudhary et al., 2012; Arivazhagan et al., 2013; Wspanialy and Moussa, 2016), weed control (Slaughter et al., 2008), and crop estimation (Gongal et al., 2016), most of these tasks tend to deal with a simple plant structure (small seedling) at an early growth stage or large scale analysis (weed). However, 2D images are not robust enough to address the problem of complex structure plant canopies or the occlusion problem of overlapping leaves.

To overcome this problem, 3D imaging technology has been introduced for analysing 3D properties of plants.

The literature reports many articles dealing with image analysis of leaves for the purpose of species identification using shape, texture and colour properties (Sections 2.1.2 and 2.3.1). The segmentation and counting of individual leaves remains challenging when leaves are overlapping (Scharr et al., 2016). Studies in the literature have developed some autonomous methods for multiple leaf detection and leaf occlusion separation using the colour and depth fusion method (Wallenberg et al., 2011), colour and active shape model (Xia et al., 2013), and colour, depth and shape properties (Xia et al., 2015); however, all these trials were under greenhouse or indoor conditions which invite the need for development of a plant leaf detection algorithm for outdoor conditions.

Outdoor lighting conditions are a big challenge for precision agriculture applications. Segmentation using colour features is widely used in outdoor agricultural applications. Colour features have limiting disadvantages under outdoor varying ambient lighting conditions. This limitation makes adding other features such as texture, shape or depth necessary for plant image segmentation. Since plants are 3D objects, introducing depth has the potential to isolate a plant from the image background and also for the segmentation within the foreground objects.

The identification of plant growth parameters is important for monitoring plant growth and assessing crop management practices. A multiple leaf segmentation and counting process using a stereo vision sensor for measuring plant canopies under a variety of outdoor lighting conditions, as a growth estimation indicator, is not heavily researched in the literature which indicates a new gap in the current research area. This study intends to use the combination of 3D image information

(colour, depth) for identifying plant parts (leaf, stem) and to solve leaf occlusion problems. Depth information will also be used for plant parts localisation and for reconstructing plant segmented parts in a 2.5D model.

# Chapter 3

## Evaluation of the stereo vision system

### 3.1 Introduction

The information gathered by the 2D image sensors are useful for identifying small plants' parameters for those that have limited depth (e.g. weeds), and with a known position (e.g. on the ground) (Chien and Lin, 2002; Meyer and Neto, 2008). Stereo vision techniques enhance 2D image features to obtain more accurate localisation of fruit and plant structures. Recently stereo vision techniques have been successfully used through the application of harvesting robots for this purpose. Depth information was used to enhance the detection of adhered or overlapped fruits (Xiang et al., 2014), therefore, it is expected that depth information can also be used to enhance the detection of plants' overlapping leaves.

This chapter presents the fundamental idea and the essential processes of stereo vision techniques including camera calibration and rectification, triangulation and

stereo corresponding process. The chapter also explains the characteristics of the depth sensor used in this study including disparity maps and their parameters to produce the required depth information for the plant parts. A wide range of disparity map parameters was tested and evaluated for optimal combination. The evaluation presents the influence of these parameters on producing an accurate disparity map that can match the desired criteria.

## 3.2 Stereo vision technique

The basic idea of stereo vision is to monitor the same points in a scene by two cameras separated only in the  $x$  direction by known distance or baseline, to produce 3D structural information of these points (e.g. range and depth information) (Trucco and Verri, 1998). This process can be implemented by finding the correspondence between the points that are seen in the left image and the same points as seen in right image. The two images have a lot of similarities and a small number of differences (Hamzah et al., 2010). When the baseline between the two cameras is known with the correspondences of these points, the 3D location of the points can be calculated. The stereo vision systems have frequently been used to provide 3D information from 2D views, without requiring a large number of views (Xia et al., 2009). In general the stereo imaging process that uses two cameras has four steps: Starting by removing image distortion and camera calibration, image rectification, feature correspondences (stereo matching) and reprojection or triangulation processes. (Bradski and Kaehler, 2008).

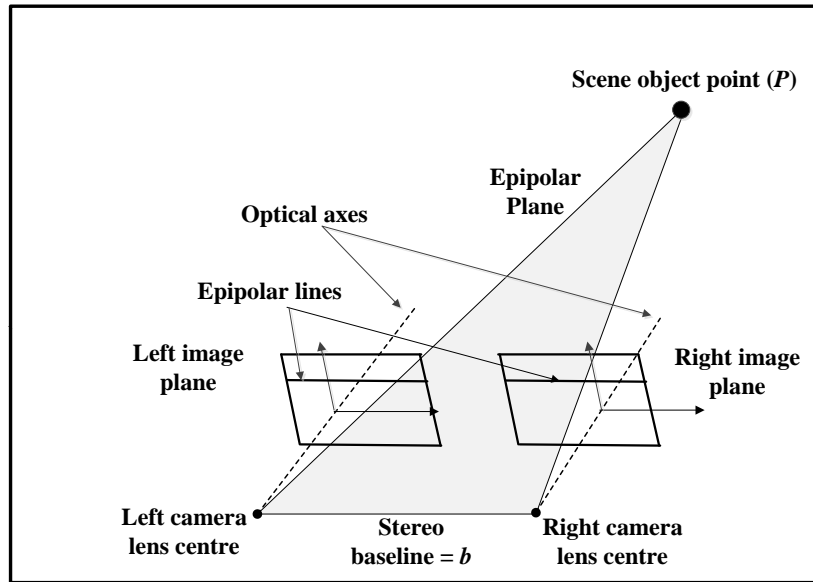
### 3.2.1 Triangulation

Figure 3.1a shows the geometry of a binocular stereo model which consists of two identical cameras separated by a baseline distance  $b$ . This model of stereo geometry presents coplanar image planes whereby every feature point in one image will lie on the same row in the second image. The plane passing through the feature point in the scene  $P$ , and the camera centers, is called the epipolar plane (Figure 3.1b). The epipolar line can be defined as the intersection of the epipolar plane with the image plane. Point  $P$  in the 3D world is viewed as  $P_l$  and  $P_r$  at different positions in the image plane by the two cameras (Figure 3.1a). The displacement between the locations of  $P_l$  and  $P_r$  in the image plane is called the disparity. The disparity is measured along the  $x$  direction only however, it might be a vertical disparity due to misregistration of the epipolar lines in practice. The vertical disparity is assumed to be zero for many formulations of binocular stereo algorithms (Jain et al., 1995).

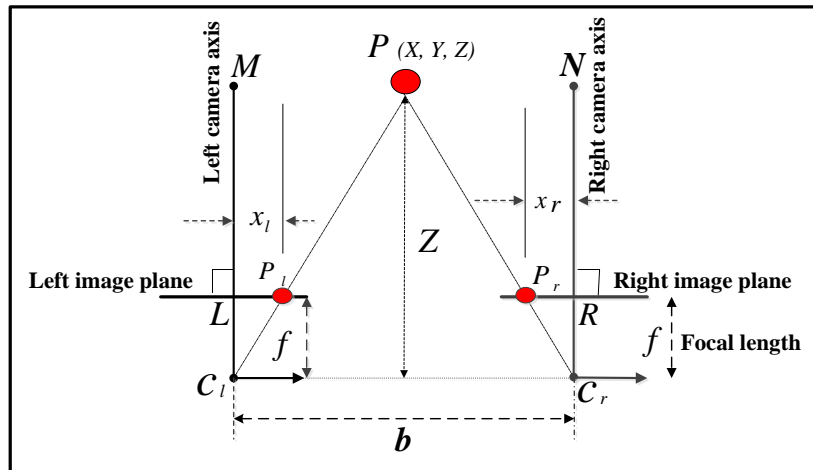
Figure 3.1b presents an undistorted, aligned and measured stereo camera system which has an exact coplanar image plane and parallel optical axes. The focal length  $f$  of the two lenses represents the distance between the image planes and the centres of each lens ( $C_l, C_r$ ). The disparity images can be defined as the horizontal position deviations of an object in the image captured by the left and right lenses of the stereo vision camera (Rovira-Más et al., 2004). The disparity between the projection points ( $P_l, P_r$ ) on the image planes is defined by  $d = x_l - x_r$ , where  $x_l$  and  $x_r$  are the left and right deviation in the image planes. By comparing the similar triangles  $PMC_l$ ,  $P_lLC_l$ ,  $PNC_r$  and  $P_rRC_r$  of Figure 3.1b the following relation can be obtained:

$$\frac{X}{Z} = \frac{x_l}{f} \quad (3.1)$$

$$\frac{X - b}{Z} = \frac{x_r}{f} \quad (3.2)$$



(a)



(b)

Figure 3.1: (a) The geometry of a binocular stereo model, and (b) an undistorted, aligned and measured stereo camera system.

Then, the depth value can be obtained by combining these equations and solving for  $Z$ :

$$Z = \frac{b \cdot f}{x_l - x_r} = \frac{b \cdot f}{d} \quad (3.3)$$

### 3.2.2 Camera calibration

The 2D camera calibration is a process used to calculate the geometry model of the camera and the distortion model of the lens. It is an essential process to improve detection accuracy and to minimize lens distortion. This process calculates the camera parameters including intrinsic and extrinsic parameters. The intrinsic parameters are the internal parameters of the camera which include: optical centre, skew coefficient and focal length, while extrinsic parameters present the position and orientation of the camera relative to the world coordinates. For the pinhole camera model (Figure 3.2), the geometric relationship between a 3D point in the world  $p_0$  and its 2D corresponding projection  $p_i$  onto the image plane, can be defined by the following equation (Hartley and Zisserman, 2003):

$$p_i = \mathbf{A} \begin{bmatrix} \mathbf{R} & \mathbf{t} \end{bmatrix} p_0, \quad \text{with} \quad \mathbf{A} = \begin{bmatrix} f_x & s_c & x_0 \\ 0 & f_y & y_0 \\ 0 & 0 & 1 \end{bmatrix} \quad (3.4)$$

where  $\mathbf{R}$  and  $\mathbf{t}$  present the  $(3 \times 3)$  rotation matrix and the  $(3 \times 1)$  translation vector respectively for the extrinsic parameters. These parameters map the 3D world coordinates system into the camera coordinates system and then, the image is transferred from camera coordinates into the image plane using camera intrinsic parameters  $\mathbf{A}$ . Where  $f_x$  and  $f_y$  present the focal length parameters,  $x_0$  and  $y_0$  present the optical center in the image plane and  $s_c$  presents skew coefficient (Hartley and



Zisserman, 2003). Typically, the chessboard pattern is recommended for the camera calibration process, as it has a calibrated image pattern and it is easy to detect its corners.

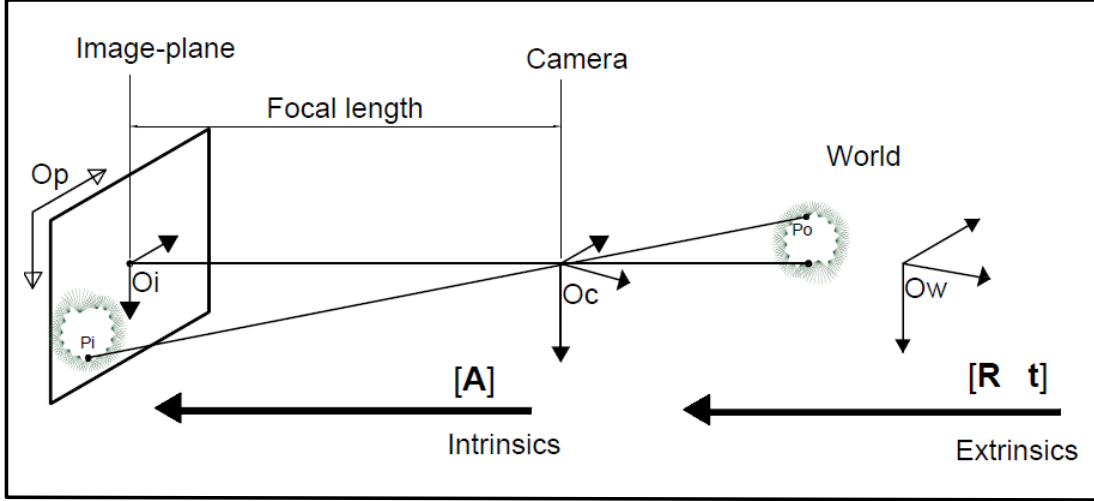


Figure 3.2: Word point mapped into the image plane using Intrinsic and Extrinsic matrix parameters in pinhole camera model.

The stereo calibration process computes the geometrical relationship model between the two cameras in the space. This is dependent on calculating the rotation matrix  $\mathbf{R}_s$  and translation vector  $\mathbf{T}_s$  between the two camera. In the calibration of a 2D camera, the process of calibration produces a list of rotation matrices and translation vectors between the camera and the chessboard pattern. In the stereo camera calibration, the process should result in a single rotation matrix and translation vector that relates the right camera to the left camera. The calibration of a pinhole camera model can be applied on the stereo calibration to put any 3D world point  $P$  in the left  $P_l = \mathbf{R}_l P + \mathbf{T}_l$  and right  $P_r = \mathbf{R}_r P + \mathbf{T}_r$  camera coordinates respectively (Bradski and Kaehler, 2008), where  $\mathbf{R}_l$ ,  $\mathbf{R}_r$ ,  $\mathbf{T}_l$ , and  $\mathbf{T}_r$  are the rotation matrix and the translation vector for the left and right cameras respectively. The two views of the point  $P$  from the two cameras are related by  $P_l = \mathbf{R}_s^T (P_r - \mathbf{T}_s)$  (Bradski and Kaehler, 2008). By solving these three relations above for rotation and translation

separately, this will produce the following relations (Bradski and Kaehler, 2008):

$$\mathbf{R}_s = \mathbf{R}_r(\mathbf{R}_l)^T \quad (3.5)$$

$$\mathbf{T}_s = \mathbf{T}_r - \mathbf{R}\mathbf{T}_l \quad (3.6)$$

The process of stereo calibration puts the right camera in the same plane with the left camera by applying the rotation matrix. It means the two image planes are coplanar but not row-aligned which is required for the stereo matching process. This task can be implemented by the stereo rectification process in the next section.

### 3.2.3 Stereo rectification

In a real stereo vision system, it is rare to find two cameras aligned perfectly with row aligned imaging planes. Stereo rectification is the process of reprojecting the image planes of the two cameras, to be exactly coplanar and row-aligned. The result of an image rectification process are two parallel epipolar lines which horizontally align along the new image planes (Kamencay et al., 2012). The stereo matching reliability and computational efficiency is then enhanced by having a one-dimensional search along horizontal lines rather than having a two-dimensional search. The results of aligning the two image planes for each camera are a distortion vector, a rotation matrix, rectified and unrectified camera matrices. From these terms, a new rectified image can be created using an interpolation process from the original image (Bradski and Kaehler, 2008). The stereo rectification step is important for a more reliable stereo matching process presented in the next section.

### 3.2.4 Stereo correspondence

The correspondence process (matching or detecting conjugate pairs) finds the corresponding point in the right image for each point in the left image. This process is required to determine two points (one in each image) by measuring the similarity of the points. The conjugate pair is two points represented by the projections of the same point in the scene, into two different images. It is necessary to assign matchable features before applying a stereo matching process. Region and edge features are usually used in stereo matching techniques (Jain et al., 1995). The epipolar line constraint can significantly limit the search space to find the conjugate pairs which means, for any pixel in the left image, there is a corresponding point in the right image that lies on the same horizontal lines (the epipolar line) (Kuhl, 2005). However, some errors in the matching point may occur due to the camera position and orientation. In this case, it is necessary to search in a small neighbourhood of the epipolar lines (Jain et al., 1995). These neighbourhood pixels can then form a block surrounding the middle pixel to be matched to the best corresponding block in the second image.

The literature reports several matching techniques based on various algorithms. These algorithms are divided on two types of matching techniques: area or region based matching, and feature based matching (Lazaros et al., 2008). The feature-based matching algorithms are based on matching intensity edges or contours between two images excluding occluded and poorly textured areas (Veksler, 2002; Veksler, 2003). These types of algorithms are faster because only a small portion from the left and right images is used for matching, however they produce semi-dense or sparse disparity maps. They are useful for some applications where fast depth computation is required and the whole image details are not required.

Other types of matching algorithms are area (region) based matching. These algorithms produce dense disparity maps which have high demand from the most contemporary applications. Each of these algorithms has to be implemented using a matching cost function between two pixels from the left and right images (Lazaros et al., 2008). The cost function finds out the distinct features between two images which could be colour, intensity features or other structural features such as edge and gradients across the image (Patil et al., 2013). The cost matching functions could be pixel-based or window-based and the cost is usually aggregated over a window with a fixed or adaptive size (Lazaros et al., 2008; Patil et al., 2013). The most common ones from cost functions are: Sum of Absolute Differences (SAD), Sum of Squared Differences (SSD) and Normalized Cross Correlation (NCC) as presented in the following equations (Lazaros et al., 2008):

$$SAD(x, y, d) = \sum_{(x,y) \in W} |I_L(x, y) - I_R(x, y - d)| \quad (3.7)$$

$$SSD(x, y, d) = \sum_{(x,y) \in W} (I_L(x, y) - I_R(x, y - d))^2 \quad (3.8)$$

$$NCC(x, y, d) = \frac{\sum_{(x,y) \in W} I_L(x, y) \cdot I_R(x, y - d)}{\sqrt{\sum_{(x,y) \in W} I_L^2(x, y) \cdot \sum_{(x,y) \in W} I_R^2(x, y - d)}} \quad (3.9)$$

where  $I_L$  and  $I_R$  are pixel intensity values of the right and left images,  $(x, y)$  are the pixel's coordinates,  $W$  is the aggregated window (mask) that surrounds the centre pixel at position  $(x, y)$ , and  $d$  is the disparity value in the  $x$  direction. The window  $W$  is centred on a left pixel  $I_L$ . This window from the left image is matched with a window from the right image by shifting the left window over the searching area of pixels in the right image. The cost functions aggregate the intensities of

all surrounding pixels in the neighbourhood for the center pixel in the left image. Then, the difference between the aggregated window of the left image pixels and the aggregated window of the right image pixels is calculated. The minimum difference over the row in the right image is selected to be the optimal matching pixel. Then, the disparity map is determined as the actual difference of the horizontal pixels. The disparity map can be an inverse function of depth, whereas, the pixel closer to the camera has a larger disparity (Van den Heuvel et al., 2003). The window size  $W$  can affect the quality of 3D disparity. A bigger window size can offer a great probability of accurate pixel disparity computed from matched points, however a bigger window will slow the process of calculation which requires more pixels to be matched.

The calculation of intensity difference between the pixels of the left and right image is the principal step for SAD and SSD cost functions. The difference between them is: SAD calculates the absolute difference of intensity while SSD squares the intensity difference instead of calculating the absolute value. The implementation time of the SSD algorithm is nearly double that of the SAD algorithm due to higher computational complexity (Kuhl, 2005; Patil et al., 2013). The square operations are implemented as a multiplication process inside the computer which takes more time compared with the calculation of absolute values. The disparity map result from applying SSD, is quite similar to the disparity map results from implementing SAD algorithm (Kuhl, 2005).

The NCC method is robust to the linear variation in brightness and produces good results with smaller aggregated windows compared with SAD and SSD which usually give good results with larger windows which add computational time (Patil et al., 2013). However, NCC method (Equation 3.9) still costs more computational time compared to SAD and SSD due to the complex calculation of divi-

sion, multiplication and square root. Furthermore, the NCC cost function tends to produce blur depth discontinuities more than other cost functions due to high errors of the outliers (Hirschmuller and Scharstein, 2007). Hence, SAD function was adopted in this study as one of the simple and fast standard cost functions (Lazaros et al., 2008; Kamencay et al., 2012), to consider computation cost and to avoid the blurred in depth discontinuities as will be discussed further in the disparity image criteria (Section 3.5).

The process of stereo vision mapping is very sensitive to error, when collapsing the data from 3D to 2D (Murray and Little, 2000). The collapsing of the 3D data encourages errors in the form of “spikes” that are propagated into the disparity map. Spikes are features of mismatches in the correspondence process of stereo vision (Kelly, 2006). Spike regions have unique attributes such as: they are stable but not large and they have discontinuities and sharp disparity at all borders (Murray and Little, 2000). Surface segmentation is a method introduced by Murray and Little (2000) to validate the disparity maps’ regions based on an assumption that they belong to a true physical surface in the disparity image, to overcome the problem of spike noise. The proposed method segments the image into continuous disparity surfaces, and according to the surface size, the algorithm can decide whether this segment is a physical 3D surface or a noise artifact (Murray and Little, 2000).

The correspondence process can be enhanced using additional techniques to validate the conjugate pair pixels from stereo images. Texture validation is another technique which can be used to determine whether disparity values are valid based on levels of texture in the correlation mask (PointGray, 2012). This is dependent on the amount of texture for the image patch and can be examined by the local sum of the Laplacian of Gaussian of the image (Murray and Little, 2000). The low textured area provides a low score sum, thus the pixel will be rejected from the

matching process due to the ambiguity and unreliable results.

### 3.3 Stereo vision specification

A stereo vision camera was selected to obtain colour and disparity images for this study. The selection of the stereo vision technique was based on its proven performance to work under natural sunlight conditions, and to deliver the depth information for the field view from two pairs of images (Plebe and Grasso, 2001; Yang et al., 2007; Biskup et al., 2007; Lati et al., 2013; Xiang et al., 2014; Kazmi et al., 2014; Si et al., 2015; Luo et al., 2016). The stereo vision camera has an advantage over Microsoft Kinect and TOF cameras (active sensors), because it can work without emitting any radiation. This advantage allows stereo vision camera to work under direct sunlight which cannot be confused by the radiation of sunlight. However, the camera has disadvantages whereby the quality resolution of depth map produced from stereo matching algorithm depends on the texture of the scenes. High-resolution depth maps can be produced from well textured scenes using stereo matching algorithms, while weak textured scenes can result in low resolution depth map. In contrast, range sensors (Microsoft Kinect and TOF camera) produce dense depth map information regardless of textured or textureless scenes but they cannot work effectively under direct sunlight conditions (Hansard et al., 2012; Kazmi et al., 2014).

The Bumblebee2 stereo vision camera (designed by Point Grey Research Company, Canada) is used to capture plant images. The camera was chosen due to its ability to produce disparity maps and work in outdoor conditions. This packaged system has two digital CCD cameras locked in a fixed assembly, that are pre-calibrated for both stereo rig and lens distortion. Disparities are calculated only in the horizontal

direction (PointGray, 2012). The focal length ( $f$ ) is equal for both cameras (2.5 mm), and they are separated by a 12 cm baseline ( $b$ ) distance. The camera pixel resolution is  $640 \times 480$  at 48 frames per second (FPS) or  $1024 \times 768$  at 20 FPS. The Bumblebee2 camera produces raw colour images, left and right calibrated and rectified colour images, disparity images/maps and 3D point cloud data. Appendix A presents more detailed about the Bumblebee2 camera specifications.

The disparity map can be rendered as a greyscale image which presents the output of stereo matching between the left and right images. The disparity map's pixels have grey level values, i.e. the darker value points are further away from the camera than the lighter points. It is expected that plant parts can be segmented according to the different intensity values in the disparity image (i.e. different depth). The disparity map produced by the Bumblebee2 camera has been optimised for efficiency through a number of validation steps (Kazmi et al., 2014). The accuracy of the disparity map can vary depending on the surface and texture correspondence algorithm (Murray and Little, 2000). The Bumblebee2 stereo vision camera offers some optional parameters that can be used to enhance the accuracy of the disparity map. The stereo and validation parameters' functions and specifications are presented in listings 3.1 and 3.2 <sup>4</sup>:

---

<sup>4</sup>The technical information about camera parameters, function and setting are collected from Point Gray website, documents, Triclops software development kit (SDK) and Flycapture application programming interface (API) references.



**Listing 3.1 Bumblebee2 Stereo parameters**

1. **Stereo mask (matching window):** is a square mask (or the aggregated window  $W$  that surrounds the centre pixel at position  $x, y$ , (Equations 3.7, 3.8, and 3.9)) from the neighbourhood pixels used to perform the matching between the stereo images. The size of the mask is specified by the user. Large mask size produces dense and smooth depth maps but the depth discontinuity's position is not precise. Small masks produce sparser and more noisy depth images, but better localization of depth discontinuities. The mask sizes must be odd numbers (PointGray, 2012).
2. **Edge mask:** is an optional filter used to generate the edge images from the rectified images which are used for pixel matching. Then, the stereo matching is performed on the change in the brightness rather than the absolute values of the pixels.
3. **Minimum and maximum disparity:** These parameters are defined as depth of field of the stereo image, where only disparity values between the minimum and maximum disparity will be processed. Minimum and maximum disparity define the range of pixels that the stereo algorithm searches to find the best match. A disparity of zero assigns an infinitely far away object. Maximum disparity defines the closest position of an object that can be measured.

**Listing 3.2 Bumblebee2 Validation parameters**

1. **Texture validation:** Determines whether there is enough texture to make the match between a bunch of pixels from the two images. The threshold of this parameter allows matching algorithm to tune the texture based rejection pixels.
2. **Surface validation size:** This parameter is used to set the minimum number of pixels that a surface can be covered and still be considered valid. It works as a filter to remove spikes caused by feature mismatches between the left and right images. The size of removed spikes depends on the value that is set to this parameter.
3. **Surface validation difference:** This parameter sets the maximum disparity difference between two adjacent pixels, that allows the two pixels to be considered as a part of the same surface.
4. **Back and forth:** Verifies the match chosen in one image which should be identical regardless of whether the left or right image is used as the reference image.

### 3.4 Cotton plants experiment setup

An experiment to capture the colour and disparity images of 16 cotton plants was implemented. The purpose of this experiment was to create a database of cotton plant images (colour/ disparity) from a stereo vision sensor at different growth stages and semi-structured outdoor environments under varying light conditions (sunny, cloudy, and shady). These images can be used to enhance automatic segmentation of the plant parts using depth properties.

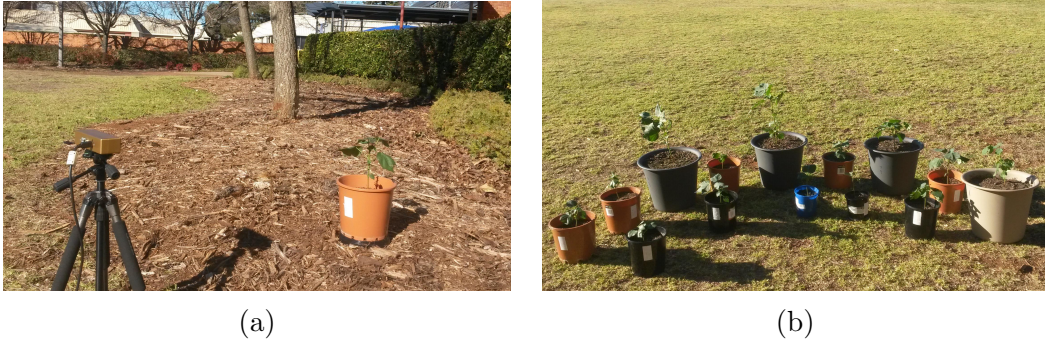


Figure 3.3: (a) Stereo vision camera during image capture. (b) Cotton plants at an early growth stage

Cotton plants were planted in April 2014 in the greenhouse. Eight data sets of images were captured during the winter and early spring of 2014 for different growth stages at outdoor environments of varying illumination conditions. The images were captured from two labeled sides of the plant (to offer different leaf orientation) and from a distance of between 0.85 - 1.25 m depending on the plants' height and size. For each growth stage of cotton plants, two image sets were taken under different illumination conditions. The main illumination conditions considered in this study are sunny (four data sets), shady (three data sets) and cloudy (one data sets). The images were captured with  $600 \times 800$  pixels to offer more details about plant parts. The Triclops software development kit (SDK) and FlyCapture (API) programming

functions were developed under Microsoft Visual C++ to capture the data sets of plant images using an 8-bit RGB colour stereo vision camera.

### **3.5 Evaluation of disparity maps for a wide range of parameters**

The disparity maps were evaluated for their ability to produce in depth information for plant parts. The purpose of this evaluation was to find the optimal combination of disparity map parameters that can fulfill the following criteria:

1. An accurate and smooth depth information for the region of interest of plant parts that focuses especially on leaves.
2. Minimisation of noise in the disparity images.
3. Resulting in a disparity map that has smooth depth information about plants parts and at the same time has an accurate depth discontinuity of leaves' boundaries. A trade-off between increasing the window size of matching function and using other stereo and validation parameters (Listing 3.1 and listing 3.2) is required.

The quality of disparity map depends on the setting of stereo and validation parameters. These parameters need to be adjusted for the best combination of values to produce good quality disparity images that coincide with all desired image criteria. Therefore, the evaluation of the disparity map is a qualitative evaluation, meaning it depends on the user requirements and it is not dependent on a constant metric.

There are a wide range of stereo and validation parameters. Different settings of these parameters produce different qualities of disparity images. Table 3.1 shows the ranges of these parameters. The ranges of these parameters were considered during the cotton plant experimentation. The disparity images for a wide range of parameters were captured. Following image capture, the disparity maps were inspected for parameters selection and to narrow their range for optimal combinations based on qualitative evaluation for disparity images.

The setting of disparity range is inversely proportional to the distance from the camera to the objects of interest. In that sense, the objects that are closer to the camera have a larger disparity range. Through inspection, it is found that keeping the minimum disparity at 0 and increasing the maximum disparity to 240, produced the required result to cover the region of interest between the camera and the plants thereby allowing for disparity in differing values.

Table 3.1: Stereo and Validation parameter ranges for the Bumblebee2 camera.

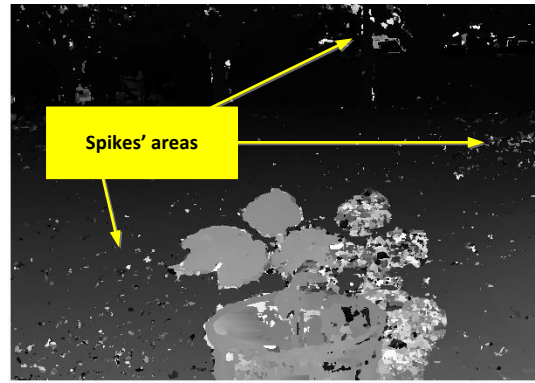
Parameter Type	Parameter name	Range values	Step of increment
Validation parameters	Surface difference	0.0 - 3.0	1.0
	Surface size	0 - 400	100
	Texture validation	0.0 - 4.0	1.0
Stereo parameters	Stereo mask	1 - 23	2
	Edge mask	1 - 11	2

The next step is to set the stereo mask parameter. The setting of this parameter controls the size of the sliding SAD window used to find matching points between the left and right images. The stereo mask was incremented by two values in each step which is ranged from 1 to 23. The small window size produces sparse and noisy disparity images but better localization of depth discontinuities. Larger window sizes smooth over small gaps in the disparity image but will also smear

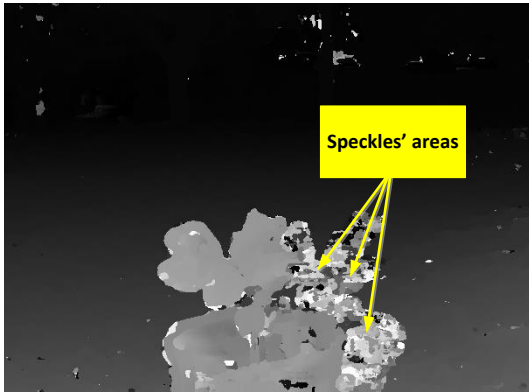
object boundaries (Figure 3.4d). Figure 3.4 presents disparity images with different stereo mask settings. It was observed that a stereo mask of size 7 (Figure 3.4b), is a good compromise for this parameter which produced disparity maps with adequate details. A stereo mask greater than 7, can cause blurred images with inaccurate leaf boundaries (Figure 3.4c and 3.4d). The block based matching method produced a “speckles” area near and behind the boundary of the plant (Figure 3.4) as the matching window catches the foreground (plant) on one side and the background (soil, grass) on the other side (Bradski and Kaehler, 2008).



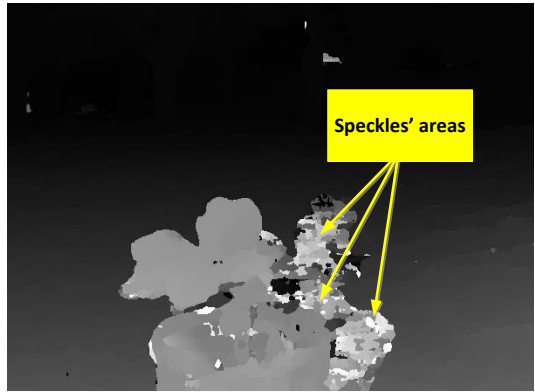
(a) Colour image



(b) Stereo mask= 7



(c) Stereo mask= 11



(d) Stereo mask= 17

Figure 3.4: Presents different settings for the stereo mask parameter. (b) The disparity map has noise “spikes” in the background and an accurate depth discontinuity for leaves’ boundaries. (c) and (d) have smooth depth and less spike areas in the background, but blur depth discontinuity for leaves’ boundaries. All disparities have a “speckles” area behind the plants.

The use of validation parameters such as surface and texture validation can enhance the accuracy of the disparity maps. The validation parameters have been adjusted in parallel with stereo mask parameter. A preliminary test was implemented to select suitable values of validation parameters including surface and texture. The surface validation is a method used to validate regions of disparity maps based on an assumption that they belong to a physical surface in the image. Two parameters were assigned to implement this task: Surface difference and surface size. The value of surface difference is used to assign the maximum value of disparity difference between two adjacent pixels, that can allow them to be considered as a part of the same surface. The size of the resulting segmented region depends thus on this difference. Larger differences produces larger regions. The value of this parameter should be greater than zero and range from 0.0 to 3.0 (PointGray, 2012). The setting of value zero can produce a blank disparity image, while an acceptable result can be observed with values ranging from 1.0 to 3.0.

The surface size parameter is used to remove noise from the disparity image by segmenting the disparity image into the connected regions according to the threshold value assigned to this parameter. The surface size works as a filter to reject spikes noise, in which any region less than the threshold value is suspected and removed from the disparity image (PointGray, 2012). A large threshold value means fewer regions will be accepted and the lower the threshold, the more surface will be accepted. The threshold values range between 0 and 400 pixels (Table 3.1).

Similarly, texture validation parameter determines whether there is enough texture for the best correlation between a bunch of pixels from the two images, which filters areas without enough texture for reliable matching. The threshold of this parameter allows tuning the texture-based rejection of pixels. The values range from 0.0 (no rejection) to 4.0 (complete rejection) but a good operating range is between 0.0 and

2.0 (PointGray, 2012). High texture threshold values may result in a blank disparity map. The default value of this parameter is equal to 1.0 (PointGray, 2012).

Figure 3.5 presents the disparity map for different settings of surface size parameter for one cotton plant image. Figure 3.5b illustrates the disparity map with stereo mask = 7, surface difference = 1.0, surface size = 0.0, and texture validation = 1.0. It is found that from the images, a small value of stereo mask produced a mismatch area as spikes noise. This noise can be reduced by increasing the values of stereo mask (from 7 to 9) and the threshold of surface size parameter (from 0.0 to 100) as shown in Figure 3.5c. Keeping the value of stereo mask equal to 9 and increasing the threshold value of surface size from 100 to 200, can improve the image and remove more spikes noise as shown in Figure 3.5d. It is observed that increasing the value of surface size more than 200 can eliminate more details from the image, therefore this parameter was set to 200 for the rest of the plants' disparity images.

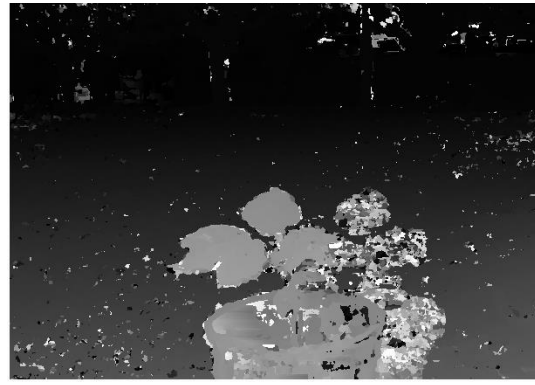
Afterwards, the value of surface difference parameters was examined. Figure 3.6 shows different threshold values of surface difference parameters which were set to 1.0 in Figure 3.6a and to 2.0 in Figure 3.6b. Other parameters were set as follows: Stereo mask = 11, surface size = 200, and texture validation = 1.0. The figure shows there is no significant difference between the two images. Larger values of these parameters (larger than 2.0) were not considered as they eliminate the small details of leaves, as larger differences produced larger regions. Therefore, this parameter was set to 1.0.

Figure 3.6c and Figure 3.6d present the effects of increasing texture validation values from 1.0 to 2.0, whereas the image of Figure 3.6c has more details about the leaves boundaries. The other parameters were set as: stereo mask= 13, surface validation =1 and surface size = 200. It was observed that some of leaf details start to disap-

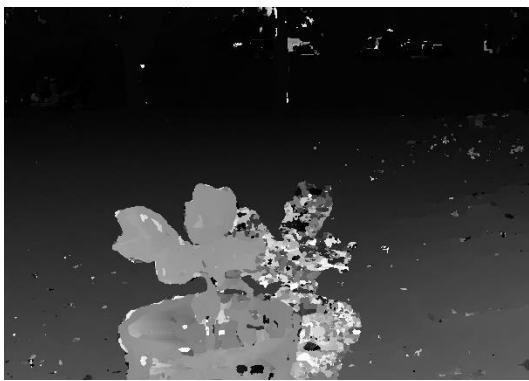




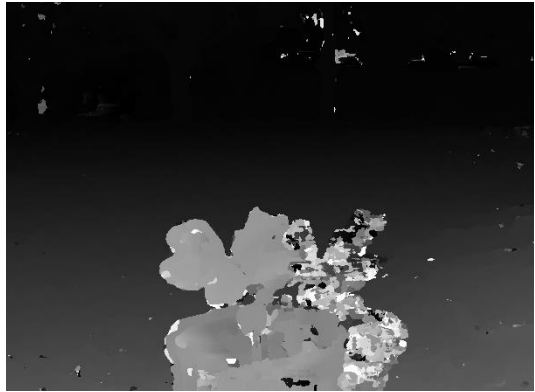
(a) Colour image



(b) Surface size = 0.0



(c) Surface size = 100



(d) Surface size = 200

Figure 3.5: Shows different settings for surface size parameters for the disparity images while the images have the same setting for surface difference = 1.0 and texture validation = 1.0. Stereo mask = 7 for (b). Stereo mask = 9 for (c) and (d).

pear when the threshold value of this parameter increased to 3.0. A high texture validation threshold might produce a blank disparity image because this parameter rejects any pixel to have texture below the threshold set value. Therefore, texture validation parameter was set to 1.0 to minimise the rejected pixels and accept more pixels in the disparity image. The backgrounds can affect the calibration of texture validation parameter. Different backgrounds mean different textures therefore, the setting of this parameter will need to be re-calibrated depending on the background of the images.

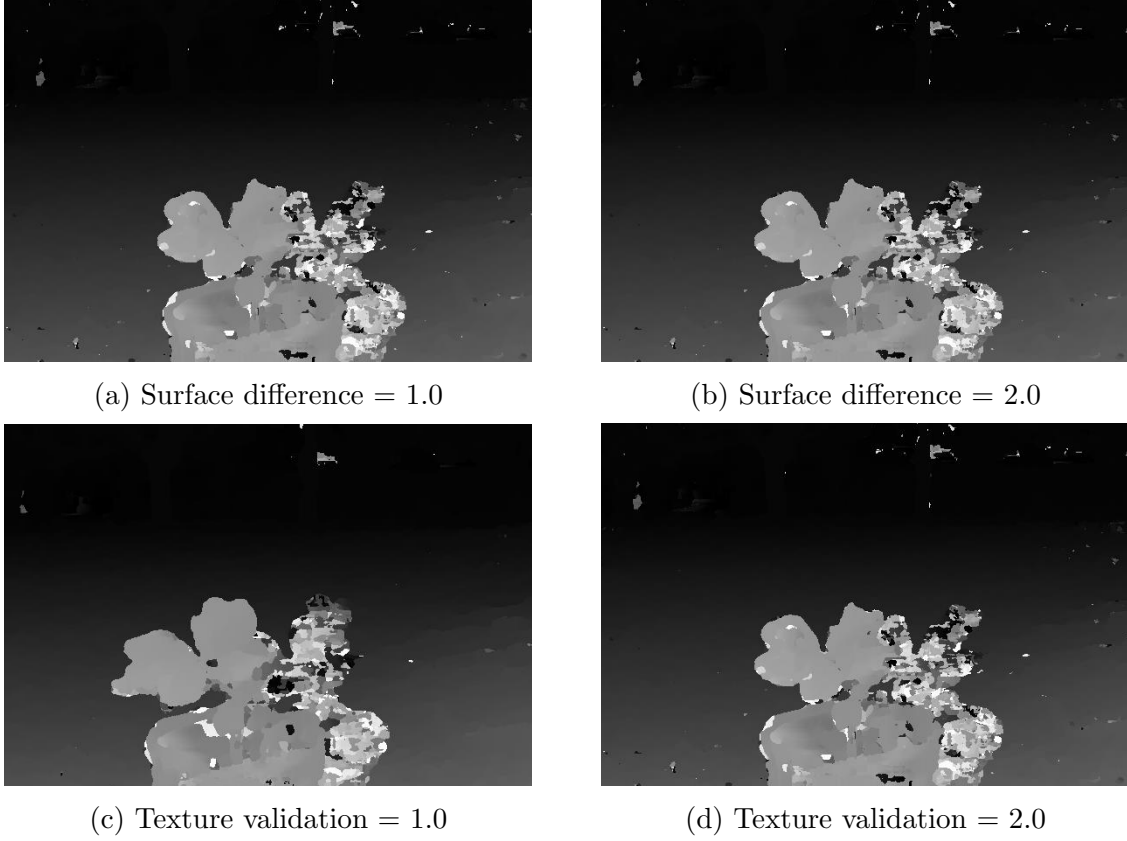


Figure 3.6: (a) and (b), present different settings for surface difference parameter. Both images have the same setting for surface size = 200, texture validation = 1.0 and Stereo mask = 11. (c) and (d), show different settings for texture validation parameter for the disparity images and have the same settings for surface size = 200, surface validation = 1 and Stereo mask = 13.

Figures 3.4, 3.5 and 3.6 present how the disparity maps were significantly enhanced by increasing the value of stereo mask. As stereo mask value increased, the mismatch area decreased. The disparity maps resulting from this setting have smooth and dense depth information but the boundaries of objects are inaccurate. As the proposed criteria relies more on accuracy of depth information rather than the dense of depth, edge mask parameters were introduced to improve the results. Edge detection is generally beneficial to stereo matching, although it introduces processing cost. Improvements can be evaluated for instance for different values of edge mask parameters in terms of number of valid disparities and matching with ground truth

(PointGray, 2012).

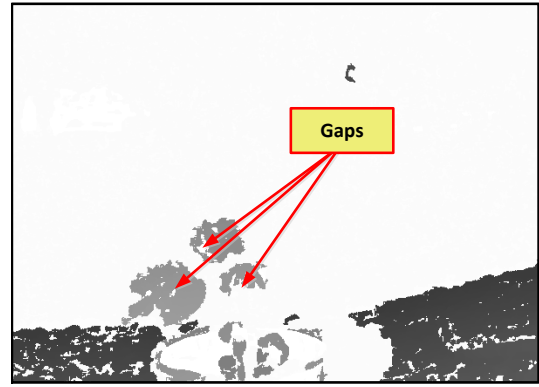
The edge mask was also examined to improve the accuracy of the disparity maps. The use of edge mask results in a smooth and an accurate depth information for the region of interest of plant parts, as matching processes were implemented in the brightness of pixels rather than the absolute values of image pixels. This parameter was tuned to narrow its range for a better combination with other parameter values. The edge mask was incremented by two for each step ranging from 1 to 11 (Table 3.1).

Figures 3.7 shows disparity maps with different settings of edge mask parameter. The setting of parameters were: Surface difference = 1.0, surface size = 200, texture validation = 1.0 and stereo mask = 7. The illustrations of Figures 3.7b, 3.7c and 3.7d present the effect of incrementing edge mask values with a fixed value of stereo mask. The images show edge mask equal to 7 can provide an acceptable result and there is no great difference between the images when this parameter was increased to 9 value. The disparity images of Figures 3.7 exhibit gaps in the leaves' areas. These gaps can be smoothed as the value of the stereo mask increased.

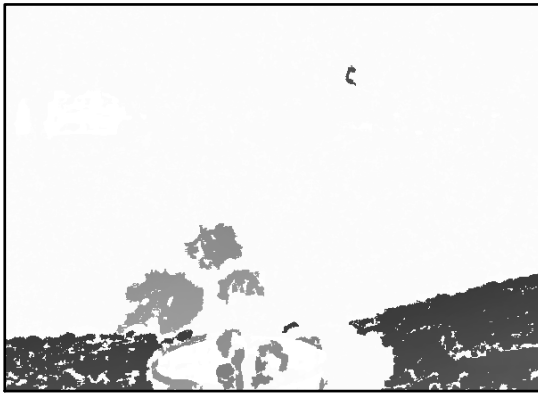
The stereo mask parameter was already examined, without turning on the edge mask, and it was found that increasing the value of this parameter (greater than 7) can blur leaves' boundaries. This parameter was examined again when the edge mask parameter was introduced with a combination of other parameters. It was observed, keeping the value of edge mask constant at 7 and increasing the value of stereo mask, has more impact on the images. Figure 3.8 illustrates the effectiveness of increasing the value of stereo mask on disparity images. Increasing the value of stereo mask smooths over small gaps of the disparity image and removes the spikes result from mismatched areas. However, a stereo mask greater than 17 can also



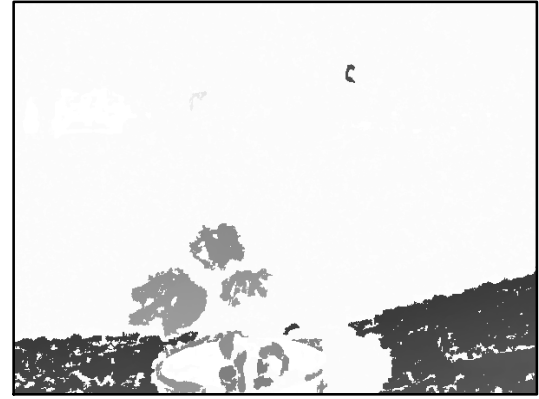
(a) Colour image



(b) Edge mask=5, Stereo mask=7



(c) Edge mask=7, Stereo mask=7



(d) Edge mask=9, Stereo mask=7

Figure 3.7: Present the effects of different settings of the stereo and edge mask parameters on the accuracy of the disparity maps.

smear leaf boundaries. On the other hand, the use of an edge mask also has a significant effect to enhance matching and remove the “speckles” area around the objects’ boundaries.

Figures 3.4 to 3.8 and their corresponding explanations present the logical order for selecting different setting values of stereo and validation parameters. Disparity maps with a wide range of these parameters have been captured to cover all the possible combinations. Then, the wide range of these parameters has been narrowed for optimal combination. To implement this task, six colour images of cotton plants (with their disparity maps) from different backgrounds and different illumination conditions were chosen. For each colour image, there are 32 disparity maps with

different settings of parameters. Thus,  $32 \times 6 = 192$  disparity maps were tested.

The 32 disparity maps consist of: twelve disparity maps that have different values of stereo mask; five disparity maps that have different values of surface size parameter and have the same value of stereo mask parameter; four disparity maps that have different values of surface difference parameter and share the same values of stereo mask and surface size parameters; five disparity maps that have different values of texture validation parameter and share the same value of stereo mask, surface size and surface difference parameters; six disparity maps that have different values of edge mask and share the same values of stereo mask, surface size, surface difference and texture validation parameters.

The first 32 disparity maps (of the first colour image) i.e. 32 from 192 maps were used to set the preliminary values of stereo and validation parameters. The remaining disparity maps (160 disparity maps) were used for performance assessment and cross validation. From all these disparity maps, a disparity map with an optimal combination of stereo and validation parameters was selected. The optimal combination of these parameters was applied for all disparity maps used to develop the proposed leaf segmentation algorithm.

It can be concluded that, after the qualitative evaluation of the stereo and validation parameters, there are three important and critical parameters that could significantly affect the quality of the disparity images which are: Stereo mask, edge mask and texture validation. The setting of other validation parameters is also required for better quality disparity images. The trade-off between these parameters is important for optimal combination. Table 3.2 shows different settings of stereo and validation parameters and their representative figures. The parameter combination shown in Figure 3.8f presents an optimal combination setting for all

### 3.5 Evaluation of disparity maps for a wide range of parameters 78

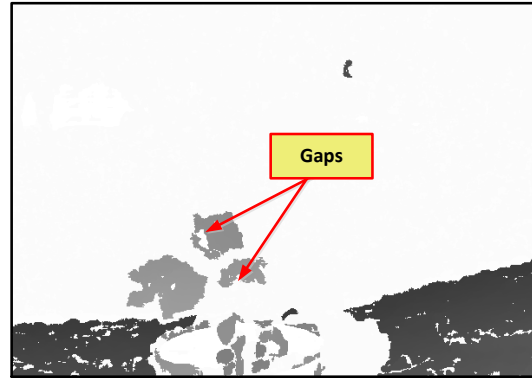
camera parameters. The set of these parameters can produce disparity maps which have: accurate and smooth depth values for the region of interest of plant parts (leaves), minimum spikes, and accurate depth discontinuity for leaves' boundaries. The setting of these parameters can fulfill the proposed criteria of the disparity images, therefore the setting of Figure 3.8f parameters was adopted for all cotton plant image data sets.

Table 3.2: The effect of changing the stereo and validation parameters on the disparity maps with their representative figures.

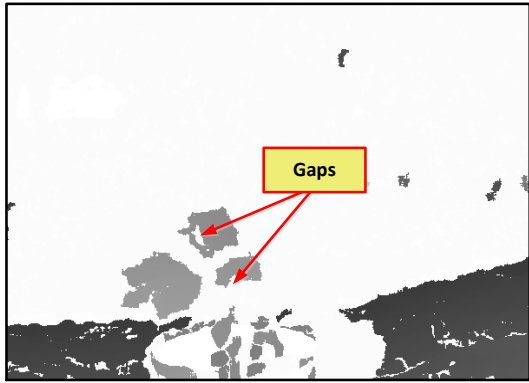
Stereo mask	Edge mask	Surface validation	Surface size	Texture validation	Presented by
7	0	1.0	0	1.0	Figures 3.4b & 3.5b
11	0	1.0	100	1.0	Figure 3.4c
17	0	1.0	200	1.0	Figure 3.4d
9	0	1.0	100	1.0	Figure 3.5c
9	0	1.0	200	1.0	Figure 3.5d
11	0	1.0	200	1.0	Figure 3.6a
11	0	3.0	200	1.0	Figure 3.6b
13	0	1.0	200	1.0	Figure 3.6c
13	0	1.0	200	2.0	Figure 3.6d
7	5	1.0	200	1.0	Figure 3.7b
7	7	1.0	200	1.0	Figure 3.7c
7	9	1.0	200	1.0	Figure 3.7d
9	7	1.0	200	1.0	Figure 3.8b
11	7	1.0	200	1.0	Figure 3.8c
13	7	1.0	200	1.0	Figures 3.8d
15	7	1.0	200	1.0	Figures 3.8e
17	7	1.0	200	1.0	Figures 3.8f



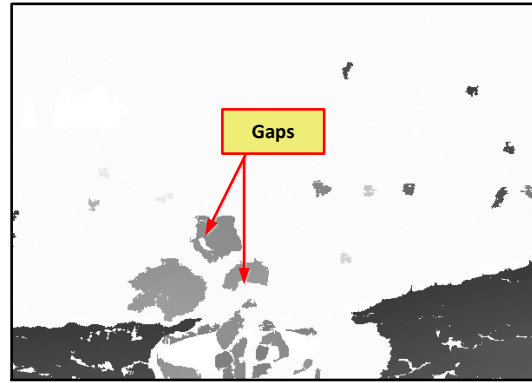
(a) colour image



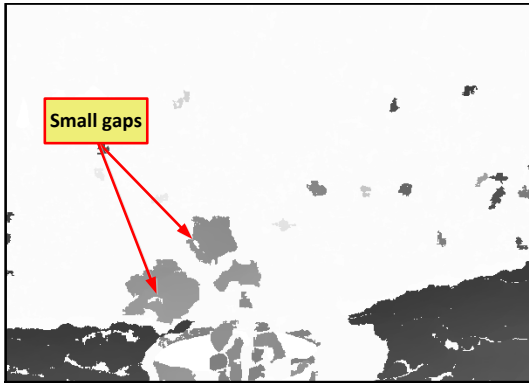
(b) Stereo mask=9, Edge mask=7



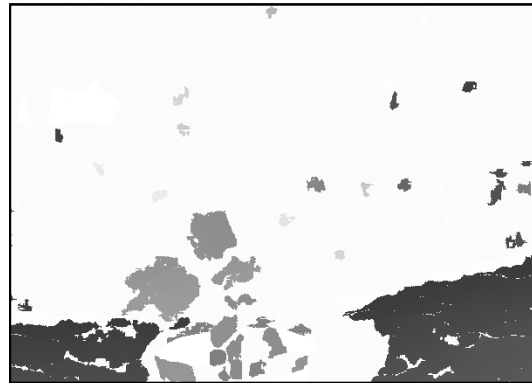
(c) Stereo mask=11, Edge mask=7



(d) Stereo mask=13, Edge mask=7



(e) Stereo mask=15, Edge mask=7



(f) Stereo mask=17, Edge mask=7

Figure 3.8: The effects of different settings of the stereo and edge mask parameters on the accuracy of the disparity maps. As the value of stereo mask increased the gaps' areas decreased.

---

## 3.6 Chapter summary

The fundamental idea and the essential processes of stereo vision techniques including camera calibration and rectification, triangulation and stereo corresponding processes have been presented in this chapter. The performance evaluation of a stereo vision sensor for producing depth information for plant parts, has been presented. The characteristics of the stereo vision sensor are explained and reflect the sensor's ability to produce depth information about plant parts in outdoor conditions. The disparity maps are very prone to error due to correspondence mismatch which can produce "spikes" and "speckles" noises. These noises could be eliminated using stereo and validation parameters. The cotton plants experiment setup and details has been illustrated and a wide range of disparity maps parameters were investigated. The specific functions of these parameters were explained. The effects of using these parameters to improve the accuracy of the disparity images were presented.

The disparity maps were evaluated in different settings of stereo and validation parameters. There were 32 disparity maps which were used to set the preliminary values of stereo and validation parameters and there were 160 disparity maps were utilised for performance assessment and cross validation. The best combination of these parameters was selected based on the qualitative evaluation of the examined disparity images. The optimal values of these parameters were applied for all disparity maps used to develop the proposed algorithms in this study. It was found that stereo mask, edge mask and texture validation are the most important parameters which could significantly affect the quality of the disparity images. The trade-off between these parameters is important for optimal combination. It was determined that, the setting of surface difference = 1.0, surface size = 200, texture validation



= 1.0, stereo mask =17 and edge mask = 7, provided the optimal combination which produced the desired outcomes for the disparity maps. The use of validation parameters and edge mask is optional and it depends on the applications' requirements. The evaluation of the disparity map was based on a qualitative evaluation and it was not based on a constant metric.

## Chapter 4

# Leaf segmentation and counting algorithm

---

## 4.1 Introduction

In this chapter, an algorithm has been developed to implement two tasks: segmenting cotton and hibiscus plant leaves from background foliage using image pre-processing and enhancement techniques, and counting and separating between the boundaries of overlapping leaves using depth discontinuity criteria. The algorithm uses depth, colour and shape properties to address the similarity in colour between neighbouring leaves, different perceived shapes of leaves (due to varying leaf orientations) and the presence of small leaves as well as older, larger leaves within the one image. The algorithm also addresses the additional complexity of larger leaves being non-coplanar. Larger leaves form a 3D structure with distinct depths across different lobes on the same leaf, compared to small leaves which are typically planar.

This chapter is organised as follows: the initial inspection of cotton and hibiscus plant images is illustrated in Section 4.2. The segmentation process designs are illustrated in Section 4.3. An image pre-processing stage was developed and applied to segment plants from foliage background and other parts of the plant and presented in Section 4.4. An segmentation method called Depth Discontinuity Segmentation (DDS) was developed based on depth difference in order to segment some complex images with touching or overlapping leaves (described in Section 4.5). The DDS applies three main techniques: beginning with the removal of noise pixels from the disparity map in Section 4.5.1; Then, two techniques which segment leaf area depending on global and local discontinuity in depth gradient are presented in Sections 4.5.2, and 4.5.3 respectively. A method that extracts a geometrical plane from the segmented leaf and presented in Section 4.6.

## 4.2 Initial image inspection and evaluation

From the visual inspection of the plant images, hibiscus has a clear structure where the number of branches and leaves can be visually counted. By contrast, the cotton plant images have a more compact structure in which individual leaves are not as clearly discernible. Plants' images with developing canopies consist of leaves that overlapped with other leaves, with a greater number of occlusions occurring on plants with denser canopies. This problem is increased with the late growth stage of plant. In addition, plant images exhibit different leaf size. Small leaves are difficult to distinguish by visual inspection, while large leaves exhibit characteristics that include bending around each lobe of the leaf. Furthermore, leaf orientation affects the perceived shape of the leaf which can provide the adequate information for a positive leaf identification. Other issues such as overexposure, shadow and low illumination phenomena were observed for some images captured under natural environments at direct sunlight, shade and sunset conditions respectively.

The focus of this study is on segmenting leaves from the plant image, and detecting overlapping leaves in plant canopies as it affects the identification of leaf parts. Therefore, the developed algorithm is concerned with leaf overlapping issues and benefits from depth information to assist segmentation. Solving other issues such as eliminating the effects of the ambient illumination conditions on the segmented images, are beyond the scope of this study. The developed algorithm is applied first to selected cotton and hibiscus plants. Six images from cotton plants and two from hibiscus plants were chosen to show the algorithm development process. The cotton images were all captured outdoors in both sunny and shadow conditions, whilst the two hibiscus plant images were chosen in both indoor and outdoor conditions. Figure 4.1 shows the six cotton plants and two hibiscus plants selected.



Figure 4.1: Sample of cotton and hibiscus plants. (a), (b), (c) and (d) cotton plants in sunny positions. (e) and (f) cotton plants in shadow conditions. (g) and (h) Hibiscus plants in indoor (g) and outdoor (sunny) positions (h).

## 4.3 Algorithm design process

Figure 4.2 describes the main steps in the segmentation algorithm. The algorithm starts by receiving colour and disparity images from the stereo vision sensor. The first step of the algorithm is conducted in the image pre-processing stage to segment leaves from the background foliage and other parts of the plant using depth, colour, shape, and image enhancement. The segmentation of the plant from the background was implemented using depth information and RGB colour transformation. Subsequently, HSV colour transformation is used to isolate green pixels from other plant pixels. Image enhancement and the geometrical analysis of leaf shapes were used to filter and analyse the ROI. Ellipse shape criteria were used to effectively segment leaves from other parts of the plant. The segmented images resulting from this algorithm consist of plant leaves that are segmented from the background and from other unwanted plant parts such as stem and branches. However, there are still some leaves that are connected or overlapped to each other.

Some standard image processing techniques were applied to separate between the overlapping leaves such as erosion and dilation operators (Sonka, 1993). The output resulting from these techniques was far from the desired requirement due to the working principles for both techniques. Erosion shrinks image objects while dilation expands them. In addition, erosion and dilation operators require a different structural element to be defined for each different shape and size object in the image. As the proposed algorithm aims to segment and separate between the overlapping leaves from different sizes, the application of these techniques could work for some leaves, but small leaves were removed by the erosion operator and other leaves were connected by the dilation operator. Furthermore, these operators might deform leaf shape and some of geometrical information could be missed also.

Hence, these techniques are not useful for such applications and their results were not considered. With this in mind, another segmentation method has been developed named Depth Discontinuity Segmentation(DDS) to implement segmentation tasks. This method has been developed based on depth discontinuity and gradient criteria, and applied on image results from the image pre-processing stage to detect and separate touching and overlapping leaves. Figure 4.2 illustrates the main steps of the proposed segmentation algorithm.

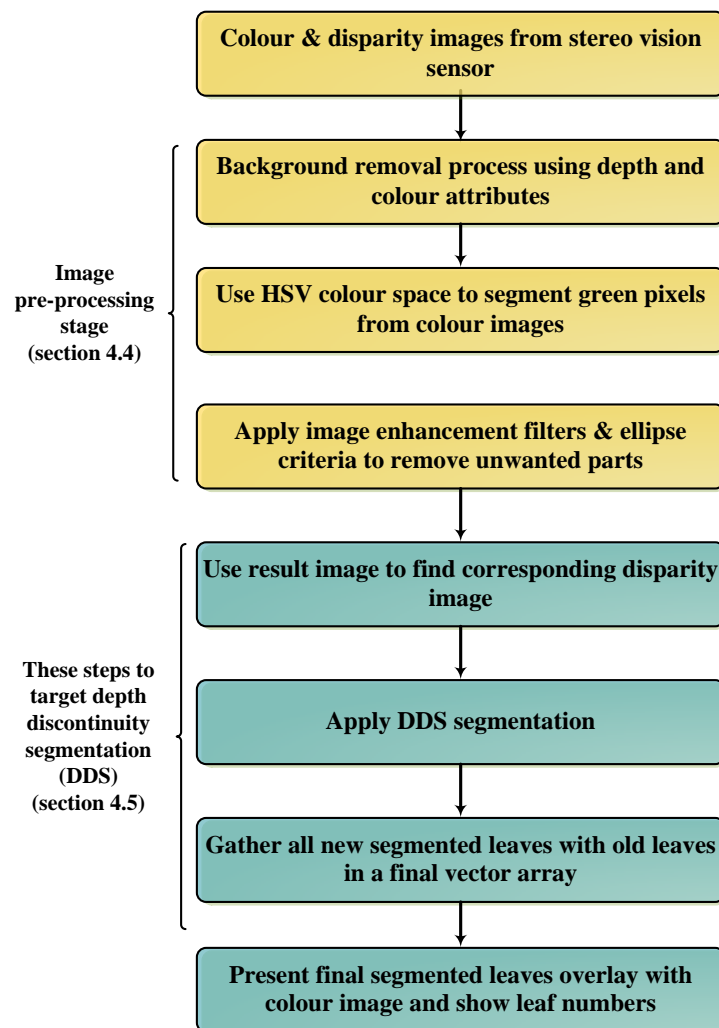


Figure 4.2: Leaf segmentation and counting algorithm.

## 4.4 Image pre-processing stage

The first stage of a plant segmentation algorithm is carried out using three segmentation steps including: Background removal using colour and depth information; image segmentation based in hue distribution; image enhancement and shape geometrical analysis. The following sections illustrate the algorithm steps and methodology.

### 4.4.1 Background removal process using depth and colour attributes

A disparity map to detect the plant Regions of Interest (ROI) from the background is used to formulate the algorithm in this instance. The disparity map obtained from the stereo vision camera presents foreground and a wide range of background objects such as foliage, sky, buildings, etc, as shown in Figure 4.3. To segment the foreground area from the background area, the following steps need to be applied:

1. A specific range of depth<sup>5</sup> was assigned as a threshold value and used as a mask to segment ROI from the original disparity map to produce a new disparity map as presented in Figure 4.4;
2. The R, G, and B colour channels were extracted from the colour image of Figure 4.1.

---

<sup>5</sup>The specific range means there are two values of depth threshold: minimum threshold, and maximum threshold, as the plant parts have different depth values with respect to the camera. These values of threshold were set only once because the images were captured from a constant distance between the camera and the plants (Section 3.4). The minimum threshold represents the closest parts of the plant while the maximum threshold presents the furthest parts.



3. The new disparity map was used as a mask for each R, G and B channel to segment the colour image from the background, the ROI of the colour image was found as shown in Figure 4.5.

After these steps, the procedures of background removal are completed. Another step is then implemented to segment plants which are presented in the following sections using colour, shape and depth properties.



Figure 4.3: Disparity map for the six selected cotton and hibiscus plants. (a), (b), (c) and (d) cotton plants in sunny condition. (e) and (f) Hibiscus plant in indoor and outdoor (sunny) conditions.

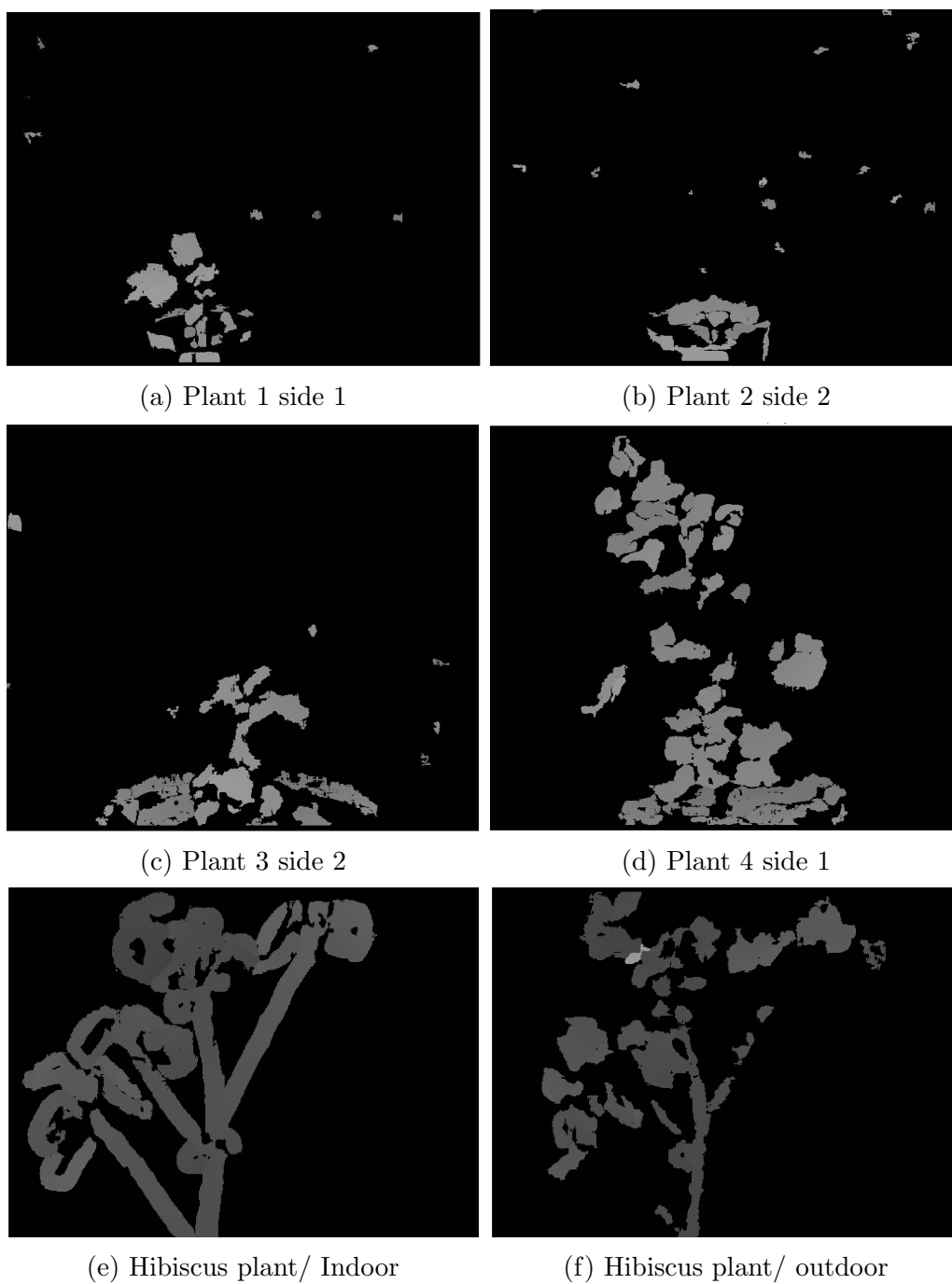


Figure 4.4: Filtered disparity map for the six selected cotton and hibiscus plants of Figure 4.1.

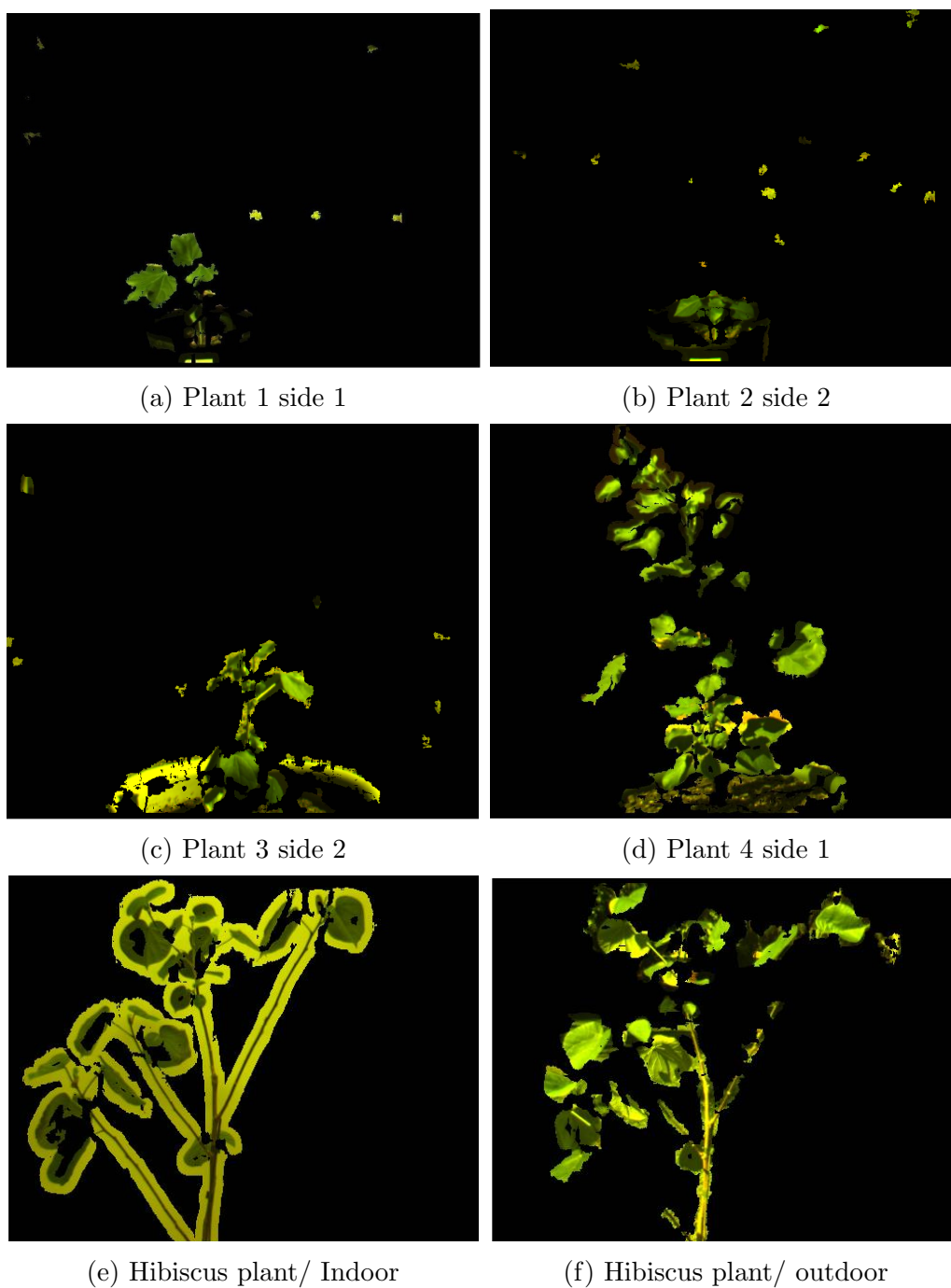


Figure 4.5: Colour image after depth mask for each of the R, G, and B colour channels for the six selected cotton and hibiscus plants of Figure 4.1.

#### 4.4.2 Image segmentation based on hue distribution

The colour images resulting from the depth mask are shown in Figure 4.5. The images show plant leaves, stem, branches, soil and pot. The HSV (Hue, Saturation, Value) colour space transformation was used to segment green from the images. The hue channel represents the colour, the Saturation channel represents the dominance of that colour and the Value channel represents the brightness (the darkness or the lightness) (Meskaldji et al., 2009). The HSV colour space is less affected by the ambient illumination at outdoor conditions compared to the RGB colour space and can retain the colour information despite differences in illumination conditions (Bjurstrøm and Svensson, 2002).

Green leaves under outdoor conditions can exhibit different illumination which can result in different hues (ranges) of green colour (light and dark green). Since HSV colour transformation can separate out the luminance from the colour information (chromaticity) (Sural et al., 2002), the Hue channel was used (from the three HSV channels) to pickup the greenness of leaves under a variety of outdoor illumination conditions and phenomena such as overexpose and shadow. The Saturation and Value channels were not used to accept different hues (ranges) of green. The distribution of green pixels can be calculated by applying image histogram method on the hue channel (Figure 4.7). Hue distribution values were used to segment the ROI of green by using the following method:

**Listing 4.1 Image segmentation using hue distribution**

**Step 1** Plot Hue distribution chart.

**Step 2** Calculate mean and standard deviation values.

**Step 3** Calculate upper and lower hue threshold values for green pixels.

**Step 4** Select the pixels from the hue channel between these threshold values.

Figure 4.6a presents the hue channel of HSV colour space. Figure 4.6b shows the histogram of normalised Hue values distribution for plant 1, side 1 as implemented in Step 1. The figure also shows the maximum bins of the histogram distribution are within the range of green in the hue channel. The normalised hue means the scale of the hue distribution chart is normalised from 360 to 1 value. Figure 4.7 shows the histogram of the normalised hue value distribution for all six selected plants in Figure 4.1.

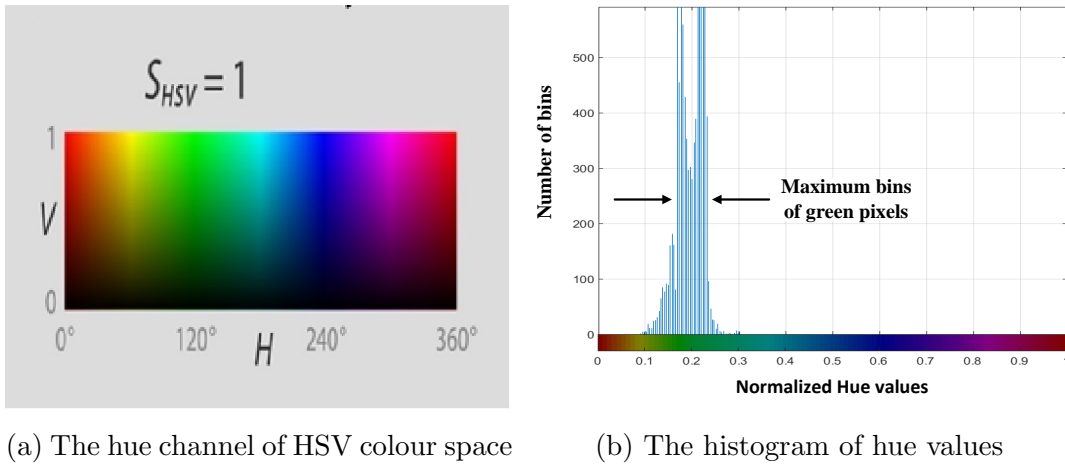


Figure 4.6: HSV colour Transformation for Plant1 side 1 of Figure 4.5

The mean ( $\mu$ ) and standard deviation ( $\sigma_h$ ) values of the the normalised hue distribution are determined. These values would vary from image to image depending on the histogram distribution of the hue. The calculated  $\mu$  and  $\sigma_h$  are used to determine the upper and lower threshold value of the hue for green pixels using the developed equations, Equation 4.1 and Equation 4.2 (Step 3, Listing 4.1).

$$LH = \begin{cases} \mu + \kappa_1 * \sigma_h & \text{if } \mu \geq \tau. \\ \mu - \kappa_1 * \sigma_h & \text{Otherwise.} \end{cases} \quad (4.1)$$

$$UH = \mu + \kappa_2 * \sigma_h \quad (4.2)$$

where;  $LH$  and  $UH$  are the upper and lower threshold values of the hue distribution for green pixels, and  $\kappa_1$ ,  $\kappa_2$  and  $\tau$  are the initialisation parameters used to calibrate equations. The initialisation parameters need to be adjusted only once, as an initial setting for the algorithm. Prior to initialisation of these parameters, the upper and the lower threshold values of multiple hue distributions of plant images selected randomly from different data sets, were visually inspected and measured to be within the range of green in the hue channel. From this prior measurement, it was observed that values of  $\kappa_1 = 0.25$ ,  $\kappa_2 = 3$  and  $\tau = 0.19$  can effectively isolate foliage pixels as shown in Figure 4.8. With current settings for these values, only green objects will be identified whereas, the assumption was to segment green leaves from the cotton plant as the main focus of this research.

After the initial calibration of Equation 4.1 and Equation 4.2 parameters. The mean, standard deviation and the upper and the lower threshold values were adaptively calculated for each single plant image. Then, the pixels between the upper and lower threshold values of the hue distribution were selected to isolate the leaves pixels from other parts of the plant pixels. Equation 4.1 and Equation 4.2 were applied on eight sets of cotton plant images (252 images) under different illumination and environmental conditions and 20 images of hibiscus plants under indoor and outdoor conditions. The results shows the developed equations can reduce most of the unwanted pixels of pots, stem and other elements of noise present in Figure 4.5. However, minor noise still exists in the green image of Figure 4.8, and this is displayed more prominently in the binary image of Figure 4.9. Further steps are required to enhance images and remove non-leaf objects which are presented in the next section.

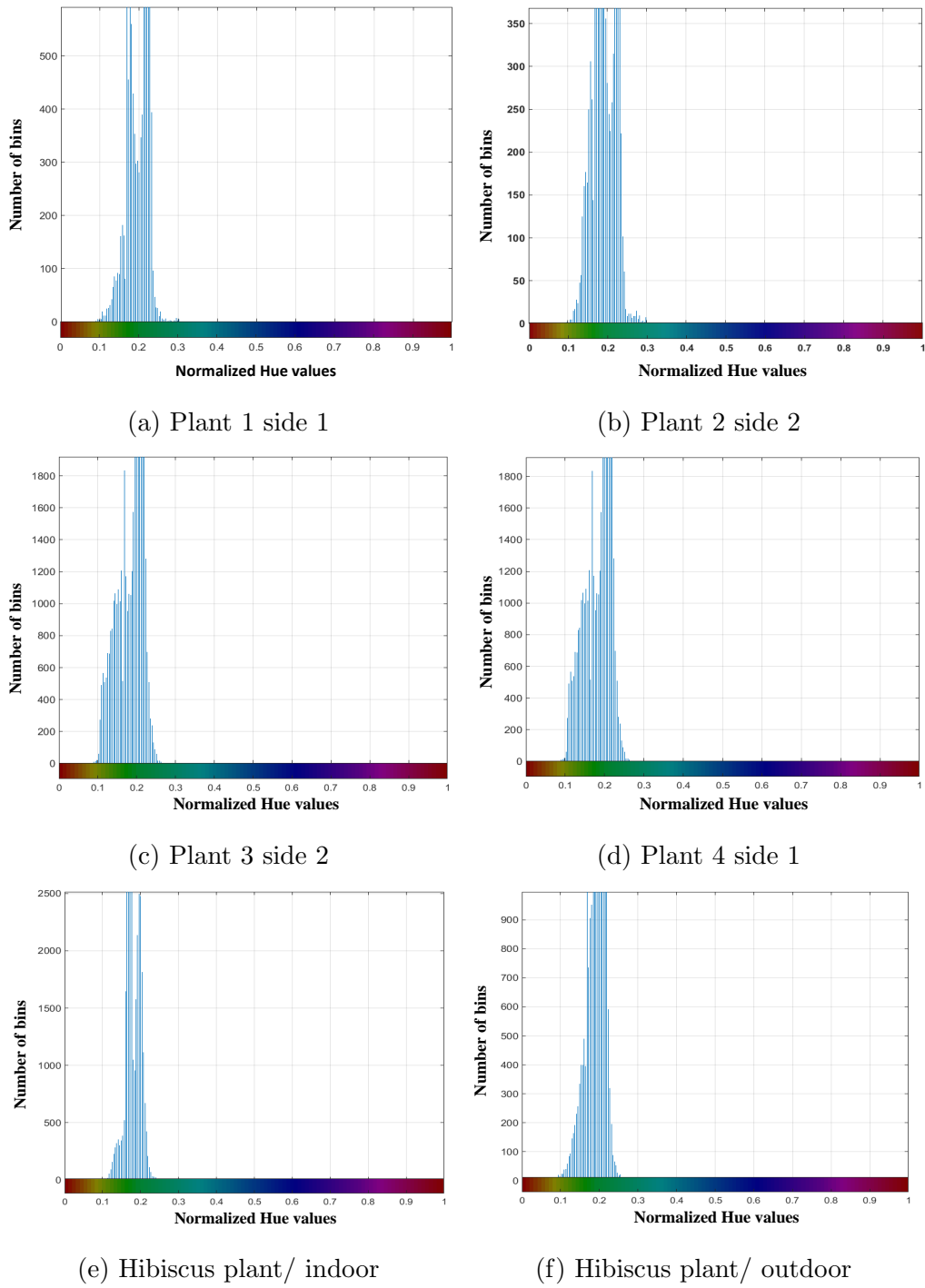


Figure 4.7: Histogram distribution of the hue channel for the colour images of the six selected cotton and hibiscus plants in Figure 4.1.



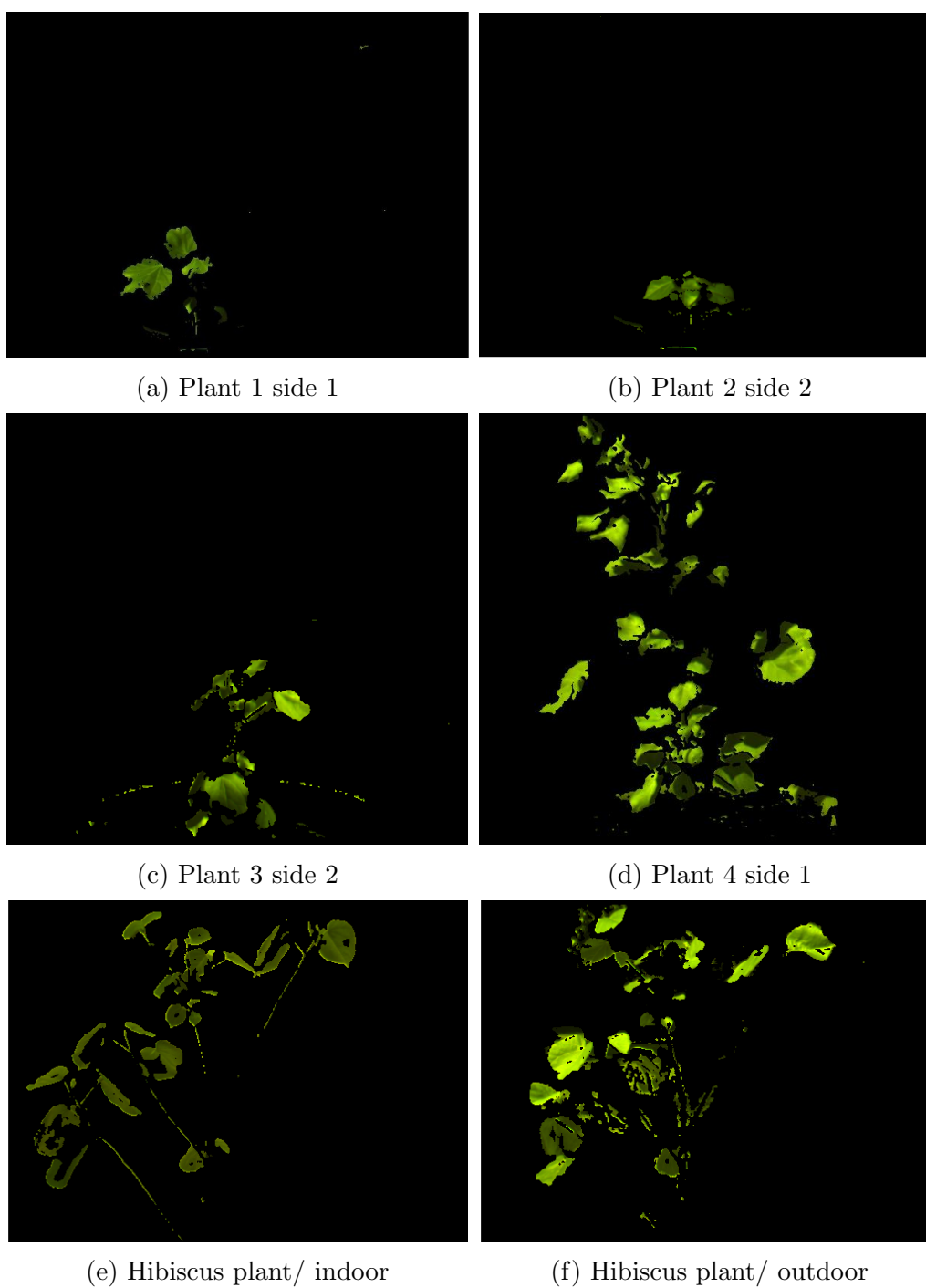


Figure 4.8: Result from HSV colour space & applying the developed equations for the six selected cotton and hibiscus plants in Figure 4.1.

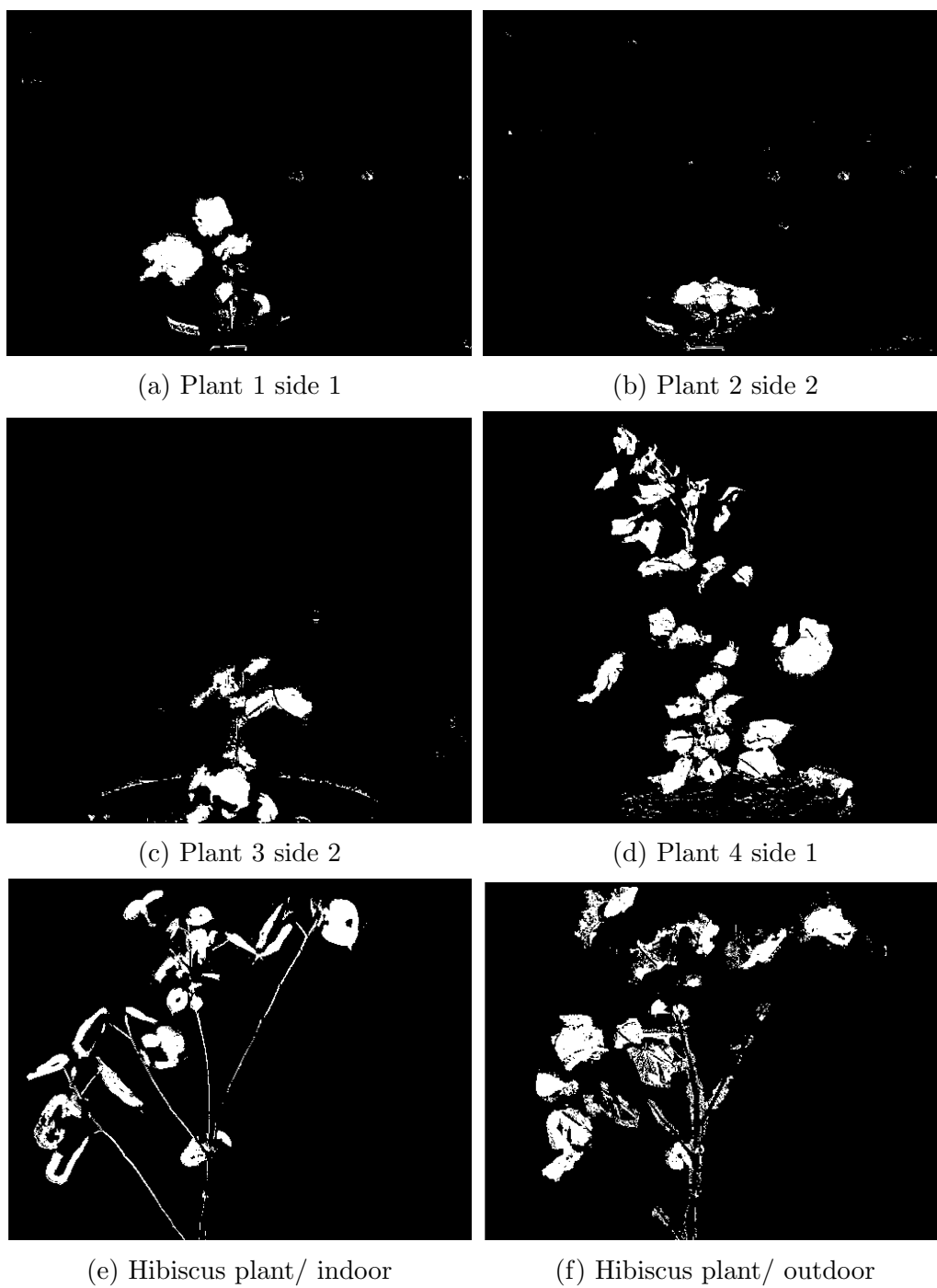


Figure 4.9: Binary image transformation for the six selected cotton and hibiscus plants in Figure 4.1

### 4.4.3 Image enhancement and shape geometrical analysis

Image enhancement processes can be implemented using different image processing techniques such image filters, regions and shape properties. A Median filter, (Lim, 1990), was applied by convolution with a  $(3 \times 3)$  kernel. This filter was employed due to its capability to simultaneously reduce noise whilst maintaining image edges (Nelikanti, 2014). The work principle of this filter is to calculate the median value in the  $3 \times 3$  neighbourhood around the corresponding pixel in the input image for each output pixel. Figure 4.10 shows the results images after using Median filter. The images show that most of the unwanted pixels, of Figure 4.9, such as pots' edges, stem and branch parts were filtered from the images.

The connected component and labeling algorithm, also known as the 'flood-fill algorithm' (Foley et al., 1982), was applied to detect the connected regions in a binary image. The desired outcome of each connected area is corresponding to one object or one leaf. This algorithm can also filter images from noise objects and confirm leaf objects according to the objects size. A suitable threshold value was assigned to the algorithm in order to accept leaf objects and remove the suspected non-leaf objects. Prior to initialisation of the threshold value, multiple plant images were selected randomly and inspected to discriminate between different leaf sizes. According to that, a 200 pixels thresholds' value was found to be an optimal value to retain plant leaves for early growth stages (i.e. dataset 1, 2, 3 and 4), and a 300 threshold value was found to be an optimal value to segment plant leaves for other growth stages (i.e. dataset 5, 6, 7 and 8). The objects below the threshold value were removed from the images. The images results from applying this algorithm are shown in Figure 4.11. The current number of objects presented by Figure 4.11 represents the initial estimation of leaf numbers in the image. Some images still have other objects such as parts of plant stem and branches therefore, further steps are

required to benefit from the geometrical analysis of leaf shape and region properties.

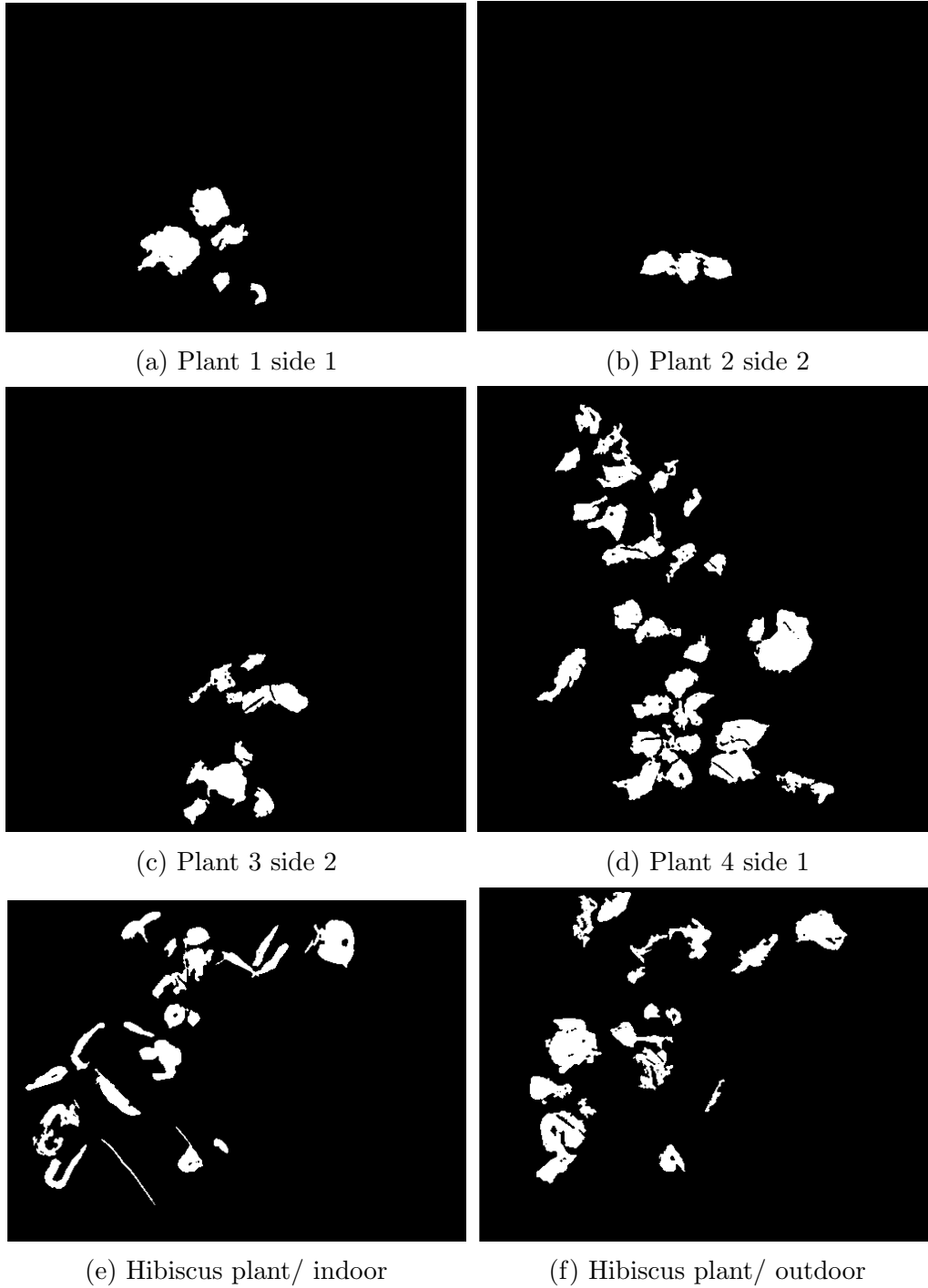


Figure 4.10: Median and size filter binary images for the six selected cotton and hibiscus plants in Figure 4.1

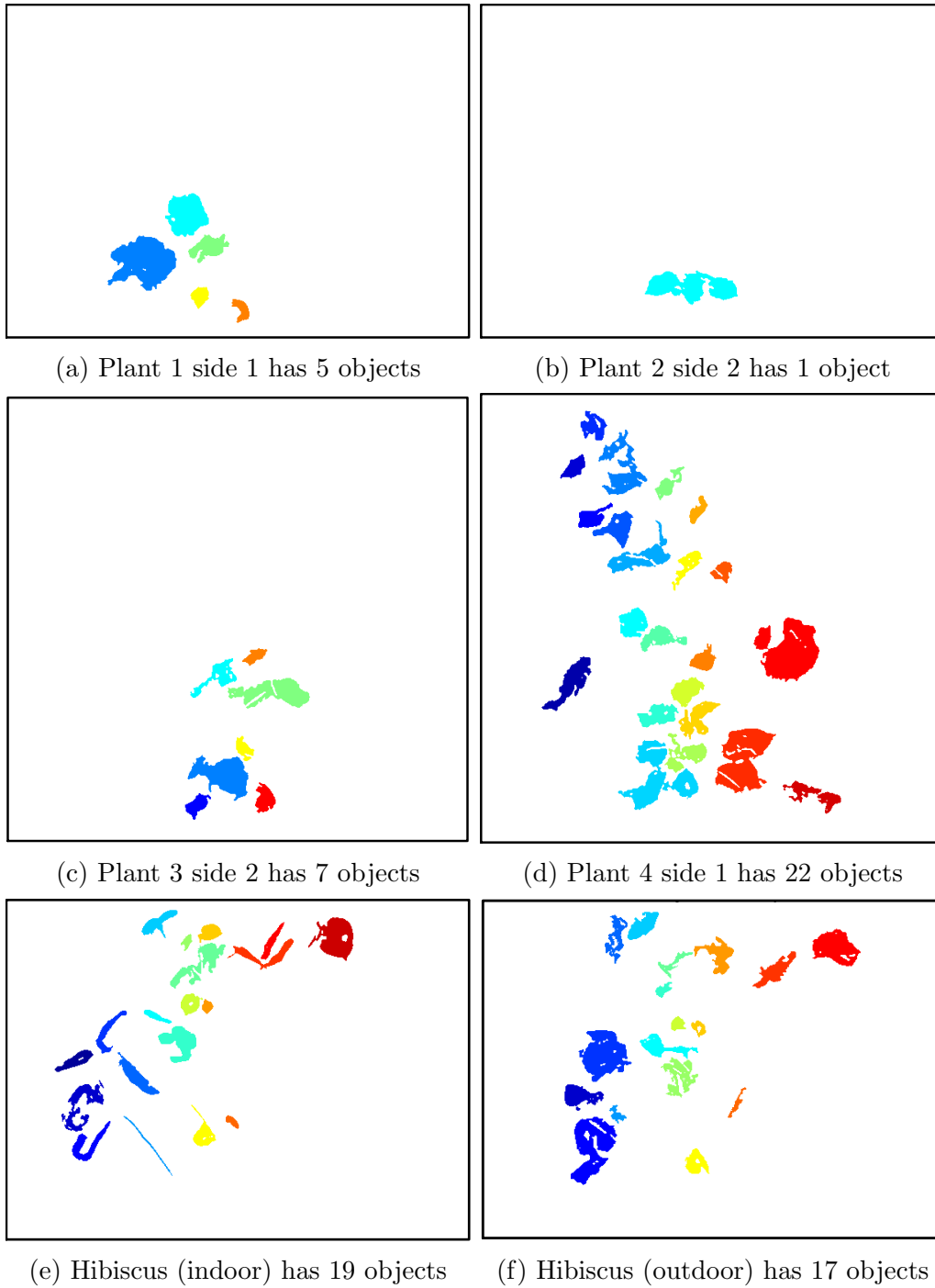


Figure 4.11: Labeled leaves with different colours for the six selected cotton and hibiscus plants in Figure 4.1

Shape is an important feature for characterising and identifying plant leaves in many studies. Here, the main concern is to segment the leaf from other parts of the plant even if the leaf is partially occluded or not facing the camera. Leaf contours with ellipse shapes are the most common method currently used to extract the important features of leaves (Valliammal and Geethalakshmi, 2011; Cerutti et al., 2013). In this sense, the geometrical measurements could be applied on plant leaves such as ellipse minor and major axis, and axis ratio (slimness)(Kadir et al., 2013). Therefore, the steps described in Listing 4.2 will be applied for each component (leaf/leaves) to segment the leaves from the stems.

**Listing 4.2 Shape geometrical analysis based on ellipse criteria**

- **Step 1** Calculate leaf major axis and axis ratio
- **Step 2** Apply threshold according to the major axis and axis ratio
- **Step 3** Find the corresponding disparity map
- **Step 4** Form a vector of multiple arrays, each array represents one leaf
- **Step 5** Counts the number of leaves
- **Step 6** Overlay the leaves with others and present the result

Prior to implementation of each step, an ellipse was fitted to each object result from applying connected component labeling algorithm. Then, the minor axis, major axis and axis ratio for each object in the image were measured. Following this step, the measured values are saved and investigated to calculate the maximum values of major axis and axis ratios for all plant leaves used in this study. These measurements were used to assign threshold values to discriminate between leaf and non-leaf objects using the following criteria:

$$MajorAxis \leq Th_1 \quad (4.3)$$

and,

$$AxisRatio = \frac{MajorAxis}{MinorAxis} \leq Th_2 \quad (4.4)$$

It is found that, objects that have a major axis greater than 190 and axis ratio more

than 5.5 can form a tall and very thin object. This object cannot be a leaf object. It could be a part of stem or branch, therefore it was removed from the image. These two values were assigned as threshold values for the developed criteria, meaning  $Th_1 = 190$ , and  $Th_2 = 5.5$ . The threshold values need to be set only once as an initial calibration. These values work effectively for all data used in this study in all instances. These values might not work with other types of plants having different leaf sizes (larger leaf sizes than cotton and hibiscus leaves). In that case, a new calibration is required for  $Th_1$  and  $Th_2$  parameters.

Figure 4.12 shows an ellipse fitted to each object in the binary image, for an image containing only leaf objects. Figure 4.13 shows the resulting binary images after using ellipse criteria. By comparing the two figures, it can be seen that the number of objects are the same for cotton plants and no object has been removed. However two objects were removed from both hibiscus plant images. These objects represented parts of a stem as shown in Figure 4.12.

The binary image resulting from ellipse criteria was used as a mask to implement Step 3 (Listing 4.2) to find the corresponding pixels in the disparity image as presented in Figure 4.14. Each leaf in the new disparity image was separated into a new array to form a new vector array involving all plant leaves (Step 4). The algorithm counts the number of leaves and gives the result for each plant (Step 5). Figure 4.15 presents each plant leaf in different colours overlying each other (to perform the first stage of the segmentation) as a result of Step 6. The figure also shows the connected/overlapped leaf areas. Figure 4.16 illustrates segmenting leaves overlying the original colour image. From Figures 4.15 and 4.16, only Plant 1 Side 1 (image ‘a’ of each figure) displays 100% segmentation accuracy using the steps developed thus far. By visual inspection, the other sample plants have a number of leaves which are segmented incorrectly due to the leaves touching or overlapping.

Hence, additional steps in the algorithm need to be developed to address touching and overlapping leaves.

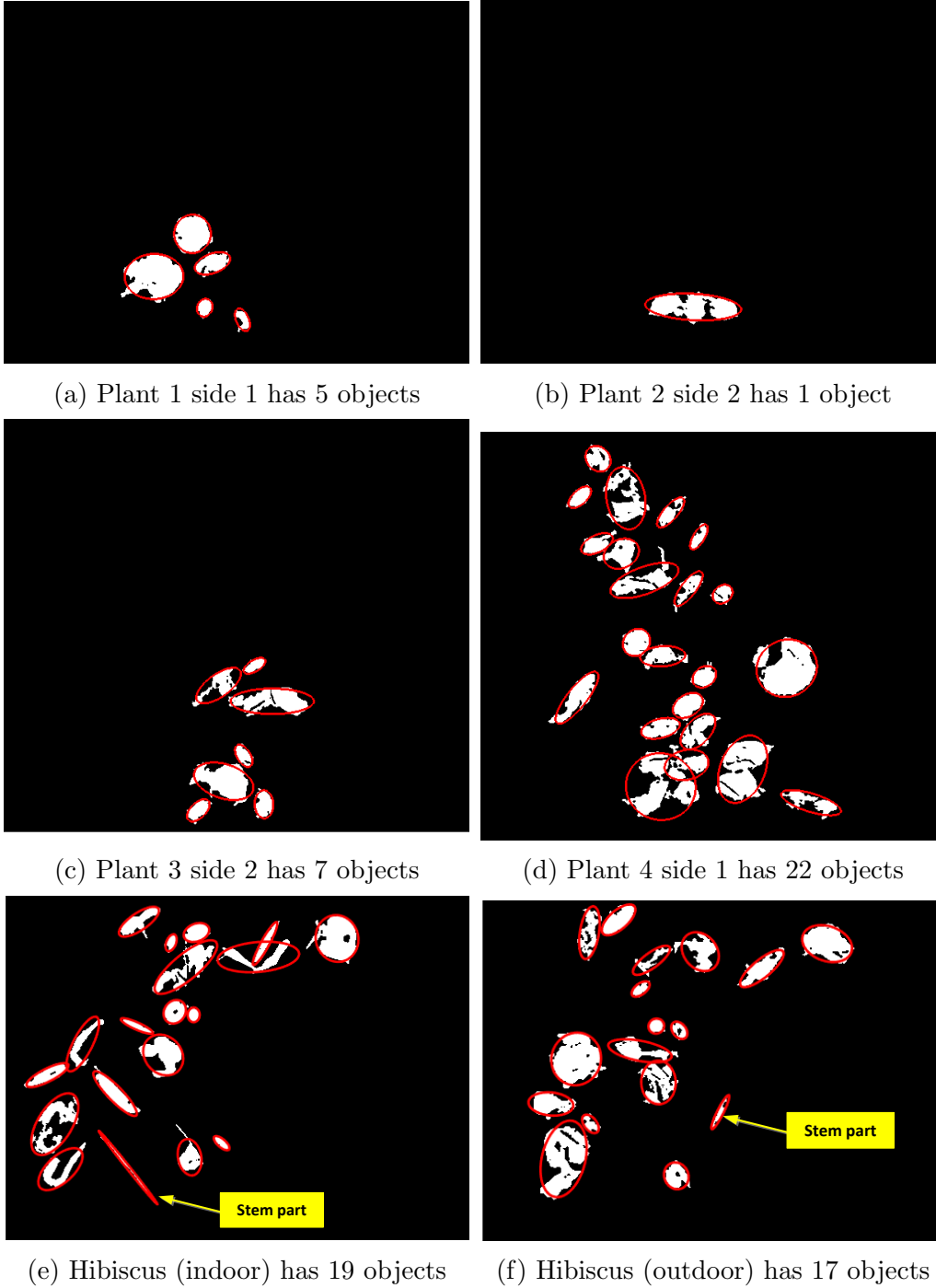


Figure 4.12: Ellipse fitted to each leaf (red outline) for the six selected cotton and hibiscus plants in Figure 4.1



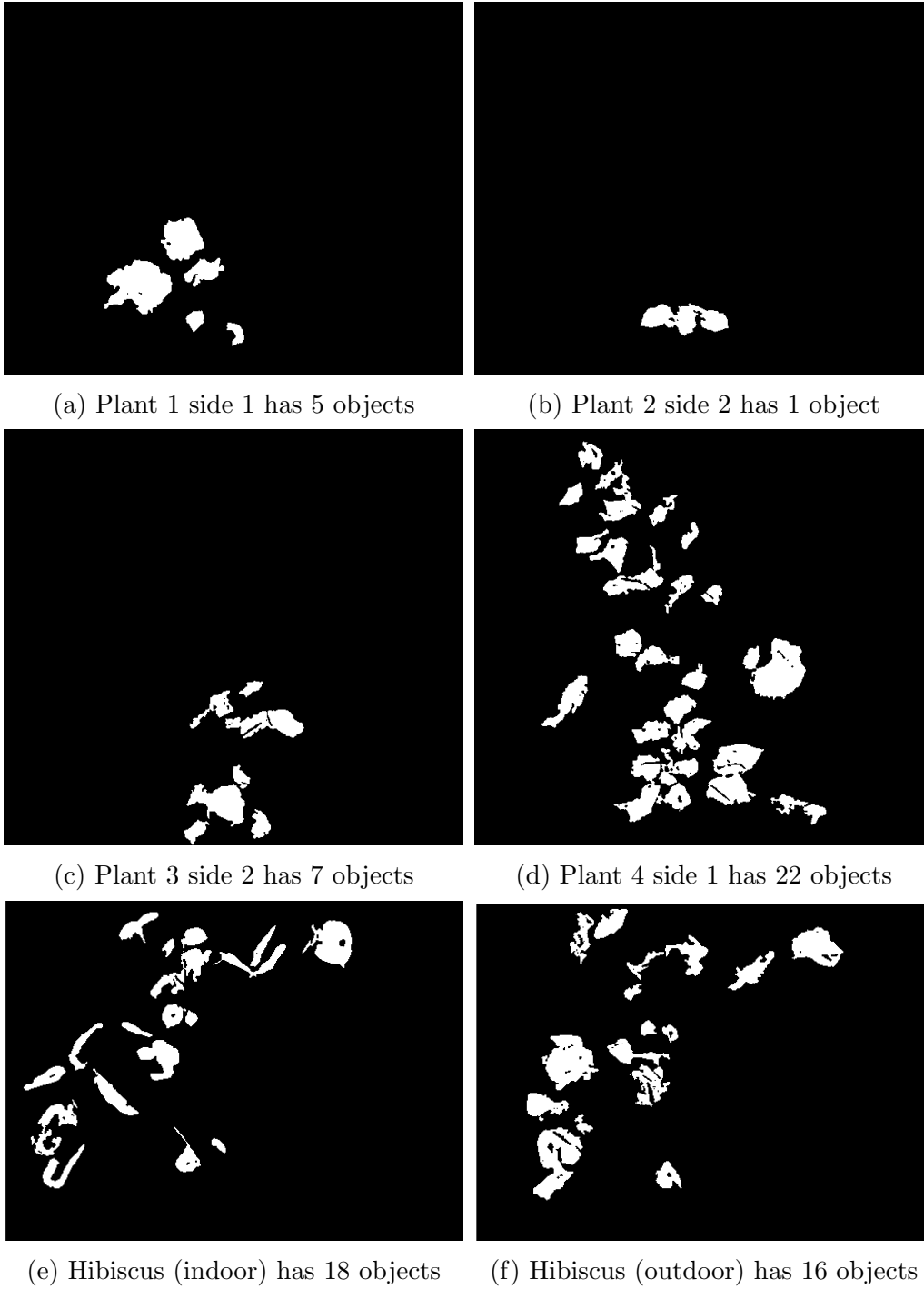


Figure 4.13: Binary images after the application of ellipse criteria for the six selected cotton and hibiscus plants in Figure 4.1. The number of objects for the hibiscus plant was decreased due to ellipse-fitted criteria.

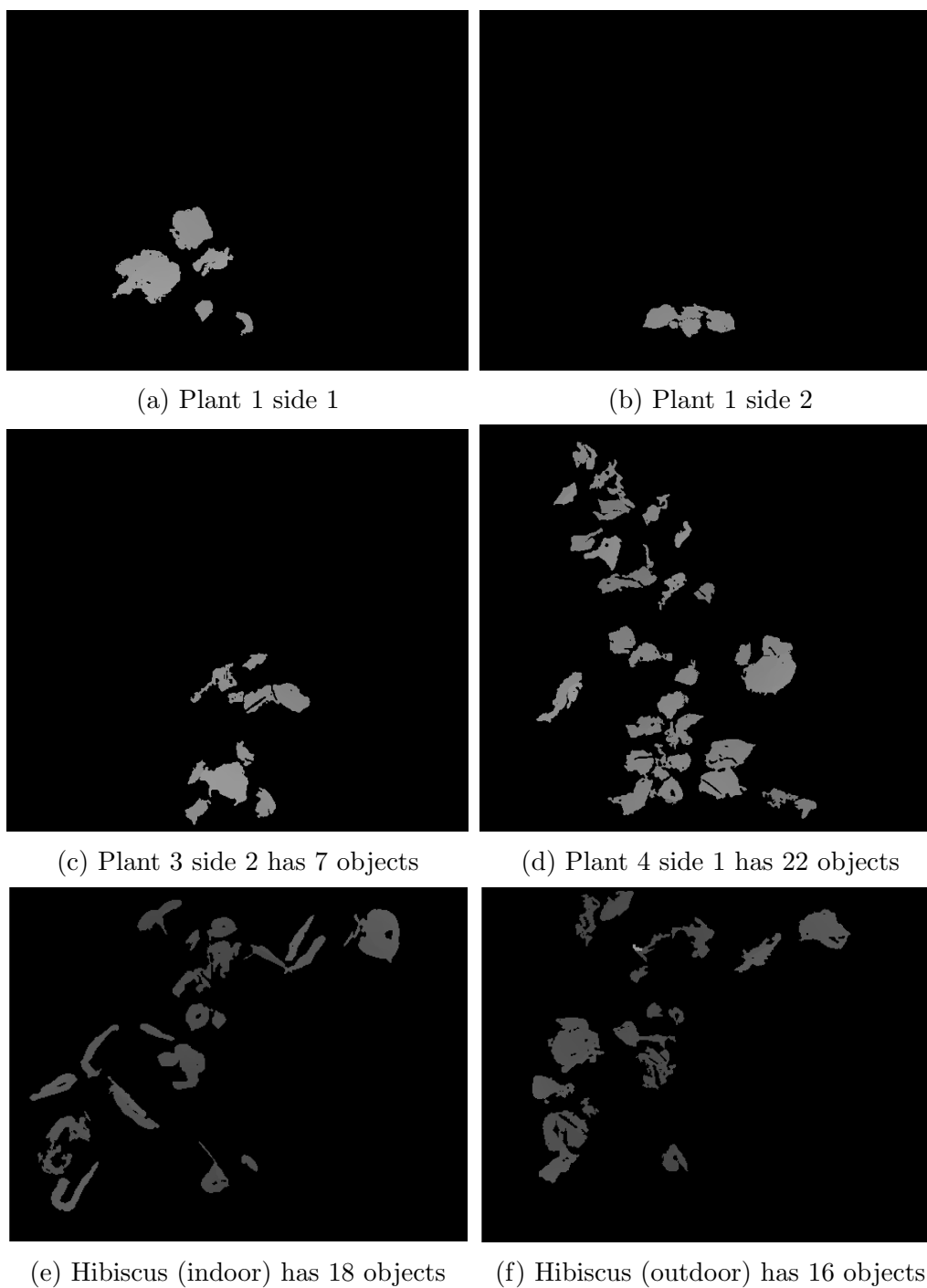


Figure 4.14: The equivalent disparity images after application of ellipse criteria for the six selected cotton and hibiscus plants in Figure 4.1

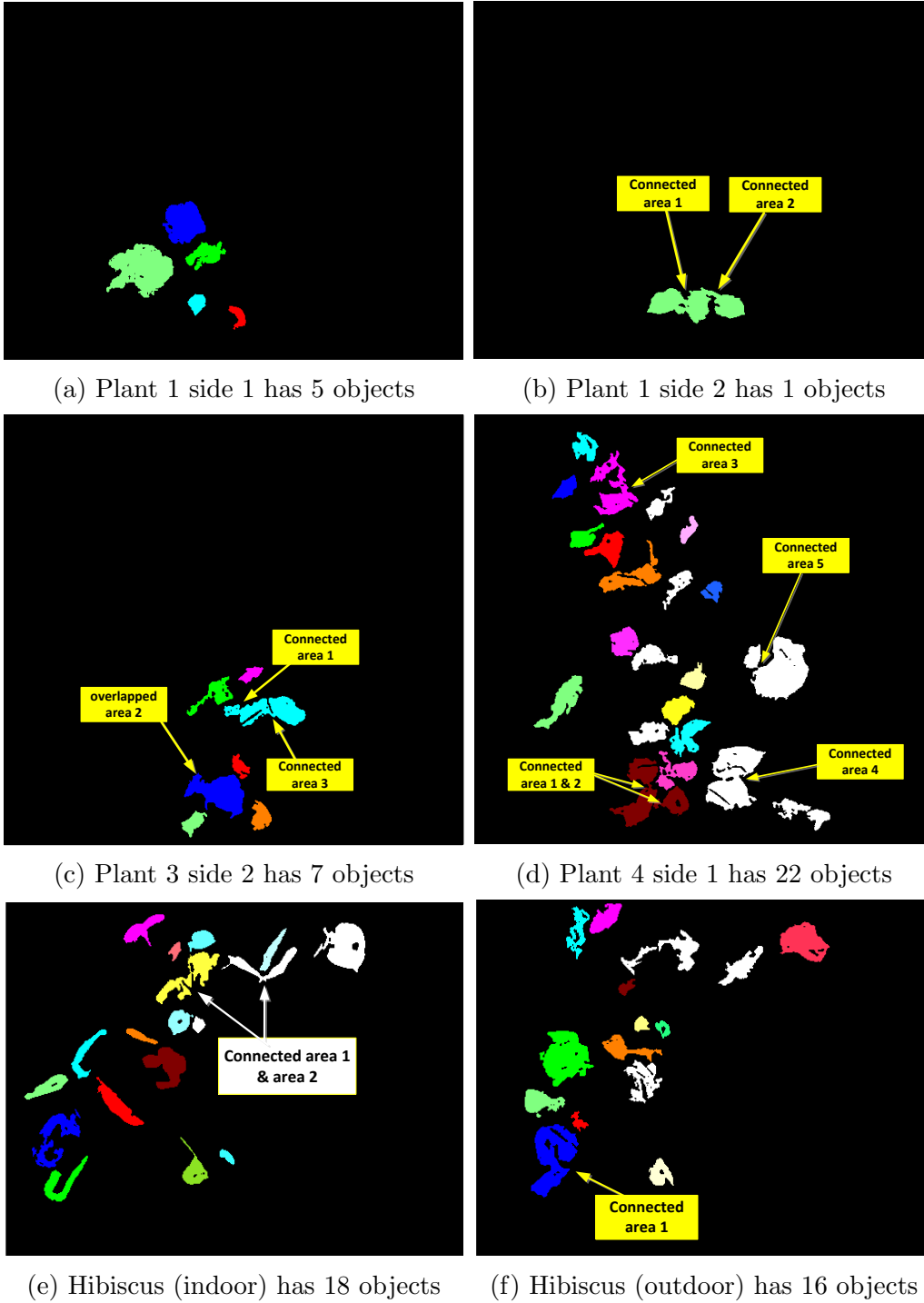
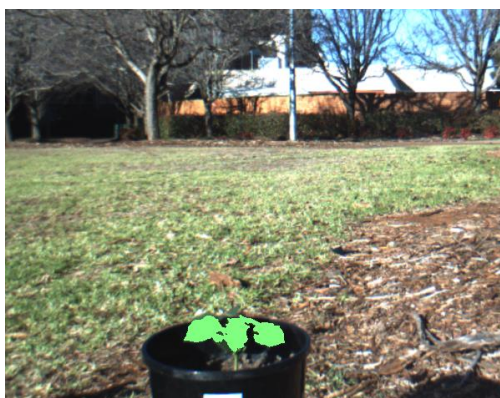


Figure 4.15: Plant leaves segmented in different colours after using ellipse criteria for the six selected cotton and hibiscus plants in Figure 4.1



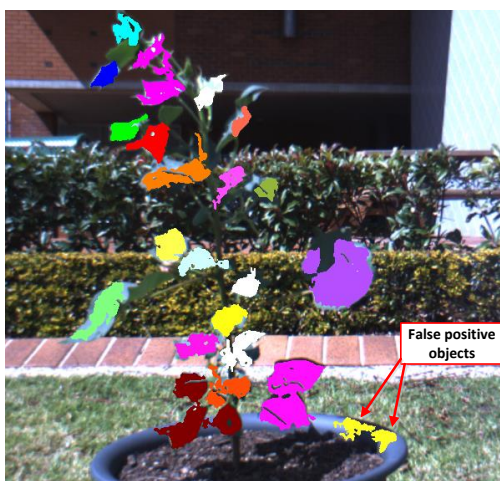
(a) Plant 1 side 1 has 5 objects



(b) Plant 1 side 2 has 1 object



(c) Plant 3 side 2 has 7 objects



(d) Plant 4 side 1 has 22 objects



(e) Hibiscus (indoor) has 18 objects



(f) Hibiscus (outdoor) has 16 objects

Figure 4.16: Plant leaves overlaying colour images for the six selected cotton and hibiscus plants in Figure 4.1

## 4.5 Depth Discontinuity Segmentation (DDS)

In this section, a segmentation method has been developed and presented to separate the overlapped leaves based on depth discontinuity criteria. The plant image in Figure 4.1a has low complexity for analysis purposes due to the absence of touching or overlapping leaves. The other plant images of the same figure have more complicated images due to touching and overlapping leaves. To segment these leaves from each other, additional steps in the segmentation process are required. Figure 4.15 shows the segmentation results after applying the image pre-processing stage (Section 4.4). The figure also presents plant images that have touching or overlapping leaf areas.

It is required to investigate the possibility of having more than one leaf in each segmented leaf (results from the pre-processing stage). The significant local change in image intensity can assign an edge in an image which is usually associated with a discontinuity in either the image intensity or the first derivative of the image intensity (Jain et al., 1995). The difference in pixel intensity (or the discontinuity of pixel values) can assign the existence of two or more leaves in the image. Typically, this difference must be obvious to be detected by the standard segmentation techniques such as edge finding correlation techniques. Therefore, some of the edge correlation finding techniques were investigated by Sobel and Feldman (1968) and Canny (1986) to solve overlap issues. It was observed that these techniques provide distinct edges for leaf boundaries but they are unable to recognise the internal discontinuity in depth values within the overlapped leaves. These unrecognised values were examined properly and the following findings were assessed: The variance in depth intensity between two overlapping regions is not distinctive enough to be recognised by edge detection techniques (also with low threshold setting) compared

with the variance in depth intensity between leaves and the background. It was noted that the smooth gradient in depth is assigned to one leaf in the image, while a depth gradient larger than three pixel values presents two different leaves. From here, it was important to measure the gradient in depth for each object (leaf) in the images and segment the images accordingly. Measuring depth gradient can be implemented by calculating the increment between the disparity map elements. Measuring depth gradient can also indicate the discontinuity in depth values for the segmented leaves. The measurement of depth discontinuity can be implemented in two different ways: global measure, and local measure. Local measure uses a direct comparison between each pixel and its neighbourhood. The value ‘global measure’ calculates the discontinuity in depth without the need to examine each pixel in the image. Both of these measurement techniques were considered in the developed algorithm which consists of three main techniques: disparity map denoising as well as global and local discontinuity segmentation. The global measure was applied first to consider the computation cost.

In order to understand the concept behind the algorithm it is important to investigate the disparity map for the intended leaf. Plant 3 side 2 (Figure 4.16c) was selected as an example to show the detailed process when applying the techniques of the depth discontinuity segmentation algorithm. Commencing in the connected area 1 of Figure 4.17, the algorithm techniques were applied sequentially to each object as in the following sections (Section 4.5.1 - Section 4.5.3).

#### **4.5.1 Disparity Map Denoising technique (DMD)**

This technique can be considered as pre-processing for the images that need to be separated by filtering the noise pixels in the disparity map. Figure 4.18a presents

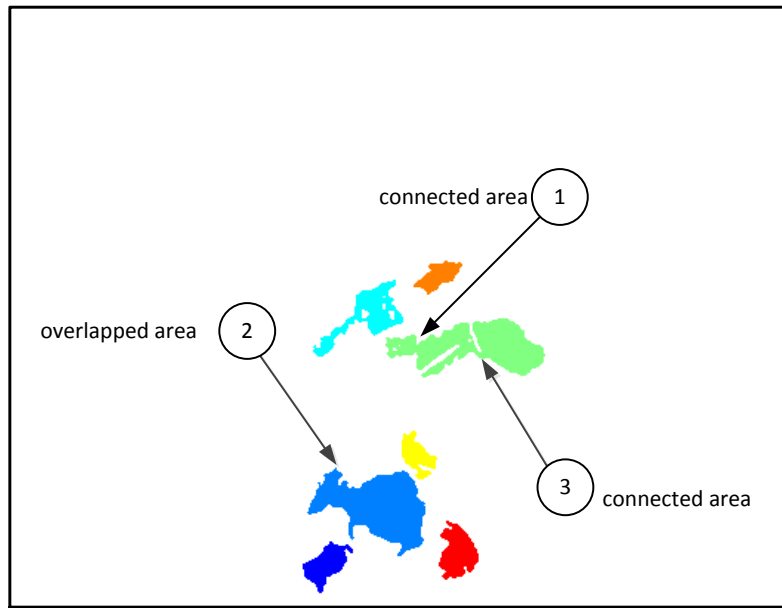


Figure 4.17: Plant 3 side 2 colour segmentation showing connected areas 1 and 3 and overlapped area 2.

the connected area (area 1) of Plant 3 side 2 of Figure 4.1c. Figure 4.18b shows one example of separation using the DMD technique. The values of disparity map's pixels ranged from 138 to 140 and presented two segmented and overlapped leaves in the disparity map. The values of these pixels are dependent on the distance between the camera and the plant parts. Larger values of disparity pixels present the furthest leaves.

The pixels valued 0 present the blank or empty area in the image. Other values ranged from 138 to 140 (Figure 4.18) are proportional to the depth values in the image. The pixels valued 1 are far from the range of depth values and they do not present the blank area as well. Therefore, those pixels are suspected to have incorrect values of depth due to an error that occurs during the calculation process of the disparity map. Errors are caused by a mismatching process due to many reasons such as overlapping, or insufficient light, shadow or overexposure. As such those pixels are considered as noise pixels.

The DMD technique was applied to change the value of noise pixels from 1 to 0. Figure 4.18b shows the disparity map after converting pixels from ones to zeros. The figure also presents a colour image of the intended leaves before and after separation. There are other connected leaves, in the already separated leaves (light blue area). This area can be separated using another technique from the DDS algorithm. Connected area 2 of plant 9 side 1 (Figure 4.15d) was also separated using the DMD technique as shown in Figure 4.19.



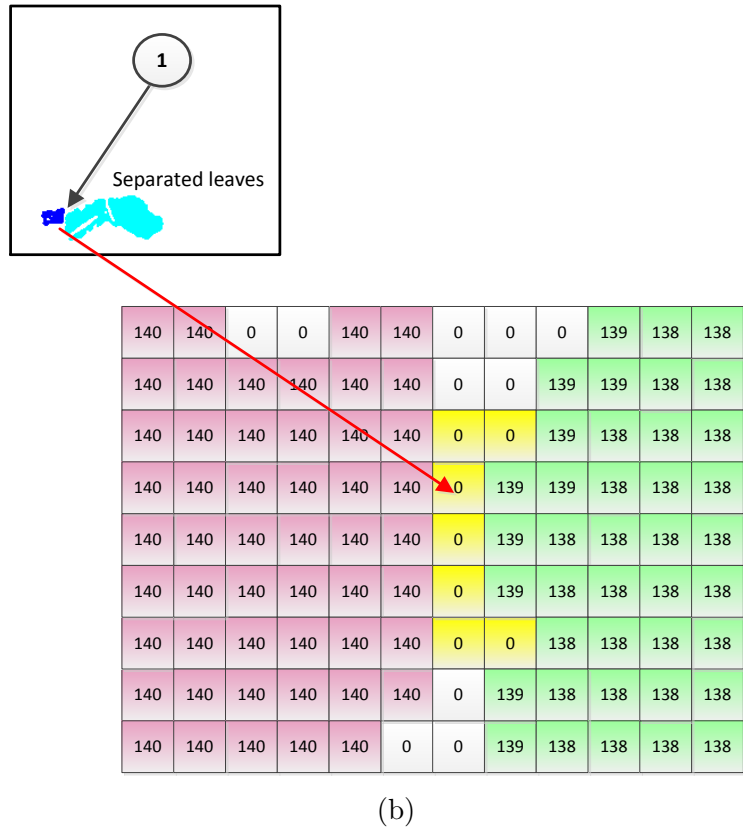
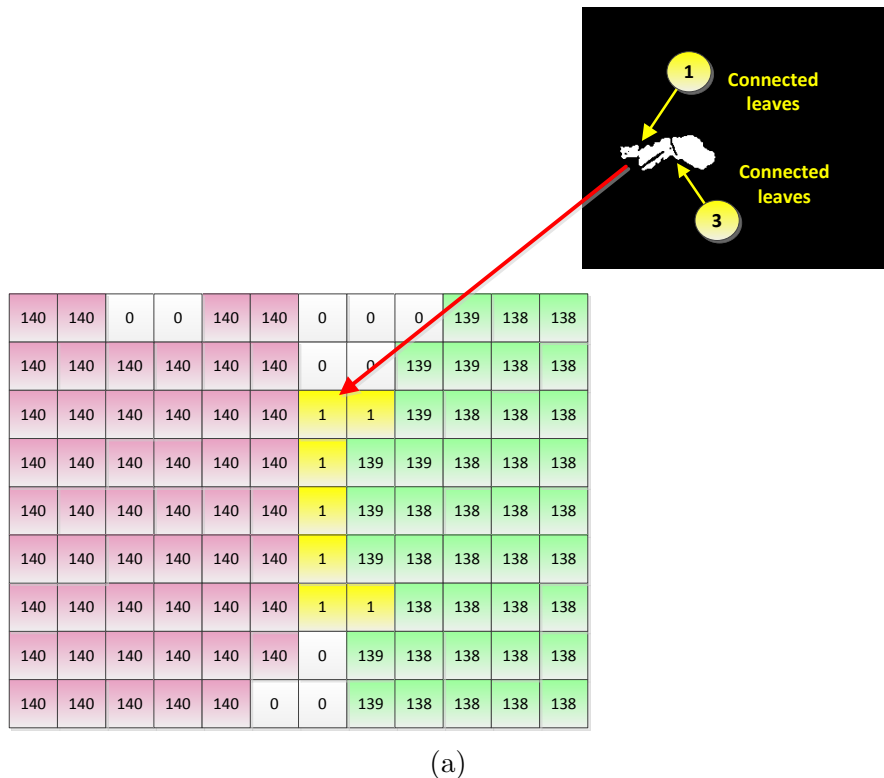


Figure 4.18: Connected leaves of area 1 for Plant 3. Colour image and disparity map (a) before separation; (b) after separation

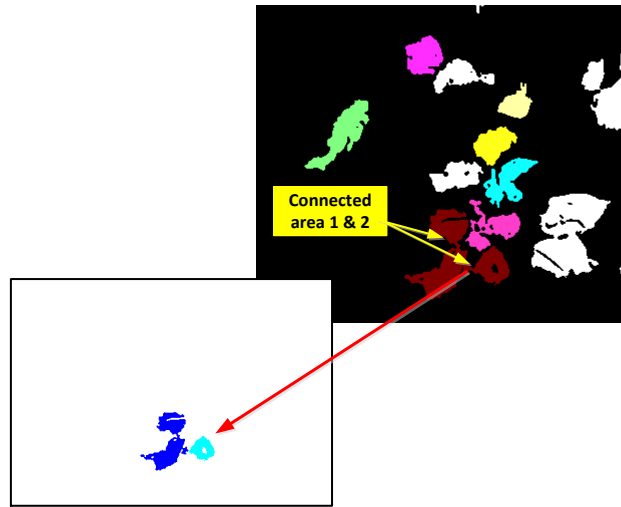


Figure 4.19: Plant 4 side 1 showing two connected areas 2 separated using the DMD technique

#### 4.5.2 Global Discontinuity Segmentation technique (GDS)

In this section, the segmentation based on global discontinuity in depth is implemented. The process begins by measuring the gradient in depth over the whole area of an examined image. For example, Figure 4.20 shows two leaves overlapping in a small area indicated by number 2 (yellow circle). The figure also shows a partial disparity map for the same specified overlapping area. The disparity map shows a distinct difference between the neighbouring pixels, ranging between 8-10. The difference indicates that there are two leaves in the examined area based on the assigned threshold. The threshold was assigned by inspecting a wide range of disparity maps with overlapping and non-overlapping leaves. The inspection shows that the smooth increment in depth between the neighbouring pixels (i.e. one or two pixel increments) in the disparity maps, assigns one small or medium leaf with a flat pose. A difference in depth equal to three pixels and more, indicates the existence of two overlapped leaves having small or medium size, or one large leaf with distinct

depths across different lobes. The gradient in depth could be measured without the need to find the difference between each contiguous pixel in the examined object. To implement this task the global discontinuity segmentation (GDS) technique has been developed to benefit from the unique property. The unique property is a method of finding the unique values in an array (MATLAB, 2015). This property was used to find the unique pixel values in the disparity map and to generate the unique vector  $U$ . The method comprises the following steps (Listing 4.3) and is explained in Equation 4.5. Figure 4.20 and Equation 4.6 show an example of two overlapping leaves which were successfully separated using GDS technique.



Figure 4.20: Two overlapping leaves (area 2 of Plant 3) and their separation process using GDS technique. The top image shows the overlapping leaves. The disparity map declares the distinct difference between pixels. The lower images present the results after separation.

**Listing 4.3 Global Discontinuity Segmentation technique**

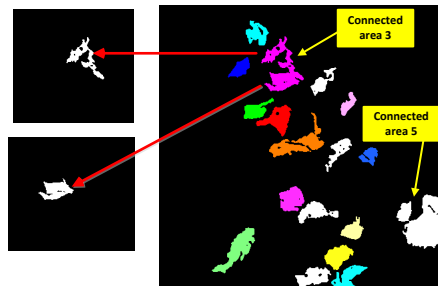
- Step 1** The unique disparity values for a single component are sorted into ascending order and stored in a vector which is called unique vector  $U$  (Equation 4.5)
- Step 2** The difference between each contiguous pixels of  $U$  vector is calculated
- Step 3** The vector is divided into smaller vectors,  $U_1$  and  $U_2, U_3, \dots, U_m$  according to the difference value (i.e. difference value  $\geq$  threshold value (threshold=3)). The number of small vectors indicates the number of overlapping leaves
- Step 3** The component is split into a group of smaller components where each component contains only those disparity values corresponding to a single vector

$$U = \begin{bmatrix} u_1 \\ u_2 \\ u_3 \\ u_4 \\ u_5 \\ u_6 \\ u_7 \\ u_8 \\ u_9 \\ \vdots \\ \vdots \\ u_n \end{bmatrix} = U_1 \begin{bmatrix} u_1 \\ u_2 \\ u_3 \end{bmatrix} \parallel U_2 \begin{bmatrix} u_4 \\ u_5 \\ u_6 \end{bmatrix} \parallel U_3 \begin{bmatrix} u_7 \\ u_8 \end{bmatrix} \parallel \dots \dots U_m \begin{bmatrix} u_9 \\ \vdots \\ \vdots \\ u_n \end{bmatrix} \quad (4.5)$$

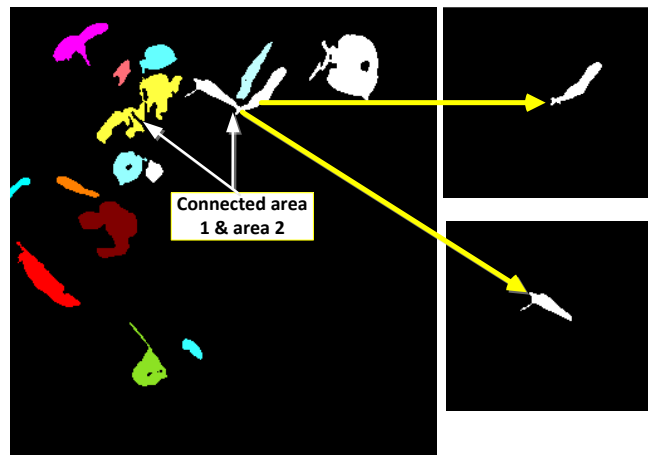
Equation 4.6 below represents an example of a unique vector which has two overlapped leaves.

$$U = \begin{bmatrix} 142 \\ 143 \\ 144 \\ 145 \\ \dots \\ 148 \\ 149 \\ 150 \\ 151 \\ 152 \\ 153 \\ 154 \end{bmatrix} = U_1 \begin{bmatrix} 142 \\ 143 \\ 144 \\ 145 \end{bmatrix} \parallel U_2 \begin{bmatrix} 148 \\ 149 \\ 150 \\ 151 \\ 152 \\ 153 \\ 154 \end{bmatrix} \tag{4.6}$$

Figure 4.21 shows Plant 4 side 1 a cotton plant and hibiscus plant (indoor conditions) with connected areas which have been separated using the GDS technique. This technique has an advantage over edge detection techniques because it measures the discontinuity in depth gradient without the need to examine each pixel, which makes it faster however, both of them are targeting the discontinuity of pixel values. In some cases, the unique vector indicates smooth increments in depth between its elements but the colour image shows there are two overlapping leaves in this particular area also confirmed by examining the disparity map. In this case, there is a requirement to search depth discontinuity using a local technique, which is developed in the next section.



(a) Plant 4 side 1, connected area 3



(b) Hibiscus plant at indoor condition

Figure 4.21: Cotton and hibiscus plants with connected areas which have been separated using the GDS technique.

### 4.5.3 Local discontinuity segmentation—Eight Neighbours Difference technique (ENBD)

This technique has been developed for certain cases where the unique vector  $U$  (Listing 4.3, Equation 4.5) presents a smooth increment in depth, i.e. only one value increment exists between the elements of  $U$  vector, but the disparity map contains more than one leaf and a large difference in depth was observed between the neighbouring pixels on the disparity map.

Figure 4.22 illustrates an example of a disparity map with a smooth unique vector  $U$  (Equation 4.7), while a sharp gradient in depth was observed in the disparity map. The vector shows a smooth increment between elements. A sharp gradient means the difference between the neighbouring pixels in the intended area of the disparity map exceeded threshold value (threshold = 3).

$$U = \begin{bmatrix} 141 & 142 & 143 & 144 & 145 & 146 & 147 & 148 \end{bmatrix} \quad (4.7)$$

The pixel values of 141 to 142 are presented by the green area while the red area contains pixel values from 145 to 147 (Figure 4.22). As the difference between the neighbouring pixels is greater than three, each area represents one leaf. The Eight Neighbours Difference technique (ENBD) was developed for targeting and separating those different areas based on the local discontinuity in depth. The idea of this technique is to measure the difference in depth between the centre pixel and its neighbouring pixels as described by the steps of Listing 4.4.

0	0	145	145	0	145	145	145	145	145	145	145
0	0	145	145	145	145	145	145	145	145	145	145
0	0	0	145	145	145	145	145	145	145	145	145
0	0	0	145	145	145	145	145	145	145	145	145
0	0	0	145	145	146	146	145	145	145	145	145
0	0	0	145	145	146	146	146	146	146	146	146
0	0	141	141	141	141	141	146	146	146	146	146
0	142	141	141	141	141	141	0	0	0	0	147
142	142	141	141	141	141	141	141	0	0	0	147
142	142	141	141	141	141	141	141	0	0	147	147

Figure 4.22: A disparity map showing a big difference in neighbouring pixels while Equation 4.7 indicates a smooth increment in unique vector  $U$ .

#### Listing 4.4 Eight Neighbours Difference technique

**Step 1** A window of nine pixels is moved across the disparity map.

**Step 2** The centre pixel is considered a reference pixel.

**Step 3** The absolute difference between the centre pixel and the other eight neighbours pixels is calculated sequentially.

**Step 4** When the absolute difference between the centre pixel and any of neighbour pixels is equal to or greater than the threshold value, the value of the neighbour pixel is set to zero.

**Step 5** When the absolute difference between the centre pixel and any of neighbour pixel is equal to zero, this value is ignored and no change is made.

**Step 6** The zero valued centre pixels are skipped and no change is made.

**Step 7** Subsequently, the nine pixel window is shifted to the right and takes another column each time.



Figures 4.23 and 4.24, illustrate the process of nine pixel windows moving over the two connected areas of the disparity map presented in Figure 4.22. They represent the state of the matrix from an arbitrary start. The replacement of pixel values was implemented in the same matrix of the disparity map. The zero valued centre pixels were skipped because the absolute difference in depth between the centre pixel and any of the neighbouring pixels is equal to the values of the neighbouring pixel itself. In this case, no change can be made otherwise, all pixels become zeros in the disparity map. The process continues until the two connected areas are separated from each other. Two new areas are produced with each area representing one leaf. All changed pixels are coloured red to declare their position after using this segmentation method as shown in Figure 4.24f. The connected component and labeling algorithm (Foley et al., 1982) (Section 4.4.3), was applied to verify the separation of the connected areas. In some instances when the separation between the connected areas was not verified, another technique was applied as in the next section.

0	0	145	145	0	145	145	145	145	145	145	145
0	0	145	145	145	145	145	145	145	145	145	145
0	0	0	145	145	145	145	145	145	145	145	145
0	0	0	145	145	145	145	145	145	145	145	145
0	0	0	145	145	146	146	145	145	145	145	145
0	0	0	145	145	146	146	146	146	146	146	146
0	0	141	141	141	141	141	146	146	146	146	146
0	142	141	141	141	141	141	0	0	0	0	147
142	142	141	141	141	141	141	141	0	0	0	147
142	142	141	141	141	141	141	141	0	0	0	147

(a) Procedure 1

0	0	145	145	0	145	145	145	145	145	145	145
0	0	145	145	145	145	145	145	145	145	145	145
0	0	0	145	145	145	145	145	145	145	145	145
0	0	0	145	145	145	145	145	145	145	145	145
0	0	0	145	145	146	146	145	145	145	145	145
0	0	0	145	145	146	146	146	146	146	146	146
0	0	141	141	141	141	141	141	146	146	146	146
0	142	141	141	141	141	141	0	0	0	0	147
142	142	141	141	141	141	141	141	0	0	0	147
142	142	141	141	141	141	141	141	0	0	0	147

(b) Procedure 2

0	0	145	145	0	145	145	145	145	145	145	145
0	0	145	145	145	145	145	145	145	145	145	145
0	0	0	145	145	145	145	145	145	145	145	145
0	0	0	145	145	145	145	145	145	145	145	145
0	0	0	145	145	146	146	145	145	145	145	145
0	0	0	145	145	146	146	146	146	146	146	146
0	0	141	141	141	141	141	141	146	146	146	146
0	142	141	141	141	141	141	0	0	0	0	147
142	142	141	141	141	141	141	141	0	0	0	147
142	142	141	141	141	141	141	141	0	0	0	147

(c) Procedure 3

0	0	145	145	0	145	145	145	145	145	145	145
0	0	145	145	145	145	145	145	145	145	145	145
0	0	0	145	145	145	145	145	145	145	145	145
0	0	0	145	145	145	145	145	145	145	145	145
0	0	0	145	145	146	146	145	145	145	145	145
0	0	0	145	145	146	146	146	146	146	146	146
0	0	141	141	141	141	141	141	146	146	146	146
0	142	141	141	141	141	141	0	0	0	0	147
142	142	141	141	141	141	141	141	0	0	0	147
142	142	141	141	141	141	141	141	0	0	0	147

(d) Procedure 4

0	0	145	145	0	145	145	145	145	145	145	145
0	0	145	145	145	145	145	145	145	145	145	145
0	0	0	145	145	145	145	145	145	145	145	145
0	0	0	145	145	145	145	145	145	145	145	145
0	0	0	145	145	146	146	145	145	145	145	145
0	0	0	145	145	146	146	146	146	146	146	146
0	0	141	141	141	141	141	146	146	146	146	146
0	142	141	141	141	141	141	0	0	0	0	147
142	142	141	141	141	141	141	141	0	0	0	147
142	142	141	141	141	141	141	141	0	0	0	147

(e) Procedure 5

0	0	145	145	0	145	145	145	145	145	145	145
0	0	145	145	145	145	145	145	145	145	145	145
0	0	0	145	145	145	145	145	145	145	145	145
0	0	0	145	145	145	145	145	145	145	145	145
0	0	0	145	145	146	146	145	145	145	145	145
0	0	0	145	145	146	146	146	146	146	146	146
0	0	141	141	141	141	141	141	146	146	146	146
0	142	141	141	141	141	141	0	0	0	0	147
142	142	141	141	141	141	141	141	0	0	0	147
142	142	141	141	141	141	141	141	0	0	0	147

(f) Procedure 6

Figure 4.23: Leaves segmented using (ENBD) technique, the red pixel presents the centre of the window, yellow pixels present the eight neighbouring pixels, the blue pixel presents the changed pixel after the application of this technique.

0	0	145	145	0	145	145	145	145	145	145	145
0	0	145	145	145	145	145	145	145	145	145	145
0	0	0	145	145	145	145	145	145	145	145	145
0	0	0	145	145	145	145	145	145	145	145	145
0	0	0	145	145	146	146	145	145	145	145	145
0	0	0	0	0	0	0	146	146	146	146	146
0	0	141	141	141	141	141	141	146	146	146	146
0	142	141	141	141	141	141	0	0	0	0	147
142	142	141	141	141	141	141	141	0	0	0	147
142	142	141	141	141	141	141	141	0	0	147	147

(a) Procedure 7

0	0	145	145	0	145	145	145	145	145	145	145
0	0	145	145	145	145	145	145	145	145	145	145
0	0	0	145	145	145	145	145	145	145	145	145
0	0	0	145	145	145	145	145	145	145	145	145
0	0	0	145	145	146	146	145	145	145	145	145
0	0	0	0	0	0	0	146	146	146	146	146
0	0	141	141	141	141	141	141	146	146	146	146
0	142	141	141	141	141	141	0	0	0	0	147
142	142	141	141	141	141	141	141	0	0	0	147
142	142	141	141	141	141	141	141	0	0	147	147

(b) Procedure 8

0	0	145	145	0	145	145	145	145	145	145	145
0	0	145	145	145	145	145	145	145	145	145	145
0	0	0	145	145	145	145	145	145	145	145	145
0	0	0	145	145	145	145	145	145	145	145	145
0	0	0	145	145	146	146	145	145	145	145	145
0	0	0	0	0	0	0	146	146	146	146	146
0	0	141	141	141	141	141	141	146	146	146	146
0	142	141	141	141	141	141	0	0	0	0	147
142	142	141	141	141	141	141	141	0	0	0	147
142	142	141	141	141	141	141	141	0	0	147	147

(c) Procedure 9

0	0	145	145	0	145	145	145	145	145	145	145
0	0	145	145	145	145	145	145	145	145	145	145
0	0	0	145	145	145	145	145	145	145	145	145
0	0	0	145	145	145	145	145	145	145	145	145
0	0	0	145	145	146	146	145	145	145	145	145
0	0	0	0	0	0	0	146	146	146	146	146
0	0	141	141	141	141	141	141	146	146	146	146
0	142	141	141	141	141	141	0	0	0	0	147
142	142	141	141	141	141	141	141	0	0	0	147
142	142	141	141	141	141	141	141	0	0	147	147

(d) Procedure 10

0	0	145	145	0	145	145	145	145	145	145	145
0	0	145	145	145	145	145	145	145	145	145	145
0	0	0	145	145	145	145	145	145	145	145	145
0	0	0	145	145	145	145	145	145	145	145	145
0	0	0	145	145	146	146	145	145	145	145	145
0	0	0	0	0	0	0	146	146	146	146	146
0	0	141	141	141	141	141	141	146	146	146	146
0	142	141	141	141	141	141	0	0	0	0	147
142	142	141	141	141	141	141	141	0	0	0	147
142	142	141	141	141	141	141	141	0	0	147	147

(e) Procedure 11

0	0	145	145	0	145	145	145	145	145	145	145
0	0	145	145	145	145	145	145	145	145	145	145
0	0	0	145	145	145	145	145	145	145	145	145
0	0	0	145	145	145	145	145	145	145	145	145
0	0	0	145	145	146	146	145	145	145	145	145
0	0	0	0	0	0	0	146	146	146	146	146
0	0	141	141	141	141	141	141	146	146	146	146
0	142	141	141	141	141	141	0	0	0	0	147
142	142	141	141	141	141	141	141	0	0	0	147
142	142	141	141	141	141	141	141	0	0	147	147

(f) Procedure 12

Figure 4.24: Leaves segmented using (ENBD) technique, the red pixel presents the centre of the window, yellow pixels present the eight neighbouring pixels, the blue pixel presents the changed pixel after applying this technique

## 4.5.3.1 Zero Neighbours Counting technique (ZNC)

The zero neighbours counting technique (ZNC) needs to be applied after ENBD in instances where connected leaves did not separate after applying ENBD. These areas in the disparity map are still connected by a few pixels, because the difference in depth is less than the threshold value. In such instances the ZNC technique has been developed and applied by counting the zero neighbours around the centre pixel on the nine window pixels. When the centre pixel is surrounded by three zeros or more, the value of the centre pixel is converted to zero in order to separate the two connected areas. Figure 4.25 shows two leaves of plant 3 (area 3) which were connected by small amounts of pixels and illustrates the corresponding disparity map of the same two leaves. The ZNC technique is outlined in Listing 4.5.

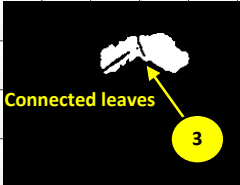
C R	C 413	C 414	C 415	C 416	C 417	C 418	C 419	C 420	C 421	C 422	C 423	C 424	C 425	C 426	C 427
R 422	134	134	134	134	0	0	0	134	134	134	134	134	134	134	134
R 423	134	134	134	134	134	0	0	134	134	134	134	134	134	134	134
R 424	134	134	134	134	134	0	0	0	134	134	134	134	134	134	134
R 425	134	134	134	134	134	134	0	0	134	134	134	134	134	134	134
R 426	134	134	134	134	134	134	0	0	0	134	134	134	134	134	134
R 427	135	134	134	134	134	134	134	0	0	134	134	134	134	134	134
R 428	0	0	0	0	134	134	134	134	134	134	134	134	134	134	134
R 429	0	0	0	0	0	134	134	134	134	134	134	134	134	134	134
R 430							0	134	134	134	134	134	134	134	134
R 431							0	0	134	134	134	134	134	134	134
R 432							0	0	0	0	134	134	0	0	0
R 433							0	0	0	0	0	0	0	0	0
R 434							0	0	0	0	0	0	0	0	0

Figure 4.25: Two areas of plant 3 connected by small pixels and the disparity map of the same connected area.

**Listing 4.5 Zero Neighbours Counting technique**

- Step 1** The technique starts to work in two loops. The first loop takes the first column of the non-zero pixel from the disparity map and the second loop takes all rows sequentially.
- Step 2** A window of nine pixels was moved over the current row and first column.
- Step 3** The centre pixel is set as a reference pixel.
- Step 4** When the centre pixel has three zero neighbours or more, the value of the centre pixel is set to zero.
- Step 5** Subsequently, the algorithm takes the next column to complete loop one.
- Step 6** The connected component algorithm is applied after each column's loop to verify the segmentation process.
- Step 7** If the separation is not accrued, the process will continue and the window will move over to the next row until the separation process is completed and the process ends.

Figure 4.26 shows the algorithm process. When the algorithm loops reach the region of interest (connected leaf areas), the number of zero neighbours for each pixel was calculated and the required action then applied. The connected component and labeling algorithm (Foley et al., 1982) (Section 4.4.3), was applied to confirm segmentation when the window was moved over all columns for each row. When the segmentation is confirmed and the separated leaves are labeled using the connected algorithm, the process will stop and there is no need to examine all elements of the disparity map. This step is important to preserve most of the disparity map data and leaf shape to develop another algorithm which extracts a plane from each segmented leaf. The ZNC technique cannot be applied unless the discontinuity in depth is detected by the ENBD technique but the separation process was not completely implemented.

$\begin{smallmatrix} C \\ R \end{smallmatrix}$	C 413	C 414	C 415	C 416	C 417	C 418	C 419	C 420	C 421	C 422	C 423	C 424	C 425	C 426	C 427
R 422	134	134	134	134	0	0	0	134	134	134	134	134	134	134	134
R 423	134	134	134	134	134	0	0	134	134	134	134	134	134	134	134
R 424	134	134	134	134	134	0	0	0	134	134	134	134	134	134	134
R 425	134	134	134	134	134	0	0	0	134	134	134	134	134	134	134
R 426	134	134	134	134	134	0	0	0	134	134	134	134	134	134	134
R 427	135	134	134	134	134	134	134	0	0	134	134	134	134	134	134
R 428	0	0	0	0	0	134	134	134	134	134	134	134	134	134	134
R 429	0	0	0	0	0	134	134	134	134	134	134	134	134	134	134
R 430	0	0	0	0	0	0	134	134	134	134	134	134	134	134	134
R 431	0	0	0	0	0	0	0	134	134	134	134	134	134	134	134
R 432	0	0	0	0	0	0	0	0	134	134	0	0	0	0	0
R 433	0	0	0	0	0	0	0	0	0	0	0	0	0	0	0

(a)

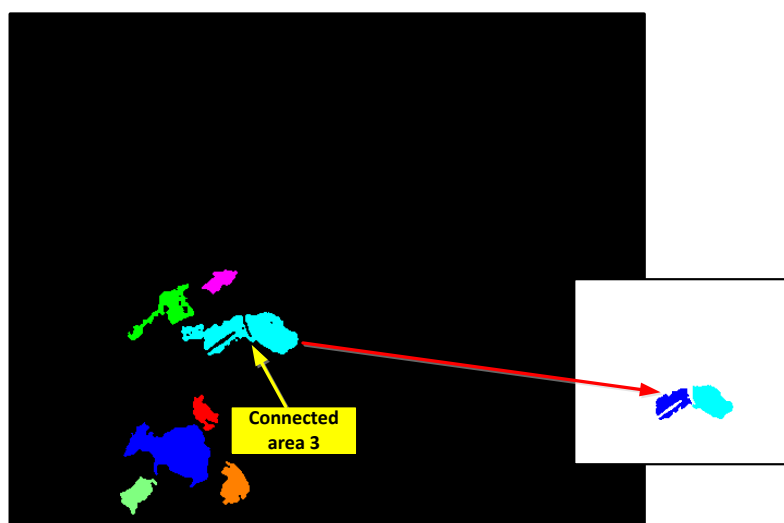
$\begin{smallmatrix} C \\ R \end{smallmatrix}$	C 413	C 414	C 415	C 416	C 417	C 418	C 419	C 420	C 421	C 422	C 423	C 424	C 425	C 426	C 427
R 422	134	134	134	0	0	0	0	134	134	134	134	134	134	134	134
R 423	134	134	134	134	0	0	0	134	134	134	134	134	134	134	134
R 424	134	134	134	134	0	0	0	0	134	134	134	134	134	134	134
R 425	134	134	134	134	134	0	0	0	134	134	134	134	134	134	134
R 426	134	134	134	134	134	0	0	0	0	134	134	134	134	134	134
R 427	135	0	0	0	134	0	134	0	0	134	134	134	134	134	134
R 428	0	0	0	0	0	0	134	134	134	134	134	134	134	134	134
R 429	0	0	0	0	0	134	134	134	134	134	134	134	134	134	134
R 430	0	0	0	0	0	0	134	134	134	134	134	134	134	134	134
R 431	0	0	0	0	0	0	0	134	134	134	134	134	134	134	134
R 432	0	0	0	0	0	0	0	0	134	134	0	0	0	0	0
R 433	0	0	0	0	0	0	0	0	0	0	0	0	0	0	0

(b)

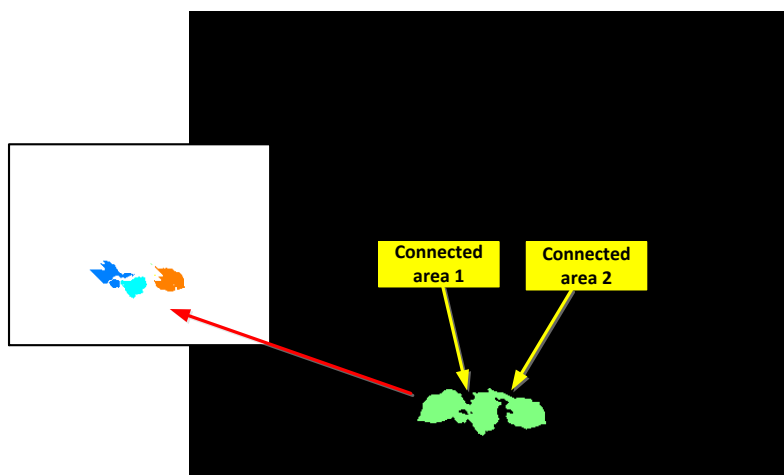
Figure 4.26: Disparity map of area 3 connected leaves, (a) sequence of the ZNC technique, (b) disparity map after the separation of the two connected areas using the ZNC technique.

Figures 4.27 and 4.28 demonstrate the operation of the ENBD and ZNC techniques to separate individual leaves. As per the labels in Figure 4.28, some components were separated into individual leaves using only the ENBD technique and others used both ENBD and then ZNC techniques where necessary.

The ENBD and ZNC techniques have an advantage over the erosion dilation operators as follows: The ENBD technique is able to recognise the internal discontinuity in depth within an object and segment the connected area accordingly, while erosion dilation operators shrink objects which might affect leaf shape, deleting some leaf boundaries and losing depth information. In addition, erosion and dilation operators require a different structural element to be defined for each different shape and size object in the image. Their working principles are not useful for images having connected leaves of different sizes, which might need multiple interventions from the user to set the structure parameters for each connected area in the image. The result of applying the ZNC technique (only) might be similar to the erosion (operators for some images) where both try to separate connected objects, however the working principles are different. In many cases there is no need to apply the ZNC technique after the ENBD technique, as the connected area is separated already by using ENBD or GDS techniques.



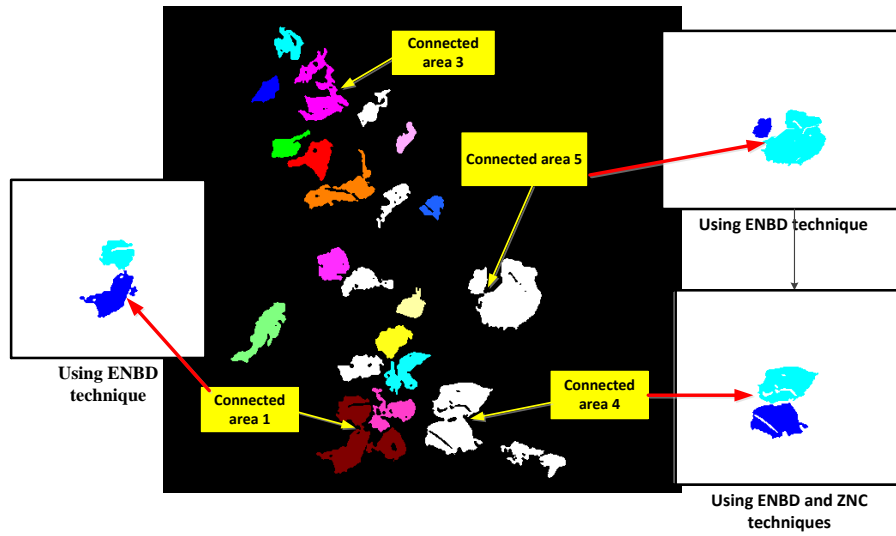
(a) Plant 3 side 2



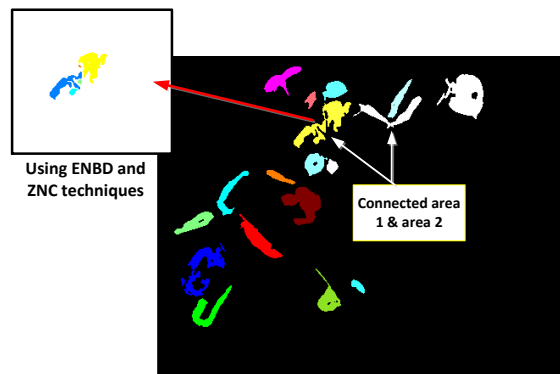
(b) Plant 2 side 2

Figure 4.27: (a) Colour image of area 3, plant 3 after separation using ENBD and ZNC techniques, (b) Plant 2 final segmentation image after using DDS techniques.

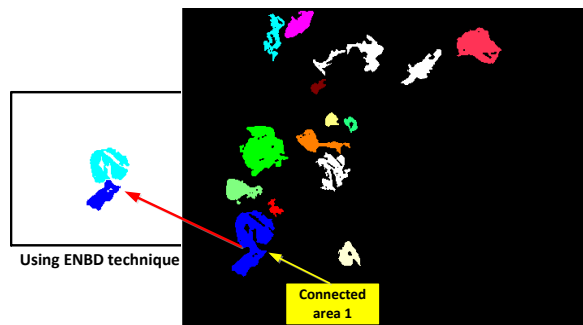




(a) Plant 4 side 1



(b) Indoor condition Hibiscus image



(c) Outdoor condition Hibiscus image

Figure 4.28: Cotton and hibiscus plants with connected areas separated using ENBD and ZNC techniques.

#### 4.5.4 Final leaf segmentation

Figures 4.29 and 4.30 show the final plant leaf segmentations of all selected cotton and hibiscus plants in Figure 4.1. Although some leaves are still missing from the final segmentation results as shown in column two of both figures, the results have been improved after using the developed DDS. The improvement can be recognised by the difference between the numbers of leaves in relevant columns.

The missing leaves or false negative leaves are due to the poor illumination conditions (shadow) and the brightness areas (overexposure). The indoor hibiscus plant has one false negative leaf due to the poor illumination (Figure 4.30f). A false negative leaf can also be observed in the outdoor hibiscus plant images due to the overexposed area (Figure 4.30h). Moreover, three false positive leaves/objects can be recognised in the segmentation results for Plant 4 side 1 (Figure 4.29h) and two false positive objects in the results for Plant 6 side 1 (Figure 4.30d). The false positive objects for these two plants were caused by the shadow appearing on the pot's edge.

These false negative and positive leaves are expected to be affected by lighting conditions and other factors such as leaf direction and leaf size which will be further explained in different data sets in the next chapter. Table 4.1 presents the incremental increase in accuracy as the proposed technique was added to the leaf segmentation algorithm for the 8 selected cotton and hibiscus plants in Figures 4.29 and 4.30, increasing from 72% to 91% accuracy with all techniques applied. Table 4.1 also shows the number of leaves of each plant calculated from the visual inspection of each image. Furthermore, the performance of the developed algorithm will be evaluated further using an extended dataset in Chapter 5.

Table 4.1: Final leaf segmentation results for the 8 selected cotton and hibiscus plants in Figures 4.29 and 4.30.

Name of technique	Total leaf auto-count	Total leaf visual image count	False negative	False positive	Total true segments	Accuracy%
Image pre-processing	95	122	4	31	91	72
DMD	98	122	4	28	94	75
GDS	106	122	4	20	102	81
ENBD	112	122	5	15	107	84
ENBD+ZNC	120	122	5	7	115	91

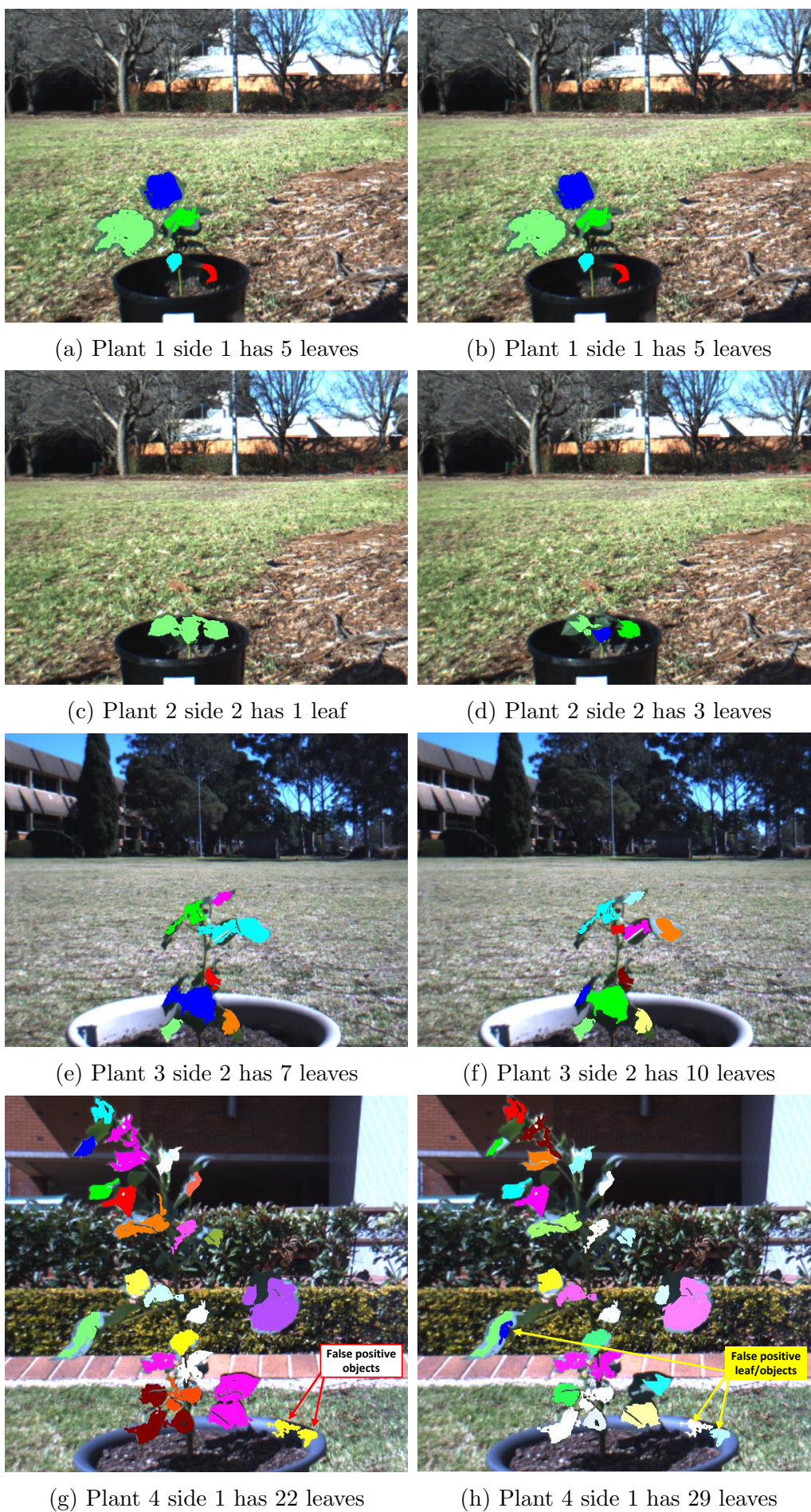


Figure 4.29: Final leaf segmentations. Column 1 presents results after using the image pre-processing algorithm, column 2 shows result after using DDS.



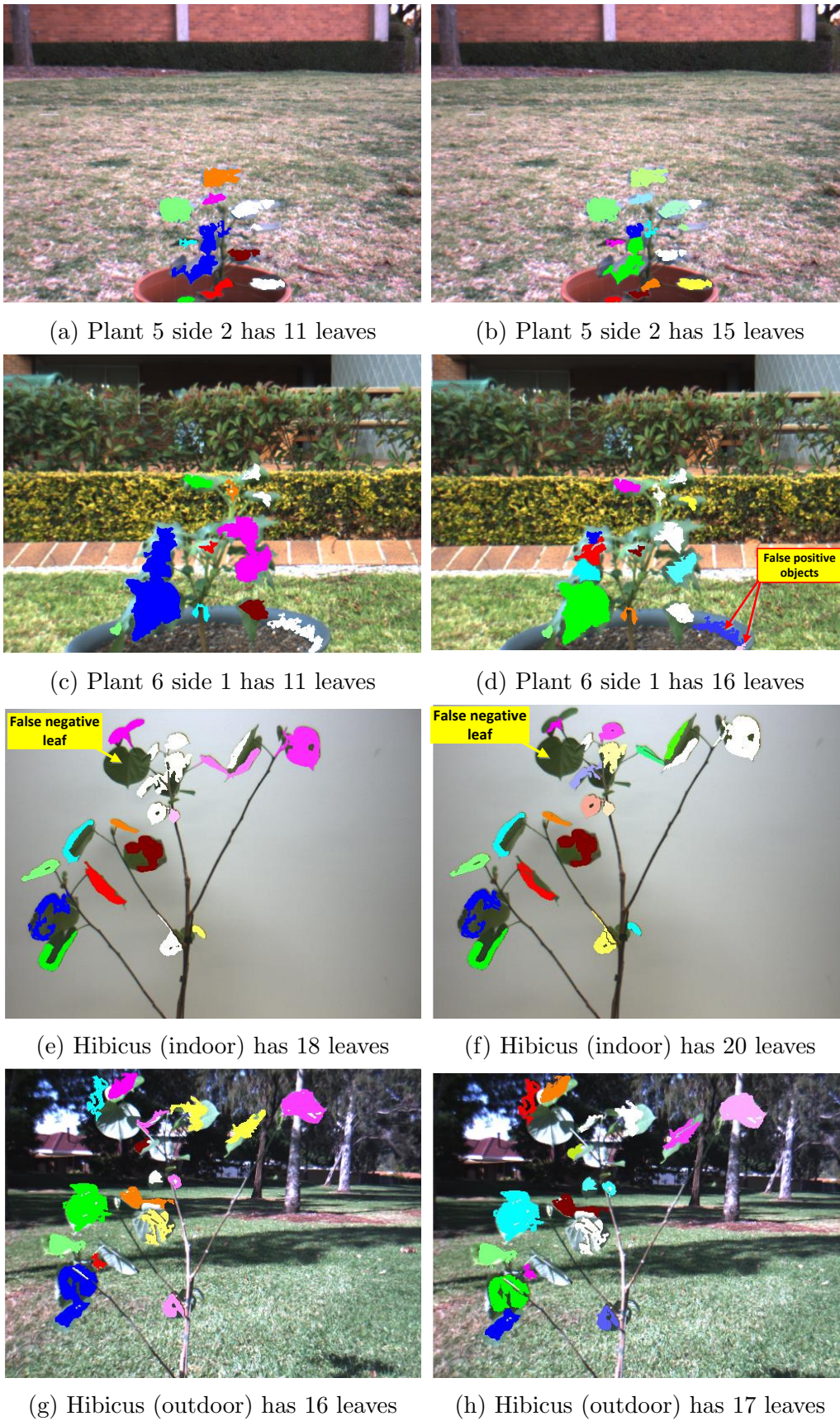


Figure 4.30: Final leaf segmentations. Column 1 presents results after using image pre-processing algorithm, column 2 shows result after using DDS.

## 4.6 Leaf plane extraction

In this section, a method that extracts a geometrical plane from leaf vertices using  $x$ ,  $y$ ,  $z$  coordinates of leaf depth image is presented. The purpose of extracting a plane from a plant leaf (in this study) is to measure the inclination angle of each leaf from the plane equation, that can inform plant drought stress or can be used to parameterise a 3D model of the imaged plant. A leaf is a three dimensional object in the space which would be more accurately presented using a curve or multiple planes with different angles. Although a plane might not be the best method for representing or modelling a leaf, however a plane can provide adequate information to measure the inclination angle of each segmented leaf which is required for this stage of the research study. Modelling plant leaves using curves or multiple planes with different angles is beyond the scope of this study.

### 4.6.1 Definition of a plane

In mathematics, a plane is a flat, two-dimensional surface spanned by two linear independent vectors. A plane can be defined in space in several different ways. For example, three non-collinear points (points which are not contained by a single line) can define a plane surface. Any line and a point not on that line can similarly define a plane surface. A plane can also be defined by two parallel lines or two intersecting lines. Planes in a three dimensional space have a natural description using a point in the plane and a vector (the normal vector) to indicate its inclination. The rectangular equation of a plane containing a point  $r_0(x_0, y_0, z_0)$  with a normal vector  $n_v = (a, b, c)$  is:

$$a(x - x_0) + b(y - y_0) + c(z - z_0) + d = 0 \quad (4.8)$$

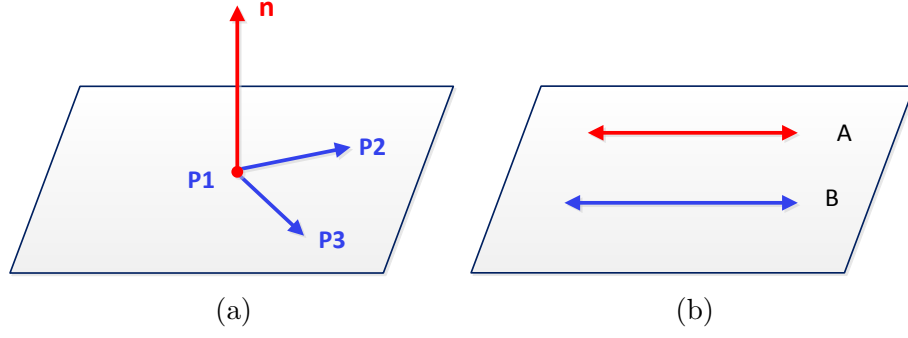


Figure 4.31: Two types of plane (a) A 3 points plane with a normal vector (b) Two parallel lines plane

A suitable normal vector  $n_v$  is given by the cross product of two vectors:

$$n_v = \overrightarrow{P_1P_2} \times \overrightarrow{P_1P_3} \quad (4.9)$$

where  $\overrightarrow{P_1P_2} = (P_1 - P_2)$  and  $\overrightarrow{P_3P_2} = (P_3 - P_2)$ , and  $P_1(x_1, y_1, z_1)$ ,  $P_2(x_2, y_2, z_2)$  and  $P_3(x_3, y_3, z_3)$  are any three given points in the space. Point  $r_0$  may be equal to any of the given points  $P_1$ ,  $P_2$  or  $P_3$ .

The normal vector can be calculated by using a Third-Order Determinant (Kreyszig, 2010) where D is equal to the determinant of a  $3 \times 3$  matrix.

$$D = \begin{bmatrix} a_{11} & a_{12} & a_{13} \\ a_{21} & a_{22} & a_{23} \\ a_{31} & a_{32} & a_{33} \end{bmatrix} = a_{11} \begin{bmatrix} a_{22} & a_{23} \\ a_{32} & a_{33} \end{bmatrix} - a_{21} \begin{bmatrix} a_{12} & a_{13} \\ a_{32} & a_{33} \end{bmatrix} + a_{31} \begin{bmatrix} a_{12} & a_{13} \\ a_{22} & a_{23} \end{bmatrix} \quad (4.10)$$

The geometric definition of a plane will be used to calculate plane equations for leaves extracted by using automatic image analysis.

### 4.6.2 Leaf plane extraction method

After segmenting leaves from each other by using image preprocessing analysis, a plane can be extracted from a leaf plane by implementing the following steps:

#### Listing 4.6 Plane extraction steps

**Step 1** Find the minimum and maximum leaf boundary values in  $x$  and  $y$  coordinates of the 2D disparity image.

**Step 2** From these values a complete four point set can be calculated where,  $P_1 = (\text{Min } x, y)$ ,  $P_2 = (\text{Max } x, y)$ ,  $P_3 = (x, \text{Max } y)$  and  $P_4 = (x, \text{Min } y)$  as illustrated in Figure 4.32a. These four points represent the four main extremities of the leaf in the image plane.

**Step 3** From these point, a polygon around the leaf can be drawn as shown in Figure 4.32a.

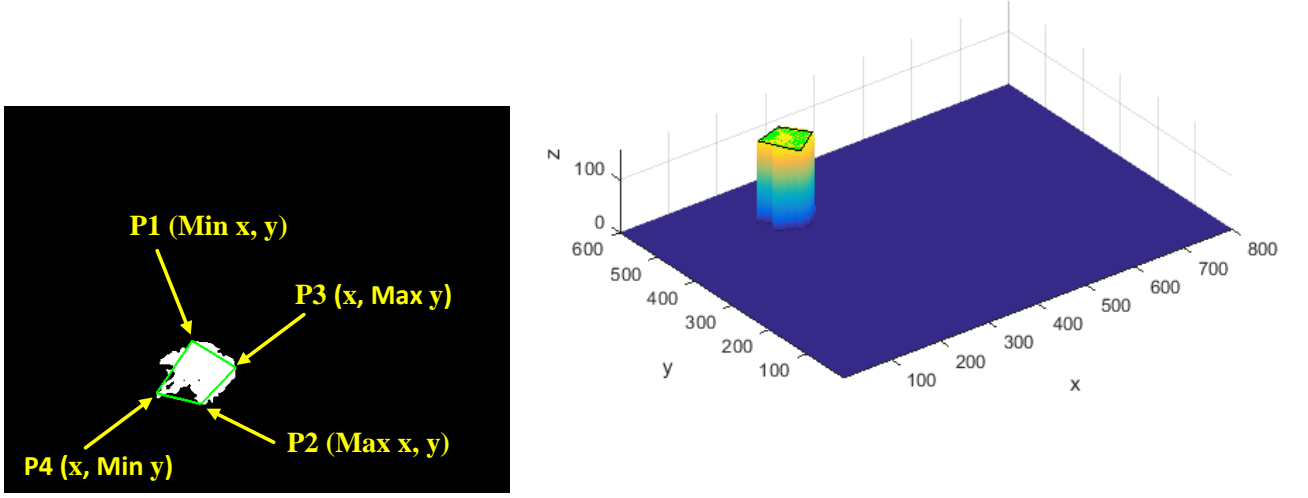
**Step 4** The corresponding  $z$  value for each point of the polygon can be calculated to plot a flat plane over a 3D disparity leaf image as shown in Figure 4.32b, where the plane surface is overlapping with the leaf surface.

**Step 5** From these four points of the polygon, three points can be chosen to drive the plane equation (Equation 4.8).

**Step 6** Since the plane equation is obtained from only three points, an interpolation process is required to find the other points of the plane. This is implemented by submitting the  $x$  and  $y$  coordinates of the disparity map in the plane equation to find the corresponding  $z$  coordinate values of the plane.

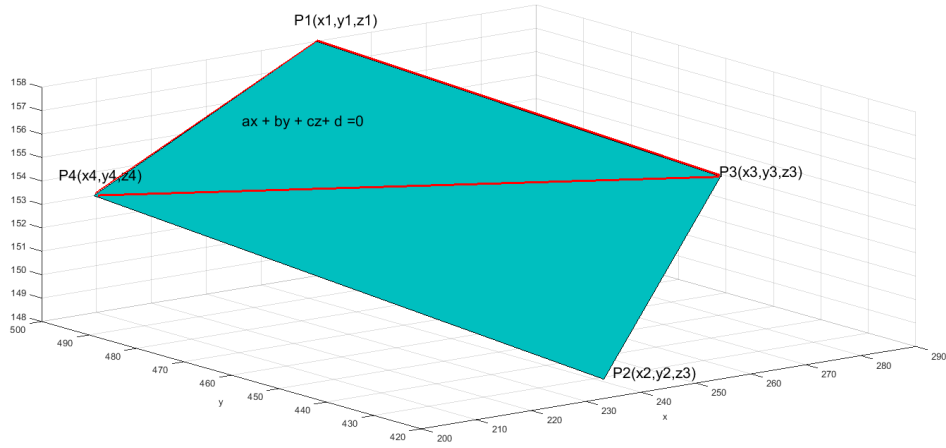
A range from minimum  $x, y$  to the maximum  $x, y$  coordinate values will be taken to cover the entire leaf area. Figure 4.32c illustrates the four points plane. The upper three points are chosen to drive the plane equation. This process results in a rectangular shape image of the plane with full interpolated  $(x, y, z)$  points.





(a) Leaf with 4 points polygon

(b) 4 points plane overlapping with 3D disparity image



(c) 4 points extracted plane, the 3 upper points are used to drive plane equation

Figure 4.32: Plane extraction process for plant leaf

### 4.6.3 Error measurement

The new interpolated plane meets the leaf plane at the three points of the equation indicated. The method that evaluates the interpolated plane depth values by calculating the error between the interpolated plane and the leaf plane is demonstrated in Listing 4.7. All depth points of the interpolated plane are involved in the cal-

culatation of error including the three extremities leaf points that used to drive the plane equation. This method measured the error by selecting which automatically-detected leaf vertices yielded the least error and verified most of the leaf plane points.

**Listing 4.7 Error measurement algorithm**

**Step 1** The difference in depth between the interpolated plane and leaf plane can be measured by subtracting the interpolated plane image from the leaf disparity image to produce a difference image (Equation 4.11).

**Step 2** The error can be measured by taking the Root Mean Square error (RMS) (Equation 4.12) for the difference image. The output of this step is a vector of error values with respect to the image columns.

**Step 3** By applying Equation 4.12 twice on the difference image ( $Dif_{Img}$ ), a vector of error values can be represented by one value named RMS2 error.

**Step 4** To minimise RMS2 error of the interpolated plane, four different plane equations can be examined from the four polygon points by choosing three points at each time alternately.

**Step 5** The minimum value of RMS2 error can be chosen to optimise the plane equation which gives minimum error and verifies more points from the leaf image.

Figure 4.33a presents the error image using different shades of grey. The variance in grey interprets the contrast in value of error from negative values (dark grey) to the positive values (light grey). The difference in images can be measured by the following equation:

$$Dif_{Img} = Leaf_{Img} - Plane_{Img} \quad (4.11)$$

Figure 4.33b shows RMS error vector with respect to the image column. The RMS error is defined by the equation below:

$$E_{RMS} = \sqrt{\frac{1}{n.m} \sum_{i=1:j=1}^{n,m} (Z_{leaf}(i,j) - Z_{plane}(i,j))^2} \quad (4.12)$$

where ( $Z_{leaf}$  and  $Z_{plane}$ ) are equal to the depth value for the leaf and the interpolated plane respectively,  $i$  and  $j$  are the dimensions of the leaf and plane images and  $n$  and  $m$  are the number of rows and columns for both images respectively.

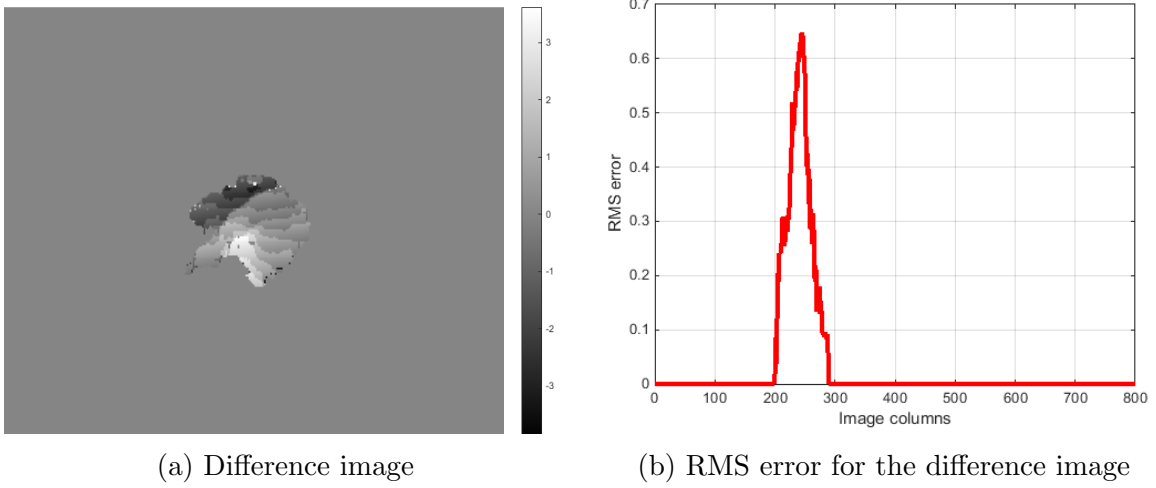
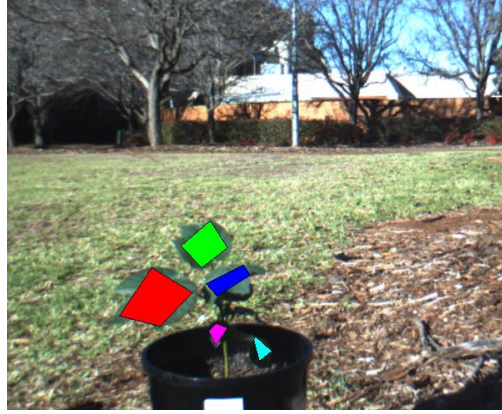
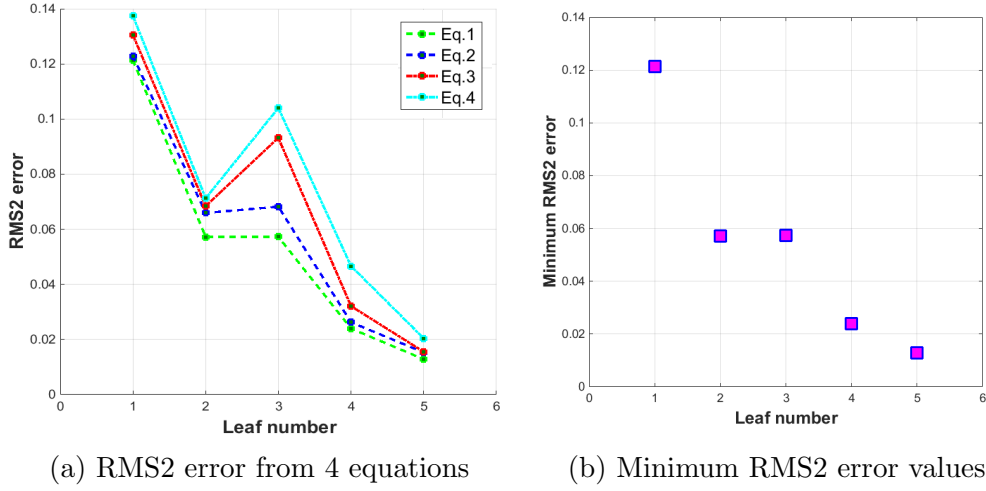


Figure 4.33: The error in depth between the leaf plane and interpolated plane

Figure 4.34c presents plant 1 side 1 with 5 segmented leaves and 5 extracted planes from each leaf. Figure 4.34a shows four values of RMS2 error for four interpolated planes for each leaf of Figure 4.34c calculated from different equations by choosing three polygon points at each time alternately (Step 3, Listing 4.7). Figure 4.34b presents minimum RMS2 error values for each leaf interpolated plane. The minimum RMS2 error can be fulfilled when the interpolated plane points involve the majority of leaf plane points. Minimum RMS2 error indicates that, the interpolated plane points are verifying most of the leaf depth values.



(c) plant 1 side1 with 5 planes

Figure 4.34: Plant 1 side 1 in Figure 4.1 with 5 extracted plane and error analysis

The accuracy of fitting the plane might be increased if the plane were not constrained to fit the extremities of the extracted leaf shape. Sophisticated 3D modelling of cotton leaf shapes and orientation using multiple planes can be achieved using computer aided geometric design (Alarcon and Sassenrath, 2011). As this thesis addresses leaf segmentation and plant modelling, such detailed modelling of individual leaves as described in (Alarcon and Sassenrath, 2011) is beyond the scope of this thesis. However, this chapter serves to demonstrate that leaf vertices extracted by automatic image analysis can be used for geometric description of individual leaves, and potentially in more sophisticated modelling with multiple planes.

---

## 4.7 Chapter summary

This chapter demonstrates a new leaf segmentation and counting algorithm. The utilisation of colour, shape and depth properties enhanced the leaves' detection and occlusion separation. The performance of the algorithm was tested with different plant structures of cotton and hibiscus. Although hibiscus plants have simpler structures in comparison to cotton plants, the leaf segmentation techniques were applied sequentially on hibiscus plant images to solve leaf occlusion problems.

The algorithm used depth information in two stages: Firstly as an effective method to isolate the foreground plant from other foliage, sky and buildings; and secondly to solve connecting and overlapping leaf problems at the final stage of the algorithm. The HSV colour space with two developed equations were used to distinguish green leaves from other plant part colours. Image noise was filtered using Median filter and image region properties. Leaf shape was tested using the fitted ellipse criteria technique.

Another algorithm to segment the connecting and overlapping leaves from each other was presented. The algorithm uses three techniques that depend on the depth gradient discontinuity values. The algorithm techniques addressed three different types of touching and overlapping leaves. DMD was used to targeting the leaves that were connected by the noise pixels, while GDS was utilised to separate leaves with distinct differences in depth using a global search by calculating the unique vector of the disparity map. Subsequently, the ENBD technique was used to discriminate between two connected leaves which have a smooth increment in unique vector, where a sharp depth gradient was observed between neighbouring pixels. The ZNC technique was applied for leaves which were isolated in space with the exception of one small region connected to a neighbouring leaf.

A method that extracted a geometrical plane from leaf vertices was demonstrated. The RMS error between leaf plain and the interpolated plane was calculated. A method that optimises a minimum error equation was proposed. This work was developed for the purposes of calculating the inclination angle of each individual leaf.

## Chapter 5

# Evaluation of automatic leaf segmentation and counting algorithm

## 5.1 Introduction

The automatic leaf segmentation and counting algorithm was evaluated on both cotton and hibiscus plant images. The data sets were collected with varying lighting and environmental conditions. This chapter presents the evaluation of the algorithm's performance under a range of conditions. The evaluation shows the algorithm's strength and its ability to work under varied illumination conditions and also addresses some current limitations of algorithm performance in some situations.

This chapter is organised as follows: the data collection protocol is presented in Section 5.2. The algorithm performance and accuracy rates are discussed in Section 5.3. This section also presents some algorithm limitations due to image issues and other leaf factors that affected the performance of the developed algorithm.

## 5.2 Data collection

A stereo vision camera was used to collect all data sets of images for both cotton and hibiscus plants as explained in Chapter 3. The images were captured from two labeled sides of a plant pot. For each cotton plant, eight data sets of images were captured at different growth rates and under different environmental and illumination conditions. The cotton plants were planted in April 2014 in two different pot sizes resulting in two different growth rates: big cotton (350 mm pot diameter); and small cotton (250 mm pot diameter). Each data set contained 16 cotton plants (4 big cotton and 12 small cotton), except dataset 1 and dataset 2 which had 15 plants each (4 big cotton and 11 small cotton). In total, the algorithm was applied to 252 images of cotton and to 20 images of hibiscus plants. The details of the data collection for different data sets are listed in Table 5.1.



Table 5.1: Cotton plants data set collection. The images were collected during Winter and early Spring of 2014.

Data sets	Image condition	Sun direction	Solar energy (Watts/ $m^2$ )
Dataset 1 (July 13, 12–4 pm)	Sunny Some overexposed and partial shading of leaves	Multiple From left, right and be- hind the camera	178–640
Dataset 2 (July 14, 10 am– 2 pm)	Shady Low illumination	N/A	N/A
Dataset 3 (August 8, 12–4 pm)	Sunny Overexposed leaves	Single From right side of the camera only	273–714
Dataset 4 (August 9, 11 am– 2 pm)	Shady Low illumination	N/A	N/A
Dataset 5 (August 28, 1–4 pm)	Sunny Wind and some bluer image	Single From behind the cam- era only	285–780
Dataset 6 (August 26, 12–3 pm)	Cloudy Complete cloud cover	N/A	77–183
Dataset 7 (September 19, 11 am –3 pm)	Sunny Some overexposed and partial shading of leaves	Single From left side of the camera only	253–892
Dataset 8 (September 19, 3–6 pm)	Shady Low illumination	N/A	N/A

The algorithm was developed initially using six selected cotton and two hibiscus plant images. The algorithm was subsequently applied to the other images to target the general problems with all images. The algorithm was tweaked to gain the major applicability for implementing a general fix for general faults for all images. Further development for the algorithm was applied in order to cope with all images from different conditions. Table 5.1 shows the three main illumination conditions and

the solar energy values at these days for cotton plant data sets at: ‘sunny’ for clear sky; ‘shady’ for sun shade; and ‘cloudy’ for complete cloud cover. These three illumination conditions were used to examine the algorithm’s reliability under a variety of situations. From the table, it can be concluded that for each grouping of sunny and shady conditions there were different cases for each data set. The same illumination conditions were used for hibiscus plant images. Hibiscus plant images were captured during Autumn 2013. The developed leaf segmentation and counting algorithm was applied on hibiscus images to evaluate the ability of the algorithm to work with plants other than cotton.

The results were subdivided according to plant size: big cotton; and small cotton for each data set. The performance of the developed algorithm was evaluated for segmenting and counting leaves and for separating occluded and overlapped leaves. The segmentation results were calculated using evaluation metrics which are defined as follows:

1. True Positive (TP): Refers to a true plant leaf correctly identified by the developed algorithm.
2. False Negative (FN): Presents a plant leaf incorrectly identified as a non-plant leaf.
3. False Positive (FP): Represents a non-plant leaf incorrectly identified as a true plant leaf, or a large and bent leaf identified twice.
4. True Negative (TN): Refers to a non-plant leaf correctly identified as non-plant leaf. This metric was not considered during accuracy calculation due to the uncountable number of objects in the image that are truly identified as non-leaf objects.

For each data set, the sensitivity (recall), precision and accuracy were calculated using Eqs. ( 5.1– 5.3) respectively (Zhu et al., 2010; Liu et al., 2017):

$$Sensitivity = \frac{TP}{TP + FN} \quad (5.1)$$

$$Precision = \frac{TP}{TP + FP} \quad (5.2)$$

$$Accuracy = \frac{TP + TN}{TP + FN + TN + FP} \quad (5.3)$$

### 5.3 Leaf counting accuracy - results and discussion

The segmentation of leaves from their background using the image pre-processing stage was conducted prior to the separation of overlapping leaves using Depth Discontinuity Segmentation method (DDS), (Section 4.4.1). The DDS method was applied to solve the issue of connected and overlapping leaves and relies on the depth feature. The main challenge was the segmentation of multiple leaves under outdoor conditions. The complex structure of cotton and the connection between leaves with many occlusion boundaries add additional challenges to the performance of the algorithms. In addition the illumination in outdoor conditions identified some issues, such as partial shadow and overexposed areas caused by sunlight reflecting from leaf surfaces. Plant leaves were efficiently segmented from the natural background according to their colour, shape and depth properties.

The accuracy of the leaf segmenting and counting algorithm was evaluated by the comparison between the number of leaves produced from automatic segmentation, and the number obtained from visual counting from plant images. The tested

data sets had 272 image pairs (colour image and disparity map) with 2453 cotton and hibiscus leaves in total. The use of developed segmentation algorithm including image pre-processing and the DDS stages was able to successfully detect 1910 leaves. The separation of occluded leaves was carried out using the proposed DDS algorithm with a high separation rate of 84%, where 484 leaves could be separated successfully from 578 connecting and overlapping leaves.

Table 5.2 below shows the overall detection rates of cotton and hibiscus plants under different illumination conditions. It can be observed from the table that, the developed segmentation algorithm shows approximately the same performance for both plants in all conditions, and there is no significant difference between the results of small and big cotton plants.

Some example images are shown in Figures 4.29 and 4.30, where many leaves in various positions and shapes (single, touching and overlapping) were detected successfully. These figures show the capability of the developed segmentation algorithm to cope with a variety of growth stages and illumination conditions. The use of the depth feature with the combination of other image features such as colour and shape, can improve the performance of the proposed algorithm; however outdoor images have many challenges and difficulties.

Table 5.2: Total segmentation rates of developed algorithm for cotton and hibiscus plants under all conditions.

Condition	All environmental & lighting conditions			
Plant size	No. of images	Accuracy%	Sensitivity%	Precision%
Big cotton	64	70	80	86
Small cotton	188	69	76	89
Hibiscus	20	73	78	92
Overall rates	272	71	78	89

Table 5.2 also demonstrates the performance of the algorithm in indoor and outdoor image conditions, for hibiscus plants. The accuracy, sensitivity and precision rates for hibiscus plants were slightly higher than for cotton. The higher results were expected due to the difference in structure between cotton and hibiscus plants and due to the fact that some images were taken in indoor conditions.

Table 5.3 illustrates cotton plant segmentation rates for different lighting and environmental conditions. From the table, it can be observed that shady and cloudy conditions reported good segmentation rates compared to sunny conditions. This is due to the images being overexposed by sun conditions or affected by partial shadow issues. However, some images taken in shady conditions presented false negative and false positive leaves due to insufficient light coverage and low illumination in the shade.

Table 5.3: Average segmentation rates for cotton plants under different illumination conditions where, A = Accuracy, S = Sensitivity and P = Precision.

Pot size	Big cotton				Small cotton			
Lighting	No. of image	A%	S%	P%	No. of image	A%	S%	P%
Sunny	32	69	76	87	94	67	73	91
Shady	24	71	84	84	70	68	79	85
Cloudy	08	71	83	83	24	73	80	90

Small cotton plants report very similar accuracy rates (68%) for both sunny and shady conditions, but report a higher accuracy rate for cloudy conditions (73%). In total, the segmentation rate of both cotton sizes was adequate; however the images were affected by outdoor environment issues such as direct sunlight and distant trees.

Similarly, the algorithm recorded different segmentation rates for hibiscus plant depending on the image capture condition. Although the sample size of hibiscus

plant images was not large like for cotton as the hibiscus plant was not the main focus of this study, high rates of accuracy were observed for indoor (80%) and shady (79%) conditions while medium rates of accuracy were recognised for sunny (67%) and cloudy (65%) conditions.

The results of the segmented images show that some images were affected by illumination issues such as leaf under shadow, low illumination or overexposure. Other images present the effects of other factors such as touching and overlapping leaves, leaf size and orientation. The effects of illumination conditions and other leaf factors on the segmented images are illustrated and discussed in the following sections:

### **5.3.1 Effect of lighting**

The algorithm was tested under sunny, shady and cloudy conditions. For each data set, a certain test was conducted to examine one illumination condition. Certain images from different data sets had insufficient light coverage such as partial shadow or low light conditions, whereas other images exhibited overexposed areas. The following subsections will analyse the impact of lighting conditions on the segmentation results.

#### **5.3.1.1 Image under partial shadow**

Partial shadow affected the performance of the proposed algorithm because it partly obscured the image. For sunny condition data sets, partial shadow was caused by sunlight coming from the left or right side with respect to the camera and plant, brightening the leaves facing the sunlight and shading on the opposite side.

The inspection of the disparity map shows that one leaf with two different areas (shaded, unshaded) could produce incorrect depth information, which could possibly be recognised as two leaves or one leaf with missing information. This is because the edge mask has been used to produce the disparity map which depends on the correlation between brightness pixels of the edge image rather than the absolute values. The inaccurate depth information from the shaded part can affect the segmentation process using depth properties. The shaded leaf might have inadequate information for a positive leaf identification.

The shaded area can also affect colour segmentation using colour properties in which shady areas could include leaves, stem, soil and pot edges that could appear as dark areas in the image. This darkness can effect the HSV colour transformation of the hue channel, where it is hard to differentiate between a leaf or non-leaf object according to its colour. Since a stereo vision camera produces disparity map information for these shaded regions, they are within the threshold value of depth that segments the plant from the background. Therefore, the image analysis algorithm may count shaded regions as a real leaf causing false positive leaf issues.

When sunlight came from the back of the camera facing the plant, shadows were cast behind the plant. In these instances, no shady areas were recognised in the colour image. This case was considered an outstanding example of capturing images under sunny conditions, however images were captured from different directions (left, right) with respect to the camera as plants can exhibit different sun direction during the day. Front sunlight direction caused camera overexposure therefore, the image analysis of front sun direction was not considered or evaluated.

Figure 5.1 shows three plants with different sun directions and shadow areas to the left and the right of the plants. Left-sun-direction is presented by Figure 5.1a for

small cotton with two small shaded leaves. The result image shows all the leaves are segmented correctly by the algorithm including leaves under shadow.

Figures 5.1c and 5.1e presents plant with back-sun-direction and right-sun-direction respectively. The plant with back-sun-direction presents higher segmentation results except one false positive leaf presents part of stem incorrectly identified as a true leaf. The plant with right-sun-direction also presents good segmentation rates including one overexposed leaf. The result image also shows one false positive leaf on the shaded soil area.

The result images of Figure 5.1 present good segmentation rates for the algorithm which can cope with leaves under shadow (Figure 5.1a) and overexposure (Figures 5.1e). This is because the colour of these leaves is still within the green area of the hue channel despite the difference in illumination between the leaves under shadow and the leaves under overexpose as the HSV transformation can separate out the luminance from the colour information (Section 4.4.2).

The segmentation results of these plants show the capability of the algorithm to segment leaves having different sun direction and illumination issues. Other images of sunny conditions exhibited the same illumination issues (shadow, overexposure) with different segmentation effects. For some overexposed images when leaves show more yellow rather than green, the algorithm may not segment these images properly which results in false negative leaf issues.



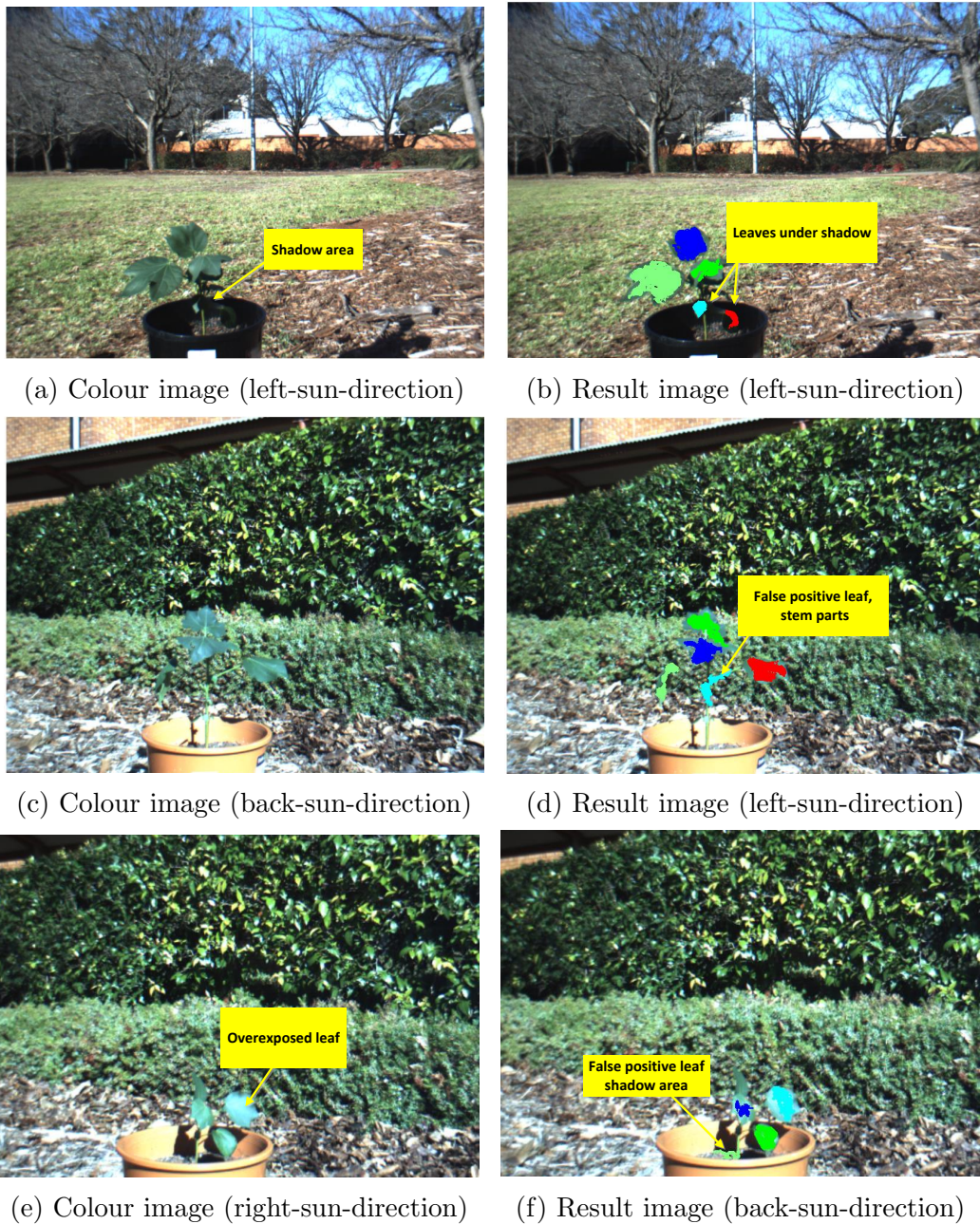


Figure 5.1: Three selected plants from dataset 1 with different sun directions.

### 5.3.1.2 Image under overexposed conditions

Overexposed areas are another problem for sunny condition images. Overexposed areas occur when the upper surface of the leaf reflects sunlight towards the camera sensors. Since the proposed segmentation algorithm depends on the HSV colour

space transformation to segment a green leaf from other parts of the plant, leaves which are overexposed show yellow rather than green. Therefore, these leaves are not segmented properly; however depth information is available for overexposed areas. Figure 5.2 presents two cotton plants with overexposed lighting issues.

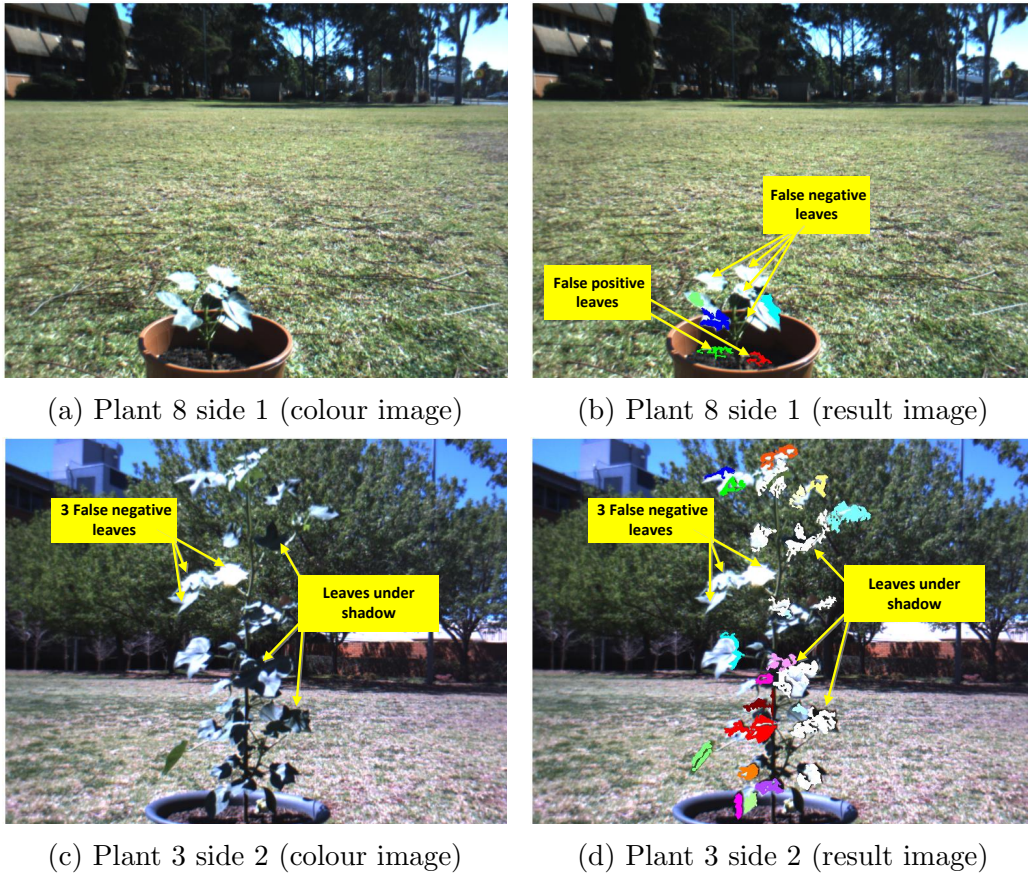
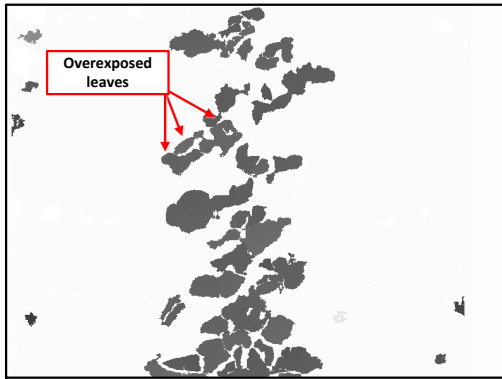


Figure 5.2: Two selected plants from dataset 3 (small cotton) and dataset 5 (big cotton) with overexposed conditions.

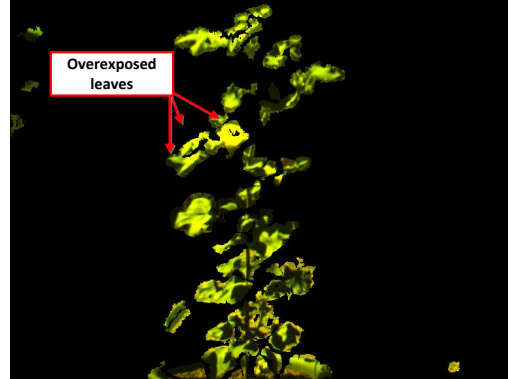
The overexposed lighting issue was investigated for the plant of Figures 5.2c which has three false negative leaves as shown in Figures 5.2d. Figure 5.3 shows the steps of segmentation for this plant. The disparity map and the RGB colour transformation (Section 4.4.1) present these overexposed leaves as shown in Figure 5.3a and 5.3b respectively. The majority of the plant's leaves show yellow rather than green as they were overexposed. The histogram distribution shows that the maximum number of bins are within the yellow area of hue channel (Figure 5.3c). Other



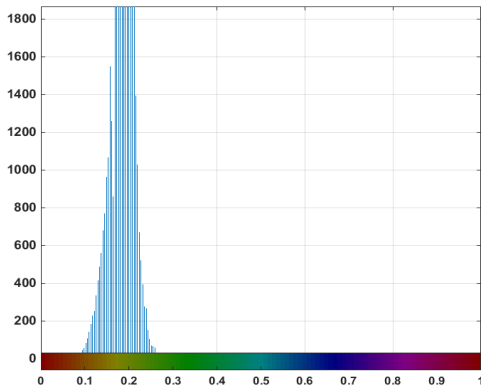
histogram bins



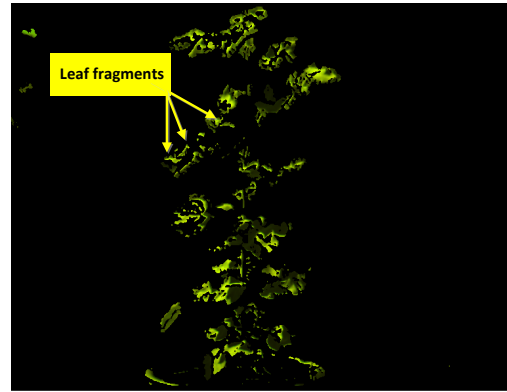
(a) Disparity map



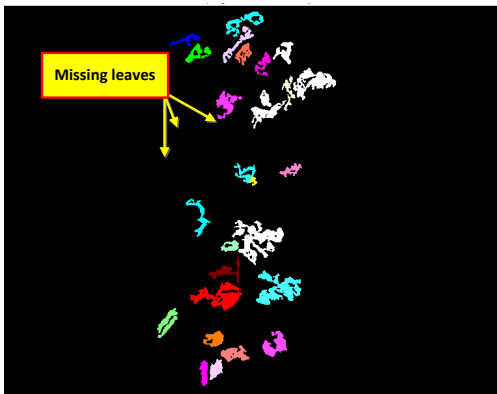
(b) RGB color transformation



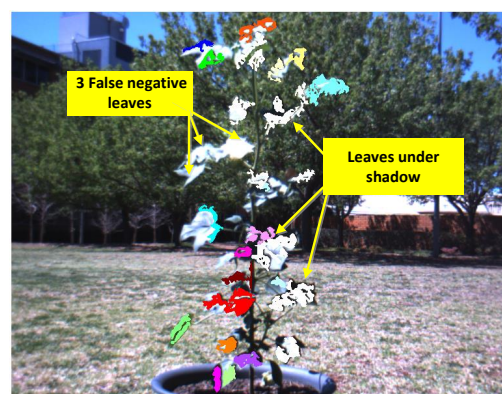
(c) Hue distribution & bins' values



(d) HSV colour transformation



(e) Final segmentation



(f) Final segmentation (colour image)

Figure 5.3: Steps of segmentation for Plant 3 side 2 from dataset 5 (big cotton) with overexposed and partial shadow conditions.

distribute on green and red areas. The developed segmentation algorithm, based on HSV color transformation (Section 4.4.2)), thresholds the hue channel for green only which eliminates yellow and preserves green areas of the plant's leaves. These

leaves appear as small fragments of green area as shown in Figure 5.3d. These small areas were removed when applying image enhancement processes (Section 4.4.3), as shown in the segmentation results of Figures 5.3e and 5.3f. Addressing this issue thereby changing the calibration's parameters of Equations 4.1 and 4.2 to accept yellow pixels from hue with green pixels caused another issue whereas non-leaf objects (stem, branches, pots' edges) can also be identified as true leaves.

The plant of Figure 5.3 shows a mix of leaves with two issues, overexposure and partial shadow. Overexposure caused false negative leaves, whilst shadow produced false positive leaves for non-leaf objects such as soil and pot edges in some instances as shown in Figure 5.2b. Leaves under shadow were segmented properly for the plant of Figure 5.3, however some leaves' parts were missing due to the shadow issue that may partially cover leaf area as discussed in Section 5.3.1.1. Overexposure issue was observed in most of the sunny condition images, hence these images exhibited the issue of false negative leaves. Overexposure is a challenging issue for machine vision at outdoor conditions which invites more studies and analysis to solve this critical problem.

### **5.3.1.3 Image under low illumination conditions**

Low illumination conditions were observed in two cases for sunny and shady conditions:

1. Case 1: In sunny conditions, low illumination conditions were observed when the image was captured at sunset (Figures 5.4a and 5.5a);
2. Case 2: In shady conditions, these conditions occurred when the plant was placed in the shade, while the camera was set between the shady source and

the plant (facing the plant). In this instance, two illumination conditions can be observed in the image: dark illumination for the plant; and overexposure for the background (Figures 5.4b and 5.5b).

A different examples of the two cases explained above is shown in Figure 5.4 and Figure 5.5. From the visual inspection of the colour images for both figures, it is hard to recognise all the leaves in these images. With this in mind, a high segmentation rate could be observed for Figure 5.4 which presents two plants' images taken in low illumination conditions at sunset (Figure 5.4a) and under shadow at morning time (Figure 5.4b). In contrast, Figure 5.5 illustrates low segmentation rates for the other two plant images taken in the same conditions as Figure 5.4. These contradictory results require an analysis for the colour images and the disparity maps.

By comparing the colour images and the disparity maps of Figure 5.4, it is clear that most of the plants' leaves were produced by the stereo vision system, while many of the plant's leaves are missing from the disparity maps of Figure 5.5. The reason for that is another factor that can affect leaf segmentation process called leaf orientation (i.e. the direction of leaf with respect to the camera). The images of Figure 5.4 present leaves with front dominant direction while Figure 5.5 shows back or obscure direction for the majority of the plants' leaves. The leaf direction can affect the correspondence process of stereo matching to produce the disparity maps. Front dominant leaf direction can preserve a complete leaf shape and offer the required leaf texture for calculating accurate and dense depth values. In contrast, the depth values might compute for a few points for the low textured object (Bradski and Kaehler, 2008). A variety of types of leaves' orientation and their effects on segmentation rate are discussed and presented in the next section.

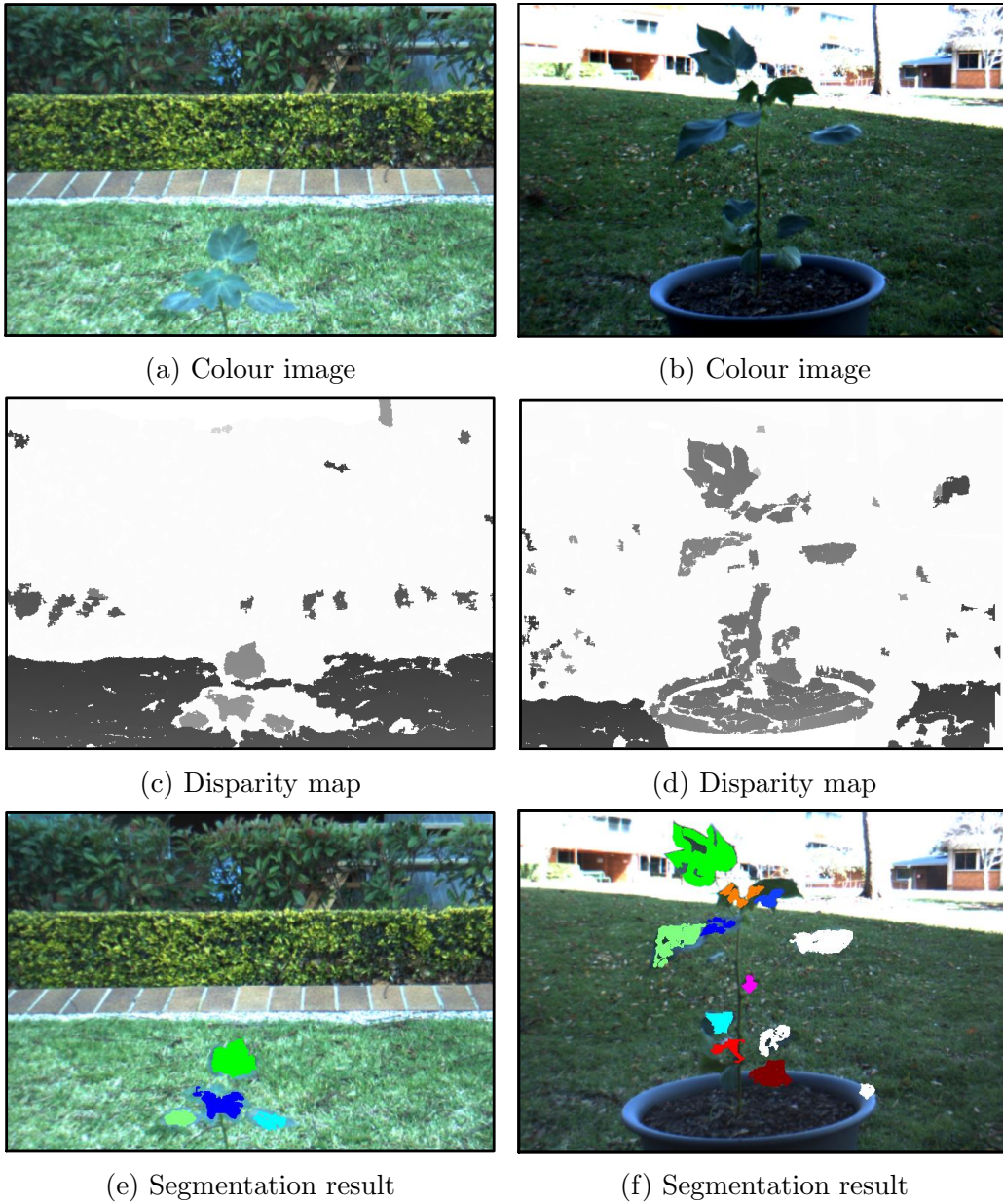


Figure 5.4: Two selected plants from different data sets with low lighting conditions and high segmentation rates, (a) Plant 11 side 2 dataset 6 presents Case 1, (b) Plant 3 side 1 dataset 2 presents Case 2.

The analysis of the effect of lighting on the segmentation result can strongly support the argument for the reliability of stereo vision system to produce depth information under different outdoor illumination conditions and environments and also shows the limitation of this system to work with a low textured scene.

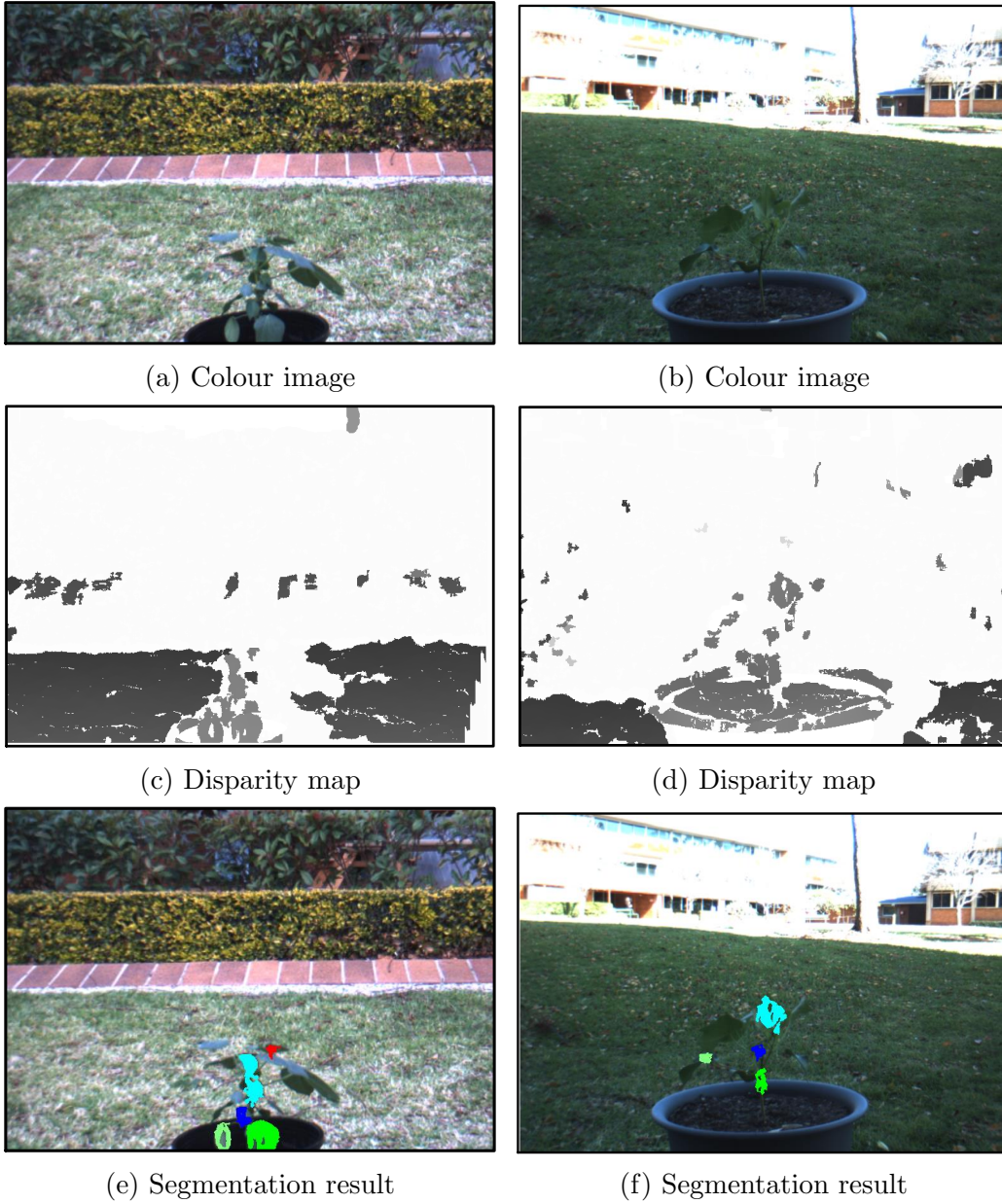


Figure 5.5: Two selected plants from different data sets with low lighting condition and low segmentation rates, (a) Plant 1 side 2 dataset 6 presents Case 1 (sunset), (b) Plant 1 side 1 dataset 2 presents Case 2 (images under shade).

### 5.3.2 Effect of leaf orientation

During data collection, images from both sides of each plant were captured to enable the effect of leaf orientation on leaf count accuracy to be quantified. The experimental setup was designed to take the images from two sides of the plant. Each side was labeled using a fixed tag on the pot edge. Ideally, side 1 was supposed to be the front or the upper side of the leaves, when all leaf upper surfaces faced the camera. Side 2 was the opposite side when all leaf lower surfaces face the camera. Typically, these two ideal cases were observed for some plants. For the majority of images, the view was mixed between front, side and back leaves.

The impact of leaf orientation on the algorithm's performance was investigated because leaf orientation affects the perceived shape of the leaf. In some images the leaf appears as a thin line, similar to a stem or branch, which is potentially insufficient information for a positive leaf identification. Leaf orientation is an important factor to provide the sufficient leaf texture for an accurate stereo matching process.

Table 5.4 presents leaf segmentation rates with respect to the leaf orientation for all cotton plants. The front dominant leaf orientation presents higher segmentation rates compared with the orientation of other leaves. The reason for these results is that front dominant leaf orientation can show a complete leaf shape with full texture information, which can enhance stereo matching and the segmentation process.



Table 5.4: All data sets segmentation results according to leaf orientation.

Plant size	Big and small cotton			
Leaf orientation	No. of image	Accuracy%	Sensitivity%	Precision%
Front dominant	35	79	86	91
Back dominant	11	70	77	89
Mix dominant	166	69	77	88
Obscure-leaf-orientation	40	65	73	85

Figures 5.6 shows four selected plants with different types of leaf orientation as presented below:

1. Front dominant: Front dominant leaf orientation is shown by Figures 5.6a and 5.6b). This orientation presents an ideal leaf orientation for plant leaves and can result in high segmentation rates;
2. Back dominant: It is hard to detect this type of leaf with insufficient colour, texture, shape and depth information being detected (Figures 5.6c and 5.6d);
3. Mixed dominant: All types of leaf orientation were found in mixed dominant leaf image (Figures 5.6e and 5.6f). This type of image shows an adequate percentage of segmentation rates, however; some leaves appeared as a thin line, similar to a stem and branches, which could not be identified correctly as a leaf when applying ellipse criteria (Section 4.4.3);
4. Obscure-leaf-orientation: Obscure orientation of the leaf can be caused by leaf movement or leaf size at an early growth stage of the plant (Figures 5.6g and 5.6h). It is hard to recognise and segment this type of leaf due to the small leaves area and they are touching each other. Leaf movement due to the wind which can cause a blurred image with obscure leaf shape and orientation.

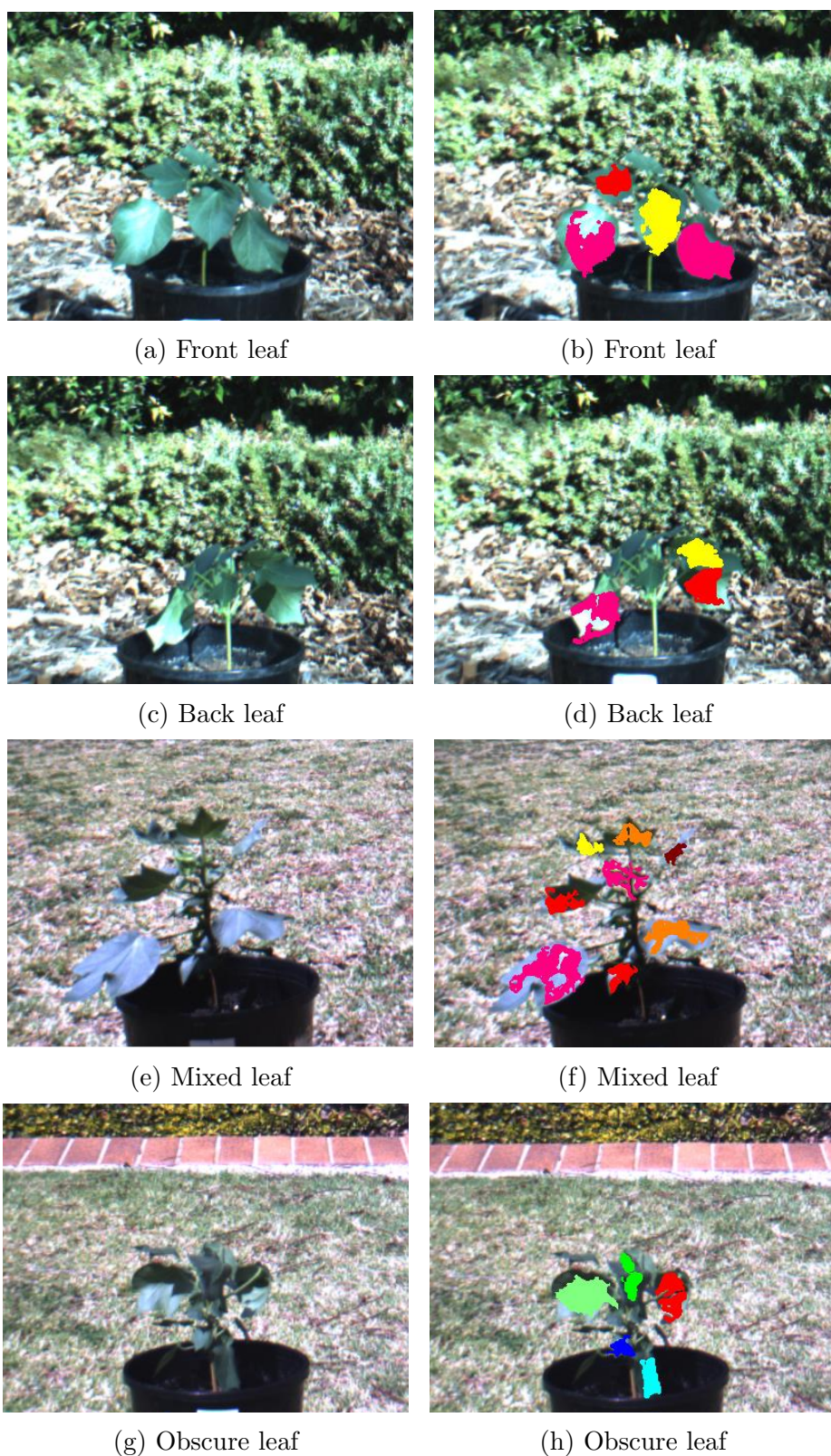


Figure 5.6: Four selected plants with different dominant leaf orientations. Column one, colour image. Column two, result image.

### 5.3.3 Effect of leaf size

As a consequence of plant growth, different sized leaves could be observed on the one plant image ranging from 1 to 10 cm. Small leaves are difficult to distinguish between using visual inspection. Figure 5.7a shows a plant with four small leaves which are incorrectly segmented as two leaves as it is hard to distinguish between them by visual inspection (Figure 5.7b).

Larger leaves exhibit bending around each lobe of the leaf, causing distinct depth differences (greater than 3 pixels in the disparity map) for different lobes of a single leaf. The DDS segmentation method considered each lobe as an independent leaf. This may cause incorrect leaf segmentation and can increase the number of false positive leaves. Large and bending leaves were significantly noticeable in big cotton plant images (more than 10 cm).

Figures 5.7d and 5.7f illustrate two plants from big cotton and the corresponding disparity maps for their large leaves. From visual inspection of these maps, some leaves are agglomerated in one part (Figure 5.7f), while others are already divided into two parts (Figure 5.7d). The DDS segmentation method was applied on each part of these leaves. Large leaves with different lobes and a flat pose can be precisely identified as one leaf as shown by leaf 2 in Figures 5.7f. This type of leaf can be segmented adequately by the algorithm. In contrast, large and bent leaves are a critical segmentation issue as they are normally divided into two parts due to the distinct difference in depth. These types of leaves are presented by leaf 1 and leaf 3 in Figure 5.7f.

From the overall algorithm performance for 252 cotton images, about 67 leaves were visually assigned as large, bent and folded leaves. These leaves produced 26 objects

as false positive leaves which is 10% from the total sum of false positive leaves. The other source of false positive leaves consisted of the shady areas and other parts of the plant such as stem, branches, soil and pot edges.



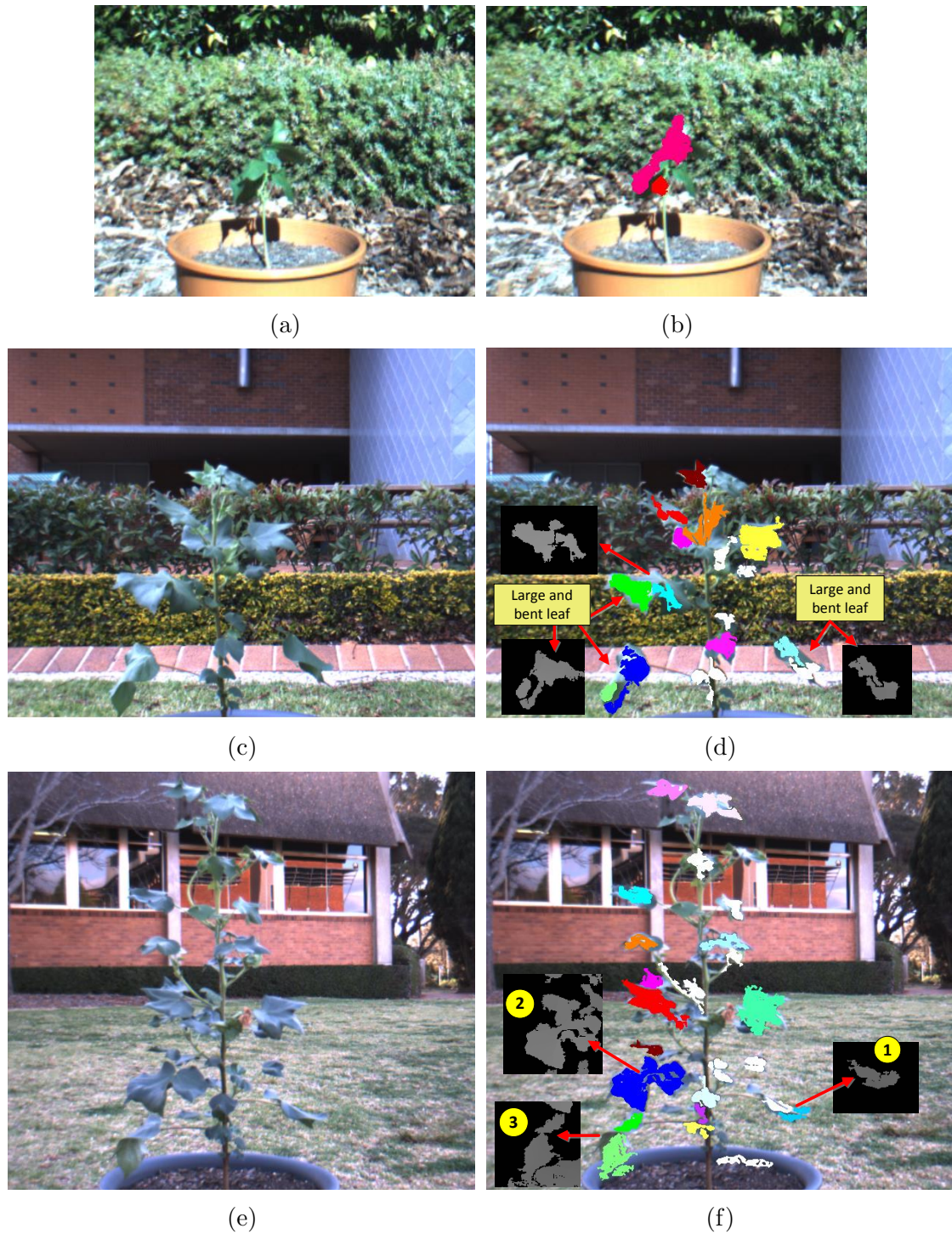


Figure 5.7: Plants with different leaf sizes (a) Small leaves; (c) Big cotton with 3 large and bent leaves showing two parts disparity for each leaf; and (e) Big cotton with 3 large and bent leaves showing one part disparity for each leaf.

### 5.3.4 Effect of overlapped leaves

Typically, images of plants with developing canopies consist of leaves that occlude other leaves, with a greater number of occlusions on plants with denser canopies. This problem is increasingly noticed with the late growth stage of the plant. The proposed algorithm was conducted with two stages of image pre-processing; and Depth Discontinuity Segmentation (DDS), as discussed in Chapter 4. The first part was conducted with leaf segmentation using colour, shape and depth properties; whereas the second part dealt with occluded and overlapping leaves using newly developed techniques.

Table 5.5 below shows the total number of connecting and overlapping leaves for cotton and hibiscus plants. From 578 connecting leaves for 272 images of cotton and hibiscus plants, the DDS segmentation successfully separated 484 leaves with 84% separation rate. The developed algorithm shows approximately the same performance for cotton and hibiscus plants under various lighting and environmental conditions. The similarity in performance can be interpreted as the ability of the algorithm to work with different types of plant rather than just cotton.

Table 5.5: Separation rate of DDS algorithm for occluded and overlapping leaves for cotton and hibiscus plants in all conditions.

Condition	All environmental & lighting conditions					
Plant type	No. of image	No. of leaf	Segmented leaf	Overlapped leaves	Separated leaves	Separation rate%
Cotton	252	2025	1578	514	431	84 %
Hibiscus	20	428	323	64	53	83 %
Overall rates	272	2453	1910	578	484	84 %

The connecting and overlapping leaves with flat poses are a critical segmentation issue for the developed algorithm. Figure 5.8 presents two cases from that type of occlusion with different segmentation results. Figure 5.8b illustrates big cotton having two overlapping leaves with a flat pose. The figure also shows the corresponding disparity map for these leaves. From visual inspection of the disparity map, a large difference in depth (more than 3 pixels value) between the neighbouring pixels of the candidate leaves can be recognised. These leaves can be correctly segmented to two leaves using depth property.

Figure 5.8a presents small cotton with four connected leaves and their corresponding disparity maps for each connected pair. The visual inspection of the disparity maps shows a smooth change in depth values between the neighbouring pixels. Since the difference between the neighbouring pixels is less than the threshold value (less than 3), these connected leaf areas were incorrectly identified as a single leaf for each pair. In this instance, the depth feature would not be beneficial to segment this particular type of occluded leaf. If the occluded and overlapping leaves cannot be separated using depth property, the algorithm would need to be modified to extract other features like certain shape attributes from the images. The leaf shape boundaries could be beneficial to identify these types of leaves. This type of identification can be implemented by training the leaf boundary classifier MLP (Xia et al., 2013) about these types of leaves.



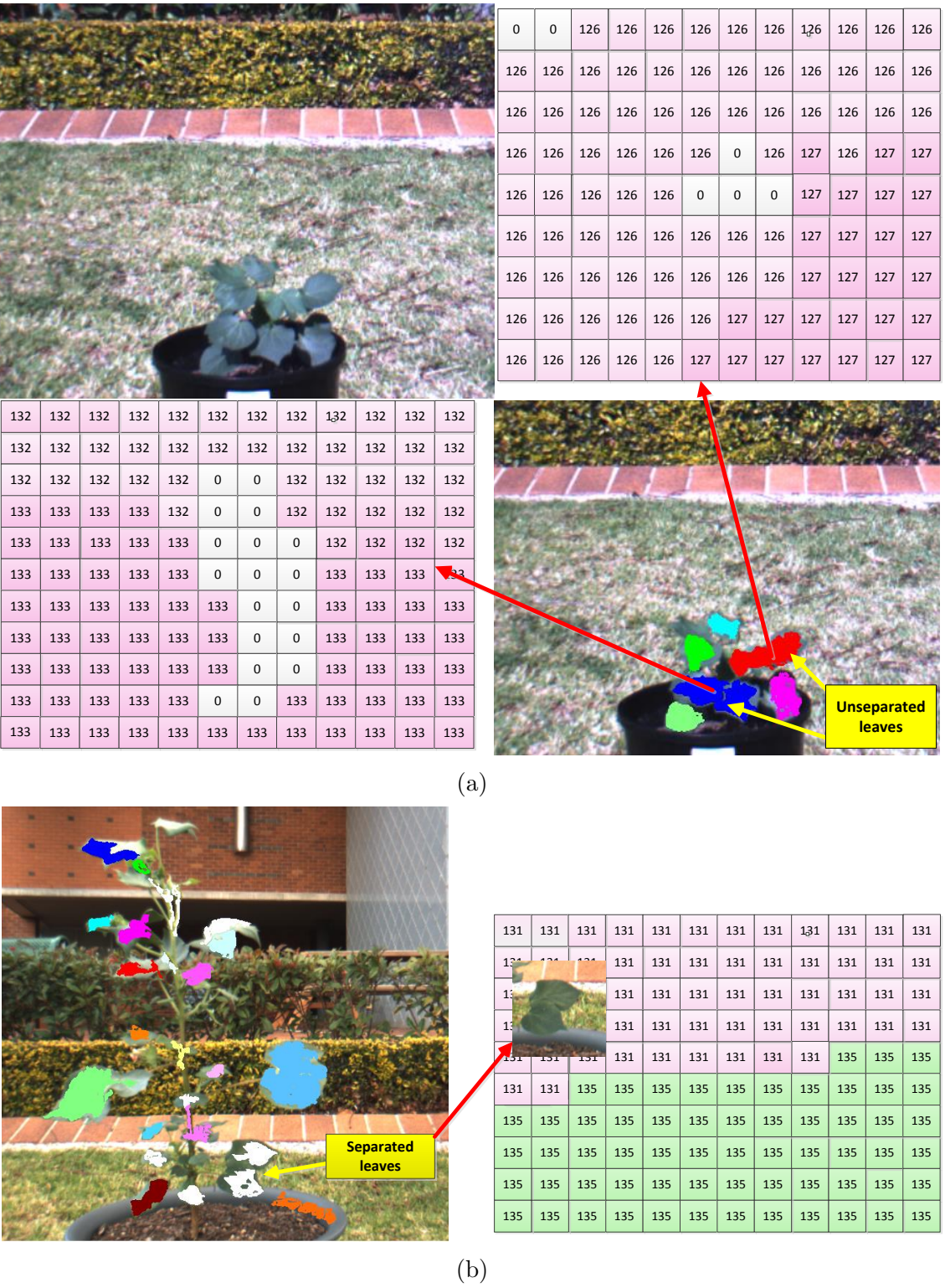


Figure 5.8: Two selected plants with overlapping leaves in flat pose and their segmentation results: (a) unseparated leaves; (b) separated leaves.



---

## 5.4 Chapter summary

The performance of the potential algorithm for automatic leaf segmenting and leaf occlusion separation, using colour, shape and depth properties was evaluated in this chapter. Eight data sets of cotton plant images (252 images) and 20 images of hibiscus plant were carried out to evaluate the performance of the algorithm. The images of cotton and hibiscus plants were captured under a variety of growth rates and environmental conditions. The results for the three labeled conditions (sunny, shady and cloudy) were presented and analysed. The proposed algorithm presents successful segmentation rates for each labeled condition.

The main image issues were demonstrated and the effects of these issues on the segmented images were analysed and evaluated. Overexposure was the main lighting issue affecting the performance of the algorithm. Partial shadow and low illumination were the other illumination issues that can affect the segmentation rate, however the algorithm can cope with these issues and produce acceptable results.

Other issues such as leaf orientation, size and overlapping can also affect results in different ways. Leaf orientation is another important factor which can preserve leaf shape and texture for positive leaf identification. Large, bent and overlapping leaves are a critical segmentation issue. Large and bent leaves are normally identified as two parts due to the distinct difference in depth. The developed algorithm addressed the leaves overlapping issue and benefited from depth information to assist segmentation. Solving other issues such as elimination of the effect of the illumination conditions on the segmented images or segmenting large and bent leaves are beyond the scope of this study.

The developed algorithm shows almost identical performance for both cotton and hibiscus, which interprets the ability of the algorithm to work with different types of plant other than cotton. The results show that it is possible to enhance results by adding depth to the other properties (colour and shape), rather than using them in isolation. Out of 2453 cotton and hibiscus plant leaves, 1910 leaves were detected successfully using DDS algorithm. The segmented leaves had 578 occluded and overlapping leaves, and DDS could separate 484 leaves successfully with a high separation rate (84%). The overall accuracy, sensitivity and precision of detecting and separating leaves were 71%, 78% and 89% respectively for all plant images in different environmental and illumination conditions. These values are highly dependent on illumination conditions, leaf orientation and on the density of the leaves in the canopy.

## Chapter 6

Automatic plant branch  
segmentation using vesselness  
measure

## 6.1 Introduction

In this chapter, a preliminary plant stem and branch segmentation algorithm is implemented on a hibiscus nursery plant. A hibiscus plant represents a plant with typical structure, with clearly discernible stem and branches. The proposed algorithm is based on vesselness measure and Hough transform techniques. This chapter is organised as follows: an overview of the main steps of stem and branches segmentation algorithm is presented in Section 6.2. Prior to the development of the proposed algorithm, two stranded edge detection techniques were investigated in their applicability to segment stem and branches in Section 6.3. The extraction process for plant stems and branches uses the vesselness measure and Hough transform techniques, which are presented in Section 6.4. The results on the ability of the algorithm to detect and count the branches automatically are shown in Section 6.5, and an initial work for reconstructing plant segmented parts to develop a structural model in 2.5D or 3D is presented in Section 6.6.

## 6.2 Stem and branches segmentation algorithm overview

A stem and branches segmentation algorithm has been developed using a combination of techniques to extract stem plant features from the colour side view of the image in both indoor and outdoor environments. Plant images were captured using an 8-bit RGB colour stereo vision camera. The resolution of the images used was  $384 \times 512$  pixels. The images were taken of a hibiscus nursery plant from a distance of 100 cm in both indoor and outdoor conditions. The algorithm consists of three main steps:

1. Extract branches from colour plant images using the vesselness measure method.
2. Apply the Hough transform technique to detect the lines of the branches.
3. Classify those branches according to the Hough transform parameters and count and uniquely label those branches.

## 6.3 Edge detection for stem and branch segmentation

Prior to the development of stem and branch profile detection algorithm, it has been important to investigate some of the standard edge detection techniques. The desired outcome is to isolate stem and branch pixels from other plant parts and background pixels. The significant local change in image intensity can assign an edge in an image (Jain et al., 1995). The stems and branches can form a distinct line in the image due to their smooth and curvilinear shape structure which can potentially be detected by an edge detection technique. A line can be considered as a type of edge where the pixel intensity changes from background intensity value to the line intensity value and back to the background intensity value (McCarthy, 2009).

From the literature, the edge detection of Sobel and Feldman (1968) and Canny (1986), have been demonstrated as an effective method for edge detection of plant parts (Xia et al., 2013; Sosa et al., 2013). Figure 6.1 shows hibiscus plant (Figure 4.1g) image's segmentation after applying edge detection techniques of Sobel and Canny. It is clear that Sobel filter detects stem, branches and leaf boundaries, while Canny filter detects stem, branches, leaf boundaries and veins. Canny's algorithm finds image edges by looking for local maxima of the gradient using a Gaussian filter which assumes to have different intensity of image pixels (Canny, 1986).

This algorithm uses two values of threshold (higher and lower) to detect strong and weak edges. Some weak edges are also included if they connect to strong edges. The value of higher (effective) threshold was determined using Otsu threshold segmentation algorithm from the gray scale images (Otsu, 1975). This algorithm uses the least squares method to calculate the high threshold based on the gradient histogram which can effectively segment the foreground from the background (LI et al., 2008; Wang and Li, 2015). The value of the Otsu threshold was assigned as a higher threshold for Canny algorithm. By examining different samples of images, it was found that, the ratio of Canny lower threshold to higher threshold is equal to: 1:2 or 1:3 and depends on the image intensity. The standard deviation of the Gaussian filter sigma was examined with different values for the best image segmentation. It was observed that sigma equal to one can provide the desired segmentation outcomes for stem and branches using Canny edge detection. The value of Otsu threshold (higher threshold) was also assigned for Sobel algorithm which detects all edges that are stronger than the higher threshold.

Figure 6.1 shows the effective segmentation of leaf and stems edges with values of 0.0239 and 0.0478 for lower and higher thresholds respectively of Canny edge detection, and with a threshold value of 0.0478 for Sobel edge detection. Other threshold values below and above these values were also examined in order to detect a clear stem and branch profile. The threshold values determined by Otsu method tried to achieve the clearest stem and branch images segmentation among the other values, but they also extracted leaves as well. The results of edge detection operators show that both leaf and branch edges revealed a strong response which limits the suitability of edge detection operators for identifying stem and branches. Since the current application is concerned with stem and branch detection, an investigation of another segmentation technique was required which could be possibly more effective for the desired application.

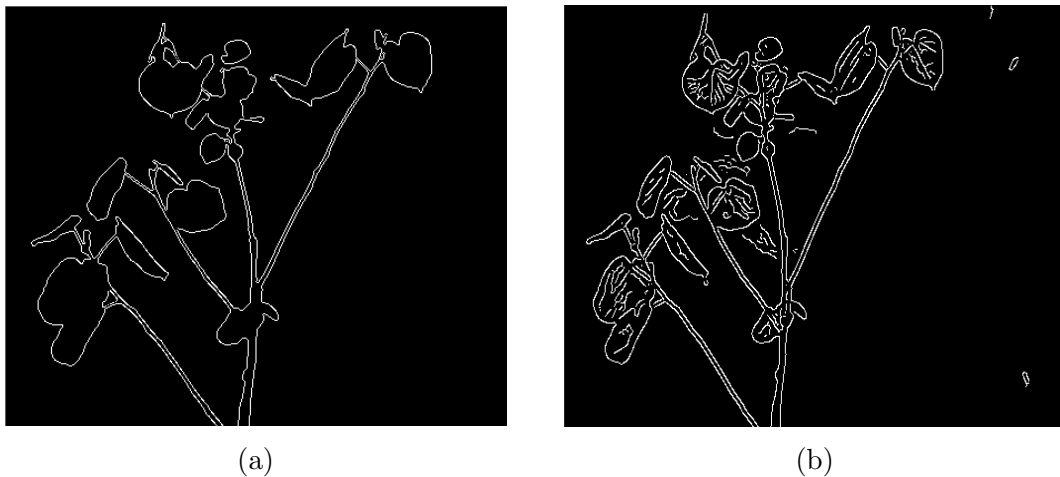


Figure 6.1: Hibiscus nursery plant (a) Sobel edge detection filter; and (b) Canny edge detection filter.

## 6.4 Branch extraction using vesselness measure

In this section, an algorithm has been developed to extract stem and branch profiles from plant colour images using a vesselness measure technique. The vesselness measure is based on detecting a typical line profile of reflected light on the colour image (Steger, 1996). Stem and branch appear as significant vessel structures in colour images (McCarthy et al. 2009; Nakarmi and Tang, 2013). The use of vesselness properties is more favourable than colour properties to identify stem and branches in the images, as stem and branch colours may range from green to brown. The vesselness measure is so named because of its original development application to extract vessels from medical images (Frangi et al., 1998). The vesselness measure technique cannot be applied to the depth image because this technique is based on detecting a typical line profile of reflected light, whereas depth image does not exhibit a typical line profile.

The vesselness measure has been used to extract vessel structures (curvilinear structure) for stem and branch detection (McCarthy et al., 2009; Nakarmi and Tang,

2013), and for complex vascular structure detection (Qian et al., 2009; Tankyevych et al., 2009). The vesselness measure technique calculates the eigenvalues and eigenvectors of the Hessian matrix ( $H$ ) to compute the likeness of an image region to vessels, according to the method described by Frangi et al. (1998):

$$H = \begin{bmatrix} I_{xx} & I_{xy} \\ I_{xy} & I_{yy} \end{bmatrix} \quad (6.1)$$

where,  $I_{ab} = \frac{\partial^2 I}{\partial a \partial b}$  for each image pixel,  $I$  is the pixel's intensity value and  $a, b$  are the pixel coordinates values (Magnus et al., 1995). The image second order derivatives are calculated by convolving the image with derivatives of a Gaussian kernel with standard deviation  $\sigma_s$  (Steger, 1996). Vessel structures and lines with different widths can be extracted by varying the standard deviation of the smoothing filter  $\sigma_s$ . Wider lines can be detected with a large value of  $\sigma_s$ . The present study is concerned with the detection of stem and branches, which are not wide, thus a low value of standard deviation  $\sigma_s$  was chosen to detect stem and branches correctly and to eliminate leaf areas.

The eigenvalues of the Hessian matrix ( $H$ ) are symbolised as  $\lambda_1$  and  $\lambda_2$  and can be used to detect the vessel region (Frangi et al., 1998). The eigenvalues decide if this pixel belongs to a tube-like or a blob-like structure. A small value of  $\lambda_1$  with a large value of  $\lambda_2$  indicates that this pixel belongs to a tube-like structure. The sign of eigenvalues indicates the brightness of the tube structure. The vesselness is a measure of the probability of the pixel belonging to a blood vessel (Frangi et al., 1998). In this special case the vesselness is a measure of the probability of the pixel belonging to the plant stem and/or branch.



The vesselness measure consists of two criteria: the ‘second order structure’  $s$ ; and ‘blobness measure’  $\mathfrak{R}_\beta$  (Frangi et al., 1998). The ‘second order structure’  $s$  is calculated by using the expression:  $s = (\lambda_1)^2 + (\lambda_2)^2$  for a 2D image which gives a low response for low image contrast. The blobness  $\mathfrak{R}_\beta$  is given by the ratio of the Hessian matrix eigenvalues  $\lambda_1 / \lambda_2$  and it has lower values for tube-like structures than blob-like structures. The vesselness measure ( $\nu_o$ ) can be combined between  $\mathfrak{R}_\beta$  and  $s$  by the expression of Equation 6.2 where  $\beta$  and  $c$  are thresholds which control the filter’s sensitivity to  $\mathfrak{R}_\beta$  and  $s$ , respectively.

$$\nu_o = \begin{bmatrix} \exp(\frac{\mathfrak{R}_\beta^2}{2\beta^2})(1 - \exp(-\frac{s^2}{2c^2})) & \text{if } \lambda_2 > 0; \\ 0 & \text{otherwise} \end{bmatrix} \quad (6.2)$$

Figure 6.2 shows a hibiscus nursery plant from an arbitrary side view under indoor conditions with different output of vesselness measure results. The plant images show different responses of the vesselness measure to the stem and branches with varying values of standard deviation  $\sigma_s$ . By increasing the value of  $\sigma_s$ , the width of the detection line increases and the detection of blob leaf areas can be recognised and increased as the blobness  $\mathfrak{R}_\beta$  increased. The brightness of detected branches can be controlled by setting a suitable value to  $\beta$  and  $c$  (the parameters of Equation 6.2).

Prior to the selection of suitable values for  $\sigma_s$  and the threshold values of  $\beta$  and  $c$ , a wide range of these parameters was investigated. It was found that the values of ( $\sigma_s = 0.55$ ,  $\beta = 0.5$  and  $c = 7$ ) can provide the optimal segmentation results for stems and branches only, without including edges of leaves as shown Figure 6.2. The calibration of these parameters as an initial setting is required only once during the development of the algorithm. The same values of these parameters were applied then for all plant images which produce satisfactory results.

Figure 6.3 demonstrates the output of vesselness measure after applying a morphological area opening operation. Applying the area opening operation based on the area of the objects to eliminate unwanted parts, is important at this stage, in order to remove most of the unwanted leaf parts from the image. Then the Hough transform technique was applied for detecting stem and branch lines as applied this technique before removing unwanted parts, could produce more false positive lines for leaf edges, which could be similar to the small twigs. The area opening operation works under the concept of the connected components algorithm, which removes all connected components (objects) having an area fewer than the selected  $x_c$  pixels. The value of  $x_c$  can be any integer value.

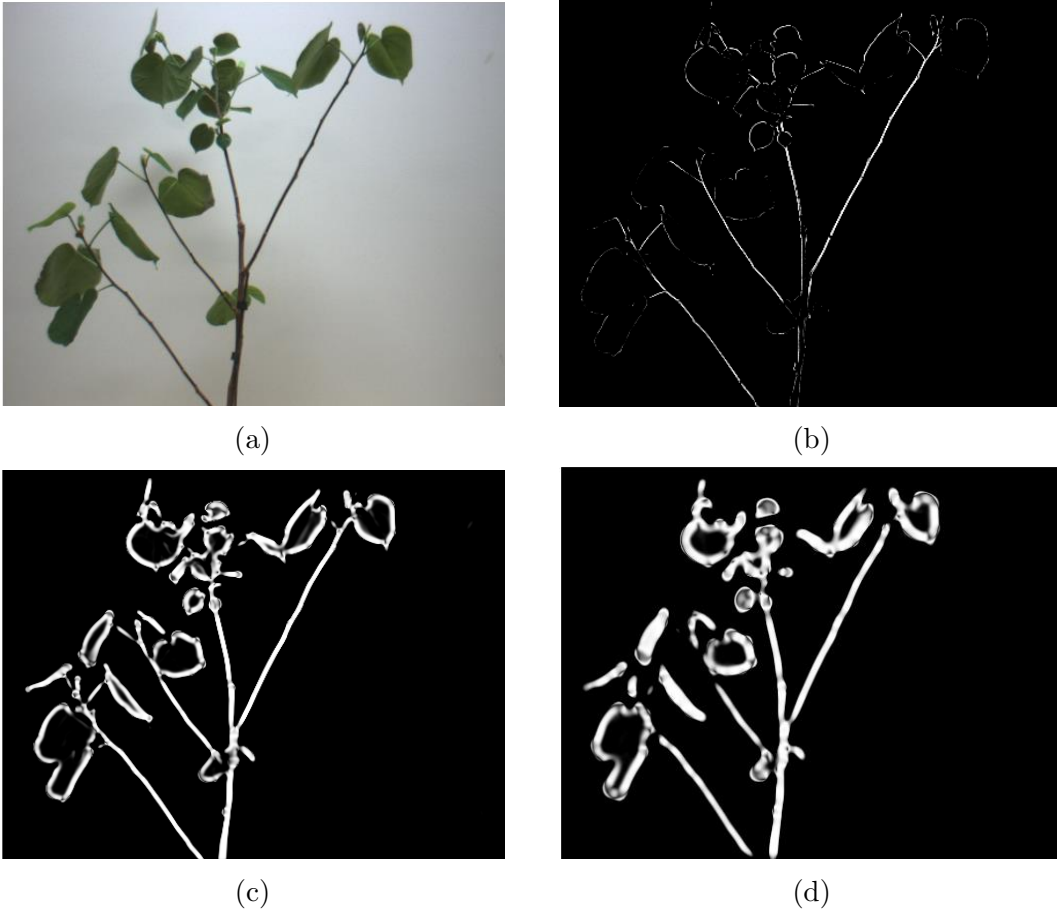


Figure 6.2: Hibiscus nursery plant (a) RGB image, (b), (c) and (d) illustrate output of Frangi vesselness filter with standard deviation  $\sigma_s = 0.55, 2.55$  and  $4.55$  respectively.

By examining different values of  $x_c$  it is recognised that,  $x_c = 50$  could produce an optimal segmentation result to eliminate leaf areas and preserve stem and branches areas. Figure 6.3 presents plant images when applying different values of  $x_c$ . The value of  $x_c$  smaller than 50 could reveal unwanted parts of plant such as leaves' edges, while  $x_c$  greater than 50 can eliminate some stem and branch parts. The setting of  $x_c$  was required only once during the development of the algorithm. The optimized value of  $x_c$  was applied for the rest of the hibiscus plant images at indoor and outdoor conditions which produced the desired outcomes.

The evaluation of vesselness measure technique was based on qualitative evaluation as the technique deals with plant images. This technique includes several parameters which need to be calibrated. The setting of these parameters is required only once and therefore, not for every image. The optimised values of these parameters were applied for the rest of the hibiscus plant images at indoor and outdoor conditions which produced the desired outcomes. Therefore, these values of parameters are expected to work with other types of plants that have several branches. The theoretical optimization of the algorithms parameters would be the next topic to be investigated.

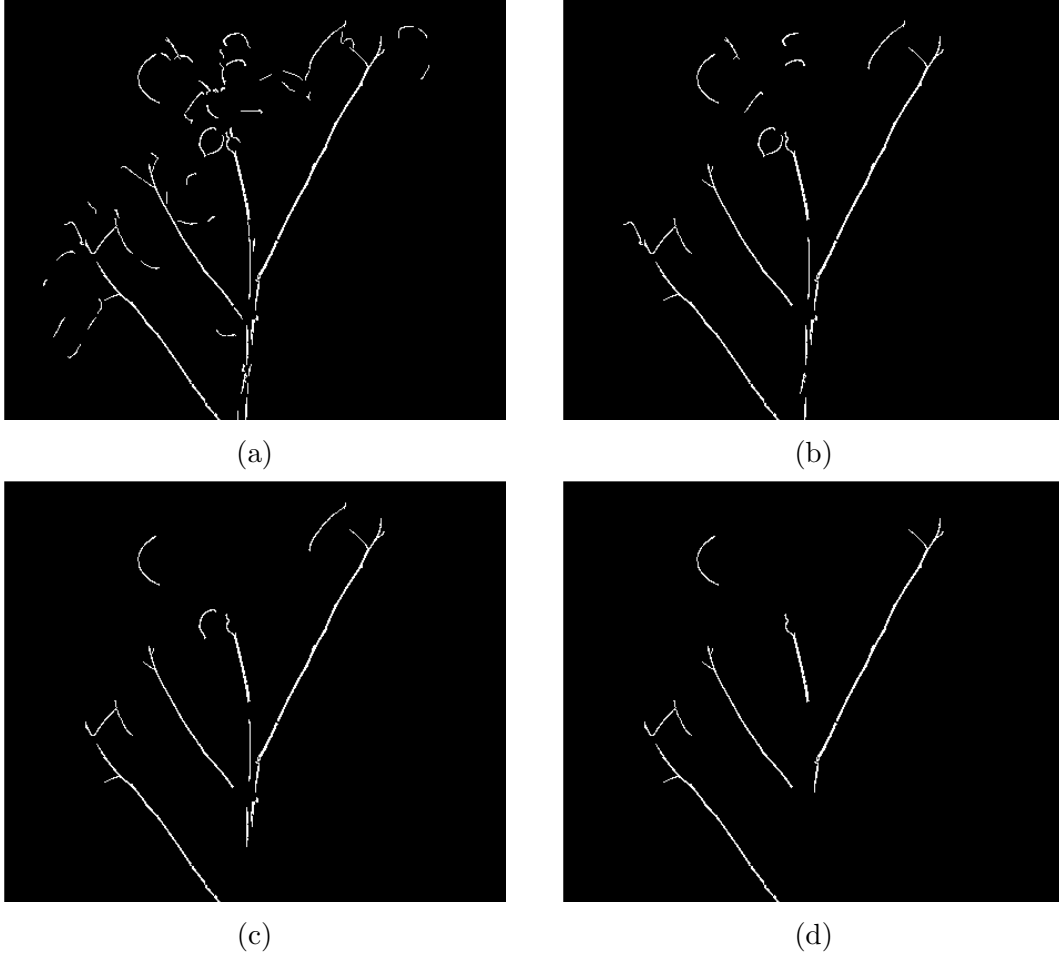


Figure 6.3: Different values of area opening operation  $x_c$  for the image of Figure 6.2b, (a)  $x_c=10$ , (b)  $x_c=30$ , (c)  $x_c=50$ , and (d)  $x_c=70$  respectively.

#### 6.4.1 Line fitting using Hough transform technique

To fit a line to the vesselness measure, the Hough transform technique (Duda and Hart, 1972) was used to identify the main stem and branches of the plant. The Hough transform uses a voting technique to identify points located on the same line and performs well to detect the main stem and branches. Typical figures of branch segmentation algorithm steps are shown in Figure 6.4. Figure 6.4d displays excellent Hough transform lines overlay on a hibiscus plant, however, the Hough transform lines were less visible on individual branches on outdoor plants under variable lighting conditions.

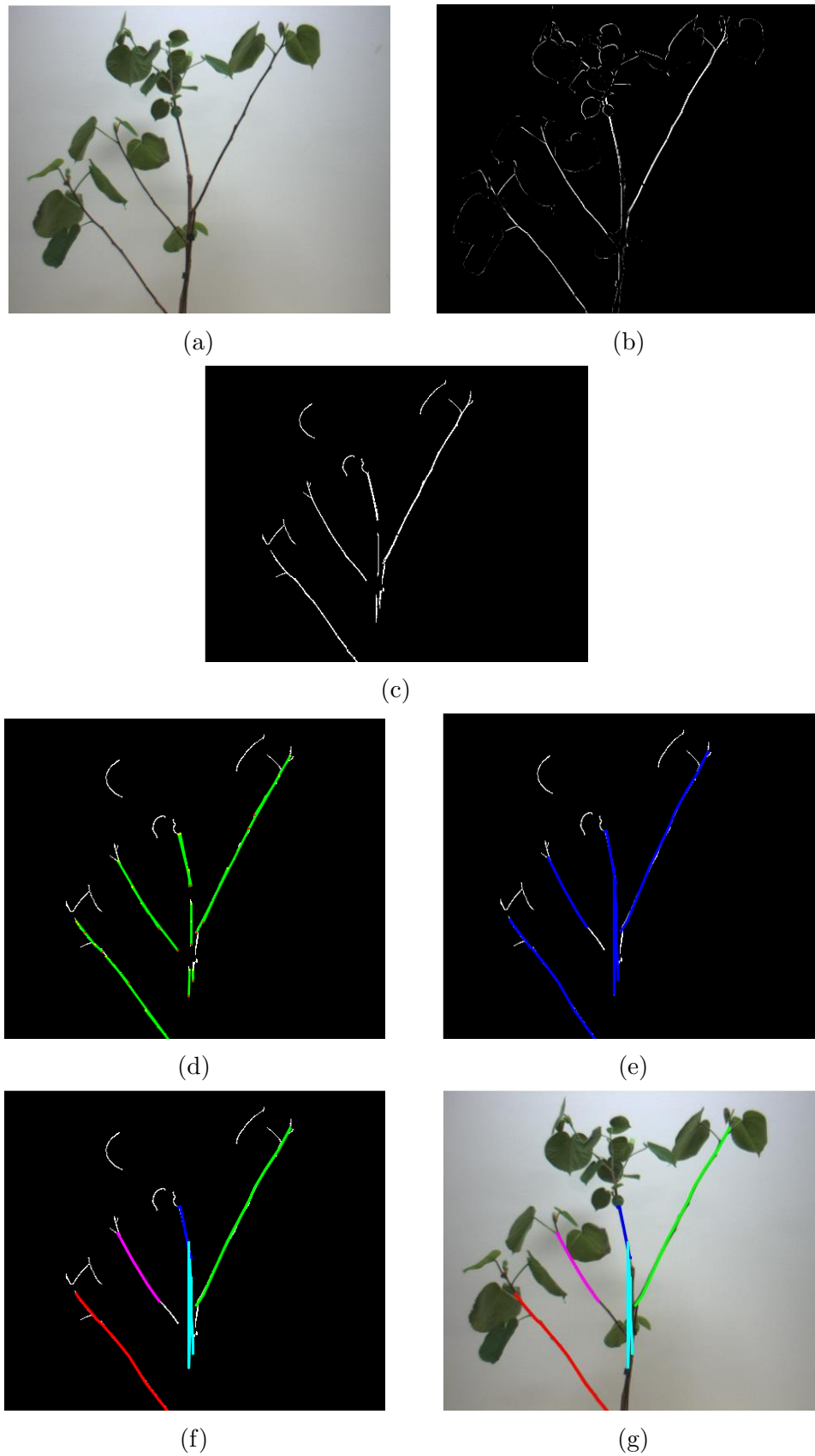


Figure 6.4: Typical steps of the branch segmented algorithm: (a) RGB image; (b) vesselness measure output; (c) area opening operation  $x_c=50$ ; (d) Hough transform multiple lines output; (e) single line for each branch; (f) assigning different colour for each line; and (g) overlapping those lines with the RGB image.

Figure 6.5 shows the output of the Hough transform accumulator. The small black square points represent the values for each stem detected by the Hough transform technique. There are five groups of points which represent the detection of five branches. The Hough transform technique puts all these groups in one bin as explained in stem and branch detection algorithm steps (Listing 6.1).

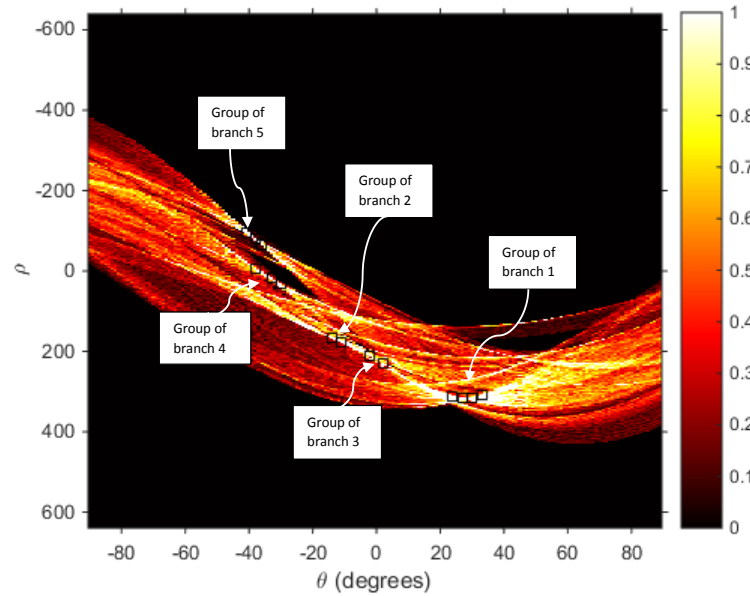


Figure 6.5: Hough transform Accumulator output for the images in Figure 6.6a and 6.6b. The groups are numbered as branch numbers for the image in Figure 6.6a.

The Hough transform represents each branch by multiple lines as shown in Figure 6.4d. The developed algorithm minimises multiple lines to one single line for each branch as shown in Figures 6.4e to 6.4g following the steps in Listing 6.1:

**Listing 6.1 Stem and branch detection algorithm steps**

1. Apply vesselness measure filter (Equation 6.2) on the gray scale image to segment stem and branches.
2. Use morphological area opening operation to remove non-branch objects.
3. Apply Hough transform (lines) to find the segmented branches.
4. Use Hough transform parameters ( $\rho$ ,  $\theta$ ) to classify detected lines and store the lines which share the same parameters (or close values) in the same bin.
5. Count the number of branches by counting the numbers of bins.
6. Hough transform draws multiple lines for each segmented branch, the developed algorithm uses other parameters of the Hough transform (the values of  $x$  and  $y$  coordinates for each line point) to arrange the points in ascending order and draws a single line for each branch.
7. Validate the points of each line and delete any points greater than the allocated threshold distance. The threshold distance was set where points from the same line should have less than  $\pm 20^\circ$  difference in  $\theta$ .
8. Classify each branch and present it in a different colour. Figure 6.4 shows the process steps of the developed algorithm

## 6.5 Results evaluation and discussion

### 6.5.1 Indoor results

The algorithm was applied on 12 images of hibiscus nursery plants. Figure 6.6 shows samples of these images and their results from different perspectives and different indoor illumination conditions. Two indoor illumination conditions were investigated: artificial light; and diffused sunlight through a glass window. Fig-

ures 6.6a and 6.6b present plants under the first illumination condition (artificial light). It can be seen that the stem and all branches are segmented successfully by the developed algorithm. Figures 6.6c and 6.6d, show the hibiscus plant from another aspect under diffuse sunlight conditions. The results for these images show that there was one undetected branch due to a shadow being cast by other branch leaves.

The same problem was observed for the images in Figures 6.6e and 6.6f, where one or two branches were omitted from the segmented branches. Although those branches can be perceived in the colour images, there is no typical reflected line profile from the shaded branches to be detected by the vesselness measure technique. As the vesselness measure technique is based on detecting a typical line profile of reflected light on the colour image (Section 6.4), the vesselness measure was not able to detect the line profile for these branches. Table 6.1 illustrates the results of stem and branch segmentation algorithm for hibiscus plant images under indoor illumination conditions. The table shows a dissimilar number of branches for each image of the same plant. The number of branches changed according to the side view of the image. From Table 6.1 it can be observed that images 1 and 12 show an optimal result, where all branches are segmented successfully by the proposed algorithm. There is a variance in the other results due to different indoor lighting conditions.



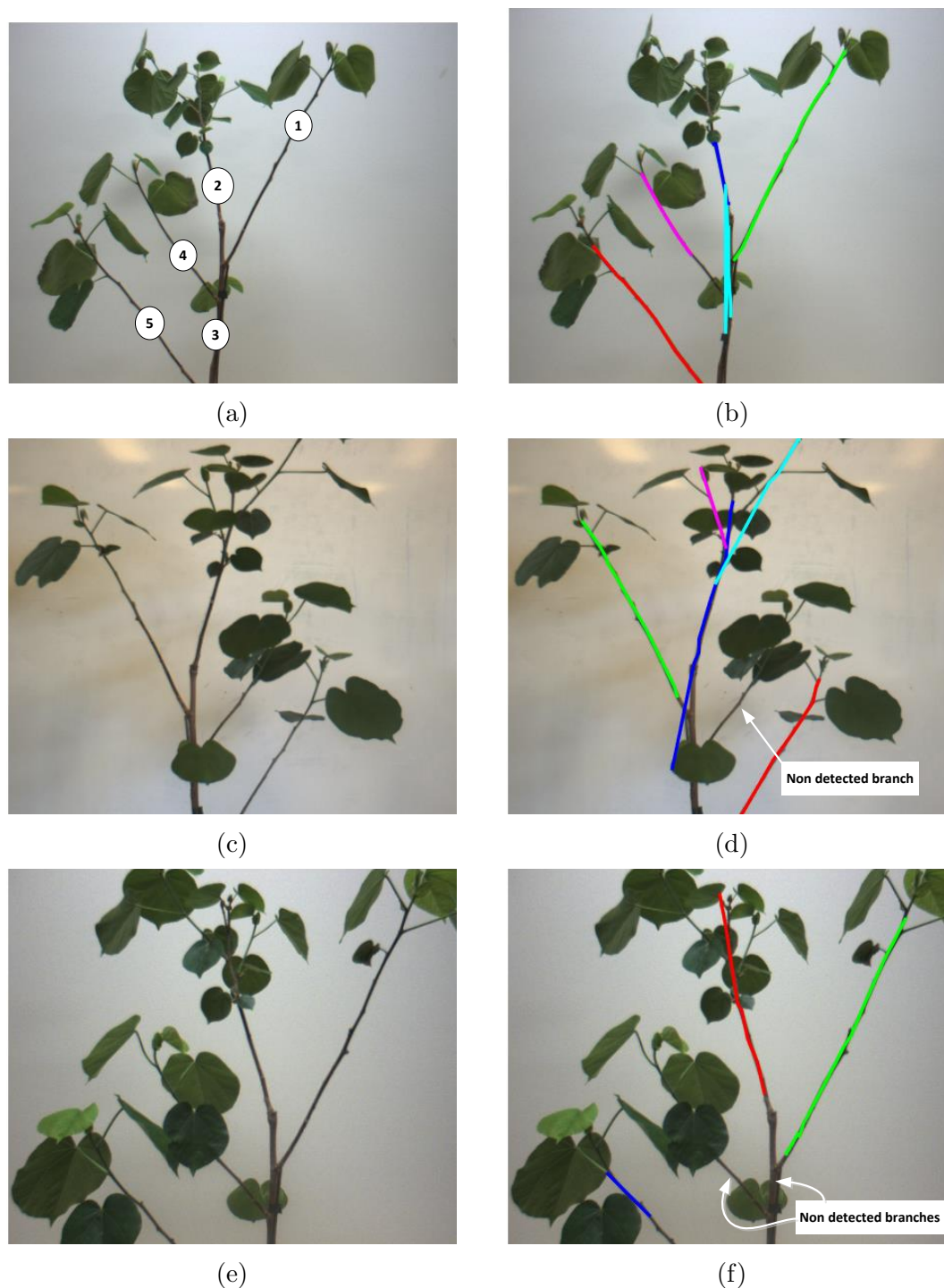


Figure 6.6: Image of hibiscus nursery plant from different aspects (Column one); the results after stem and branch segmentation algorithm is applied (Column two). The images were taken under indoor conditions, (a), (b), (e) and (f) with artificial light, (c), and (b) with diffuse sunlight

Table 6.1: Stem and branch segmentation results for 12 hibiscus plant images under indoor conditions.

Image No.	Branch no.	Automatic count	Light type	Accuracy%	Sensitivity%	Precision%
Image 1	5	5	Artificial light	100	100	100
Image 2	8	7	Diffused sunlight	88	88	100
Image 3	4	3	Artificial light	75	75	100
Image 4	5	4	Diffused sunlight	80	80	100
Image 5	5	6	Diffused sunlight	83	100	83
Image 6	6	4	Diffused sunlight	67	67	100
Image 7	5	4	Diffused sunlight	80	80	100
Image 8	7	5	Artificial light	71	71	100
Image 9	5	4	Artificial light	80	80	100
Image 10	7	4	Artificial light	57	57	100
Image 11	5	4	Diffused sunlight	80	80	100
Image 12	5	5	Artificial light	100	100	100

## 6.5.2 Outdoor result

### 6.5.2.1 Hibiscus plant

The algorithm was applied to seven hibiscus plant images taken in sunny conditions at midday, in the afternoon, and at sunset. In an outdoor environment, the resulting images showed many unwanted lines due to extensive noise in the background. Hence, an additional step was included which checked the values of the Hough transform parameters  $(\rho, \theta)$  and removed extra lines in the images not related to plant branch and stem.

Figure 6.7 presents three selected images with different responses to the algorithm. The images were taken from different aspects of the plant at midday and in the afternoon. Not all branches are shown clearly due to sunlight reflection and partial shadow areas in the images. As the vesselness measure is affected by the illumination conditions, the algorithm failed to detect branches under shadow or in overexposed areas. An acceptable response was shown by the images in Figures 6.7b and 6.7d, whereas a low response was indicated in Figure 6.7f.

The average accuracy, sensitivity and precision for the hibiscus plant in indoor and outdoor conditions are illustrated in Table 6.2. High rate results were obtained by the indoor plant images with 81%, 82%, 98.6% for accuracy, sensitivity and precision respectively. In contrast, poor results were observed for the hibiscus plant of outdoors.

Table 6.2: Final average of accuracy, sensitivity and precision for the hibiscus plant in indoor and outdoor conditions.

Total Average of	No. of images	Accuracy %	Sensitivity %	Precision %
Hibiscus plant / indoor	12	81	82	98.6
Hibiscus plant / outdoor	7	49.5	49.5	100

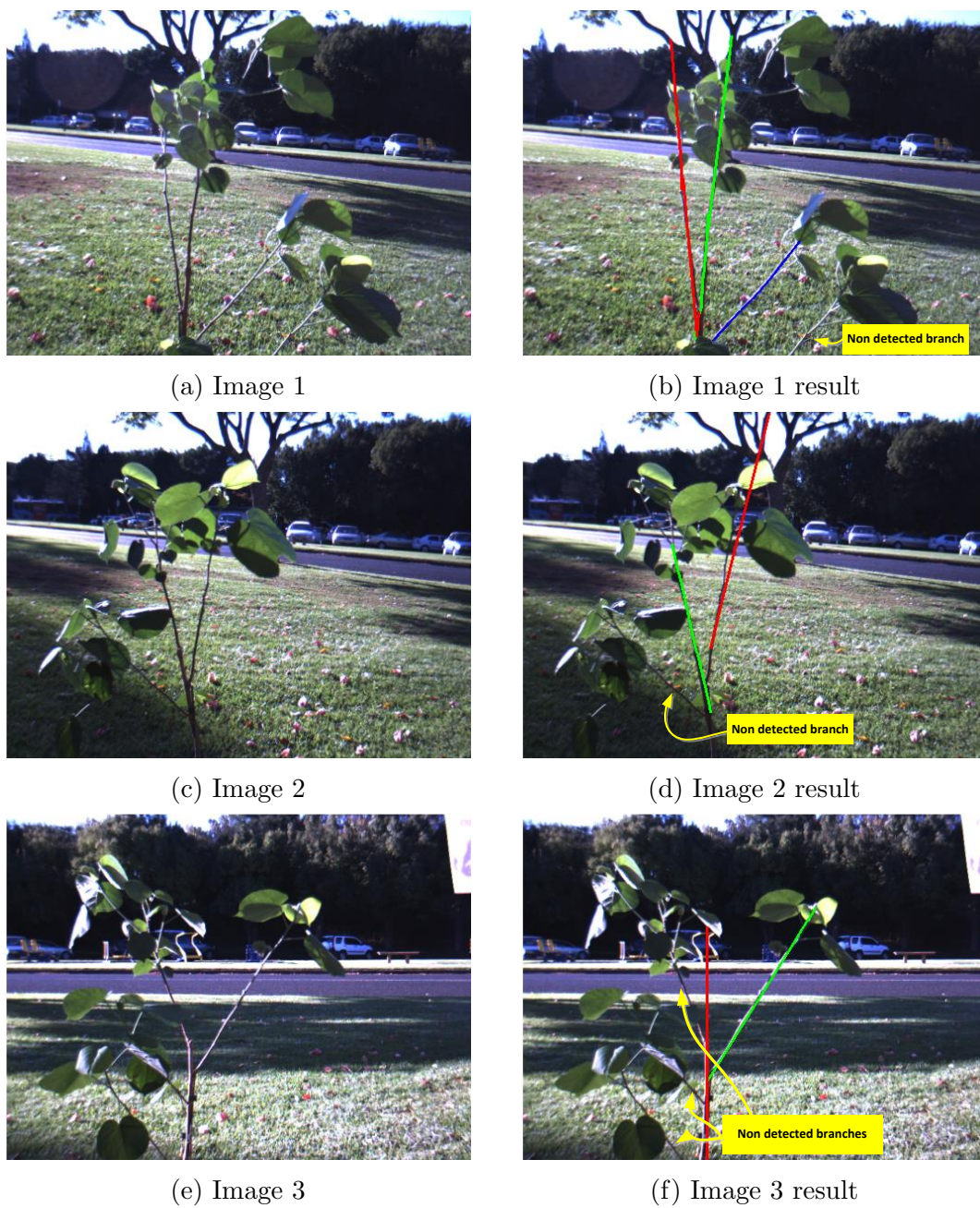


Figure 6.7: Hibiscus nursery plant, (a), (c) and (e) RGB image; (b), (d) and (e) stem and branch detection results.

### 6.5.2.2 Cotton Plant

The stem and branch detection algorithm was applied to big pot cotton plant images (350 mm pot diameter). Cotton plants are different from hibiscus plants in that petioles (the stalk that joins a leaf to a stem) are more obvious on cotton plants than they are on the hibiscus. The algorithm was applied to 48 images taken on both sunny and shady days at different times: midday, afternoon, and sunset. The results show that the stem was detected successfully for only 10/48 images, which is a low segmentation rate (21%).

The low segmentation rate was expected to be due to leaves hiding the stem, therefore it is hard to detect a complete stem profile which is normally covered by leaves. Partial shadow due to poor illumination conditions was another issue for certain parts of the stem that faced the camera. Figure 6.8 presents four examples of cotton plant images where stems were detected successfully.

Extra work and trials are discussed in Chapter 7 to cope with direct sunlight conditions, however detecting the stem and branches under direct sunlight is a big challenge using the vesselness measure technique. The literature reports two previous attempts to detect the stem using vesselness measure technique: Firstly, by using camera enclosure to establish ideal light conditions for the plants facing the camera (McCarthy et al., 2009); and secondly by using an active sensor at night (Nakarmi and Tang, 2013). After segmenting important plant parts (leaf, stem, branch), a method of reconstructing these parts in 2.5D model will be proposed in the next section.



(a)



(b)



(c)



(d)

Figure 6.8: The result of stem detection for 4 big pot cotton plants (350 mm diameter) in sunny conditions

## 6.6 Reconstruction of plant segmented parts and 3D localisation

Depth information can enhance the process of plant parts reconstructing and modelling by adding a third dimension, depth, to produce a 3D model. A reconstruction plant model from 3D images has distinct advantages over a 2D image for quantifying the structural information of plants such as leaf angle distribution and leaf area (Lià et al., 2015). The 3D geometrical and accurate plant model can enhance accuracy measurements and modelling of biological processes, such as yield prediction, plant growth modelling and photosynthesis (Golbach et al., 2016).

In this study, the results of leaf segmentation using depth imaging can be integrated with the results of stem detection to reconstruct a plant model. The stem and branch extraction method was implemented using 2D colour images. Then,  $x$  and  $y$  coordinate values for stem and branches could be determined from the 2D colour images. Afterwards, depth values were assigned to the stem and branches from the disparity map. Similarly, depth values were assigned to the segmented leaves. Then, a 2.5D model of the plant could be generated by integrating the plant segmented leaves and plant extracted stem and branches in a 3D coordinate image. Figure 6.9 presents a 2.5D model reconstruction of two hibiscus plant images captured from different aspects.



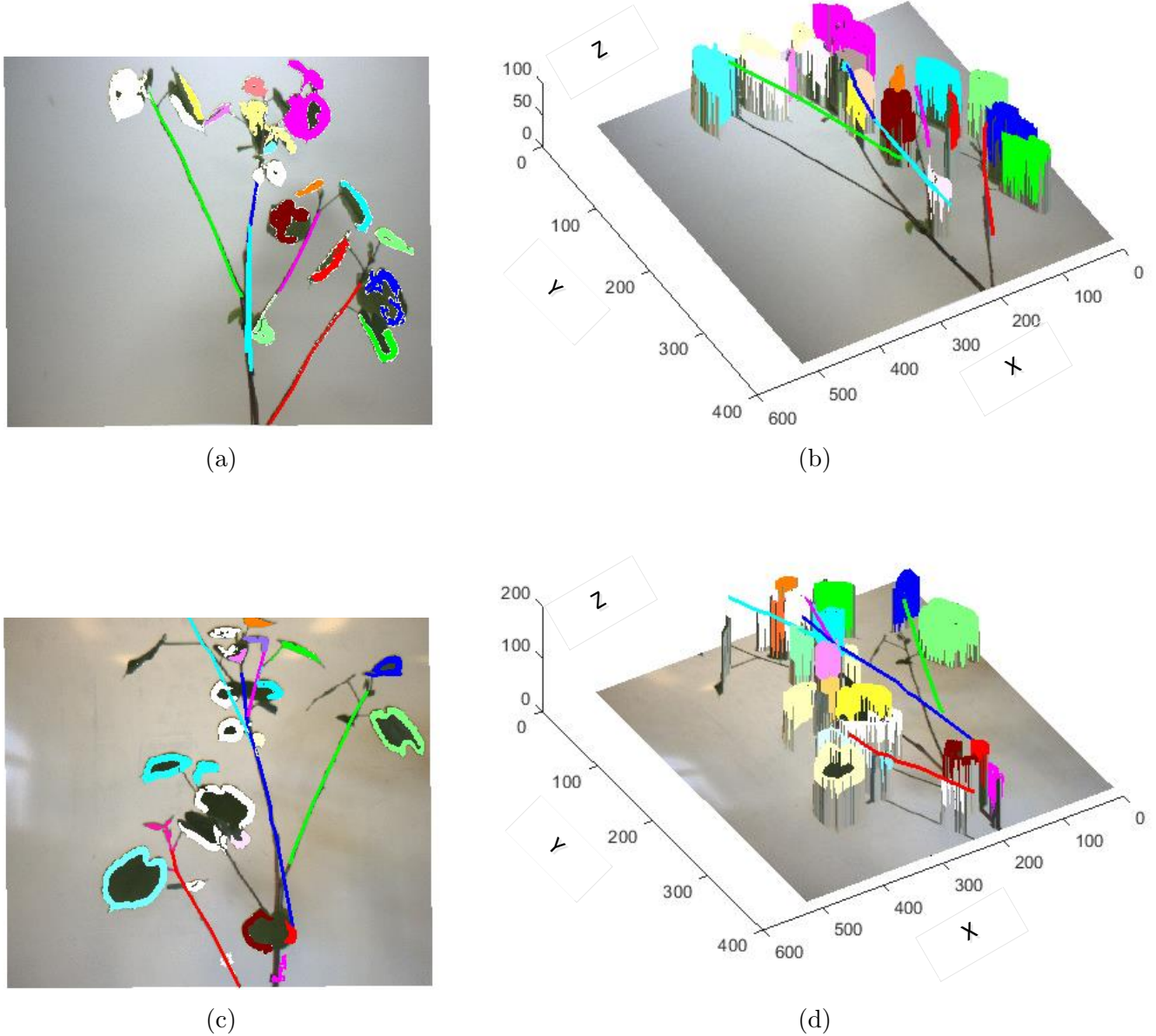


Figure 6.9: Plant part reconstruction of two images of a hibiscus plant to generate a 2.5D model

A 2.5D model obviously cannot present as much information as a full 3D model because it is generated from one colour and one disparity image only. However, it shows plant geometry in  $x, y, z$  image coordinates. This model can be extracted from depth images while a real 3D model of the plant can be generated from the dense point cloud data (Paulus et al., 2014). To generate a 3D model of a plant which would more accurately describe plant parts and positions, further work needs



to be undertaken with more than one image that needs to be taken from different aspects of the plant. The method proposed in Chapter 4, which extracted leaf plane from leaf vertices, can be used for geometric description of individual leaves. This method can potentially measure individual leaf orientation for the purpose of generating a 3D plant model. A point cloud library is another method which can be used to implement a 3D model of the plant (Santos and Rodrigues, 2015). The use of different sensors such as 3D laser scanner (Chaudhury et al., 2015), (Hétroy-Wheeler et al., 2016) is usually the most common method of producing a 3D plant model. Further work and more ideas that can be implemented in plant modelling using the stereo vision techniques that are recommended in Chapter 7.

For plant part localization, the distance formula of Equation 6.3 will be applied on the disparity image to find the position of each leaf in  $X$ ,  $Y$ ,  $Z$  world coordinates and also to find the distance from each leaf to the camera

$$Z_{depth} = \frac{b \cdot f}{d_s} \quad (6.3)$$

where,  $Z_{depth}$  = the distance along the camera's  $Z$  axis in meters,  $b$  = the baseline of the camera (in metres - 0.12 m for Bumblebee2),  $f$  = the focal length of the lenses and  $d_s$  = disparity (in pixels). The  $X$  and  $Y$  components of the Euclidean coordinates can be determined by triangulation and could be calculated by the Equations 6.4 and 6.5.

$$X = \frac{x \cdot Z_{depth}}{f} \quad (6.4)$$

$$Y = \frac{y \cdot Z_{depth}}{f} \quad (6.5)$$

where  $x$  and  $y$  represent the image coordinates of the left point of a corresponding pair of images.

## 6.7 Chapter Summary

The automatic detection and counting of the plant branches algorithm was demonstrated. The detection of branches was achieved by applying the vesselness measure and the Hough transform technique. The vesselness measure was more effective in detecting branches than edge detection filters (Sobel, Canny) as edge detection filters detect all the details of plant structures such as leaves and leaf veins. Hibiscus and cotton plants were used to evaluate the performance of the new algorithm.

An experimental test was conducted first on 12 colour images of a hibiscus plant taken randomly from different aspects in indoor conditions. The results showed that 2 of 12 images were completely detected by the algorithm, 7 of 12 were detected with one branch missing or an extra number of branches, while the remaining three were presented with two or three undetected branches. Two parameters clearly affected stem and branch segmenting results: a clear view of the plant from the camera; and good illumination conditions. The average accuracy, sensitivity and precision were 81%, 82% and 98.6% respectively in indoor environment.

Further work to enhance the algorithm was implemented to deal with outdoor images and remove extra lines of background regions which are not related to plant branch and stem. The algorithm was applied to 7 images of hibiscus plants taken at different times on a sunny day and 48 images of cotton plants under different light conditions. The outdoor images have a lower response to the algorithm than the indoor images. The low response was due to both differing illumination conditions

and complex backgrounds. The average accuracy was 49.5% for hibiscus and 21% for cotton with 100% precision rate for both plants in outdoor conditions. As the indoor images have a much higher accuracy than the outdoor images, a shade hood for the stereo vision camera and crop or nursery plants is a possible option to increase the accuracy in outdoor environments.

Depth information can enhance the process by adding the third dimension to the plant image and produce the a 2.5D model of the plant. A method for reconstructing the segmented parts of hibiscus plants has been presented. The method can generate a 2.5D model and present the 3D plant information. This model was generated by integrating one colour image with disparity map information.

# Chapter 7

## Conclusions and Future work

The principal contribution of this research is the development of an image analysis system using colour and depth information to segment, count and separate between overlapping leaf boundaries using depth gradient discontinuity. This algorithm can work in a semi-structured outdoor environments under a variety of sunlight conditions (sunny, shady and cloudy). The developed system has the capability of detecting, classifying and counting plant stems and branches automatically using colour features and the vesselness measure techniques in both indoor and outdoor conditions. This system is also able to reconstruct the segmented plant parts to generate a 2.5D plant model which can be used to monitor plant characteristics for various growth stages. The image analysis system presents a method to extract a geometrical plane from each segmented leaf. This geometric plane can be used to parameterise a 3D model of the plant image. Another contribution of this study is the collection of a detailed data set of cotton plant images at different growth stages under varying outdoor lighting conditions. These data sets could be added to the plant image data sets to be beneficial for other research studies.

This chapter presents the conclusions of this study with respect to the achievement of the objectives listed in Section 1.7. It also provides suggestions for potential future applications and recommendations for further development of the research.

## 7.1 Conclusions

This section provides an overview of the performance of the algorithms which have been developed in this research study. Their evaluations are as follows:

1. **Leaf detection and counting.** A leaf segmentation process which has the ability to segment plant leaves from both a complex background and other parts of the plant was developed in Chapter 4. An effort was made to find the best method of consistently segmenting leaves from different aspects of plant images in a variety of outdoor environments. Depth information was effectively used to segment the plant from background objects, while colour transformation, image enhancement techniques and ellipse criteria were utilised to isolate the leaf pixels from other plant part pixels. The developed process can segment the individual leaf from the plant canopies; however, some leaves still appear to be connected or overlapped. To address this problem, a method for separating the overlapped leaf boundaries was presented in Chapter 4. This method named Depth Discontinuity Segmentation (DDS), contains three main techniques based on searching for discontinuity in depth using global and local methods.

The capability of this method for separating the overlapping leaves was evaluated with two differently structured plants, cotton and hibiscus. The hibiscus plant has a simpler structure to cotton, however the leaf segmentation

techniques were applied sequentially on hibiscus to solve the overlapping leaf problem. The developed algorithm was applied on cotton plant images (252 images at different growth stages) and 20 images of hibiscus plant. The results for the three different illumination conditions (sunny, shade and cloudy) were presented and analysed in Chapter 5. Certain issues affected leaf segmentation accuracy such as overexposure, leaf orientation and the occlusion between leaf boundaries. Other issues such as shadow, low illumination and leaf size also affected the segmentation accuracy in different rates. These issues were presented and analysed in detail in Chapter 5. In total, from approximately 2453 leaves, 78% of these leaves were detected successfully by the developed algorithm. The segmented leaves included 578 occluded and overlapped leaves. There were 484 leaves separated successfully with a high separation rate (84%). The results show, an enhancement in leaf detection was observed when utilising a combination of image features such as colour, shape and depth, rather than using each feature separately. The overall sensitivity, precision and accuracy of detecting and separating leaves were 78%, 89% and 71% respectively for all plant images under different environmental and illumination conditions.

2. **Geometric plane extraction.** A method has been developed that extracted a geometrical plane from the vertices of each leaf. This geometric plane can be used to parameterise a 3D model of the plant image. The purpose of this work is to measure the inclination angle of each individual leaf. The measured angles will be useful for reconstructing plant leaves in different orientations to develop a 3D model of the plant.
3. **Stem and branch detection.** In this study, the automatic detection and counting of a plant branch algorithm was developed (Chapter 6). A stem and

branch detection algorithm was achieved by applying both vesselness measure and Hough transform techniques. The proposed algorithm was reliant on the colour feature to extract stem and branch profiles. Experimental tests were conducted with 12 colour images of a hibiscus plant taken randomly from different aspects in indoor conditions. Further work on enhancing the algorithm was recently implemented with hibiscus and cotton plant images in outdoor conditions. The stem and branch detection algorithm was evaluated by its ability to extract these features in a plant using big cotton and hibiscus plants. The outdoor images have a lower response to the algorithm than the indoor images. The low response was caused by differing illumination conditions and the complexity of the background. The average accuracy, sensitivity and precision were 81%, 82% and 98.6% respectively for indoor images. In outdoor conditions, both accuracy and sensitivity had the same values, 49.5% for hibiscus and 21% for cotton, while the precision rate was 100% for both plants.

4. **Reconstruction of plant parts.** A method to reconstruct a 2.5D model of a hibiscus plant was developed in Chapter 6. The results of the stem and branch segmentation algorithm have been integrated with the results of the leaf detection algorithm, to reconstruct plant parts in 3D coordinates and produce a 2.5D model of the plant. This model of the plant does not represent a real 3D model because it only uses one colour image and disparity map information (as illustrated in Chapter 4), however, the model presents the geometry data of the plant in  $x, y, z$  image coordinates. This model can be used to monitor plant characteristics for various growth stages.

For each objective, the research work was implemented under different lighting conditions as working outdoors needs to consider different lighting and different plant

aspects with respect to the sun. The algorithm was also applied to different growth stages of plants in order to evaluate the performance of the algorithm with different levels of plant complexity. From the overview of the algorithm's performance for each objective and the results obtained, the following can be concluded, which adequately answers the research questions listed in Section 1.6:

1. The developed algorithms can extract plant stems, segment individual leaves and count the number of leaves automatically. Each of these plant parts has a different visual feature. For example, stem and branches have thin, straight and vessel shapes which can be segmented using vesselness measure and line detection techniques. Leaves have other distinct features such as colour, shape and smoothness of depth change within themselves. The difference in depth between leaf boundaries is another feature which can be beneficial to segment overlapping leaves from each other. The developed algorithm can segment each of these plant parts according to its visual feature using different image analysing techniques. The results show, cotton leaves are more obvious to be detected from plant images than stem, which is usually covered by leaves. Therefore, leaves in cotton can be segmented more accurately than stems. The detection and counting of leaves in cotton can help inform some plant characteristics such as leaf density and vegetative growth information. This information is useful for estimating growth stages and enhancing crop management practices. The results also present each plant's features including stems, branches and leaves that can be segmented accurately for hibiscus plants due to the structural difference of hibiscus plants from cotton plants. The leaf segmentation results can be integrated with stem detection results to reconstruct the plant model. This model could be useful to calculate further information such as plant height, width and volume which could provide good



estimations for plant growth. The estimation of plant growth could be beneficial for many agricultural tasks such as yield estimation and input resource optimisation to reduce costs and increase crop productivity.

2. The stereo vision system used in this research study can successfully extract the important features of a plant (e.g. leaf, stem). A combination of image features such as colour, shape and depth was used to implement plant segmentation. The colour feature was used to distinguish between the green of leaves and other parts of the plant. Shape elliptical property was useful to detect leaves and eliminate unwanted objects from plant images. The depth feature was used, in the first stage of the algorithm, to segment the plant image from the complex background. The depth feature can also enhance the leaf detection algorithm by targeting the occlusion in leaf boundaries and separating them according to the discontinuity in depth gradient. As leaves have 3D shape properties, they can benefit from depth property more than other parts of a plant.
3. Overexposure, partial shadow and low illumination are the main ambient lighting issues that affected the performance of the stereo vision sensor at different rates. Overexposure was the main lighting issue affecting the performance of the algorithm when leaves show yellow rather than green colour. Overexposure caused false negative leaves, whilst shadow produced false positive leaves. The algorithm can cope with some images having these issues and produces acceptable results. In some particular cases, it was hard to recognise all the leaves in a plant image when the illumination condition was low with obscure leaf orientation.

Leaf orientation, size and occlusion also affected results in different ways. Small leaves are difficult to distinguish between using visual inspection. Larger

leaves exhibit bending around each lobe causing distinct depth differences for different lobes of a single leaf. The impact of leaf orientation on the algorithm's performance was investigated, which affects the perceived shape of the leaf. Overlapped leaves may exist in most of the plant images. The developed algorithm separated overlapped leaves relying on discontinuity in depth gradient values. The developed algorithms could be applied to many machine vision applications and could enhance the precision of agricultural operations.

## **7.2 Potential application of the research work**

The machine vision system developed in this study can be applied to several commercial and scientific applications for the agricultural mobile robot as described below:

### **7.2.1 Plant inspection and growth monitoring**

As a routine agricultural task, plant inspection is normally undertaken by the farmer in order to have up-to-date information about growing plants. Routine agricultural tasks are usually repetitive operations which are highly labour intensive and consume long hours. Mobile robots have the potential for compensating human inspection routines and being more robust to implement the potentially risky agricultural operations currently undertaken by humans (de Oliveira Neris et al., 2007). Inspection mobile robots should have intelligent machine vision systems to sense the environment and complement different agricultural tasks.

The stereo vision system used in this study (with the developed algorithms) can recognise the important features of plants (leaf, stem, branches) which can help monitoring plants of different agriculture practices. Plant leaf images can support farmers with the required information needed to identify certain problems related to plant growth and health, such as water stress, wilting, nitrogen deficiency, damage and disease attack.

The stereo vision system can also analyse data, count the number of leaves and find the position of each individual in X, Y, Z coordinates. From this information, further information can be calculated such as plant height, width, and volume. Moreover, the distance between the camera and each individual leaf can be calculated. As the distance between plant leaf and the stereo vision sensor can be calculated, the mobile robot can position itself closer to the specified leaf and capture another closer image. This closer image will more effectively examine leaf health and disease, leaf area, water stress, and nutrient deficiency. This image could also be used for plant species identification.

### **7.2.2 Leaf inclination angle measurement**

Leaf inclination angle distribution is an effective indicator of drought stress and leaf wilt (Mizuno et al., 2007). Plant leaf orientation usually presents the response of the plant to environmental change. Measuring individual leaf angle distributions manually tends to be labour-intensive (Biskup et al., 2007). To overcome this problem, the proposed algorithm uses a plane extraction method to find the most accurate plane tailored with each leaf as explained in Section 4.6. When the plane equations are known, the leaf inclination angle can be measured. The leaf inclination angle will be useful to find the orientation of the leaf. Thus, the mobile robot arm

can be projected to the particular leaf with the same angle of orientation and perform specific functions.

Furthermore, leaf inclination angle measurement is important for plant water stress indicators, and the automated irrigation of plants can be controlled by visual monitoring of the plant (Farkas, 2011). Another benefit of inclination angle measurement is in finding the orientation of each leaf in order to implement the 3D model reconstruction of the plant canopy. The generation of 3D realistic-looking models of plants from images is useful for simulating and analysing the silent response of plants to the environmental effects, stresses, and climate changes.

## 7.3 Future work and recommendations

### 7.3.1 Development of leaf detection algorithm

The performance of a leaf detection algorithm could be enhanced by implementing further recommended developments as follows:

1. Adding additional features such as leaf texture can enhance the recognition capability of the leaf detection algorithm.
2. Developing an interactive or fused approach for colour and depth information to isolate the foreground (ROI) from the background of plant image. This method would require the use of both a disparity map and colour image used in parallel to implement the segmentation. The fusion of the colour and the depth data can be implemented using a neural network classifier with tuning thresholds for colour and depth values to effectively isolate the plant pixels

from background pixels.

3. Neural network technology could be investigated and trained for some plant leaves' irregular shapes and areas. As the algorithm detected plant leaves with a variety of areas from different aspects and orientations, this training will have the potential to distinguish between single leaves and clusters of overlapping leaves, depending on the average leaf area.

### 7.3.2 Detection of large and bent leaves

The depth discontinuity segmentation algorithm (DDS) discussed in Chapter 4 was applied to a variety of leaf sizes and shapes. One of the limitations of this algorithm is large leaf size and bent leaves as discussed in Chapter 5. The DDS algorithm segments these types of leaves according to the depth gradient property which produces two or more areas. A training leaf boundary classifier MLP (Xia et al., 2013) could be investigated to overcome this problem, whereas leaf shape boundaries could be used for training the classifier to identify these types of leaves.

### 7.3.3 Development of stem detection algorithm

The stem detection algorithm could be enhanced as follows:

1. Using a shade hood for the stereo vision camera and crop or nursery plants is a possible option to increase the accuracy in outdoor environments.
2. For cotton plants, the stem position and height can be estimated using segmented leaf information such as the distance between the boundary leaves

on both sides of the plant. Suitable functions such as fitting line and curve interpolation algorithms could be used to reconstruct the plant stem.

3. The new colour transformation method proposed by Ji et al. (2016) could be investigated to enhance stem extraction from other parts of the plant and background in outdoor conditions.

#### 7.3.4 Development of 3D model reconstruction

The reconstruction of plant parts in 3D coordinates could be developed using a different method as follows:

1. Leaf inclination angles can be calculated from the geometrical plane which is extracted from each leaf by the method proposed in Chapter 4. The measured angles, along with the leaf position information in 3D coordinates, can be used to enhance the reconstruction of plant leaves with respect to the plant stem and branch position. The values of these angles can be used to project and model the missing petioles or small twigs between leaves and stems or branches.
2. The reconstruction of plant parts in a 3D model can be enhanced by using more than one image captured from different poses of plant position with the aid of depth information. This method can be implemented by examining and developing the fast 3D reconstruction method proposed by (Golbach et al., 2016) for high-throughput seedling phenotyping.

# References

- Alarcon, V. J. and Sassenrath, G. F. (2011), ‘Modeling cotton (gossypium spp.) leaves and canopy using computer aided geometric design (cagd)’, *Ecological modelling* **222**(12), 1951–1963.
- Andersen, H. J., Reng, L. and Kirk, K. (2005), ‘Geometric plant properties by relaxed stereo vision using simulated annealing’, *Computers and electronics in agriculture* **49**(2), 219–232.
- Arivazhagan, S., Shebiah, R. N., Ananthi, S. and Varthini, S. V. (2013), ‘Detection of unhealthy region of plant leaves and classification of plant leaf diseases using texture features’, *Agricultural Engineering International: CIGR Journal* **15**(1), 211–217.
- Armada, M. A., Muscato, G., Prestifilippo, M., Abbate, N. and Rizzuto, I. (2005), ‘A prototype of an orange picking robot: past history, the new robot and experimental results’, *Industrial Robot: An International Journal* **32**(2), 128–138.
- Åstrand, B. and Baerveldt, A.-J. (2004), Plant recognition and localization using context information, in ‘Proc. of the IEEE Conference Mechatronics and Robotics’, pp. 13–15.
- Bakhshipour, A., Jafari, A. and Hosseini, M. (2012), ‘Recognition of pomegranate

- on tree and stereoscopic locating of the fruit [-j]', *American-Eurasian J Agric Environ* **12**(10), 1288–1294.
- Billingsley, J., Milella, A., Reina, G. and Foglia, M. (2006), 'Computer vision technology for agricultural robotics', *Sensor Review* **26**(4), 290–300.
- Billingsley, J. and Schoenfisch, M. (1997), 'The successful development of a vision guidance system for agriculture', *Computers and electronics in agriculture* **16**(2), 147–163.
- Birchfield, S. and Tomasi, C. (1999), 'Depth discontinuities by pixel-to-pixel stereo', *International Journal of Computer Vision* **35**(3), 269–293.
- Biskup, B., Scharr, H., Schurr, U. and Rascher, U. (2007), 'A stereo imaging system for measuring structural parameters of plant canopies', *Plant, cell & environment* **30**(10), 1299–1308.
- Bjurstrøm, H. and Svensson, J. (2002), Assessment of grapevine vigour using image processing, Master's thesis.
- Blatt, M., Wiseman, S. and Domany, E. (1996), 'Superparamagnetic clustering of data', *Physical review letters* **76**(18), 3251.
- Bradski, G. and Kaehler, A. (2008), *Learning OpenCV: Computer vision with the OpenCV library*, " O'Reilly Media, Inc."
- Bréda, N. J. (2003), 'Ground-based measurements of leaf area index: a review of methods, instruments and current controversies', *Journal of experimental botany* **54**(392), 2403–2417.
- Breiman, L., Friedman, J., Olshen, R. and Stone, C. (1984), 'Classification and regression trees. wadsworth & brooks/cole advanced books & software', *Pacific California* .



- Bulanon, D., Burks, T. and Alchanatis, V. (2010), 'A multispectral imaging analysis for enhancing citrus fruit detection', *Environment control in biology* **48**(2), 81–91.
- Canny, J. (1986), 'A computational approach to edge detection', *Pattern Analysis and Machine Intelligence, IEEE Transactions on* (6), 679–698.
- Cerutti, G., Tougne, L., Mille, J., Vacavant, A. and Coquin, D. (2013), 'Understanding leaves in natural images—a model-based approach for tree species identification', *Computer Vision and Image Understanding* **117**(10), 1482–1501.
- Chapron, M., Ivanov, N., Boissard, P. and Valery, P. (1993), Visualization of corn acquired from stereovision, in 'Systems, Man and Cybernetics, 1993.' Systems Engineering in the Service of Humans', Conference Proceedings., International Conference on', Vol. 5, IEEE, pp. 334–338.
- Chaudhary, P., Chaudhari, A. K., Cheeran, A. and Godara, S. (2012), 'Color transform based approach for disease spot detection on plant leaf', *International Journal of Computer Science and Telecommunications* **3**(6), 65–70.
- Chaudhury, A., Ward, C., Talasaz, A., Ivanov, A. G., Huner, N. P., Grodzinski, B., Patel, R. V. and Barron, J. L. (2015), Computer vision based autonomous robotic system for 3d plant growth measurement, in 'Computer and Robot Vision (CRV), 2015 12th Conference on', IEEE, pp. 290–296.
- Cheein, F. A. A. and Carelli, R. (2013), 'Agricultural robotics: Unmanned robotic service units in agricultural tasks', *IEEE Industrial Electronics Magazine* **7**(3), 48–58.
- Chen, X. and Yang, S. X. (2013), 'A practical solution for ripe tomato recognition and localisation', *Journal of real-time image processing* **8**(1), 35–51.

- Chéné, Y., Rousseau, D., Lucidarme, P., Bertheloot, J., Caffier, V., Morel, P., Belin, É. and Chapeau-Blondeau, F. (2012), ‘On the use of depth camera for 3d phenotyping of entire plants’, *Computers and Electronics in Agriculture* **82**, 122–127.
- Chi, Y.-T., Chien, C.-F. and Lin, T.-T. (2003), ‘Leaf shape modeling and analysis using geometric descriptors derived from bezier curves’, *Transactions of the ASAE* **46**(1), 175.
- Chien, C. and Lin, T. (2002), ‘Leaf area measurement of selected vegetable seedlings using elliptical hough transform’, *Transactions of the ASAE* **45**(5), 1669–1677.
- Chien, C. and Lin, T. (2005), ‘Non-destructive growth measurement of selected vegetable seedlings using orthogonal images’, *Transactions of the ASAE* **48**(5), 1953–1961.
- Comaneci, D. and Shift, P. M. M. (2002), ‘A robust approach toward feature space analysis’, *IEEE Transactions on Pattern Analysis and Machine Intelligence* **24**(5), 313–329.
- Cubero, S., Aleixos, N., Moltmez-Sanchis, J. and Blasco, J. (2011), ‘Advances in machine vision applications for automatic inspection and quality evaluation of fruits and vegetables’, *Food and Bioprocess Technology* **4**(4), 487–504.
- de Oliveira Neris, L., Roda, V. O. and Trindade, O. (2007), A method for agricultural machine guidance on row crops based on the vanishing point, in ‘Vehicular Electronics and Safety, 2007. ICVES. IEEE International Conference on’, IEEE, pp. 1–6.
- Duda, R. O. and Hart, P. E. (1972), ‘Use of the hough transformation to detect lines and curves in pictures’, *Communications of the ACM* **15**(1), 11–15.

- Ehleringer, J. and Hammond, S. (1987), ‘Solar tracking and photosynthesis in cotton leaves’, *Agricultural and Forest Meteorology* **39**(1), 25–35.
- English, A., Ross, P., Ball, D. and Corke, P. (2014), Vision based guidance for robot navigation in agriculture, in ‘2014 IEEE International Conference on Robotics and Automation (ICRA)’, IEEE, pp. 1693–1698.
- Farkas, I. (2011), Plant drought stress: detection by image analysis, in ‘Encyclopedia of Agrophysics’, Springer, pp. 608–609.
- Foley, J. D., Van Dam, A. et al. (1982), *Fundamentals of interactive computer graphics*, Vol. 2, Addison-Wesley Reading, MA.
- Fountas, S., Blackmore, B. S., Vougioukas, S., Tang, L., Sørensen, C. G. and Jørgensen, R. (2007), ‘Decomposition of agricultural tasks into robotic behaviours’, *Agricultural Engineering International: CIGR Journal* **32**(Manuscript PM 07 006).
- Frangi, A. F., Niessen, W. J., Vincken, K. L. and Viergever, M. A. (1998), Multiscale vessel enhancement filtering, in ‘International Conference on Medical Image Computing and Computer-Assisted Intervention’, Springer, pp. 130–137.
- Franz, E. (1989), Identifying weed seedlings by computer vision using leaf shape and spectral information, PhD thesis, University of Missouri-Columbia.
- Franz, E., Gebhardt, M. and Unklesbay, K. (1991a), ‘Shape description of completely visible and partially occluded leaves for identifying plants in digital images’, *Transactions of the ASAE* **34**(2), 673–6681.
- Franz, E., Gebhardt, M. and Unklesbay, K. (1991b), ‘The use of local spectral properties of leaves as an aid for identifying weed seedlings in digital images’, *Transactions of the ASAE* **34**(2), 682–6687.

- Franz, E., Gebhardt, M. and Unklesbay, K. (1995), 'Algorithms for extracting leaf boundary information from digital images of plant foliage', *Transactions of the ASAE* **38**(2), 625–633.
- Funnell, A. (2015), 'Robots and the future of agriculture', <http://www.abc.net.au/radionational/programs/futuretense/aswarm-of-agbots/6968940>.
- Gai, J., Tang, L. and Steward, B. (2016), Plant localization and discrimination using 2d+ 3d computer vision for robotic intra-row weed control, in '2016 ASABE Annual International Meeting', American Society of Agricultural and Biological Engineers, p. 1.
- Golbach, F., Kootstra, G., Damjanovic, S., Otten, G. and van de Zedde, R. (2016), 'Validation of plant part measurements using a 3d reconstruction method suitable for high-throughput seedling phenotyping', *Machine Vision and Applications* **27**(5), 663–680.
- Gongal, A., Silwal, A., Amatya, S., Karkee, M., Zhang, Q. and Lewis, K. (2016), 'Apple crop-load estimation with over-the-row machine vision system', *Computers and Electronics in Agriculture* **120**, 26–35.
- Granlund, G. (1999), Does vision inevitably have to be active?, in 'Proceedings of the Scandinavian Conference on Image Analysis', Vol. 1, pp. 11–20.
- Guijarro, M., Pajares, G., Riomoros, I., Herrera, P., Burgos-Artizzu, X. and Ribeiro, A. (2011), 'Automatic segmentation of relevant textures in agricultural images', *Computers and Electronics in Agriculture* **75**(1), 75–83.
- Guo, W., Rage, U. K. and Ninomiya, S. (2013), 'Illumination invariant segmentation of vegetation for time series wheat images based on decision tree model', *Computers and electronics in agriculture* **96**, 58–66.

- Guyer, D. E., Miles, G., Schreiber, M., Mitchell, O. and Vanderbilt, V. (1986), 'Machine vision and image processing for plant identification', *Transactions of the ASAE* **29**(6), 1500–1507.
- Hamuda, E., Glavin, M. and Jones, E. (2016), 'A survey of image processing techniques for plant extraction and segmentation in the field', *Computers and Electronics in Agriculture* **125**, 184–199.
- Hamzah, R. A., Rahim, R. A. and Rosly, H. N. (2010), Depth evaluation in selected region of disparity mapping for navigation of stereo vision mobile robot, in 'Industrial Electronics & Applications (ISIEA), 2010 IEEE Symposium on', IEEE, pp. 551–555.
- Hanawa, K., Yamashita, T., Matsuo, Y. and Hamada, Y. (2012), 'Development of a stereo vision system to assist the operation of agricultural tractors', *Japan Agricultural Research Quarterly: JARQ* **46**(4), 287–293.
- Hansard, M., Lee, S., Choi, O. and Horaud, R. P. (2012), *Time-of-flight cameras: principles, methods and applications*, Springer Science & Business Media.
- Hartley, R. and Zisserman, A. (2003), *Multiple view geometry in computer vision*, Cambridge university press.
- Hayashi, S., Shigematsu, K., Yamamoto, S., Kobayashi, K., Kohno, Y., Kamata, J. and Kurita, M. (2010), 'Evaluation of a strawberry-harvesting robot in a field test', *Biosystems engineering* **105**(2), 160–171.
- He, D., Matsuura, Y., Kozai, T. and Ting, K. (2003), 'A binocular stereovision system for transplant growth variables analysis', *Applied Engineering in Agriculture* **19**(5), 611.
- Hétroy-Wheeler, F., Casella, E. and Boltcheva, D. (2016), 'Segmentation of tree

- seedling point clouds into elementary units', *International Journal of Remote Sensing* **37**(13), 2881–2907.
- Hirschmuller, H. and Scharstein, D. (2007), Evaluation of cost functions for stereo matching, in 'Computer Vision and Pattern Recognition, 2007. CVPR'07. IEEE Conference on', IEEE, pp. 1–8.
- Hu, R., Jia, W., Ling, H. and Huang, D. (2012), 'Multiscale distance matrix for fast plant leaf recognition', *IEEE transactions on image processing* **21**(11), 4667–4672.
- Huck, M. G. and Klepper, B. (1977), 'Water relations of cotton. ii. continuous estimates of plant water potential from stem diameter measurements', *Agronomy Journal* **69**(4), 593–597.
- Husin, Z., Shakaff, A., Aziz, A., Farook, R., Jaafar, M., Hashim, U. and Harun, A. (2012), 'Embedded portable device for herb leaves recognition using image processing techniques and neural network algorithm', *Computers and Electronics in Agriculture* **89**, 18–29.
- Ivanov, N., Boissard, P., Chapron, M. and Andrieu, B. (1995), 'Computer stereo plotting for 3-d reconstruction of a maize canopy', *Agricultural and Forest Meteorology* **75**(1), 85–102.
- Jain, R., Kasturi, R. and Schunck, B. G. (1995), *Machine vision*, Vol. 5, McGraw-Hill New York.
- Ji, W., Qian, Z., Xu, B., Tao, Y., Zhao, D. and Ding, S. (2016), 'Apple tree branch segmentation from images with small gray-level difference for agricultural harvesting robot', *Optik-International Journal for Light and Electron Optics* **127**(23), 11173–11182.

- Ji, W., Zhao, D., Cheng, F., Xu, B., Zhang, Y. and Wang, J. (2012), ‘Automatic recognition vision system guided for apple harvesting robot’, *Computers & Electrical Engineering* **38**(5), 1186–1195.
- Jin, J. and Tang, L. (2009), ‘Corn plant sensing using real-time stereo vision’, *Journal of Field Robotics* **26**(6-7), 591–608.
- Jonckheere, I., Fleck, S., Nackaerts, K., Muys, B., Coppin, P., Weiss, M. and Baret, F. (2004), ‘Review of methods for in situ leaf area index determination: Part i. theories, sensors and hemispherical photography’, *Agricultural and forest meteorology* **121**(1), 19–35.
- Jukan, A., Masip-Bruin, X. and Amla, N. (2017), ‘Smart computing and sensing technologies for animal welfare: A systematic review’, *ACM Computing Surveys (CSUR)* **50**(1), 10.
- Kacira, M. and Ling, P. (2001), ‘Design and development of an automated and non-contact sensing system for continuous monitoring of plant health and growth’, *Transactions of the ASAE* **44**(4), 989.
- Kadir, A., Nugroho, L. E., Susanto, A. and Santosa, P. I. (2011a), ‘A comparative experiment of several shape methods in recognizing plants’, *International Journal of Computer Science & Information Technology (IJSIT)* **3**(3), 256–263.
- Kadir, A., Nugroho, L. E., Susanto, A. and Santosa, P. I. (2011b), ‘Foliage plant retrieval using polar fourier transform, color moments and vein features’, *Signal & Image Processing: An International Journal* **2**(3), 1–13.
- Kadir, A., Nugroho, L. E., Susanto, A. and Santosa, P. I. (2013), ‘Leaf classification using shape, color, and texture features’, *International Journal of Engineering Trends and Technology* **2**(1), 225–230.

- Kalyoncu, C. and Toygar, Ö. (2015), ‘Geometric leaf classification’, *Computer Vision and Image Understanding* **133**, 102–109.
- Kamencay, P., Breznan, M., Jarina, R., Lukac, P. and Zachariasova, M. (2012), ‘Improved depth map estimation from stereo images based on hybrid method.’, *Radioengineering* **21**(1), 70–78.
- Kaminuma, E., Heida, N., Tsumoto, Y., Yamamoto, N., Goto, N., Okamoto, N., Konagaya, A., Matsui, M. and Toyoda, T. (2004), ‘Automatic quantification of morphological traits via three-dimensional measurement of arabidopsis’, *The Plant Journal* **38**(2), 358–365.
- Kane, K. E. and Lee, W. S. (2007), Multispectral imaging for in-field green citrus identification, in ‘2007 ASAE Annual Meeting’, American Society of Agricultural and Biological Engineers, p. 1.
- Kaur, G. and Kaur, G. (2012), ‘Classification of biological species based on leaf architecture’, *International Journal of Engineering Research and Development* **1**(6), 35–42.
- Kazmi, W., Foix, S., Alenyà, G. and Andersen, H. J. (2014), ‘Indoor and outdoor depth imaging of leaves with time-of-flight and stereo vision sensors: Analysis and comparison’, *ISPRS journal of photogrammetry and remote sensing* **88**, 128–146.
- Kelly, B. (2006), Structure from stereo vision using optical flow, Master’s thesis, University of Canterbury.
- Kise, M. and Zhang, Q. (2008), ‘Development of a stereovision sensing system for 3d crop row structure mapping and tractor guidance’, *Biosystems Engineering* **101**(2), 191–198.



- Kise, M., Zhang, Q. and Rovira Más, F. (2005), 'A stereovision-based crop row detection method for tractor-automated guidance', *Biosystems Engineering* **90**(4), 357–367.
- Kreyszig, E. (2010), *Advanced engineering mathematics*, John Wiley & Sons.
- Kuhl, A. (2005), Comparison of stereo matching algorithms for mobile robots, Master's thesis, The University of Western Australia Faculty of Engineering, Computing and Mathematics.
- Kurtulmus, F., Lee, W. S. and Vardar, A. (2011), 'Green citrus detection using eigenfruit, color and circular gabor texture features under natural outdoor conditions', *Computers and Electronics in Agriculture* **78**(2), 140–149.
- Lamm, R. D., Slaughter, D. C. and Giles, D. K. (2002), 'Precision weed control system for cotton', *Transactions of the ASAE* **45**(1), 231.
- Lati, R. N., Filin, S. and Eizenberg, H. (2013), 'Estimating plant growth parameters using an energy minimization-based stereovision model', *Computers and Electronics in Agriculture* **98**, 260–271.
- Lazaros, N., Sirakoulis, G. C. and Gasteratos, A. (2008), 'Review of stereo vision algorithms: from software to hardware', *International Journal of Optomechatronics* **2**(4), 435–462.
- Lee, K.-B. and Hong, K.-S. (2013), 'An implementation of leaf recognition system using leaf vein and shape', *International Journal of Bio-Science and Bio-Technology* **5**(2), 57–66.
- Lee, W. S. (2006), 'Spectral sensing of different citrus varieties for precision agriculture', *American Society of Agricultural and Biological Engineers* (061065).

- Lee, W. and Slaughter, D. (2004), ‘Recognition of partially occluded plant leaves using a modified watershed algorithm’, *Transactions of the ASAE* **47**(4), 1269.
- Lexer, C., Joseph, J., van Loo, M., Prenner, G., Heinze, B., Chase, M. W. and Kirkup, D. (2009), ‘The use of digital image-based morphometrics to study the phenotypic mosaic in taxa with porous genomes’, *Taxon* **58**(2), 349–364.
- LI, H.-q., YU, Q.-c. and Fang, M. (2008), ‘Application of otsu thresholding method on canny operator [j]’, *Computer Engineering and Design* **29**(9), 2297–2299.
- Li, X., Li, Y., Zhang, Z. and Li, X. (2015), ‘Influences of environmental factors on leaf morphology of chinese jujubes’, *PloS one* **10**(5), e0127825.
- Li, Y., Xia, C. and Lee, J. (2009), Vision-based pest detection and automatic spray of greenhouse plant, in ‘Industrial Electronics, 2009. ISIE 2009. IEEE International Symposium on’, IEEE, pp. 920–925.
- Lià, J., zaragoza, p., kuffner, p. and Ansel, chuong nguyen, h. d. (2015), Growth measurment of arabidopsis in 2.5d from a high throughput phenotyping platform, in ‘Modelling and Simulation, 21 st International congress on’, csiro, pp. 517–523.
- Lim, J. S. (1990), *Two-dimensional signal and image processing*, Englewood Cliffs, NJ, Prentice Hall, 1990, 710 p.
- Lin, F.-Y., Zheng, C.-H., Wang, X.-F. and Man, Q.-K. (2008), ‘Multiple classification of plant leaves based on gabor transform and lbp operator’, *Advanced Intelligent Computing Theories and Applications. With Aspects of Contemporary Intelligent Computing Techniques* pp. 432–439.
- Lin, K.-y., Wu, J. and Xu, L. (2005), ‘A survey on color image segmentation techniques’, *Journal of Image and Graphics* **10**(1), 1–10.

- Linker, R., Cohen, O. and Naor, A. (2012), ‘Determination of the number of green apples in rgb images recorded in orchards’, *Computers and Electronics in Agriculture* **81**, 45–57.
- Liu, S., Cossell, S., Tang, J., Dunn, G. and Whitty, M. (2017), ‘A computer vision system for early stage grape yield estimation based on shoot detection’, *Computers and Electronics in Agriculture* **137**, 88–101.
- Lu, Z. and Neumann, P. M. (1999), ‘Water stress inhibits hydraulic conductance and leaf growth in rice seedlings but not the transport of water via mercury-sensitive water channels in the root’, *Plant Physiology* **120**(1), 143–152.
- Luo, L., Tang, Y., Zou, X., Ye, M., Feng, W. and Li, G. (2016), ‘Vision-based extraction of spatial information in grape clusters for harvesting robots’, *Biosystems Engineering* **151**, 90–104.
- Magnus, J. R., Neudecker, H. et al. (1995), *Matrix differential calculus with applications in statistics and econometrics*.
- Manh, A.-G., Rabatel, G., Assemat, L. and Aldon, M.-J. (2001), ‘Automation and emerging technologies: Weed leaf image segmentation by deformable templates’, *Journal of agricultural engineering research* **80**(2), 139–146.
- Matas, J., Galambos, C. and Kittler, J. (2000), ‘Robust detection of lines using the progressive probabilistic hough transform’, *Computer Vision and Image Understanding* **78**(1), 119–137.
- MATLAB (2015), *MATLAB version 8.5.0.197613 (R2015a)*, The Mathworks, Inc., Natick, Massachusetts.
- McCarthy, C. (2009), Automatic non-destructive dimensional measurement of cotton plants in real-time by machine vision, PhD thesis, University of Southern Queensland.

- McCarthy, C., Hancock, N. and Raine, S. (2009), ‘Automated internode length measurement of cotton plants under field conditions’, *Transactions of the ASABE* **52**(6), 2093–2103.
- McKenzie, D. (1998), ‘Soilpak for cotton growers, 3rd edn. orange’, *New South Wales Agriculture* .
- McLellan, T. and Endler, J. A. (1998), ‘The relative success of some methods for measuring and describing the shape of complex objects’, *Systematic Biology* **47**(2), 264–281.
- Meskaldji, K., Boucherkha, S. and Chikhi, S. (2009), Color quantization and its impact on color histogram based image retrieval accuracy, *in* ‘Networked Digital Technologies, 2009. NDT’09. First International Conference on’, IEEE, pp. 515–517.
- Meyer, G. E. (2011), Machine vision identification of plants, *in* ‘Recent Trends for Enhancing the Diversity and Quality of Soybean Products (ISBN: 978-953-307-533-4)’, InTech, Rijeka, Croatia, pp. 401–420.
- Meyer, G. E. and Davison, D. A. (1987), ‘An electronic image plant growth measurement system’, *Transactions of the ASAE* **30**(1), 242–0248.
- Meyer, G. E., Hindman, T. W. and Laksmi, K. (1998-a), Machine vision detection parameters for plant species identification, *in* ‘Precision Agriculture and Biological Quality’, Vol. 3543, International Society for Optics and Photonics, pp. 327–336.
- Meyer, G. E. and Neto, J. C. (2008), ‘Verification of color vegetation indices for automated crop imaging applications’, *Computers and Electronics in Agriculture* **63**(2), 282–293.

- Meyer, G. E., Neto, J. C., Jones, D. D. and Hindman, T. W. (2004), ‘Intensified fuzzy clusters for classifying plant, soil, and residue regions of interest from color images’, *Computers and electronics in agriculture* **42**(3), 161–180.
- Meyer, G., Mehta, T., Kocher, M., Mortensen, D. and Samal, A. (1998-b), ‘Textural imaging and discriminant analysis for distinguishing weeds for spot spraying’, *Transactions of the ASAE* **41**(4), 1189.
- Meyer, W. S. and Walker, S. (1981), ‘Leaflet orientation in water-stressed soybeans’, *Agronomy Journal* **73**(6), 1071–1074.
- Mitchell, O. R. and Grogan, T. A. (1984), ‘Global and partial shape discrimination for computer vision’, *Optical Engineering* **23**(5), 235484–235484.
- Mizuno, S., Noda, K., Ezaki, N., Takizawa, H. and Yamamoto, S. (2007), ‘Detection of wilt by analyzing color and stereo vision data of plant’, *Computer Vision/Computer Graphics Collaboration Techniques* pp. 400–411.
- Mozos, O. M., Mizutani, H., Kurazume, R. and Hasegawa, T. (2012), ‘Categorization of indoor places using the kinect sensor’, *Sensors* **12**(5), 6695–6711.
- Murray, D. and Little, J. J. (2000), ‘Using real-time stereo vision for mobile robot navigation’, *Autonomous Robots* **8**(2), 161–171.
- Nakarmi, A. and Tang, L. (2012), ‘Automatic inter-plant spacing sensing at early growth stages using a 3d vision sensor’, *Computers and electronics in agriculture* **82**, 23–31.
- Nakarmi, A. and Tang, L. (2013), ‘Stem detection algorithm for cotton plants: Proof of concept’, *Automated inter-plant spacing sensing of corn plant seedlings and quantification of laying hen behaviors using 3D computer vision* p. 61.

- Nelikanti, A. (2014), ‘Image enhancement using image fusion and image processing techniques’, *COMPUSOFT, An international journal of advanced computer technology* **3**(10), 1193–1197.
- Nesaratnam, J. and BalaMurugan, C. (2015), Identifying leaf in a natural image using morphological characters, in ‘Innovations in Information, Embedded and Communication Systems (ICIIECS), 2015 International Conference on’, IEEE, pp. 1–5.
- Neto, J. C., Meyer, G. E. and Jones, D. D. (2006), ‘Individual leaf extractions from young canopy images using gustafson–kessel clustering and a genetic algorithm’, *Computers and Electronics in Agriculture* **51**(1), 66–85.
- Neto, J. C., Meyer, G. E., Jones, D. D. and Samal, A. K. (2006), ‘Plant species identification using elliptic fourier leaf shape analysis’, *Computers and electronics in agriculture* **50**(2), 121–134.
- Okamoto, H. and Lee, W. (2009), ‘Green citrus detection using hyperspectral imaging’, *Computers and Electronics in Agriculture* **66**(2), 201–208.
- Oosterhuis, D. (2001), ‘Physiology and nutrition of high yielding cotton in the usa’, *Informações Agronômicas Piracicaba* **95**, 18–24.
- Oosterhuis, D. M. and Kerby, T. A. (2008), ‘Measures of cotton growth and development’, *Crop Management System* p. 21.
- Oshio, H., Asawa, T., Hoyano, A. and Miyasaka, S. (2015), ‘Estimation of the leaf area density distribution of individual trees using high-resolution and multi-return airborne lidar data’, *Remote Sensing of Environment* **166**, 116–125.
- Otsu, N. (1975), ‘A threshold selection method from gray-level histograms’, *Automatica* **11**(285-296), 23–27.

- Pan, J. and He, Y. (2008), Recognition of plants by leaves digital image and neural network, *in* 'Computer Science and Software Engineering, 2008 International Conference on', Vol. 4, IEEE, pp. 906–910.
- Park, J., Hwang, E. and Nam, Y. (2008), 'Utilizing venation features for efficient leaf image retrieval', *Journal of Systems and Software* **81**(1), 71–82.
- Patil, S., Nadar, J. S., Gada, J., Motghare, S. and Nair, S. S. (2013), 'Comparison of various stereo vision cost aggregation methods', *International Journal of Engineering and Innovative Technology* **2**(8), 222–226.
- Paulus, S., Behmann, J., Mahlein, A.-K., Plümer, L. and Kuhlmann, H. (2014), 'Low-cost 3d systems: suitable tools for plant phenotyping', *Sensors* **14**(2), 3001–3018.
- Pauwels, E. J., de Zeeuw, P. M. and Ranguelova, E. B. (2009), 'Computer-assisted tree taxonomy by automated image recognition', *Engineering Applications of Artificial Intelligence* **22**(1), 26–31.
- Payne, A. B., Walsh, K. B., Subedi, P. and Jarvis, D. (2013), 'Estimation of mango crop yield using image analysis–segmentation method', *Computers and Electronics in Agriculture* **91**, 57–64.
- Perez, A., Lopez, F., Benlloch, J. and Christensen, S. (2000), 'Colour and shape analysis techniques for weed detection in cereal fields', *Computers and electronics in agriculture* **25**(3), 197–212.
- Plebe, A. and Grasso, G. (2001), 'Localization of spherical fruits for robotic harvesting', *Machine Vision and Applications* **13**(2), 70–79.
- PointGray (2012), 'Stereo accuracy and error modeling', <https://www.ptgrey.com/support/downloads/10403>. [Online; accessed February-2016].

- Popovic, V., Seyid, K., Cogal, Ö., Akin, A. and Leblebici, Y. (2017), *Design and Implementation of Real-Time Multi-Sensor Vision Systems*, Springer.
- QFF (2012), ‘Cotton industry’, <http://www.qff.org.au/farming-in-qlld/cotton-industry/>. [Online; accessed February-2013].
- Qian, X., Brennan, M. P., Dione, D. P., Dobrucki, W. L., Jackowski, M. P., Breuer, C. K., Sinusas, A. J. and Papademetris, X. (2009), ‘A non-parametric vessel detection method for complex vascular structures’, *Medical image analysis* **13**(1), 49–61.
- Quan, L., Tan, P., Zeng, G., Yuan, L., Wang, J. and Kang, S. B. (2006), Image-based plant modeling, *in* ‘ACM Transactions on Graphics (TOG)’, Vol. 25, ACM, pp. 599–604.
- Rees, S., McCarthy, C., Artizzu, X., Baillie, C. and Dunn, M. (2009), Development of a prototype precision spot spray system using image analysis and plant identification technology, *in* ‘Proceedings of the 2009 CIGR International Symposium of the Australian Society for Engineering in Agriculture (SEAg 2009)’, Engineers Australia, pp. 343–349.
- Rojanamontien, M., Sihanatkathakul, P., Piemkaroonwong, N., Kamales, S. and Watchareeruetai, U. (2016), Leaf identification using apical and basal features, *in* ‘2016 8th International Conference on Knowledge and Smart Technology (KST)’, IEEE, pp. 234–238.
- Rojas-Hern, R., Rojas-Hern, C. A. et al. (2016), Plant identification using new geometric features with standard data mining methods, *in* ‘2016 IEEE 13th International Conference on Networking, Sensing, and Control (ICNSC)’, IEEE, pp. 1–4.



- Rosenfeld, A. (1975), 'A characterization of parallel thinning algorithms', *Information and control* **29**(3), 286–291.
- Ross, J. (2012), *The radiation regime and architecture of plant stands*, Vol. 3, Springer Science & Business Media.
- Rovira-Más, F., Zhang, Q. and Reid, J. (2004), 'Automated agricultural equipment navigation using stereo disparity images', *Transactions of the ASAE* **47**(4), 1289.
- Rovira-Más, F., Zhang, Q. and Reid, J. (2008), 'Stereo vision three-dimensional terrain maps for precision agriculture', *Computers and Electronics in Agriculture* **60**(2), 133–143.
- Sakamoto, T., Gitelson, A. A., Nguy-Robertson, A. L., Arkebauer, T. J., Wardlow, B. D., Suyker, A. E., Verma, S. B. and Shibayama, M. (2012), 'An alternative method using digital cameras for continuous monitoring of crop status', *Agricultural and Forest Meteorology* **154**, 113–126.
- Santos, T. T. and Rodrigues, G. C. (2015), 'Flexible three-dimensional modeling of plants using low-resolution cameras and visual odometry', *Machine Vision and Applications* pp. 1–13.
- Sarfraz, M. (2005), *Computer-aided intelligent recognition techniques and applications*, Wiley Online Library.
- Scharr, H., Minervini, M., French, A. P., Klukas, C., Kramer, D. M., Liu, X., Luenigo, I., Pape, J.-M., Polder, G., Vukadinovic, D. et al. (2016), 'Leaf segmentation in plant phenotyping: a collation study', *Machine vision and applications* **27**(4), 585–606.
- Si, Y., Liu, G. and Feng, J. (2015), 'Location of apples in trees using stereoscopic vision', *Computers and Electronics in Agriculture* **112**, 68–74.

- Slaughter, D., Giles, D. and Downey, D. (2008), ‘Autonomous robotic weed control systems: A review’, *Computers and electronics in agriculture* **61**(1), 63–78.
- Sobel, I. and Feldman, G. (1968), ‘A 3x3 isotropic gradient operator for image processing’, *a talk at the Stanford Artificial Project in* pp. 271–272.
- Söderkvist, O. (2001), Computer vision classification of leaves from swedish trees, Master’s thesis, Linköping University.
- Sonka, M., H. V. . B. R. (1993), *Image Processing, Analysis and Machine Vision*, London: Chapman and Hall.
- Sosa, J. P. M., Solano, G. A. and Obico, J. A. (2013), ‘An application using canny edge detection and multilayer perceptron for recognizing leaves of tropical plants’, *Mathematics and Computers in Biology and Biomedical Informatics* pp. 53–61.
- Steger, C. (1996), Extracting curvilinear structures: A differential geometric approach, *in* ‘European Conference on Computer Vision’, Springer, pp. 630–641.
- Strickland, R. N. and Hahn, H. I. (1997), ‘Wavelet transform methods for object detection and recovery’, *IEEE Transactions on image processing* **6**(5), 724–735.
- Sural, S., Qian, G. and Pramanik, S. (2002), Segmentation and histogram generation using the hsv color space for image retrieval, *in* ‘Image Processing. 2002. Proceedings. 2002 International Conference on’, Vol. 2, IEEE, pp. II–II.
- Takizawa, H., Ezaki, N., Mizuno, S. and Yamamoto, S. (2005), Measurement of plants by stereo vision for agricultural applications, *in* ‘Signal and Image Processing: Proceedings of the Seventh IASTED International Conference’.
- Tang, L., Tian, L. and Steward, B. L. (2003), ‘Classification of broadleaf and grass

- weeds using gabor wavelets and an artificial neural network', *Transactions of the ASAE* **46**(4), 1247.
- Tang, X., Liu, M., Zhao, H. and Tao, W. (2009), Leaf extraction from complicated background, in 'Image and Signal Processing, 2009. CISP'09. 2nd International Congress on', IEEE, pp. 1–5.
- Tankyevych, O., Talbot, H., Dokládál, P. and Passat, N. (2009), Direction-adaptive grey-level morphology. application to 3d vascular brain imaging, in '2009 16th IEEE International Conference on Image Processing (ICIP)', IEEE, pp. 2261–2264.
- Tian, L. F. and Slaughter, D. C. (1998), 'Environmentally adaptive segmentation algorithm for outdoor image segmentation', *Computers and electronics in agriculture* **21**(3), 153–168.
- Tillett, N. D., Hague, T. and Miles, S. (2001), 'A field assessment of a potential method for weed and crop mapping on the basis of crop planting geometry', *Computers and Electronics in Agriculture* **32**(3), 229–246.
- Trucco, E. and Verri, A. (1998), *Introductory techniques for 3-D computer vision*, Vol. 201, Prentice Hall Englewood Cliffs.
- Valliammal, N. and Geethalakshmi, S. (2011), 'Automatic recognition system using preferential image segmentation for leaf and flower images', *Computer Science and Engineering: an international Journal* **1**, 13–25.
- Van den Heuvel, J. C., Kleijweg, J., van der Mark, W., Liewers, M., Kester, L. et al. (2003), Obstacle detection for people movers using vision and radar, in '10th World Conference on Intelligent Transport Systems and Services, Madrid, Spain'.

- Van Henten, E. J., Hemming, J., Van Tuijl, B., Kornet, J., Meuleman, J., Bontsema, J. and Van Os, E. (2002), ‘An autonomous robot for harvesting cucumbers in greenhouses’, *Autonomous Robots* **13**(3), 241–258.
- Veksler, O. (2002), ‘Dense features for semi-dense stereo correspondence’, *International Journal of Computer Vision* **47**(1), 247–260.
- Veksler, O. (2003), Extracting dense features for visual correspondence with graph cuts, in ‘Computer Vision and Pattern Recognition, 2003. Proceedings. 2003 IEEE Computer Society Conference on’, Vol. 1, IEEE, pp. I–I.
- Wachs, J., Stern, H., Burks, T. and Alchanatis, V. (2010), ‘Low and high-level visual feature-based apple detection from multi-modal images’, *Precision Agriculture* **11**(6), 717–735.
- Wallenberg, M., Felsberg, M., Forssén, P.-E. and Dellen, B. (2011), Channel coding for joint colour and depth segmentation, in ‘Joint Pattern Recognition Symposium’, Springer, pp. 306–315.
- Wang, C., Zou, X., Tang, Y., Luo, L. and Feng, W. (2016), ‘Localisation of litchi in an unstructured environment using binocular stereo vision’, *Biosystems Engineering* **145**, 39–51.
- Wang, Q., Nuske, S., Bergerman, M. and Singh, S. (2012), Automated crop yield estimation for apple orchards, in ‘13th International Symposium on Experimental Robotics’.
- Wang, X.-F., Huang, D.-S., Du, J.-X., Xu, H. and Heutte, L. (2008), ‘Classification of plant leaf images with complicated background’, *Applied mathematics and computation* **205**(2), 916–926.
- Wang, Y. and Li, J. (2015), An improved canny algorithm with adaptive threshold selection, in ‘MATEC Web of Conferences’, Vol. 22, EDP Sciences.

- Wang, Y., Zhu, X. and Ji, C. (2008), 'Machine vision based cotton recognition for cotton harvesting robot', *Computer And Computing Technologies In Agriculture, Volume II* pp. 1421–1425.
- Wang, Z., Chi, Z., Feng, D. and Wang, Q. (2000), Leaf image retrieval with shape features, in 'Visual', Springer, pp. 477–487.
- Watson, D. J. (1947), 'Comparative physiological studies on the growth of field crops: I. variation in net assimilation rate and leaf area between species and varieties, and within and between years', *Annals of Botany* **11**(41), 41–76.
- Weiss, M., Baret, F., Smith, G., Jonckheere, I. and Coppin, P. (2004), 'Review of methods for in situ leaf area index (lai) determination: Part ii. estimation of lai, errors and sampling', *Agricultural and forest meteorology* **121**(1), 37–53.
- Weiss, U. and Biber, P. (2011), 'Plant detection and mapping for agricultural robots using a 3d lidar sensor', *Robotics and autonomous systems* **59**(5), 265–273.
- Woebbecke, D., Meyer, G., Von Bargen, K. and Mortensen, D. (1995), 'Color indices for weed identification under various soil, residue, and lighting conditions', *Transactions of the ASAE* **38**(1), 259–269.
- Wolf, D., Carson, E. and Brown, R. (1972), 'Leaf area index and specific leaf area determinations', *J. Agr. Edu* **1**, 24–27.
- Wspanialy, P. and Moussa, M. (2016), 'Early powdery mildew detection system for application in greenhouse automation', *Computers and Electronics in Agriculture* **127**, 487–494.
- Wu, S., Bao, F., Xu, E., Wang, Y., Chang, Y. and Xiang, Q. (2007), A leaf recognition algorithm for plant classification using probabilistic neural network, in 'Signal Processing and Information Technology, 2007 IEEE International Symposium on', IEEE, pp. 11–16.

- Xia, C., Lee, J.-M., Li, Y., Song, Y.-H., Chung, B.-K. and Chon, T.-S. (2013), 'Plant leaf detection using modified active shape models', *biosystems engineering* **116**(1), 23–35.
- Xia, C., Li, Y., Chon, T.-S. and Lee, J.-M. (2009), A stereo vision based method for autonomous spray of pesticides to plant leaves, in 'Industrial Electronics, 2009. ISIE 2009. IEEE International Symposium on', IEEE, pp. 909–914.
- Xia, C., Wang, L., Chung, B.-K. and Lee, J.-M. (2015), 'In situ 3d segmentation of individual plant leaves using a rgb-d camera for agricultural automation', *Sensors* **15**(8), 20463–20479.
- Xiang, R., Jiang, H. and Ying, Y. (2014), 'Recognition of clustered tomatoes based on binocular stereo vision', *Computers and Electronics in Agriculture* **106**, 75–90.
- Xu, C. and Prince, J. L. (1998), 'Snakes, shapes, and gradient vector flow', *IEEE Transactions on image processing* **7**(3), 359–369.
- Yaghoubi, S., Akbarzadeh, N. A., Bazargani, S. S., Bazargani, S. S., Bamizan, M. and Asl, M. I. (2013), 'Autonomous robots for agricultural tasks and farm assignment and future trends in agro robots', *International Journal of Mechanical & Mechatronics Engineering IJMME-IJENS* **13**(03), 1–6.
- Yahiaoui, I., Hervé, N. and Boujemaa, N. (2006), Shape-based image retrieval in botanical collections, in 'Pacific-Rim Conference on Multimedia', Springer, pp. 357–364.
- Yamamoto, K., Guo, W. and Ninomiya, S. (2016), 'Node detection and internode length estimation of tomato seedlings based on image analysis and machine learning', *Sensors* **16**(7), 1044.

- Yang, L., Dickinson, J., Wu, Q. and Lang, S. (2007), A fruit recognition method for automatic harvesting, *in* 'Mechatronics and Machine Vision in Practice, 2007. M2VIP 2007. 14th International Conference on', Ieee, pp. 152–157.
- Yanikoglu, B., Aptoula, E. and Tirkaz, C. (2014), 'Automatic plant identification from photographs', *Machine vision and applications* **25**(6), 1369–1383.
- Yuan, T., Li, W., Feng, Q. and Zhang, J. (2010), Spectral imaging for greenhouse cucumber fruit detection based on binocular stereovision, *in* '2010 Pittsburgh, Pennsylvania, June 20-June 23, 2010', American Society of Agricultural and Biological Engineers, p. 1.
- Zecha, C., Link, J. and Claupein, W. (2013), 'Mobile sensor platforms: Categorisation and research applications in precision farming', *Journal of Sensors and Sensor Systems* **2**(1), 51–72.
- Zemel, R. S., Dayan, P. and Pouget, A. (1998), 'Probabilistic interpretation of population codes', *Neural computation* **10**(2), 403–430.
- Zhang, C. and Chaisattapagon, N. (1995), 'Effective criteria for weed identification in wheat fields using machine vision', *Transactions of the ASAE* **38**(3), 965–974.
- Zhang, N., Wang, M. and Wang, N. (2002), 'Precision agriculture worldwide overview', *Computers and electronics in agriculture* **36**(2), 113–132.
- Zhang, T. and Suen, C. Y. (1984), 'A fast parallel algorithm for thinning digital patterns', *Communications of the ACM* **27**(3), 236–239.
- Zhao, D., Xie, D., Zhou, H., Jiang, H. and An, S. (2012), 'Estimation of leaf area index and plant area index of a submerged macrophyte canopy using digital photography', *PloS one* **7**(12), e51034.

- Zhao, J., Tow, J. and Katupitiya, J. (2005), On-tree fruit recognition using texture properties and color data, *in* 'Intelligent Robots and Systems, 2005.(IROS 2005). 2005 IEEE/RSJ International Conference on', IEEE, pp. 263–268.
- Zhou, R., Damerow, L., Sun, Y. and Blanke, M. (2012), 'Using colour features of cv. 'gala' apple fruits in an orchard in image processing to predict yield', *Precision Agriculture* pp. 1–13.
- Zhu, W., Zeng, N., Wang, N. et al. (2010), 'Sensitivity, specificity, accuracy, associated confidence interval and roc analysis with practical sas implementations', *NESUG proceedings: health care and life sciences, Baltimore, Maryland* **19**.



# Appendix A

## Stereo vision camera and specifications

## A.1 Stereo vision camera

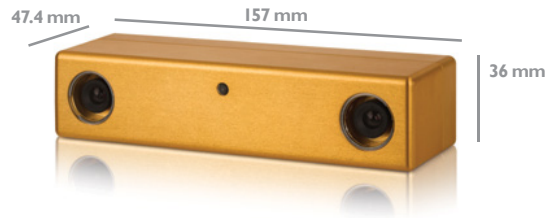
The Bumblebee2 is pre-calibrated for lens distortions and camera misalignments. The camera does not require in-field calibration, as this information is pre-loaded on the camera. A stereo rig is used to calibrate the cameras. The images have to be mapped using a pin-hole camera model. The resulting image is called ‘rectified’. The camera synchronises by itself which is particularly useful for acquiring 3D data from multiple points of view. The camera pixel resolution is  $640 \times 480$  at 48 frames per second (FPS) or  $1024 \times 768$  at 20 FPS. The camera is pre-calibrated within 0.1 pixel RMS error, based on a stereo resolution of  $640 \times 480$  and is valid for all camera models. Calibration accuracy will vary from camera to camera.

When the camera produces the disparity image, two kinds of stereo errors can be found: mismatch; and estimation. Mismatch error means the disparity map is wrong, while estimation error interpolates that there are some errors in the estimating of values for the position of the sub pixel disparity value and the correlation match was correct. Validation was used to remove mismatch errors only. The Texture Validation and Surface Validation are the most effective combination to use (PointGray, 2012).

## A.2 Camera specifications

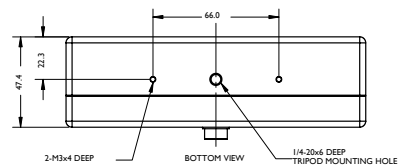
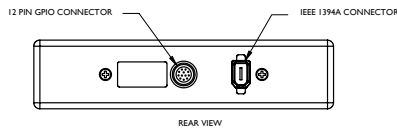
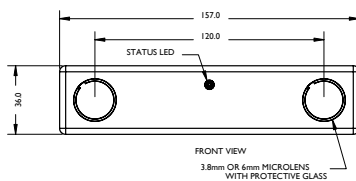
The following data sheets presents Bumblebee2 camera characteristics, design and specifications:

# FLIR *BUMBLEBEE®2* 1394a



## PRE-CALIBRATED AGAINST DISTORTION AND MISALIGNMENT

The Bumblebee®2 stereo vision camera provides a balance between 3D data quality, processing speed, size and price. Developed as a drop-in replacement for the original Bumblebee camera, the Bumblebee2 also features increased frame rate and a GPIO connector for external trigger and strobe functionality.

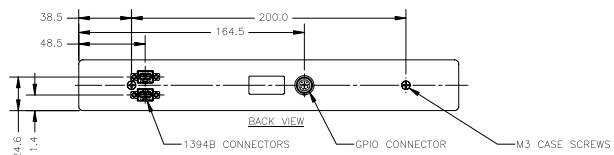
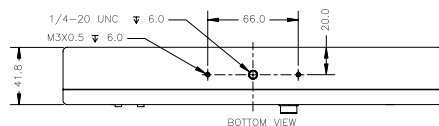
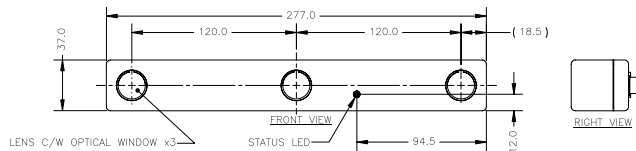
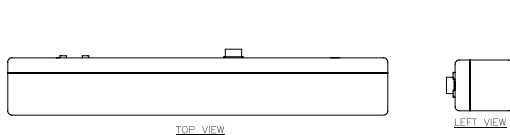


# FLIR *BUMBLEBEE®XB3* 1394b



## PRE-CALIBRATED + MULTI-BASLINE + 3 SENSORS

The Bumblebee® XB3 is a 3-sensor multi-baseline IEEE-1394b (800Mb/s) stereo camera designed for improved flexibility and accuracy. It features 1.3 mega-pixel sensors and has two baselines available for stereo processing. The extended baseline and high resolution provide more precision at longer ranges, while the narrow baseline improves close range matching and minimum-range limitations.



## Specifications

Specification	BB2-03S2	BB2-08S2	BBX3
Image Sensor Type	Sony® 1/3" progressive scan CCD		
	ICX424 (648x488 max pixels)	ICX204 (1032x776 max pixels)	ICX445 (1280x960 max pixels)
	7.4µm square pixels	4.65µm square pixels	3.75µm square pixels
Baseline	12 cm		12 cm and 24 cm
Focal Lengths	2.5mm with 97° HFOV (BB2 only) or 3.8mm with 66° HFOV or 6mm with 43° HFOV		
Aperture	f/2.0 (2.5mm and 3.8mm focal length), f/2.5 (6.0mm focal length)		
A/D Converter	12-bit analog-to-digital converter		
White Balance	Automatic / Manual (Color model)		Manual (Color model)
Frame Rates	48 FPS	20 FPS	16 FPS
Interfaces	6-pin IEEE-1394a for camera control and video data transmission 4 general-purpose digital input/output (GPIO) pins		2 x 9-pin IEEE-1394b for camera control and video data transmit 4 general-purpose digital input/output (GPIO) pins
Voltage Requirements	8-30V via IEEE-1394 interface or GPIO connector		
Power Consumption	2.5W at 12V		4W at 12V
Gain	Automatic/Manual		
Shutter	Automatic/Manual, 0.01ms to 66.63ms at 15 FPS		
Trigger Modes	DCAM v1.31 Trigger Modes 0, 1, 3, and 14		DCAM v1.31 Trigger Modes 0, 1, 3, and 14
Signal To Noise Ratio	60dB		54dB
Dimensions	157 x 36 x 47.4mm		277 x 37 x 41.8mm
Mass	342 grams		505 grams
Camera Specification	IIDC 1394-based Digital Camera Specification v1.31		
Lens mount	2 x M12 microlens mount		3 x M12 microlens mount
Emissions Compliance	Complies with CE rules and Part 15 Class A of FCC Rules		
Operating Temperature	Commercial grade electronics rated from 0° to 45°C		
Storage Temperature	-30° to 60°C		

### FLIR Integrated Imaging Solutions

#### CANADA

12051 Riverside Way  
Richmond, BC, Canada  
V6W 1K7  
T: +1 866.765.0827 (toll free)  
T: +1 604.242.9937  
F: +1 604.242.9938  
E: mv-sales@flir.com  
www.flir.com/iis

#### USA

T: +1 866.765.0827 (toll free)  
E: mv-na-sales@ptgrey.com

#### EUROPE

T: +49 7141 488817-0  
F: +49 7141 488817-99  
E: mv-eusales@flir.com

#### CHINA

T: +86 10 8215 9938  
F: +86 10 8215 9936  
E: mv-chinasales@flir.com

#### ASIA

E: mv-asiasales@ptgrey.com

### DISTRIBUTORS

#### JAPAN

ViewPLUS Inc. (www.viewplus.co.jp)

#### KOREA

CYLOD Co., Ltd. (www.cylod.com)

#### CHINA

LUSTER LightVision (www.lusterinc.com)

#### SINGAPORE, THAILAND, MALAYSIA

Voltrium Systems (www.voltrium.com.sg)

#### TAIWAN

Apo Star Co., Ltd. (www.apostar.com.tw)

#### UNITED KINGDOM AND IRELAND

ClearView Imaging (www.clearviewimaging.co.uk)

©2017 FLIR® Integrated Imaging Solutions Inc. All rights reserved. Names and marks appearing on the products herein are either registered trademarks or trademarks of FLIR® Systems, Inc. and/or its subsidiaries.